AD-A131 159 BEHAVIOUR OF SHORT CRACKS IN AIRFRAME COMPONENTS CONFERENCE PROCEEDINGS O..(U) ADVISORY GROUP FOR AEROSPACE RESEARCH AND DEVELOPMENT NEUILLY.. APR 83 AGARD-CP-328 F/G 1/3 NL

1/3

UNCLASSIFIED

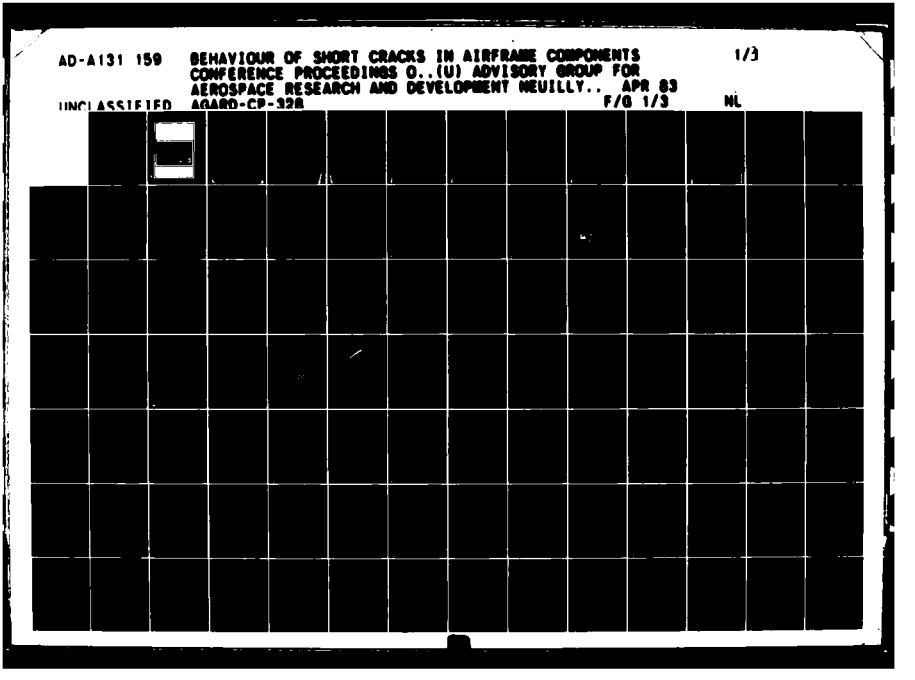

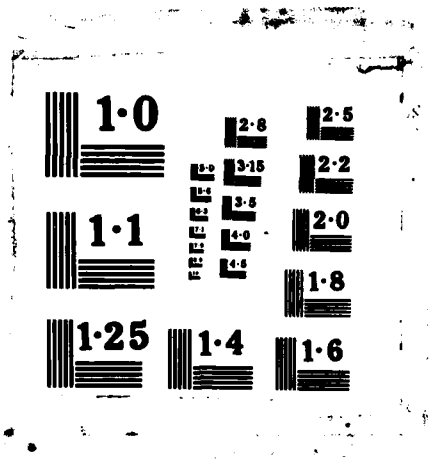
1·0
1·1
1·25
2·8
3·15
3·5
4·0
4·5
1·4
2·5
2·2
2·0
1·8
1·6

AGARD

ADVISORY GROUP FOR AEROSPACE RESEARCH & DEVELOPMENT

AGARD CONFERENCE PROCEEDINGS No. 328

Behaviour of Short Cracks in Airframe Components

NORTH ATLANTIC TREATY ORGANIZATION

AGARD-CP-328

NORTH ATLANTIC TREATY ORGANIZATION

ADVISORY GROUP FOR AEROSPACE RESEARCH AND DEVELOPMENT

(ORGANISATION DU TRAITE DE L'ATLANTIQUE NORD)

AGARD Conference Proceedings No.328

BEHAVIOUR OF SHORT CRACKS IN AIRFRAME COMPONENTS

Papers presented at the 55th Meeting of the AGARD Structures and Materials Panel in Toronto, *Canada on 19–24 September 1982.*

THE MISSION OF AGARD

The mission of AGARD is to bring together the leading personalities of the NATO nations in the fields of science and technology relating to aerospace for the following purposes:

- Exchanging of scientific and technical information;
- Continuously stimulating advances in the aerospace sciences relevant to strengthening the common defence posture;
- Improving the co-operation among member nations in aerospace research and development;
- Providing scientific and technical advice and assistance to the North Atlantic Military Committee in the field of aerospace research and development;
- Rendering scientific and technical assistance, as requested, to other NATO bodies and to member nations in connection with research and development problems in the aerospace field;
- Providing assistance to member nations for the purpose of increasing their scientific and technical potential;
- Recommending effective ways for the member nations to use their research and development capabilities for the common benefit of the NATO community.

The highest authority within AGARD is the National Delegates Board consisting of officially appointed senior representatives from each member nation. The mission of AGARD is carried out through the Panels which are composed of experts appointed by the National Delegates, the Consultant and Exchange Programme and the Aerospace Applications Studies Programme. The results of AGARD work are reported to the member nations and the NATO Authorities through the AGARD series of publications of which this is one.

Participation in AGARD activities is by invitation only and is normally limited to citizens of the NATO nations.

Published April 1983

ISBN 92-835-1444-0

Printed by Specialised Printing Services Limited
40 Chigwell Lane, Loughton, Essex IG10 3TZ

REPORT DOCUMENTATION PAGE			
1. Recipient's Reference	2. Originator's Reference AGARD-CP-328	3. Further Reference ISBN 92-835-1444-0	4. Security Classification of Document UNCLASSIFIED

5. Originator: Advisory Group for Aerospace Research and Development
North Atlantic Treaty Organization
7 rue Ancelle, 92200 Neuilly sur Seine, France

6. Title

BEHAVIOUR OF SHORT CRACKS IN AIRFRAME COMPONENTS

7. Presented at

the 55th Meeting of the AGARD Structures and Materials Panel in Toronto, Canada on 19–24 September 1982.

8. Author(s)/Editor(s)	9. Date
Various	April 1983
10. Author's/Editor's Address	**11. Pages**
Various	214

12. Distribution Statement: This document is distributed in accordance with AGARD policies and regulations, which are outlined on the Outside Back Covers of all AGARD publications.

13. Keywords/Descriptors

Airframes
Cracks
Crack propagation
Fracturing
Fracture properties

14. Abstract

In the Fall of 1982 the AGARD Structures and Materials Panel arranged a Specialists' Meeting to examine the accuracy and applicability of linear fracture mechanics to the growth behaviour of short cracks. These Conference Proceedings include fourteen of the fifteen papers presented at the meeting, together with a report of the round table discussion. The paper give an overview of the existing state of the art of fracture mechanics as applied to short cracks.

COMPONENT PART NOTICE

THIS PAPER IS A COMPONENT PART OF THE FOLLOWING COMPILATION REPORT:

(TITLE): Behaviour of Short Cracks in Airframe Components, Conference Proceedings of the Meeting of the AGARD Structures and Materials Panel (55th) Held at Toronto, Canada on 19-24 September 1982.

(SOURCE): Advisory Group for Aerospace Research and Development, Neuilly-sur-Seine (France).

TO ORDER THE COMPLETE COMPILATION REPORT USE AD-A131 159.

THE COMPONENT PART IS PROVIDED HERE TO ALLOW USERS ACCESS TO INDIVIDUALLY AUTHORED SECTIONS OF PROCEEDINGS, ANNALS, SYMPOSIA, ETC. HOWEVER, THE COMPONENT SHOULD BE CONSIDERED WITHIN THE CONTEXT OF THE OVERALL COMPILATION REPORT AND NOT AS A STAND-ALONE TECHNICAL REPORT.

THE FOLLOWING COMPONENT PART NUMBERS COMPRISE THE COMPILATION REPORT:

AD#:	TITLE:
P001 602	Mechanics and Physics of the Growth of Small Cracks.
P001 603	Fatigue Damage Mechanisms and Short Crack Growth.
P001 604	An Assessment of the Importance of Small Crack Growth to Aircraft Design.
P001 605	A Nonlinear Fracture Mechanics Approach to the Growth of Small Cracks.
P001 606	Damage Tolerance Evaluation of Structures with Small Cracks.
P001 607	Fracture Mechanics Analysis of Short Cracks at Loaded Holes.
P001 608	Probabilistic Fracture Mechanics Analysis Methods for Structural Durability.
P001 609	The Effects of Compressive Overloads on the Threshold Stress Intensity for Short Cracks.
P001 610	Crack Propagation at Short Crack Lengths under Variable Amplitude Loading (2nd Report).
P001 611	Spectrum Effects on the Growth of Short Cracks.
P001 612	A Study of Small Crack Growth under Transport Spectrum Loading.
P001 613	Small Cracks in Large Forgings.
P001 614	'Short Crack' Fatigue Design Considerations: Modelling, Characterization Interpretation, Detection: Prediction of Behavior.

PREFACE

Following on publication of AGARDograph 257 "Practical Applications of Fracture Mechanics", interest amongst engineers has centred on the present state-of-the-art in relation to the prediction of short crack growth behaviour. In particular, some current airworthiness requirements demand an analytical demonstration that very small flaws (of specified shape and of length very much less than one millimetre) should not cause excessive cracking within the structure during the aircraft's designed service life. The applicability of linear elastic fracture mechanics in these circumstances has been questioned, because data from some crack propagation tests has shown growth rates in excess of those predicted by theory. The problem was discussed in two pilot papers presented at the fifty-second SMP Meeting, and now being published together as AGARD Report 696.

It was subsequently decided to call a Specialists Meeting in the Fall of 1982 to examine the accuracy and applicability of methods based on linear elastic fracture mechanics currently available for predicting short crack behaviour. These Conference Proceedings include the fifteen papers presented there together with a report of the round table discussion.

Many varied views were expressed on the data obtained from experimental investigation, but there was no consensus of opinion. Some tests appeared to confirm the existence of short crack effects, whereas other experimenters did not confirm these findings. During the round table discussion however, it emerged that the tests which did not confirm the existence of short crack effects had not included compressive loading cycles. The outcome of the meeting was a proposal to encourage further activity which would aim to determine the reasons for apparently contradictory results in crack growth data; the way to perform this task has yet to be defined.

In the meantime, this document describes the state of the existing fracture mechanics art when applied to the analysis of short cracks; it provides a sound base from which to further consider the problems.

I wish to express my sincere thanks to the authors and all those who contributed to this document including those who evaluated the main topics of the round table discussion.

H.J.ZOCHER
Chairman, Sub-Committee
Behaviour of Short Cracks in
Airframe Components

CONTENTS

*not available at time of printing

assumed to be inherently conservative.

Current practice in the determination of the relevant crack growth law for a particular material in a given application is to utilize the existing data-base of laboratory-determined fatigue crack propagation results, characterized in terms of the linear elastic stress intensity range ΔK. However, the majority of these data has been determined from test-piece geometries containing crack sizes of the order of 25 mm or so, whereas many defects encountered in service are far smaller than this, particularly in turbine disk- and blade applications, for example. In the relatively few instances where the fatigue behavior of such short cracks has been experimentally studied (for reviews see refs. 1-4), it has been found, almost without exception, that at the same nominal driving force, the growth rates of short cracks are greater than (or equal to) the corresponding growth rates of long cracks. This implies a breakdown in the similitude concept generally assumed in fracture mechanics, whereby for, say, nominal linear elastic conditions, different-sized cracks subjected to the same stress intensity K_I will have identical local stress and strain fields at their crack tips and correspondingly should undergo equal amounts of crack extension. Furthermore, it suggests that the use of existing (long crack) data for defect-tolerant life-time calculations in components, where the growth of short flaws represents a large proportion of the life, has the potential for ominously non-conservative life predictions.

There are several factors which constitute a definition of a short crack, namely, i) cracks which are of a length comparable with the scale of microstructure (e.g., $\sim$ grain size, typically $\lesssim$ 1-50 μm), ii) cracks which are of a length comparable to the scale of local plasticity (e.g., $\sim$ plastic zone size, typically $\lesssim 10^{-2}$ mm in ultrahigh strength materials to $\lesssim$ 0.1-1 mm in low strength materials), and iii) cracks which are simply physically small (e.g., $\lesssim$ 0.5-1 mm). Most investigations to date have focussed on the first two factors which represent, respectively, a continuum mechanics limitation and a linear elastic fracture mechanics (LEFM) limitation to current analysis procedures. Presumably here, with an appropriate micro- or macro-mechanics characterization of crack advance, a correspondence between long and short crack growth rate data should be achieved. However, physically-short flaws, which are "long" in terms of continuum and LEFM analyses, have also been shown to propagate at rates faster than equivalent long cracks (at the same driving force) [4], indicating that the lack of correspondence between results also may reflect basic differences in the physical micro-mechanisms associated with the crack extension of long and short flaws.

In the present paper, we review the existing data on the growth of short fatigue cracks in engineering materials and discuss where behavior may differ from that of equivalent long cracks in terms of i) the appropriate fracture mechanics characterizations and ii) the physics and mechanisms involved in crack advance. In the former case, the short-crack problem is treated in terms of elastic-plastic fracture mechanics (EPFM) analyses which incorporate the effects of local crack tip plasticity and strain fields of notches, whereas in the latter case behavioral differences are examined in terms of the roles of crack size and shape, microstructure, environment, crack closure and crack extension mechanisms. We begin, however, with a brief summary of the fracture mechanics procedures used to characterize fatigue crack propagation for both long and short flaws.

2. FRACTURE MECHANICS CHARACTERIZATION OF FATIGUE CRACK GROWTH

The essential features of fracture mechanics involve characterization of the local stress and deformation fields in the vicinity of the crack tip. Under linear elastic conditions, the local crack tip stresses (σ_{ij}) at a distance r ahead of a nominally stationary crack subjected to tensile (Mode 1) opening can be so characterized in terms of the K_I singular field:

$$\sigma_{ij}(r,\theta) \rightarrow \frac{K_I}{\sqrt{2\pi r}} f_{ij}(\theta) , \quad \text{as } r \rightarrow 0 \qquad (2)$$

where K_I is the Mode I stress intensity factor, θ the polar angle measured from the crack plane and f_{ij} a dimensionless function of θ [5]. The use of K_I to uniquely characterize the local linear elastic crack tip field is meaningful only when small-scale yielding conditions exist. This implies that the region of local yielding at the crack tip, denoted by the plastic zone size (r_y),

$$r_y \approx \frac{1}{2\pi}\left(\frac{K_I}{\sigma_o}\right)^2 , \qquad (3)$$

where σ_o is the yield strength of the material, is small compared to the in-plane dimensions of the body, namely crack length (a) and remaining ligament depth (b) [6]. Specifically, small-scale yielding conditions [7], i.e., that a K_I based description of crack tip fields is relevant, requires

$$r_y << a,b , \quad \text{typically} < \frac{1}{15}(a,b) . \qquad (4)$$

MECHANICS AND PHYSICS OF THE GROWTH OF SMALL CRACKS

by
R. O. Ritchie and S. Suresh
Materials and Molecular Research Division, Lawrence Berkeley Laboratory,
and Department of Materials Science and Mineral Engineering,
University of California
Berkeley, CA 94720
U.S.A.

SUMMARY

The mechanics and physics of the sub-critical propagation of small fatigue cracks are reviewed in terms of reported differences in behavior between long and short flaws based on fracture mechanics, microstructural and environmental viewpoints. Cracks are considered short when their length is small compared to relevant microstructural dimensions (a continuum mechanics limitation), when their length is small compared to the scale of local plasticity (a linear elastic fracture mechanics limitation), and when they are merely physically-small (e.g., <0.5-1 mm). For all three cases, it is shown that, at the same nominal driving force, the growth rates of the short flaws are likely to be greater than (or at least equal to) the corresponding growth rates of long flaws; a situation which can lead to non-conservative defect-tolerant lifetime predictions where existing (long crack) data are utilized. Reasons for this problem of similitude between long and short flaw behavior are discussed in terms of the roles of crack driving force, local plasticity, microstructure, crack shape, crack extension mechanism, premature closure of the crack, and local crack tip environment.

1. INTRODUCTION

Fatigue, involving the progressive failure of materials via the incipient growth of flaws under cyclically-varying stresses, can be regarded as the principal cause of in-service failures in most engineering structures and components. Whether under pure mechanical loading or in association with sliding and friction between surfaces (fretting-fatigue), rolling contact between surfaces (rolling contact fatigue), active environments (corrosion fatigue) or elevated temperatures (creep fatigue), fatigue fractures probably account for over 80% of all service failures. However, the process of these failures can be characterized into several related phenomena involving i) initial cyclic damage (cyclic hardening or softening), ii) the formation of initial microscopic flaws (micro-crack initiation), iii) the coalescence of these micro-cracks to form an initial "fatal" flaw (micro-crack growth), iv) the subsequent macroscopic propagation of this flaw (macro-crack growth) and v) final catastrophic failure or instability. In engineering terms, the first three stages, involving deformation and micro-crack initiation and growth, are generally embodied into the single process of (macro-) crack initiation representing the formation of an "engineering-size" detectable crack (i.e., of the order of several grain diameters in length). Thus in such terms, the total fatigue life (N) can be defined as the number of cycles to initiate a (macro-) crack (N_i) plus the number of cycles to propagate it sub-critically to final failure (N_p), i.e.,

$$N = N_i + N_p \quad . \tag{1}$$

From the perspective of fatigue design or lifetime prediction, this distinction between initiation and propagation lives can be critical. Conventional fatigue design approaches, on the one hand, classically involve the use of S-N curves, representing the *total life* N resulting from a stress, or strain, amplitude S, suitably adjusted to take into account effects of mean stress (using, for example, Goodman diagrams), effective stress concentrations at notches (using fatigue-strength reduction factors or local strain analysis), variable-amplitude loading (using the Palmgren-Miner cumulative-damage law or rainflow counting methods), multiaxial stresses, environmental effects, and so forth. Although based on total life, this approach, which is in widespread use, essentially represents design against *crack initiation*, since near the fatigue limit, especially in smooth specimens, the major portion of the lifetime is spent in the formation of an engineering-size crack. For safety-critical structures, especially with welded and riveted components, on the other hand, there has been a growing awareness that the presence of defects in a material below certain size must be assumed and taken into account at the design stage. Under such circumstances, the integrity of a structure will depend upon the lifetime spent in crack propagation, and since the crack-initiation stage will be small, the use of conventional S/N total life analyses may lead to dangerous overestimates of life. Such considerations have led to the adoption of the so-called defect-tolerant approach, where the fatigue lifetime is assessed in terms of the time, or number of cycles, to *propagate* some arbitrary undetected crack (estimated by non-destructive evaluation or proof tests) to failure (defined by the fracture toughness, limit load or some allowable strain criteria). This approach, which is used exclusively for certain applications in the nuclear and aerospace industries, for example, relies on integration of a crack-growth expression, representing a fracture mechanics characterization of relevant fatigue crack propagation data suitably modified to account for mean stress effects (e.g., using the Forman equation), variable-amplitude loading (e.g., using the Wheeler or Willenborg models), environmental effects, and so forth, as required [1]. Since the crack initiation life is taken to be zero, such defect-tolerant life predictions are

Under cyclic loading, the range of stress intensity ΔK, given by the difference between the maximum (K_{max}) and minimum (K_{min}) stress intensities in the cycle, is commonly used to correlate to crack extension, through power-laws of the form [8]:

$$\frac{da}{dN} = C\,\Delta K^m \quad , \tag{5}$$

where C and m are scaling constants. Here the extent of local yielding is defined in terms of maximum (monotonic) and cyclic plastic zones (r_{max} and r_Δ, respectively), given approximately by [7]:

$$r_{max} \approx \frac{1}{2\pi}\left(\frac{K_{max}}{\sigma_o}\right)^2 \quad ,$$

and

$$r_\Delta \approx \frac{1}{2\pi}\left(\frac{\Delta K}{2\sigma_o}\right)^2 \quad . \tag{6}$$

The numerical values of the stress intensity factors at the crack tip, i.e., K_I, ΔK, etc., remain undetermined from the asymptotic analysis, yet can be computed from the overall geometry and applied loading conditions. In fact solutions for K_I applicable to a wide variety of situations are now tabulated in handbooks [9]. A useful example of such K_I solutions, which is particularly relevant to the short crack problem, is that of a crack (length ℓ) growing from a notch (length 2c)(Fig. 1) [10]. Assuming a circular hole in an infinite plate under a remotely applied tensile stress σ, the limiting analytical solution for a short crack emanating from the notch is given as:

$$K_s = 1.12\ k_t\sigma\sqrt{\pi\ell} \quad , \tag{7}$$

where k_t is the elastic stress concentration factor (equal to 3 in this case) and 1.12 is the free surface correction factor. However, when the crack becomes long, the limiting stress intensity is obtained by idealizing the geometry so that the notch becomes part of a long crack of dimension $a = c + \ell$, such that

$$K_\ell = F\,\sigma\sqrt{\pi a} \quad , \tag{8}$$

where F is a dimensionless function of geometry, such as a finite width correction factor. The numerically-determined K_I solution for any crack emanating from a notch, shown by the dashed line in Fig. 1, can be seen to be given by these short and long crack limiting cases. As shown by Dowling [10], the transition crack size ℓ_o, which can be interpreted as the extent of the local notch field, can then be obtained by combining Eqs. (7) and (8) as:

$$\ell_o = \frac{c}{(1.12\ k_t/F)^2 + 1} \quad . \tag{9}$$

Values of ℓ_o are generally a small fraction of the notch root radius ρ, and for moderate to sharp notches generally fall in the range $\rho/20$ to $\rho/4$. Dowling [10] has further noted that $k_t\sigma$ values only 20-30% above σ_o are sufficient to generate a notch tip plastic zone which engulfs the small crack region ℓ_o, and thus far small cracks at notches, LEFM analysis will often be suspect.

The above example serves to illustrate one aspect of the short crack problem where the crack length is comparable with the notch tip plastic zone size. A similar situation, where small-scale yielding conditions may not apply, is where the plastic zone at the tip of the fatigue crack itself is comparable with the crack length, i.e., when $a \sim r_y$. Since the use of K_I singular fields is no longer appropriate in such instances, alternative asymptotic analyses have been developed to define the crack tip stress and strain fields in the presence of more extensive local plasticity. Based on the deformation theory of plasticity (i.e., non-linear elasticity), the asymptotic form of these local fields, for non-linear elastic power hardening solids of constitutive law $\sigma \propto \varepsilon^n_{plastic}$, is given by the Hutchinson, Rice, Rosengren (HRR) singularity as [11,12]:

$$\sigma_{ij}(r,\theta) \to \left(\frac{E'\,J}{\sigma_o^2\,r}\right)^{n/n+1} \sigma_o\, f^1_{ij}(\theta,n) \quad ,$$

$$\varepsilon_{ij}(r,\theta) \to \left(\frac{E'\,J}{\sigma_o^2\,r}\right)^{1/n+1} f^{11}_{ij}(\theta,n) \quad , \tag{10}$$

as $r \to 0$, where n is the work hardening exponent, E' the appropriate elastic modulus (= E for plane stress or $E/(1-\nu^2)$ for plane strain) and f_{ij}, f_{ij} are universal functions of their arguments depending upon whether plane stress or plane strain is assumed. The amplitude of this field is the so-called J-integral [13], and analogous to K_I, J uniquely and autonomously characterizes the crack tip field under elastic-plastic conditions *provided some degree of strain hardening exists*. Further, for small-scale

yielding, J can be directly related to the strain energy release rate G, and hence K_I, i.e.,

$$J = G = K_I^2/E' \qquad \text{(linear elastic)} \qquad (11)$$

Despite difficulties in the precise meaning of J as applied to a description of crack growth of cyclically-stressed (non-stationary) cracks, certain authors [14,15] have proposed a power-law correlation of fatigue crack growth rates under elastic-plastic conditions to the range of J, i.e.,

$$\frac{da}{dN} \propto \Delta J^{m'} \quad . \qquad (12)$$

Provided such analysis is fundamentally justified, the use of ΔJ does present a feasible approach to characterize the growth of short cracks which are comparable in size to the extent of local yielding, as discussed below. However, as alluded to above, the validity of the ΔJ approach is often questioned since it appears to contradict a basic assumption in the definition of J that stress is proportional to the *current* plastic strain. This follows because J is defined from the deformation theory of plasticity (i.e., non-linear elasticity) which does not allow for the elastic unloading and non-proportional loading effects which accompany crack advance [13]. By recognizing, however, that constitutive laws for *cyclic* plasticity (i.e., the cyclic stress-strain curve) can be considered in terms of *stable* hysteresis loops, and that such loops can be mathematically shifted to a common origin after each reversal, the criterion of stress proportional to current plastic strain can be effectively satisfied for cyclic loading [16].

An alternative treatment of elastic/plastic fatigue crack growth, which is not subject to such restrictions required by non-linear elasticity, is to utilize the concept of crack tip opening displacement (CTOD). From Eq. (10), it is apparent that the opening of the crack faces varies at $r \to 0$ as $r^{n/n+1}$, such that this separation can be used to define the CTOD (δ_t) as the opening where 45° lines emanating back from the crack tip intercept the crack faces, i.e.,

$$\delta_t = d(\varepsilon_o, n)\,\frac{J}{\sigma_o^2} \quad , \qquad \text{(elastic/plastic)} \quad ,$$

$$\propto \frac{K_I^2}{\sigma_o E'} \quad , \qquad \text{(linear elastic)} \quad , \qquad (13)$$

where d is a proportionality factor ($\sim$ 0.3 to 1) dependent upon the yield strain ε_o, the work hardening exponent n, and whether plane stress or plane strain is assumed [17]. Since δ_t, like J, can be taken as a measure of the intensity of the elastic-plastic crack tip fields, it is feasible to correlate rates of fatigue crack growth to the range of δ_t, i.e., the cyclic crack tip opening displacement (ΔCTOD), as

$$\frac{da}{dN} \propto \Delta\text{CTOD} \quad , \qquad \text{(elastic/plastic)} \quad ,$$

$$\propto \frac{\Delta K_I^2}{2\sigma_o E'} \quad , \qquad \text{(linear elastic)} \quad . \qquad (14)$$

Approaches based on J and δ_t are basically equivalent, and are of course valid under both elastic/plastic and linear elastic conditions. They therefore are applicable to a continuum description of the growth rate behavior of cracks considered small because their size is comparable with the scale of local plasticity. Thus, for such short cracks, the use of elastic/plastic, rather than linear elastic, fracture mechanics may be expected to normalize differences in behavior between long and short flaws. However, the use of EPFM cannot necessarily be expected to normalize behavior between long and microstructurally-short or physically-short flaws, where other factors are important. These other factors are related to microstructural, environmental and closure effects and are discussed in detail below.

3. REVIEW OF EXPERIMENTAL RESULTS

Microstructural Effects

The first definition of a short fatigue crack involves cracks which are comparable in size with the scale of microstructural features. Several recent experimental studies [1,18-23] on the initiation and growth of cracks in a wide range of materials have revealed that short cracks, initiated near regions of surface roughening caused by the to and fro motion of dislocations or at inclusions and grain boundaries, propagate at rates which are different from those of equivalent long cracks, when characterized in terms of conventional fracture mechanics concepts. For example, it was first shown by Pearson [23] in precipitation hardened alloys that cracks, of a size comparable with the grain size, grew several times faster than long cracks at nominally identical stress intensity values. Such variation in the growth rate behavior of long and microstructurally-short cracks as a function of the stress intensity range is shown in Fig. 2 for 7075-T6

aluminum alloy, taken from the work of Lankford [24]. It is apparent from this figure that the growth rates associated with the short cracks are up to two orders of magnitude faster than those of the long cracks, and further that such accelerated short crack advance occurs at stress intensities well below the so-called fatigue threshold stress intensity range (ΔK_o), below which *long cracks* remain dormant or grow at experimentally-undetectable rates [25]. The initially higher growth rates of the short cracks can be seen to progressively decelerate (and even arrest in certain cases) before merging with the long crack data at stress intensities close to ΔK_o, similar to observations reported elsewhere by Morris et al. [26], Kung et al. [20] and Tanaka et al. [27,28]. Such short crack behavior has been attributed to a slowing down of short crack advance through interaction with grain boundaries [20-22,24,26-28]. Using arguments based on microplasticity and crack closure effects, Morris and co-workers [22,26] have modelled the process in terms of two factors, namely a cessation of propagation into a neighboring grain until a sizeable plastic zone is developed, and a retardation in growth rates due to an elevated crack closure stress. Tanaka et al. [21,27,28] similarly considered the impeded growth of microstructurally-short cracks in terms of the pinning of slip bands, emanating from the crack tip, by grain boundaries. The results of Lankford [24] in Fig. 2 indicate that the crack growth rate minimum corresponds to a crack length roughly equal to the smallest grain dimension (i.e., $a \sim d_g$). Further, the extent, or depth, of the deceleration "well," shown in this figure, appeared to be determined by the degree of microplasticity involved in the crack traversing the boundary. For example, when the orientation between the grain containing the crack and the neighboring grain was similar, little deceleration in growth rates at the boundary was seen to occur. Thus a consensus from these studies is that despite their accelerated propagation rates, compared to long crack data, short cracks are apparently impeded by the presence of grain boundaries, which in general would be unlikely to significantly affect the local propagation rates of long cracks.

From such experimental studies, it is readily apparent that threshold stresses, or stress intensities, associated with long and short cracks are likely to be very different. Although conventional fracture mechanics arguments infer that the threshold stress intensity range (ΔK_{TH}) for a particular material should be independent of crack length (i.e., $\Delta K_{TH} = \Delta K_o$ (the long crack threshold) = constant); Kitagawa and Takahashi [29] first showed that below a critical crack size, the threshold ΔK_{TH} for short cracks actually decreased with decreasing crack length, where the threshold *stress* $\Delta\sigma_{TH}$ approached that of the smooth bar fatigue limit $\Delta\sigma_e$ at very short crack lengths (Fig. 3). Several workers have shown that this critical crack size (below which ΔK_{TH} is no longer constant with crack length) is dependent upon microstructural and mechanical factors [25,28-37], but from continuum arguments it is approximately given by $1/\pi\ (\Delta K_o/\Delta\sigma_e)^2$, where both ΔK_o and $\Delta\sigma_e$ are corrected for a common load ratio. Values of this dimension, which effectively represent the limiting crack size for valid LEFM analysis (see next section), range from typically 1-10 μm in ultrahigh strength materials (i.e., $\sigma_o \sim 2000$ MPa) to 0.1-1 mm in low strength materials (i.e., $\sigma_o \sim 200$ MPa).

Based on these results, it has been suggested [30,38,39] that the threshold condition for no growth for long cracks is one of a constant *stress intensity*, i.e., ΔK_o, whereas the threshold condition for short cracks is one of a constant stress, i.e., the fatigue limit $\Delta\sigma_e$ or endurance strength. Such a premise has been shown to be consistent with the modelling studies of Tanaka et al. [28] where the threshold for short crack propagation is governed by whether the crack tip slip bands are blocked, or can traverse, the grain boundary between an adjacent grain.

Local Plasticity Effects

The second definition of a short crack involves cracks which are small compared to the scale of local plasticity, generated either by the crack itself, i.e., the crack tip plastic zone, or by the presence of a larger stress concentrator, i.e., the strain field of a notch. The propagation of such cracks involves crack extension under elastic-plastic conditions, and from comparisons of their behavior with equivalent long cracks using LEFM analyses, i.e., at the same nominal ΔK, it is invariably seen that the short cracks appear to grow much faster [10,31-35,40,41]. However, part of the reason for such results lies not in any physical difference between long and short crack behavior but mostly with the inappropriate use of linear elastic analyses. This was shown particularly clearly by Dowling [40] who monitored the growth of small surface cracks in smooth bar specimens of A533B nuclear pressure vessel steel subjected to fully-reversed strain cycling. By analyzing the growth rates (da/dN) in terms of ΔJ, where J values were computed from the stress-strain hysteresis loops, a closer correspondence was found between long and short crack behavior (Fig. 4). However, even with the more appropriate characterization afforded by elastic-plastic fracture mechanics, it is still apparent in Fig. 4 that short cracks propagate at somewhat faster rates.

In order to account for this apparent breakdown in continuum mechanics concepts, also noticeable in the threshold results in Fig. 3, El Haddad and co-workers [33-35] introduced the notion of an intrinsic crack length a_o. These authors redefined the stress intensity factor in terms of the physical crack length plus a_o, such that the stress intensity range which characterizes the growth of fatigue cracks independent of crack length is given by:

$$\Delta K = Q\ \Delta\sigma^{\infty}\sqrt{\pi(a + a_o)}\ , \qquad (15)$$

where Q is the geometry factor. The material-dependent constant a_o was estimated from the limiting conditions of crack length where the nominal stress $\Delta\sigma^\infty$ approaches the fatigue limit $\Delta\sigma_e$ when $a \to 0$ and $\Delta K = \Delta K_o$, i.e.,

$$a_o \approx \frac{1}{\pi}\left(\frac{\Delta K_o}{\Delta\sigma_e}\right)^2 , \qquad (16)$$

and can be seen to be equivalent to the critical crack size (above which $\Delta K_{TH} = \Delta K_o$) in Fig. 3. By recomputing both ΔK and ΔJ to include this a_o concept, these authors [33] re-analyzed the short crack data of Dowling [40], shown in Fig. 4, and claimed to achieve a closer correspondence between long and short crack growth results [35].

Although such intrinsic crack length arguments successfully rationalize many apparent anomalies between the growth rate kinetics of long and short cracks limited by LEFM analyses, there is currently no available physical interpretation for the parameter a_o. Comparisons of a_o with the characteristic scales of microstructural dimensions have failed to reveal any convincing correspondence.

A somewhat different approach to rationalizing the behavior of long and short cracks, specifically with respect to the threshold condition, was presented by Usami and co-workers [36,37]. To replace the notion that the threshold condition for short cracks was one of a constant stress, compared to one of a constant stress intensity range for long cracks, these authors proposed a single criterion that the cyclic plastic zone dimension (r_Δ) at the threshold is a material constant. Using the Dugdale solution to approximate plastic zone sizes, this approach was shown to reproduce the form of the $\Delta\sigma_{TH}$ vs. a curves shown in Fig. 3 and further to rationalize effects of stress ratio and yield strength on short crack behavior. However, experimental conformation of the constancy of r_Δ at the threshold for long and short cracks was not presented.

Effects of local plasticity also play an important role in influencing the initiation and growth of short cracks emanating from notches, where cracks are considered short when their lengths are comparable in size to the extent of the strain field of the notch tip plastic zone (Fig. 5). The linear elastic K_I solutions for such short flaws have been discussed previously in Section 2. Phillips, Frost and others [42,43] first showed that such cracks initiated from notches can arrest completely and become so-called non-propagating cracks (NPC) after growing a short distance. Many subsequent studies [31,32, 35,44-47] have confirmed the existence of such NPC's although a precise understanding of the mechanisms for their occurrence is still lacking. Stress-strain/life analyses, however, have revealed that NPC's only form at sharp notches above a critical stress concentration factor k_t [47]. Hammouda and Miller [32] argue that the total plastic shear displacement, which is taken as the sum of the shear displacement arising from (notch) bulk plasticity and that due to the local crack tip plastic zone for LEFM controlled growth, determines the growth kinetics of such short cracks. Where the crack is completely submerged in the notch tip plastic zone (Fig. 5), bulk plasticity conditions dominate behavior. Here it is argued that the growth rates of the short cracks will progressively decrease until they arrest or merge with the long crack LEFM curve where behavior is dominated by local plasticity conditions within the crack tip plastic zone (Fig. 6). Several continuum mechanics explanations for such observations of decreasing growth rates of short cracks within the notch tip plastic zone have been claimed based on the above total plastic shear displacement argument [32], on elastic-plastic J-based analyses incorporating the a_o concept [45] and on the concept that the reversed plastic zone size is a material concept (independent on crack length) [37]. The physical reasons for such behavior, however, are difficult to comprehend, particularly since a striking similarity exists between Fig. 6 and Fig. 2. In the latter case the progressive deceleration in short crack growth rates was reported [24] in the absence of a notch and attributed to impeded growth at grain boundaries. With this in mind, we must conclude that the precise mechanism for the occurrence of decelerated short crack growth and NPC's is currently unclear but we do recognize that factors such as notch-tip plasticity, micro-plasticity, grain boundary blocking of slip-bands, cessation of growth and crystallographic reorientation of growth at grain boundaries, and crack closure (see Section 4) all may play a significant role. In this regard, it has been claimed that since small cracks are capable of propagating below the long crack threshold ΔK_o value, they may propagate for some distance until the combination of their size and local stress cause them to arrest at or below the ΔK_o value [2]. Although this is a convenient statement to rationalize the behavior schematically illustrated in Figs. 2 and 6, physically based mechanistic interpretations of such behavior are still uncertain.

Physically-Short Flaws

The third definition of a short crack, and perhaps the most ominous from a design viewpoint, is the physically-short flaw where the crack is long compared to both the scale of microstructure and the scale of local plasticity, yet simply physically small, i.e., typically less than 0.5-1 mm in length. Since both continuum mechanics and LEFM characterizations of the behavior of such flaws would be expected to be valid, it is perhaps surprising to find that under certain circumstances [4,48-52] even physically-short cracks show growth rates in excess of those of long cracks under nominally identical driving force conditions (i.e., at the same ΔK). This realization represents a significant breakdown in the similitude argument engrained in fracture mechanics analyses of sub-critical crack growth and has been currently attributed to two basic factors. The first of these pertains to the phenomenon of crack closure where, due to interference

microstructural factors (Fig. 2) [24]. Certainly no linear elastic analysis of the case of a notch plus short crack [62] has demonstrated that the crack driving force (e.g., K_I) goes through a minimum, as the crack extends from the notch, to rationalize such behavior, and to our knowledge there is no formal elastic-plastic analysis available which similarly predicts the appropriate variation in crack driving force (without incorporation of crack closure effects). Whilst we cannot refute the experimental data on short crack growth at notches, in the absence of a complete continuum mechanics analysis we must conclude that part of the reason for the differing growth rate behavior of the short cracks in this instance may similarly result from the interaction of the short flaw with microstructural features and from the role of crack closure, as described below.

With respect to microstructural features, it is generally accepted that the presence of grain boundaries, hard second phases, inclusions, etc. play a somewhat minimal role in influencing the growth of long fatigue cracks [25] (at least over the range of growth rates below $\sim 10^{-3}$ mm/cycle), because behavior is governed primarily by average bulk properties. However, this clearly will not be the case for small micro-cracks whose length will be comparable to the size of these microstructural features. For example, for micro-cracks contained within a single grain, cyclic slip will be strongly influenced by the crystal orientation and the proximity of the grain boundary, resulting in locally non-planar crack extension [3]. There is now a large body of evidence that shows that the growth of small cracks is impeded by the presence of grain boundaries by such mechanisms as the blocking of slip bands [21] or containment of the plastic zone [22] within the grain, reorientation and re-initiation of the crack as it traverses the boundary [24], and simply cessation of growth at the boundary [22]. The latter effect has also been demonstrated for the presence of harder second phases, where in duplex ferritic-martensitic steels, micro-cracks were observed to initiate and grow in the softer ferrite only to arrest when they encountered the harder martensite [63]. Such considerations do not explain why short cracks can propagate below the long crack threshold ΔK_o, yet they do provide a feasible interpretation for the progressively decreasing growth rates observed in this region (Fig. 2).

A further factor which may contribute to differences in the behavior of long and short cracks is the question of crack shape [3]. Even long cracks, which encompass many grains, are known to possess certain irregularities in their geometry (*on a microscale level*) due to local interactions with microstructural features [64], yet, at a given ΔK, the overall growth behavior would be expected to be similar. However, on comparing a macro-crack and a micro-crack contained within a few grains, this similarity would seem to be questionable. Moreover, the early stages of fatigue damage often involve the multi-initiation of micro-cracks such that the subsequent growth of a particular small flaw is likely to be strongly influenced by the presence of other micro-cracks [1,19].

Differences in the behavior of long and short cracks may also result from the fact that, at the same nominal ΔK, the crack extension mechanisms may be radically different. As pointed out by Schijve [3], the restraint of the elastic surrounding on a small crack near a free surface is very different from that experienced at the tip of a long crack inside the material. For a small grain-sized crack, the low restraint on cyclic slip will predominately promote single slip on the system with the highest critical resolved shear stress resulting in a Mode II + Mode I slip band cracking mechanism akin to Forsyth's Stage I. For the long crack, however, which spans many grains, maintaining such slip-band cracking in a single direction in each grain is incompatible with a coherent crack front. The resulting increased restraint on cyclic plasticity will tend to activate further slip-systems leading to a non-crystallographic mode of crack advance by alternating or simultaneous shear, commonly referred to as striation growth (Forsyth's Stage II). At near-threshold levels where the extent of local plasticity is contained within a single grain, even long cracks propagate via this single shear mechanism but, in contrast to the short crack case, the orientation of the slip-band cracking will change at each grain boundary leading to a faceted or zig-zag crack path morphology (Fig. 10) [3,59]. As discussed below, the occurrence of this shear mode of crack extension, together with the development of a faceted fracture surface, has major implications with respect to the magnitude of crack closure effects [59,60], which further may lead to differences in long and short crack behavior [50].

The origin of the differences in behavior resulting from the contribution from crack closure arises from the fact that such closure effects predominate in the *wake* of the crack tip. Since short cracks by definition will possess a limited wake, it is to be expected that in general such cracks will be subjected to less closure. Thus, at the same *nominal* ΔK, short cracks may experience a larger *effective* ΔK compared to the equivalent long crack. As outlined in Section 3, this can arise from two sources. First, with respect to plasticity-induced closure, plastic deformation in the wake of the crack has to build up before it can be effective in reducing ΔK_{eff}. From analogous studies of the role of dilatant inelasticity (generated by phase transformations) on reducing the effective stress intensity at the crack tip in ceramics [65], it has been found that the full effect of this closure is only felt when the transformed zone extends a distance five times its forward extent in the wake of the crack. Although this analysis has not been performed for plastic deformation in metals, it is to be expected that the role of the compressive stresses in the plastic zone encompassing the wake of the crack would be limited for small cracks of a length comparable with the forward extent of this zone (i.e., for $a \sim r_y$). We believe that this is one of the major reasons (at least from the perspective of continuum mechanics) for non-propagating cracks and why short cracks and cracks emanating from notches can propagate below the long crack threshold ΔK_o. Essentially they can initiate and grow at nominal stress intensities below ΔK_o due to the absence of closure effects, but, as they increase in length, the build-up of plasticity in their wake promotes a

and physical contact between mating fracture surfaces in the *wake* of the crack tip, the crack can be effectively closed at positive loads during the fatigue cycle. Since the crack cannot propagate whilst it remains closed, the net effect of closure is to reduce the nominal stress intensity range (ΔK), computed as $K_{max} - K_{min}$ from applied loads and crack length measurements, to some lower effective value (ΔK_{eff}) actually experienced at the crack tip, i.e., $\Delta K_{eff} = K_{max} - K_{cl}$, where K_{cl} is the stress intensity at closure ($\geq K_{min}$) [53]. Closure can arise from a number of sources, such as the constraint of surrounding elastic material on the residual stretch in material elements previously plastically-strained at the tip (plasticity-induced closure) [53], the presence of corrosion debris within the crack (oxide-induced closure) [54-56], and the contact at discrete points between faceted or rough fracture surfaces where significant Mode II crack tip displacements are present (roughness-induced closure) [52,56-60]. These mechanisms of crack closure are schematically illustrated in Fig. 7 [59], and are particularly relevant to short crack behavior simply because their action predominates in the *wake* of the crack tip. Since for small cracks the extent of this wake is limited, it is to be expected that the effect of crack closure will be different for long and short cracks, and specifically that the short crack is likely to be subjected to a smaller influence of closure. Evidence for the extent of crack closure being a function of crack size has been reported by Morris et al. [51] for the growth of short flaws in titanium alloys. Here, by monitoring the surface crack opening displacement (at zero load) for crack sizes ranging from 50 to 500 μm (Fig. 8), these authors concluded that for cracks less than approximately 160 μm in length, the extent of crack closure, specifically roughness-induced, decreased with decreasing crack length. A further influence of roughness-induced closure was inferred in the work of McCarver and Ritchie [50] on the crystallographic growth of long and physically-short fatigue cracks in René 95 nickel-base superalloy. In this latter study, threshold ΔK_{TH} values for short cracks ($a \sim 0.01$-0.20 μm) at low mean stresses ($R = 0.1$) were found to be 60% smaller than for long cracks ($a \sim 25$ mm), yet at high mean stresses ($R = 0.7$) where closure effects are minimal, this difference was not apparent. Thus, at equivalent nominal ΔK levels, physically-short flaws may be expected to propagate faster (and show lower thresholds) than corresponding long flaws simply due to a smaller influence of closure producing larger effective stress intensity ranges at the crack tip. Specific mechanisms for this effect are discussed in more detail in the following section.

However, a second factor which may also produce accelerated growth rates for short cracks is associated with chemical and electrochemical effects and is relevant to the growth of physically-short flaws in differing environments [4,48,49,61]. Experiments by Gangloff [4,48] on high strength 4130 steels tested in NaCl solution revealed corrosion fatigue crack propagation rates of short cracks (0.1-0.8 mm) to be up to two orders of magnitude faster than corresponding rates of long cracks (25-60 mm) at the same ΔK level, although behavior in inert atmospheres was essentially similar (Fig. 9). A complete understanding of this phenomenon is as yet lacking but preliminary analysis indicated that the effect could be attributed to differences in the local crack tip environments in the long and short flaws, principally resulting from different electrochemically-active surface-to-volume ratios of the cracks and from the influence of crack length on the solution renewal rate in the crack tip region [48].

4. DISCUSSION

In this paper, an attempt has been made to draw from the literature the salient points relevant to the mechanics and physics of the growth of short fatigue cracks. From the preceding discussion it is apparent that such cracks may present difficulties in fatigue design simply because their growth rate behavior is somewhat unpredictable when based on current (long crack) analyses and methodologies (e.g., using long crack LEFM data). It is also apparent that the latter procedures are liable to yield non-conservative predictions of lifetimes in the presence of short flaws because, at the same nominal driving force, the short crack invariably propagates at a faster rate than the corresponding long crack. This problem of similitude between long and short crack behavior can be considered to arise for a number of reasons, such as i) local plasticity effects resulting in the inappropriate characterization of the crack driving force for short cracks, ii) local microstructural features which in general do not perturb macro-crack growth yet which are of a size that they can interact strongly with the growth of small cracks, iii) similitude of crack shape and geometry, iv) interaction with other micro-cracks, v) similitude of crack extension mechanism, vi) crack closure effects, and vii) differences in the local crack tip environments. We now examine each of these factors in turn.

Questions concerning the inappropriate use of linear elastic fracture mechanics to characterize the growth of short cracks in the presence of extensive plasticity have been largely resolved through the use of J, or CTOD-based, methodologies, as evidenced by the results of Dowling [40] in Fig. 4. It is now apparent that much earlier data indicating differences in long and short crack behavior can be traced to the fact that growth rates were compared at equivalent ΔK values, and that the use of this LEFM parameter did not provide an adequate characterization of the short crack tip fields where $a \sim r_y$. However, for the case of short cracks emanating from notches, where initial growth is occurring within the plastic zone of the notch (Fig. 5), a continuum mechanics description of behavior is less clear. Certainly there is experimental evidence that such short cracks can propagate below the long crack threshold at progressively decreasing growth rates (Fig. 6) and even arrest to form non-propagating cracks [31,32,45], but such behavior has been also shown in the absence of a notch and attributed alternatively to

contribution from crack closure, which progressively decreases the effective ΔK experienced at the crack tip resulting in a progressive reduction in crack growth rate and sometimes complete arrest. 1-9

An analogous situation can arise due to the contribution from roughness-induced crack closure promoted by rough, irregular fracture surfaces, particularly where the crack extension mechanism involves a strong single shear (Mode II + Mode I) component [50,59,60]. Since a crack of zero length can have no fracture surface and hence no roughness-induced closure, it is to be expected that the development of such closure will be a strong function of crack size [50-52], as demonstrated by the experimental data of Morris et al. [51] in Fig. 8. A lower bound estimate for the transition crack size below which roughness-induced closure will be ineffective (at near-threshold levels) can be appreciated from Fig. 11 [50]. The long crack, which encompasses several grains, will at near-threshold levels have developed a faceted morphology and, due to incompatibility between mating crack surfaces from the Mode II crack tip displacements, will be subjected to roughness-induced closure in the manner depicted in Fig. 7. The short crack, however, will be unable to develop such closure whilst its length remains less than a grain diameter since, although it is advancing via the same single shear mechanism, it will not have changed direction at a grain boundary and accordingly will not have formed a faceted morphology.

In general, since the majority of results showing differences in long and short crack growth rates have been observed at low stress intensity ranges, and since the fatigue crack propagation behavior of long cracks in this near-threshold regime is known to be strongly influenced by crack closure effects, it is our belief that the major reason for the faster growth of short cracks and the fact that they can propagate below the long crack threshold ΔK_0 is associated with a decreasing role of closure at decreasing crack sizes. In this regard it would be useful to compare short crack data with data for long cracks *at high load ratios*, since closure effects are minimal here even for long cracks. Where this has been done, i.e., for crystallographic near-threshold fatigue in nickel-base alloys [50], the threshold for short cracks, despite being 60% smaller than the long crack threshold at $R = 0.1$, was approximately equal to the long crack threshold at $R = 0.7$.

Finally, large differences in the behavior of long and short cracks can arise at stress intensities well outside the threshold regime due to environmental factors [4,48,49]. As shown in Fig. 8, the results of Gangloff [4,48] have demonstrated that the corrosion fatigue crack growth rates of physically-short cracks in 4130 steel tested in aqueous NaCl solution can be 1-2 orders of magnitude faster than the corresponding growth rates of long cracks at the same ΔK value. This unique environmentally-assisted behavior of short cracks was attributed to differing local crack tip environments as a function of crack size. Specifically, the local concentration of the embrittling species within the crack was reasoned to depend on the surface to volume ratio of the crack, on the diffusive and convective mass transport to the crack tip, and on the distribution and coverage of active sites for electrochemical reaction, all processes sensitive to crack depth, opening displacement and crack surface morphology [48]. Analogous, yet less spectacular, environmental crack size effects may also arise in gaseous environments, where for example the presence of hydrogen may induce an intergranular fracture mode. The rough nature of this failure mechanism would promote roughness-induced closure which again act to primarily influence the long crack behavior by reducing ΔK_{eff}.

These examples of the differences in behavior of fatigue cracks of varying size are a clear indication of where the fracture mechanics similitude concept can break down. The stress intensity, although adequately characterizing the mechanical driving force for crack extension, cannot account for the chemical activity of the crack tip environment, or the *local* interaction of the crack with microstructural features. Since these factors, together with the development of crack closure, are a strong function of crack size, it is actually unreasonable to expect identical crack growth behavior for long and short cracks. Thus, in the absence of the similitude relationship, the analysis and utilization of laboratory fatigue crack propagation data to predict the performance of in-service components, where short cracks are present, becomes an extremely complex task, a task which immediately demands a major effort in fatigue research from both academics and practical engineers alike.

5. CONCLUDING REMARKS

The problem of short cracks must now be recognized as one of the most important topics facing current researchers in fatigue. Not only is it a comparatively unexplored area academically, but it raises doubts in the universal application of fracture mechanics to the characterization of sub-critical flaw growth and accordingly has the potential, from the engineering viewpoint, for creating unreliable, non-conservative defect-tolerant lifetime predictions. In the current paper, we have attempted to provide an overview of the recent experimental studies on the growth of small fatigue cracks, and specifically to outline the mechanical, metallurgical and environmental reasons, as to why the behavior of such cracks should differ from the behavior of long cracks. Our intent was not to present a formal analysis of each of these factors, since in most cases such analysis simply does not exist, but rather to thoroughly review the many inter-disciplinary factors which may be relevant. We conclude that behavioral differences between the short and long flaw are to be expected, and such differences can arise from a number of distinct phenomena, namely: i) inadequate characterization of the crack tip stress and deformation fields of short cracks due to extensive local plasticity, ii) notch tip stress and

deformation field effects, iii) interaction of short cracks with microstructural features, e.g., grain boundaries, inclusions, second phases, etc., of dimensions comparable in size with the crack length, iv) differences in crack shape and geometry, v) differences in crack extension mechanisms, vi) differences in the contribution from crack closure mechanisms (specifically plasticity- and roughness-induced) with crack length, and finally vii) differences in the local crack tip environments. Each of these factors represents a formidable challenge in fatigue research, because of the complex nature of both experimental and theoretical studies, yet their importance is undeniable. We trust that the proceedings of this conference will provide a significant step in increasing our understanding of this important topic.

6. REFERENCES

1. M.E. Fine and R. O. Ritchie: "Fatigue-Crack Initiation and Near-Threshold Crack Growth," in Fatigue and Microstructure, Amer. Soc. Metals, Metals Park, OH, 1968, pp. 245-278.
2. S. J. Hudak: "Small Crack Behavior and the Prediction of Fatigue Life," J. Eng. Matls. Tech., Trans. ASME Ser. H, vol. 103, 1981, pp. 26-35.
3. J. Schijve: "Differences between the Growth of Small and Large Fatigue Cracks: The Relation to Threshold K-Values," in Fatigue Thresholds, eds. J. Bäcklund, A. Blom, and C. J. Beevers, EMAS Ltd., Warley, U.K., vol. 2, 1981, pp. 881-908.
4. R. P. Gangloff: "Electrical Potential Monitoring of the Formation and Growth of Small Fatigue Cracks in Embrittling Environments," in Advances in Crack Length Measurement, ed. C. J. Beevers, EMAS Ltd., Warley, U.K., 1982, in press.
5. M. L. Williams: "On the Stress Distribution at the Base of a Stationary Crack," J. Appl. Mech., vol. 24, 1957, pp. 109-117.
6. G. R. Irwin: "Fracture Mechanics," in Structural Mechanics, Proc. 1st. Symp. on Naval Structural Mechanics, eds. J. Goodier and N. Huff, Pergamon Press, New York, 1960.
7. J. R. Rice: "Mathematical Analysis in the Mechanics of Fracture," in Fracture: An Advanced Treatise, ed. H. Liebowitz, Academic Press, New York, vol. 2, 1968, pp. 191-311.
8. P. C. Paris and F. Erdogan: "A Critical Analysis of Crack Propagation Laws," J. Basic Eng., Trans. ASME Ser. D, vol. 85, 1963, pp. 528-534.
9. H. Tada, P. C. Paris, and G. R. Irwin: in The Stress Analysis of Cracks Handbook, Del Research Corp., Hellertown, PA, 1973.
10. N. E. Dowling: "Notched Member Fatigue Life Predictions Combining Crack Initiation and Propagation," Fat. Eng. Matls. Struct., vol. 2, 1979, pp. 129-138.
11. J. W. Hutchinson: "Singular Behavior at the End of a Tensile Crack in a Hardening Material," J. Mech. Phys. Solids, vol. 16, 1968, pp. 13-31.
12. J. R. Rice and G. R. Rosengren: "Plane Strain Deformation Near a Crack Tip in a Power Hardening Material," J. Mech. Phys. Solids, vol. 16, 1968, pp. 1-12.
13. J. R. Rice: "A Path Independent Integral and the Approximate Analysis of Strain Concentration by Notches and Cracks," J. Appl. Mech., vol. 35, 1968, pp. 379-385.
14. N. E. Dowling: "Geometry Effects and the J-Integral Approach to Elastic-Plastic Fatigue Crack Growth," in Cracks and Fracture, ASTM STP 601, Am. Soc. Test. Matls., 1976, pp. 19-32.
15. N. E. Dowling and J. A. Begley: "Fatigue Crack Growth During Gross Plasticity and the J-Integral," in Mechanics of Crack Growth, ASTM STP 590, Am. Soc. Test. Matls., 1976, pp. 82-103.
16. R. O. Ritchie: "Why Ductile Fracture Mechanics?," J. Eng. Matls. Tech., Trans. ASME Ser. H, vol. 104, 1982, in press.
17. C. F. Shih: "Relationships Between the J-Integral and Crack Opening Displacement for Stationary and Extending Cracks," J. Mech. Phys. Solids, vol. 29, 1981, pp. 305-330.
18. A. R. Jack and A. T. Price: "The Initiation of Fatigue Cracks from Notches in Mild Steel Plates," Acta Met., vol. 6, 1970, pp. 401-409.
19. Y. H. Kim, T. Mura, and M. E. Fine: "Fatigue Crack Initiation and Microcrack Growth in 4140 Steel," Met. Trans. A, vol. 9A, 1978, pp. 1679-1683.
20. C. Y. Kung and M. E. Fine: "Fatigue Crack Initiation and Microcrack Growth in 2024-T4 and 2124-T3 Aluminum Alloys," Met. Trans. A, vol. 10A, 1979, pp. 603-610.
21. S. Taira, K. Tanaka and M. Hoshina: "Grain Size Effect on Crack Nucleation and Growth in Long-Life Fatigue of Low Carbon Steel," in Fatigue Mechanisms, ASTM STP 675, Am. Soc. Test. Matls., 1979, pp. 135-173.
22. W. L. Morris: "The Noncontinuum Crack Tip Deformation Behavior of Surface Microcracks," Met. Trans. A, vol. 11A, 1980, pp. 1117-1123.
23. S. Pearson: "Initiation of Fatigue Cracks in Commercial Aluminum Alloys and the Subsequent Propagation of Very Short Cracks," Eng. Fract. Mech., vol. 7, 1975, pp. 235-247.

24. J. Lankford: "The Growth of Small Fatigue Cracks in 7075-T6 Aluminum," Fat. Eng. Matls. Struct., vol. 5, 1982, in press.

25. R. O. Ritchie: "Near-Threshold Fatigue Crack Propagation in Steels," Intl. Metals Rev., vol. 20, 1979, pp. 205-230.

26. W. L. Morris, M. R. James, and O. Buck: "Growth Rate Models for Short Surface Cracks in Al 2219-T851," Met. Trans. A, vol. 12A, 1981, pp. 57-64.

27. S. Taira, K. Tanaka, and Y. Nakai: "A Model of Crack Tip Slip Band Blocked by Grain Boundary," Mech. Res. Comm., vol. 5, 1978, pp. 375-381.

28. K. Tanaka, Y. Nakai, and M. Yamashita: "Fatigue Growth Threshold of Small Cracks," Intl. J. Fract., vol. 17, 1981, pp. 519-533.

29. H. Kitagawa and S. Takahashi: "Applicability of Fracture Mechanics to Very Small Cracks or the Cracks in the Early Stage," in Proc. 2nd Intl. Conf. on Mech. Beh. of Materials, 1979, pp. 627-631.

30. R. A. Smith: "On the Short Crack Limitations of Fracture Mechanics," Intl. J. Fract., vol. 13, 1977, pp. 717-719.

31. R. A. Smith and K. J. Miller: "Prediction of Fatigue Regimes in Notched Components," Intl. J. Mech. Sci., vol. 20, 1978, pp. 201-206.

32. M. M. Hammouda and K. J. Miller: "Elastic-Plastic Fracture Mechanics Analyses of Notches," in Elastic-Plastic Fracture, ASTM STP 668, Amer. Soc. Test. Matls., 1979, pp. 703-719.

33. M. H. El Haddad, K. N. Smith, and T. H. Topper: "Fatigue Crack Propagation of Short Cracks," J. Eng. Matls. Tech., Trans. ASME Ser. H, vol. 101, 1979, pp. 42-46.

34. M. H. El Haddad, T. H. Topper, and B. Mukherjee: "Review of New Developments in Crack Propagation Studies," J. Test. Eval., vol. 9, 1981, pp. 65-81.

35. M. H. El Haddad, N. E. Dowling, T. H. Topper, and K. N. Smith: "J-Integral Applications for Short Cracks at Notches," Intl. J. Fract., vol. 16, 1980, pp. 15-30.

36. S. Usami and S. Shida: "Elastic-Plastic Analysis of the Fatigue Limit for a Material with Small Flaws," Fat. Eng. Matls. Struct., vol. 1, 1979, pp. 471-481.

37. S. Usami: "Applications of Threshold Cyclic-Plastic-Zone-Size Criterion to Some Fatigue Limit Problems," in Fatigue Thresholds, eds. J. Bäcklund, A. Blom, and C. J. Beevers, EMAS Ltd., Warley, U.K., vol. 1, 1982, pp. 205-238.

38. R. O. Ritchie: "Discussion on Microstructural Aspects of the Threshold Condition for Nonpropagating Fatigue Cracks in Martensitic-Ferritic Structures," in Fatigue Mechanisms, ASTM STP 675, Amer. Soc. Test. Matls., 1979, pp. 364-366.

39. J. Lankford: "On the Small Crack Fracture Mechanics Problem," Intl. J. Fract., vol. 16, 1980, pp. R7-R9.

40. N. E. Dowling: Crack Growth During Low Cycle Fatigue of Smooth Axial Specimens," in Cyclic Stress-Strain and Plastic Deformation Aspects of Fatigue Crack Growth, ASTM STP 637, Amer. Soc. Test. Matls., 1977, pp. 97-121.

41. R. A. Smith and K. J. Miller: "Fatigue Cracks at Notches," Intl. J. Mech. Sci., vol. 19, 1977, pp. 11-22.

42. C. E. Phillips: "Discussion on Non-Propagating Fatigue Cracks in Low-Carbon Steel," in Proc. Colloquium on Fatigue, IUTAM Stockholm, 1955, Springer, Berlin, 1956, p. 210.

43. N. E. Frost and D. S. Dugdale: "Fatigue Tests on Notched Mild Steel Plates with Measurement of Fatigue Cracks," J. Mech. Phys. Solids, vol. 5, 1957, pp. 182-192.

44. P. Lukáš and M. Klesnil: "Fatigue Limit of Notched Bodies," Mater. Sci. Eng., vol. 34, 1978, pp. 61-66.

45. M. H. El Haddad, K. N. Smith, and T. H. Topper: "Prediction of Non-Propagating Cracks," Eng. Fract. Mech., vol. 11, 1979, pp. 573-584.

46. B. N. Leis and T. P. Forte: "Fatigue Growth of Initially Physically Short Cracks in Notched Aluminum and Steel Plates," in Fracture Mechanics, ASTM STP 743, Amer. Soc. Test. Matls., 1982, pp. 100-124.

47. N. E. Frost, K. J. Marsh, and L. P. Pook: in Metal Fatigue, Clarendon Press, Oxford, 1974.

48. R. P. Gangloff: "The Criticality of Crack Size in Aqueous Corrosion Fatigue," Res. Mech. Let., vol. 1, 1981, pp. 299-306.

49. B. F. Jones: "The Influence of Crack Depth on the Fatigue Crack Propagation Rate for a Marine Steel in Seawater," J. Matls. Sci., vol. 17, 1982, pp. 499-507.

50. J. F. McCarver and R. O. Ritchie: "Fatigue Crack Propagation Thresholds for Long and Short Cracks in René 95 Nickel-Base Superalloy," Mater. Sci. Eng., vol. 55, 1982, pp. 63-67.

51. W. L. Morris, M. R. James, and O. Buck: "A Simple Model of Stress Intensity Range Threshold and Crack Closure Stress," Eng. Fract. Mech., vol. 14, 1982, in press.

52. M. R. James and W. L. Morris: "Effect of Fracture Surface Roughness on Short Fatigue Crack Growth," Met. Trans. A, vol. 13A, 1982, in press.

53. W. Elber: "The Significance of Fatigue Crack Closure," in Damage Tolerance in Aircraft Structures, ASTM STP 486, Amer. Soc. Test. Matls., 1971, pp. 230-242.

54. R. O. Ritchie, S. Suresh, and C. M. Moss: "Near-Threshold Fatigue Crack Growth in 2¼Cr-1Mo Pressure Vessel Steel in Air and Hydrogen," J. Eng. Matls. Tech., Trans. ASME Ser. H, vol. 102, 1980, pp. 293-299.

55. A. T. Stewart: "The Influence of Environment and Stress Ratio on Fatigue Crack Growth at Near-Threshold Stress Intensities in Low-Alloy Steels," Eng. Fract. Mech., vol. 13, 1980, pp. 463-478.

56. S. Suresh, G. F. Zamiski, and R. O. Ritchie: "Oxide-Induced Crack Closure: An Explanation for Near-Threshold Corrosion Faitgue Crack Growth Behavior," Met. Trans. A, vol. 12A, 1981, pp. 1435-1443.

57. N. Walker and C. J. Beevers: "A Fatigue Crack Closure Mechanism in Titanium," Fat. Eng. Matl. Struct., vol. 1, 1979, pp. 135-148.

58. K. Minakawa and A. J. McEvily: "On Crack Closure in the Near-Threshold Regime," Scripta Met., vol. 15, 1981, pp. 633-636.

59. R. O. Ritchie and S. Suresh: "Some Considerations on Fatigue Crack Closure at Near-Threshold Stress Intensities Due to Fracture Surface Morphology," Met. Trans. A, vol. 13A, 1982, pp. 937-940.

60. S. Suresh and R. O. Ritchie: "A Geometric Model for Fatigue Crack Closure Induced by Fracture Surface Roughness," Met. Trans. A, vol. 13A, 1982, in press.

61. J. Lankford: "The Effect of Environment on the Growth of Small Fatigue Cracks," Fat. Eng. Matls. Struct., vol. 5, 1982, in press.

62. J. Schijve: "The Stress Intensity Factor of Small Cracks at Notches," Fat. Eng. Matls. Struct., vol. 5, 1982, pp. 77-90.

63. T. Kunio and K. Yamada: "Microstructural Aspects of the Threshold Condition for Non-Propagating Fatigue Cracks in Martensitic-Ferritic Structures," in Fatigue Mechanisms, ASTM STP 675, Amer. Soc. Test. Matls, 1979, pp. 342-370.

64. J. Schijve: "The Effect of an Irregular Crack Front on Fatigue Crack Growth," Eng. Fract. Mech., vol. 14, 1981, pp. 467-475.

65. R. M. McMeeking and A. G. Evans: "Mechanics of Transformation-Toughening in Brittle Materials," J. Amer. Cer. Soc., vol. 65, 1982, pp. 242-246.

7. ACKNOWLEDGEMENTS

The work was performed under Grant No. AFOSR-82-0181 from the Air Force Office of Scientific Research. The authors wish to thank Dr. Alan Rosenstein of AFOSR for his support and encouragement, and Kimberly A. Johnston and Madeleine M. Penton for their help in preparing the manuscript.

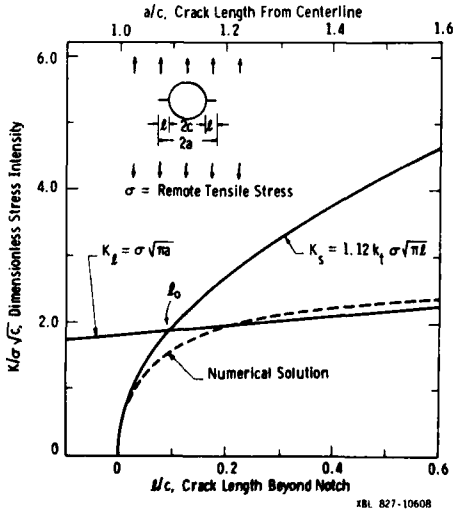

Fig. 1: Linear elastic K_I solutions for a crack, length ℓ, emanating from a circular notch, radius c, in an infinite plate subjected to a remotely applied uniaxial tensile stress σ. Short (K_s) and long (K_ℓ) crack limiting solutions and numerical solution are shown. After Dowling (1978).

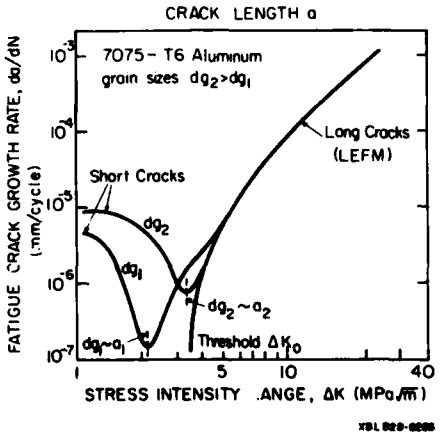

Fig. 2: Effect of grain size (d_g) on the growth of microstructurally-short fatigue cracks in 7075-T6 aluminum alloy (σ_o = 515 MPa). Micro-crack growth rate (da/dN) data, for two grain sizes ($d_{g_2} > d_{g_1}$), show growth rate minima approximately where crack length $a \sim d_g$, below the long crack threshold ΔK_o. After Lankford (1982).

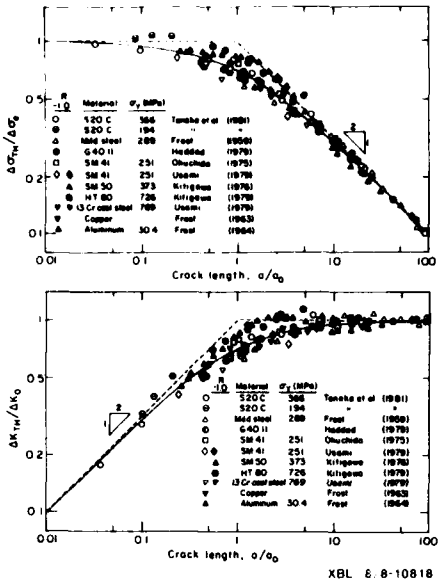

Fig. 3: Variation of threshold stress ($\Delta\sigma_{TH}$), normalized with respect to the smooth bar fatigue limit ($\Delta\sigma_e$), and threshold stress intensity (ΔK_{TH}), normalized with respect to the long crack threshold (ΔK_o), with crack length (a), normalized with respect to the intrinsic crack length ($a_o = 1/\pi[\Delta K_o/\Delta\sigma_e]^2$). After Tanaka et al (1981).

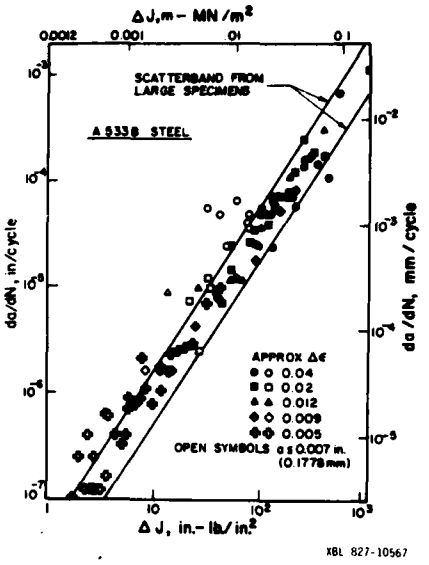

Fig. 4: Variation of fatigue crack growth rate (da/dN) for long ($a \gtrsim 25$ mm) and short ($a \lesssim 0.18$ mm) cracks in A533B steel (σ_o = 480 MPa) under plastic loading, where data are analyzed in terms of ΔJ. After Dowling (1977).

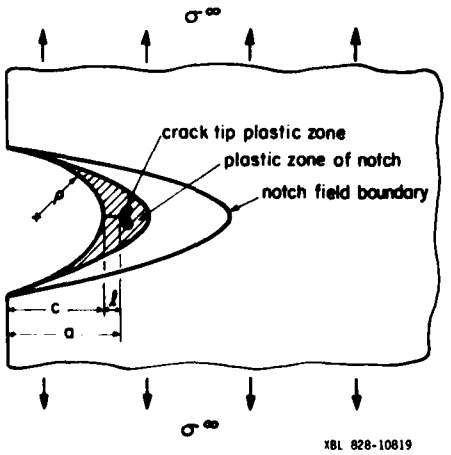

Fig. 5: Schematic illustration of crack tip notch plastic strain field associated with the growth of a short crack, length ℓ, emanating from a notch of depth c and root radius ρ. After Hammouda and Miller (1979).

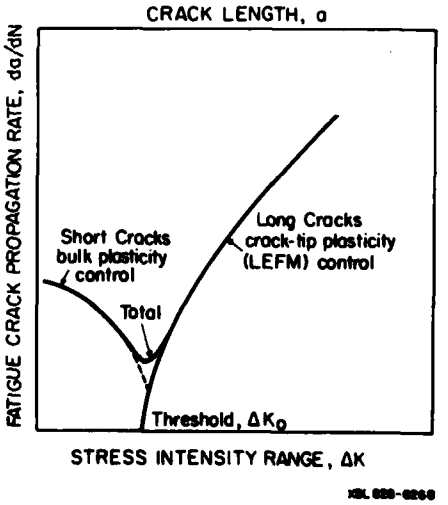

Fig. 6: Schematic illustration of the elastic-plastic and linear elastic characterization of the kinetics of crack growth for a short crack propagating from a notch (as shown in Fig. 5). After Hammouda and Miller (1979).

1-14

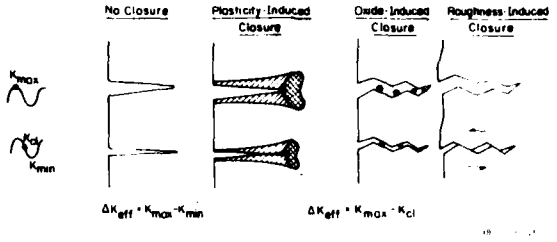

Fig. 7: Schematic illustration of the mechanisms of fatigue crack closure induced by plasticity effects, corrosion debris and rough fracture morphologies. ΔK_{eff} is the effective stress intensity range, defined as $K_{max} - K_{cl}$, where K_{cl} is the stress intensity to close the crack ($K_{cl} \geq K_{min}$). After Ritchie and Suresh (1982)

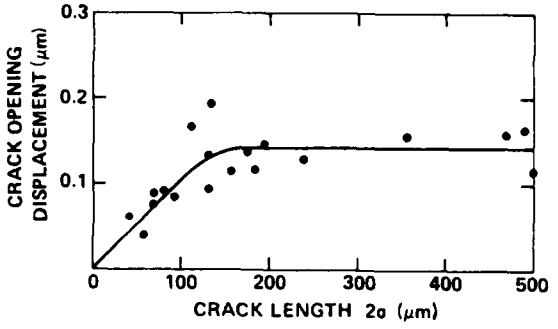

Fig. 8: Variation in crack mouth opening displacement (at zero load), with crack length a, of small surface cracks in 6Al-2Sn-4Zn-6Mo titanium alloy (σ_o = 1140 MPa), primary α grain size = 4 μm, β grain size = 12 μm), showing reduction in crack closure with decreasing crack size. After Morris et al. (1982).

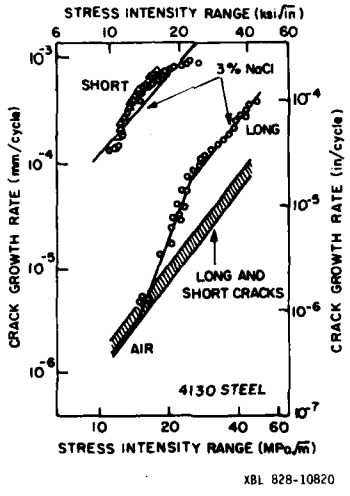

Fig. 9: Variation in fatigue crack growth rate (da/dN) as a function of ΔK for long (a ∿ 50 mm) and physically-short (a = 0.1-0.8 mm) cracks in 4130 steel (σ_o = 1300 MPa) tested in moist air and aqueous 3% NaCl solution. After Gangloff (1981).

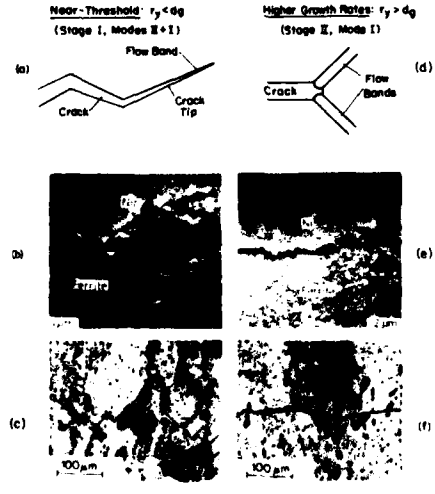

Fig. 10: Crack opening profiles and resulting long crack path morphologies for (a), (b), (c) near-threshold (Stage I) and (d), (e), (f) higher growth rate (Stage II) fatigue crack propagation. (b) and (e) are nickel-plated fracture sections in 1018 steel (after Minakawa and McEvily, 1981), and (c) and (f) are metallographic sections in 7075-T6 aluminum alloy (after Louwaard, 1977, quoted in ref. 3). After Suresh and Ritchie (1982).

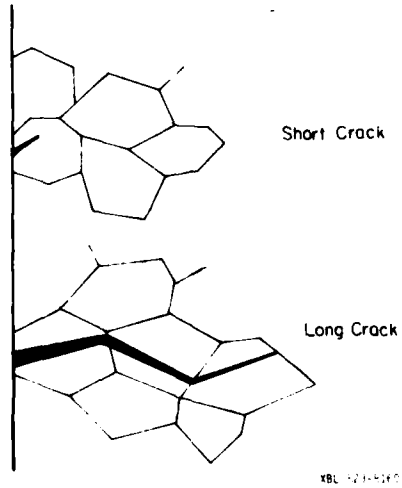

Fig. 11: Idealization of a microstructurally-short and a microstructurally-long crack propagating at near-threshold levels by single-shear Stage I mechanism. Note, with reference to Fig. 7, how roughness-induced crack closure will be promoted only in the long crack case. After Suresh and Ritchie (1982).

FATIGUE DAMAGE MECHANISMS AND SHORT CRACK GROWTH

by

I. Le May
Professor
Department of Mechanical Engineering
University of Saskatchewan
Saskatoon, Sask.
Canada S7N OWO

SUMMARY

The growth of short fatigue cracks, where the Paris law does not appear to hold, is discussed. In this regime the mechanisms of fatigue damage are of importance to an understanding of the role of microstructure in affecting growth rate. The paper reviews the operative mechanisms and their effect on short crack growth.

1. INTRODUCTION

Fatigue failures continue to occur in service components despite the vast increase in knowledge of fatigue mechanisms which has taken place during the past twenty years, in particular. Instead of attempting to design on the basis of a fatigue or endurance limit and seeking to keep stresses sufficiently low that fatigue failure can be considered unlikely, designers have developed the approach based on linear elastic fracture mechanics (LEFM), which considers that all structures contain defects and that the rate of growth of such defects, in the form of fatigue cracks, can be predicted from a knowledge of the stress spectrum applied and of the material constants C and m in the Paris Law [1],

$$da/dN = C(\Delta K)^m \qquad (1)$$

where a is crack length, N is number of load cycles, and ΔK is the range of stress intensity factor.

Subsequently, a number of deviations from this simplistic approach have become recognized. These include the following:

- Environmental effects can markedly alter crack growth rate and the conditions for crack initiation.
- Where there are high local stresses leading to local plasticity, LEFM approaches may break down and elastic-plastic fracture mechanics (EPFM) techniques of analysis may be required.
- A threshold condition in terms of ΔK is observed, below which a fatigue crack will not grow.
- Cracks may become non-propagating after growing for some time.
- Overloads may cause retardation of subsequent crack growth rate.
- Short cracks (less than, say, a few grain diameters in length, or a longer crack contained in a more extensive plastic zone) do not follow LEFM in their growth behaviour, but can grow much more quickly.
- Crack closure, leading to a reduction in the effective value of the range of stress intensity factor, causes crack growth predictions to vary from those obtained from Eq. (1).
- Microstructural effects, which are normally considered to be relatively unimportant in fatigue crack growth predictions, can become very significant when dealing with short cracks and threshold conditions.

In the context of aircraft structures, with the introduction of the concept of damage tolerant design [2] and consideration of the distribution of cracks in a structure, it has been shown that small cracks can affect the residual strength of a member [3, 4]. Thus it is of considerable importance to be able to estimate the growth rate of short cracks in predicting the safe life of aircraft structures.

The present paper attempts to outline and review aspects of the short fatigue crack problem with some emphasis on microstructural and mechanistic aspects.

2. THE FRACTURE MECHANICS APPROACH

It is appropriate to review briefly the fracture mechanics approach to fatigue crack propagation because of its widespread use, and to illustrate its limitations.

2-2

The Paris law given in Eq. (1) represents the linear portion only of the log (da/dN) versus log (ΔK) plot shown in Fig. 1. At low values of ΔK there is a threshold, ΔK_{th}, approaching which cracks propagate more slowly than might be predicted from the Paris law, while reaching final fracture the growth rate accelerates as the maximum value of stress intensity factor $K_{max} \rightarrow K_c$. However, it has been observed that at short crack lengths, cracks can grow at values of $\Delta K < \Delta K_{th}$, and, with increase in its length, the crack may either become non-propagating or subsequently grow according to the conventional growth curve. This is illustrated in the schematic plot of Fig. 2. Our discussion will be concerned primarily with the regime of the crack growth curve at and below the long crack threshold condition.

The work of Elber [5, 6] and others [7, 8, 9] has shown that crack closure commonly occurs, particularly in plane stress conditions, so that the Paris law has to be modified to the form

$$da/dN = C' (\Delta K_{eff})^m \tag{2}$$

where C' is a material constant and $K_{eff} = K_{max} - K_{op}$, K_{op} being the stress intensity factor when the crack starts to open. Alternatively, we may write

$$da/dN = C'(U\Delta K)^m \tag{3}$$

where the effective stress range factor U, is defined in terms of the maximum, minimum and crack opening stress as $(\sigma_{max} - \sigma_{op})/(\sigma_{max} - \sigma_{min})$. U depends on the stress ratio R ($= \sigma_{min}/\sigma_{max}$), the ratio of applied stress to yield stress, and the cyclic strain hardening exponent, n [10, 11]. In the near threshold regime, the effect of crack closure may be greater and ΔK_{eff} can depend on R to a considerable extent [12]. At higher values of R, where closure does not occur to a significant degree, if at all, ΔK_{th} is expected to become independent of R.

At the threshold condition for "long" fatigue cracks, a crack either stops growing or will just start to grow, and

$$\Delta K_{th} = \Delta\sigma\sqrt{\alpha\pi a} \tag{4}$$

α being a geometrical factor. For a surface crack,

$$\Delta K_{th} = 1.12\ \Delta\sigma\sqrt{\pi a} \tag{5}$$

Thus, to avoid fatigue crack growth, and neglecting the effect of closure which can be accommodated as already outlined, we have the condition that, for a surface crack,

$$\Delta K = 1.12\ \Delta\sigma\sqrt{\pi a} \leq \Delta K_{th} \tag{6}$$

Crack initiation can be considered in terms of the local stress range being above that at the fatigue limit; or, for no initiation, the applied stress range

$$\Delta\sigma \leq \Delta\sigma_o/k_t \tag{7}$$

$\Delta\sigma_o$ being the fatigue limit and k_t being the local elastic stress concentration factor. However, it has been shown that a better correlation exists for notched specimens using the relation [13]

$$\Delta\sigma \leq \Delta\sigma_o/k_f \tag{8}$$

where k_f, the fatigue strength reduction factor, is given by

$$k_f = [1 + 7.69(c/\rho)^{1/2}]^{1/2} \tag{9}$$

in which c and ρ define the notch geometry, as shown in Fig. 3.

It may be seen that while Eq. (8) apparently predicts crack initiation at a notch or surface discontinuity, the propagation of a very small crack will not be expected to occur, based on a fracture mechanics approach, as $\Delta K \rightarrow 0$ as $a \rightarrow 0$ and ΔK will be $<<\Delta K_{th}$. To overcome this problem various corrections have been suggested, one of the simplest and most satisfactory being that of Smith and Miller [14], who pointed out that a crack's growth from a notch will be controlled by the notch-generated plasticity rather than crack tip plasticity, until the crack moves out of the plastic zone. This is illustrated in Figs. 3 and 4.

The minimum stress range required for crack growth from a surface crack at a notch can be written as

$$\Delta\sigma = 0.5\ \Delta K_{th} c^{-1/2} \tag{10}$$

since

$$\Delta K = \Delta\sigma\ 1.12[\pi(c + \ell)]^{1/2} = \Delta K_{th} \tag{11}$$

and $\ell << c$.

When notched and unnotched specimens are considered, the crack growth rates become identical at crack lengths of ℓ and L, respectively, under the same applied stress range, $\Delta\sigma$. Considering the notched specimen to have an equivalent crack length $L = \ell + e$, and equating ΔK in both cases (da/dN being identical), the notch contribution, e, within the notch stress field (for $\ell < 0.13(c/\rho)^{1/2}$) was determined as [14]

$$e = 7.69\ell(c/\rho)^{1/2} \tag{12}$$

and the stress intensity factor range for the equivalent crack is

$$\Delta K = [1 + 7.69\ (c/\rho)^{1/2}]^{1/2}\Delta\sigma(\pi\ell)^{1/2} \tag{13}$$

Thus, we have the conditions for propagating or non-propagating cracks and for crack initiation, as illustrated in Fig. 5.

We may also consider the condition where LEFM breaks down when the crack tip plastic zone size, r_p, is greater than the crack length. In such a case the crack growth rate will again be greater than expected from LEFM predictions using the Paris law, and EPFM procedures will apply.

3. SHORT CRACK GROWTH

Based on Eqs. (7) or (8) and (5) or (10), the limiting stress range for fatigue can be plotted as a function of crack length as shown in Fig. 6. The sloping line has a slope of -1/2 on the log/log scale, since $K \propto (a)^{1/2}$. The point of intersection of the two straight lines has been defined as being at a crack length ℓ_o [16], and this may be considered as the minimum crack size for propagation at the endurance limit. At any stress range greater than $\Delta\sigma_o$, and in the absence of any defects, a crack of length ℓ_o could be expected to form rapidly [17]. Experimental data indicate that deviations from this idealized situation occur in practice, the data of Kitagawa and Takahashi [15] being shown in Fig. 6. It may be seen that deviations from the straight lines commence at ℓ_1 and ℓ_2, and it has been found that, for cracks of length $\ell(\ell_1 < \ell < \ell_2)$, the growth rate is faster than expected from the Paris law, and the value of ΔK_{th} will be less than that obtained from long crack data.

The value of ℓ_o is easily defined without requiring experimental verification other than $\Delta\sigma_o$ and da/dN versus ΔK data. However, experimental data are required to define both ℓ_1 and ℓ_2. Little data exist for ℓ_1, the length below which cracks have no effect on fatigue strength, although there is a definite correlation between both ℓ_o and ℓ_2 and a characteristic measurement of microstructural size. This measurement is typically the grain size, or the lath spacing or lath packet size in quenched and tempered sheets, and ℓ_2 is typically of the order of several microstructural units [17, 18]. Thus, it may be suggested that ℓ_1 is probably of the order of one microstructural unit, on the basis that a crack within a grain, for example, will grow rapidly until it reaches the grain boundaries where it may be impeded.

Figure 7 shows schematically the form of the dependence of $\Delta\sigma_o$ and ΔK_{th} on grain size. As grain size is increased the fatigue limit falls and the threshold value increases. Hence, to define initiation and early growth effects more precisely, large grained specimens are to be preferred.

In the case where a short crack is driven forward by notch plasticity as illustrated in Figs. 3 and 4, for example from a hole in a lug or at a fastener hole in a structural member, microstructural effects will be of relatively little significance. Here, the crack growth rate depends on the geometry of the notch and the short crack, and on the extent of the notch plastic zone. The growth rate can be predicted using the procedures outlined by Hammouda et al. [19], for example. In this, the crack tip plastic shear displacement ϕ_t is considered as arising from the notch plasticity ϕ_p and from the plastic deformation directly generated at the crack tip, ϕ_e. Thus,

$$\phi_t = \phi_p + \phi_e \tag{14}$$

The displacement ϕ_e can be evaluated from LEFM as

$$\phi_e = (\Delta K)^2/(\sqrt{2}\ E\ \Delta\sigma_{cy}) \tag{15}$$

where $\Delta\sigma_{cy}$ is the cyclic yield stress range. ΔK can be calculated from the data of Smith and Miller [13] or Newman [20], while ϕ_t can be determined by considering a crack of length L propagating in elastically stressed bulk material at the same rate as a crack of length ℓ in the plastic zone of a notched component: ϕ_p can be determined from Eq. (14). At the point of crack initiation at the notch root $\phi_p = 0$, and at the crack exits from the notch plastic zone $\phi_p = 0$. An elastic-plastic finite element analysis and computational study has shown that the growth rate of such short cracks can be modelled successfully from initiation to their outgrowth from the notch plastic field [19].

4. MICROSTRUCTURAL AND MECHANISTIC ASPECTS

2·4 Many of the observations reported regarding the rapid growth of small cracks (in the absence of notch-plasticity), threshold conditions and the effect of R on ΔK_{th} may be rationalized when mechanistic aspects of fatigue crack growth are considered.

It is now well established that fatigue damage initiates along slip bands in surface grains, although specific exceptions occur in, for example, titanium where sub-surface crack initiation can take place [21], or with crack initiation at inclusions. A crack then forms at the side of a persistent slip band (PSB) which has developed, and grows initially in Stage I, using the nomenclature of Forsyth [22]. Such a microcrack will be contained within a simple grain and will generally be accompanied by the formation of other cracks in adjacent grains, all growing along planes most favourably oriented for slip.

The microcracks will link up to produce a crack front which is irregular and of varying orientation along its length [23]. To allow further growth with the crack front moving forward in a consistent manner as it penetrates more deeply into the material, additional slip systems must come into play, and the crack front turns to allow continued growth in Stage II, approximately at right angles to the tensile stress in an uniaxially loaded situation. Continued growth depends on the extent of crack tip plasticity and the crack tip opening in each load cycle.

Thus, in a small surface crack the early stages of growth are not greatly restrained by grain boundary or other obstacles. Only when the crack fronts of several microcracks link up and the crack is forced to turn, with several slip systems operating and the crack front moving in a coherent manner, will the growth rate slow down significantly under the influence of the microstructural obstacles present. If the crack tip plasticity is insufficient and $\Delta K < \Delta K_{th}$ the crack will stop: if $\Delta K > \Delta K_{th}$ the growth rate will accelerate until the Paris law of Eq. (1) is followed.

In the threshold regime, and considering a long crack, the growth per cycle is small and the average growth rate may be less than one lattice spacing/cycle. There is a tendency for continued slip band cracking to occur at the crack tip, together with crack branching, as illustrated in Fig. 8 [23]. The threshold fatigue regime fracture surface presents much less clearly defined striations than under faster conditions of crack growth, and in some instances no evidence of striations may be found, even although these do develop at higher values of ΔK.

The phenomena of crack branching, slip band cracking and an irregular crack front all contribute to an actual K value below that which might be expected based on crack length and applied stress. This contributes to the production of a reduced growth rate in the threshold region below that expected from simple fracture mechanics observations.

Clearly, microstructural features will have a significant influence on the fracture surface appearance, and the threshold regime crack growth rate can be affected significantly by the microstructural units which characterize the material, e.g., the grain size, inclusion or precipitate size, or lath packet size. Also, such cracks have a tendency to propagate in Mode II, shear steps showing on the fracture surface, together with a serrated crack path. Figure 9 illustrates overall Mode I growth, normal to the tensile stress axis, but involving localized Mode II shearing [24].

The effect of the stress ratio, R, on fatigue thresholds and the extent of crack closure, which is itself related closely to R, are not clear. The work of Minakawa and McEvily [24] indicated high levels of crack closure, as may be seen in Fig. 9 because of the relative displacement of A and A', and consequently a large dependence of short crack growth rate upon R. However, other workers have indicated that little, if any, closure occurs in short surface cracks, leading to a growth rate largely independent of R [17, 23]. This effect may be considered to be dependent on microstructure: if the grain size is small, the magnitude of surface asperities will be small. In addition, because of the residual plasticity produced in the wave of a large crack, a larger degree of crack closure may be expected than would be the case for a small edge crack [23].

Microstructure affects crack growth rate where the Paris law holds true, to the extent that it controls the yield stress and the size of the crack tip plastic zone. In the short crack regime for unnotched specimens the crack growth rate is very dependent upon microstructure as previously noted, and Fig. 10 illustrates this [17]. This observation led Taylor and Knott [17] to suggest that, for design purposes, it should be assumed that cracks of length ℓ_2 are already present. However, there is no obvious way to quantify the number of such cracks which might be present in a structure and they could not be taken into account in estimating the size distribution of a population of cracks in the structure.

5. CLOSING REMARKS

It is hoped that the foregoing review has illustrated the fact that the growth of short cracks in fatigue can be affected greatly by microstructural conditions. A

more complete understanding of the problem requires extensive data collection and analysis, and the effects of R on crack growth rate and on ΔK_{th} can only be determined by careful study of a wide range of material having a variety of microstructural conditions. Such studies must include metallographic and fractographic observations. 2-5

Consideration of environmental effects has been excluded here; however, such effects do need further study as they modify the mechanisms and rate of growth of short cracks.

Finally, it is hoped that short crack growth where microstructural effects are important has been separated from the situation where notch plasticity causes growth.

6. REFERENCES

[1] Paris, P.C., and Erdogan, F., "A Critical Analysis of Crack Propagation Laws", J. Basic Engng, Vol. 85, 1963, pp. 528-534.

[2] Analysis of USAF Aircraft Durability and Damage Tolerance - AIAA Lecture and Workshop Program, April, 1978.

[3] Wood, H.A., Rudd, J.D., and Potter, J.M., "Evaluation of Small Cracks in Airframe Structures", AGARD SMP Meeting, Cesme, Turkey, April, 1981.

[4] Circle, R.L., and Wood, H.A., "Fail Safety Limitation for Multiple Load Path Aircraft Structure Resulting from Service Fatigue Cracking", ICAF, The Netherlands, May, 1981.

[5] Elber, W., "Fatigue Crack Closure Under Cyclic Tension", Engng Fracture Mechanics, Vol. 2, 1970, pp. 37-45.

[6] Elber, W., "The Significance of Fatigue Crack Closure", in Damage Tolerance in Aircraft Structures, STP 486, ASTM, 1971, pp. 230-242.

[7] Cheng, Y.F., and Brunner, H., "Photoelastic Research in Progress on Fatigue Crack Closure", Int. J. Fracture Mechanics, Vol. 6, 1970, pp. 431-434.

[8] Lindley, T.C., and Richards, C.E., "The Relevance of Crack Closure to Fatigue Crack Propagation", Materials Sci. and Engng, Vol. 14, 1974, pp. 281-293.

[9] Shaw, W.J.D., and Le May, I., "Crack Closure During Fatigue Crack Propagation", in Fracture Mechanics, STP 677, ASTM, 1979, pp. 233-246.

[10] Lal, K.M., Garg, S.B.L., and Le May, I., "On the Effective Stress Range Factor in Fatigue", J. Eng. Mater. and Technology, Vol. 102, 1980, pp. 147-152.

[11] Lal, K.M., and Le May, I., "An Assessment of Crack Closure in Fatigue Using the Westergaard Stress Function", Fatigue of Engng Mater. and Structures, Vol. 3, 1982, pp. 99-111.

[12] Kirby, B.R., and Beevers, C.J., "Slow Fatigue Crack Growth and Threshold Behaviour in Air and Vacuum of Commercial Aluminum Alloys", Fatigue of Engng Mater. and Structures, Vol. 1, 1979, pp. 203-215.

[13] Smith, R.A., and Miller, K.J., "Prediction of Fatigue Regimes in Notched Components", Int. J. Mech. Sci., Vol. 20, 1978, pp. 201-206.

[14] Smith, R.A., and Miller, K.J., "Fatigue Cracks at Notches", Int. J. Mech. Sci., Vol. 19, 1977, pp. 11-22.

[15] Kitawaga, H., and Takahashi, S., "Applicability of Fracture Mechanics to Very Small Cracks or the Cracks in the Early Stage", in Proc. 2nd Int. Conf. on Mech. Behavior of Materials (ICM-II), Boston, 1976, pp. 627-631.

[16] El Haddad, M.H., Dowling, N.F., Topper, T.H., and Smith, K.N., "J-Integral Applications for Short Fatigue Cracks at Notches", Int. J. Fracture, Vol. 16, 1980, pp. 15-30.

[17] Taylor, D., and Knott, J.F., "Fatigue and Propagation Behaviour of Short Cracks; The Effect of Microstructure", Fatigue of Engng Mater. and Structures, Vol. 4, 1981, pp. 147-155.

[18] Ritchie, R.O., "Near-Threshold Fatigue-Crack Propagation in Steels", Int. Metals Rev., Vol. 24, 1979, pp. 205-230.

[19] Hammouda, M.M., Smith, R.A., and Miller, K.J., "Elastic-Plastic Fracture Mechanics for Initiation and Propagation of Notch Fatigue Cracks", Fatigue of Engng Mater. and Structures, Vol. 2, 1979, pp. 139-154.

[20] Newman, J.C., "An Improved Method of Collocation for the Stress Analysis of Cracked Plates with Various Shaped Boundaries", NASA TND-7376, 1971.

[21] Ruppen, J., Bhowal, P., Eylon, D., and McEvily, A.J., "On the Process of Subsurface Fatigue Crack Initiation in Ti-6Al-4V", in Fatigue Mechanisms, J.T. Fong, Editor, STP 675, ASTM, 1979, pp. 47-65.

[22] Forsyth, P.J.E., "A Two Stage Process of Fatigue Crack Growth", in Proceedings, Crack Propagation Symposium, The College of Aeronautics, Cranfield, U.K., 1961, pp. 76-94.

[23] Schijve, J., "Differences Between the Growth of Small and Large Fatigue Cracks in Relation to Threshold K Values", in Fatigue Thresholds: Fundamentals and Engineering Applications, J. Bäcklund, A.F. Blom and C.J. Beevers, Editors, EMAS, U.K., 1982, pp. 881-908.

[24] Minakawa, K., and McEvily, A.J., "On Near-Threshold Fatigue Crack Growth in Steels and Aluminum Alloys", in Fatigue Thresholds: Fundamentals and Engineering Applications, J. Bäcklund, A.F. Blom and C.J. Beevers, Editors, EMAS, U.K., 1982, pp. 373-390.

7. ACKNOWLEDGEMENTS

The author is grateful for support of his studies on fatigue on the Natural Sciences and Engineering Research Council of Canada.

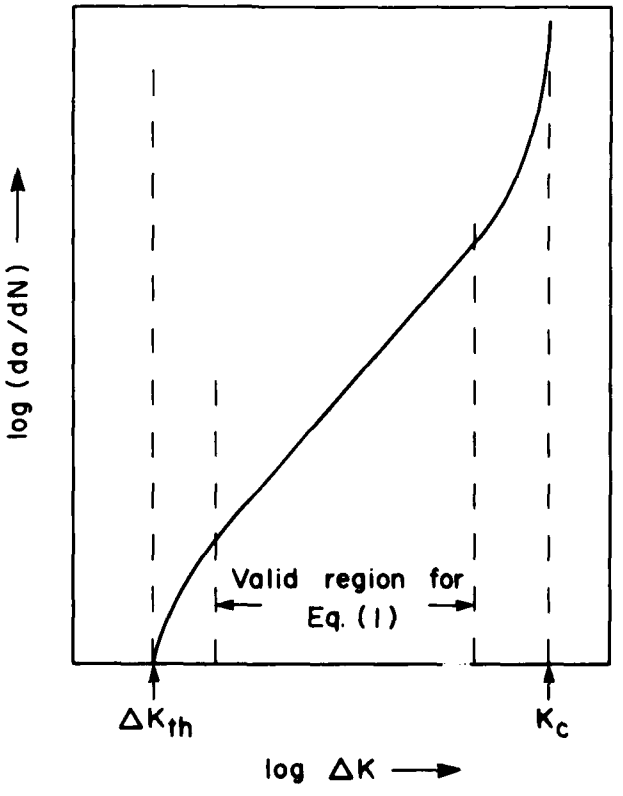

Fig. 1. Fatigue crack growth plot illustrating the region of validity for the Paris law.

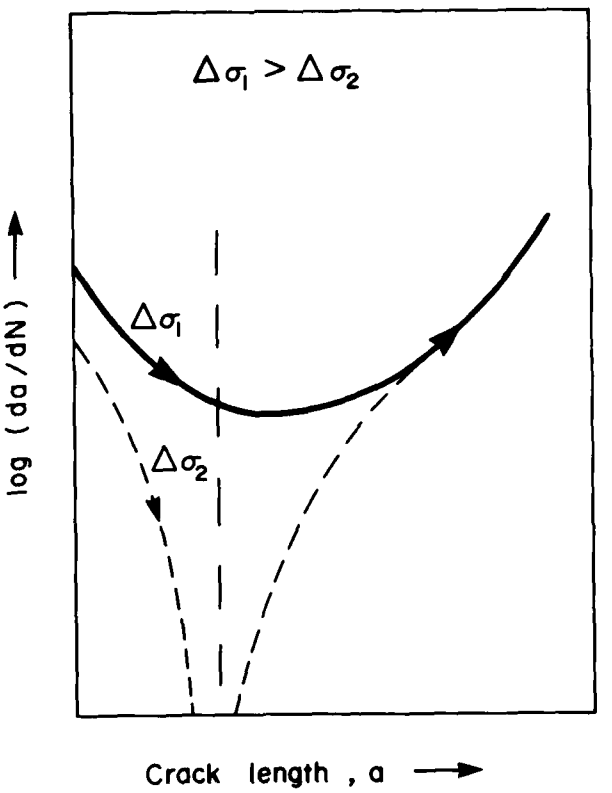

Fig. 2. Schematic plot showing the growth rate of a short fatigue crack. For $\Delta\sigma_1$ the crack continues to grow as a long crack after initial deceleration. In the case of $\Delta\sigma_2$ the crack becomes non-propagating as ΔK never reaches ΔK_{th}.

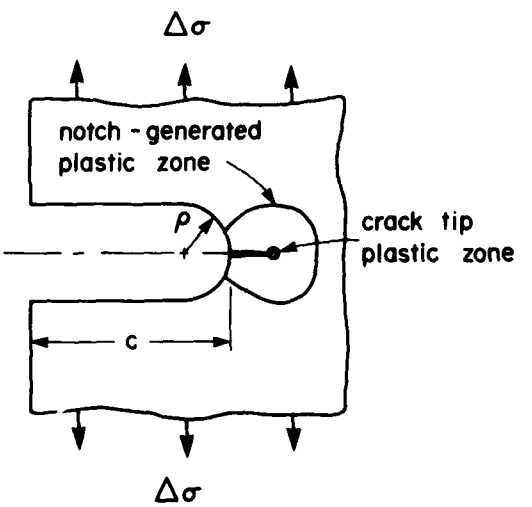

Fig. 3. A short fatigue crack growing from a notch with its growth controlled by the notch-generated plasticity.

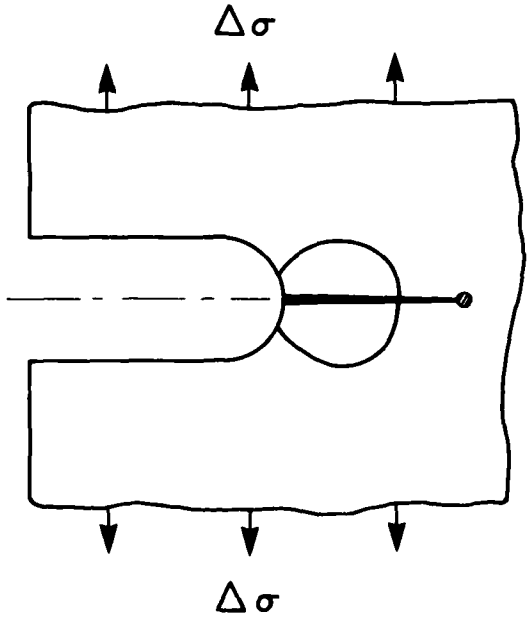

Fig. 4. The fatigue crack growing from the notch has moved out of the notch-generated plastic zone and is now driven forward by crack tip plasticity.

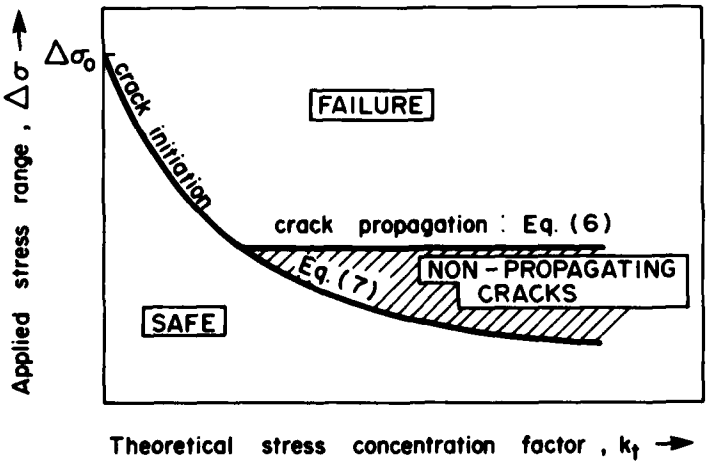

Fig. 5. The conditions for crack initiation and crack propagation in a notched component.

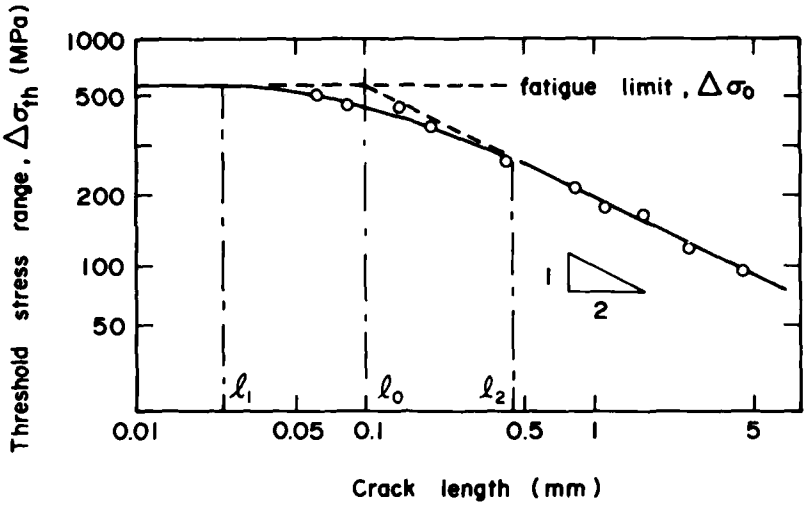

Fig. 6. The threshold stress range for fatigue failure as a function of crack length with experimental data from Ref. [15].

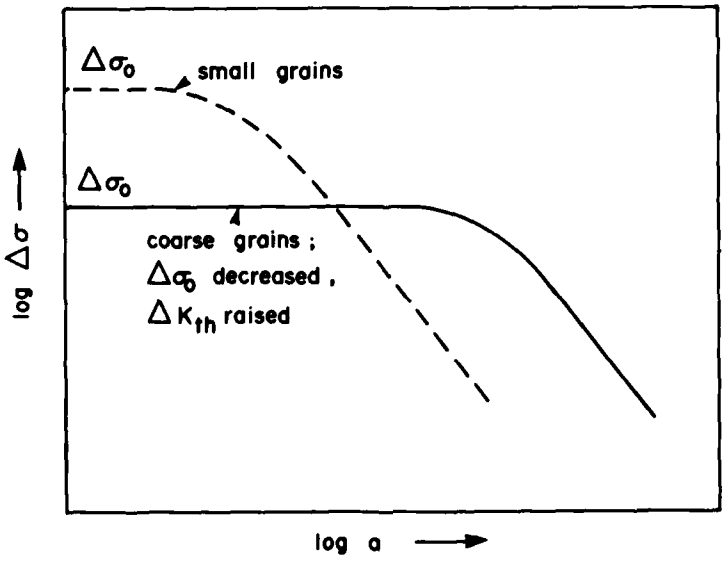

Fig. 7. Schematic showing the dependence of fatigue limit and threshold stress intensity factor range on grain size.

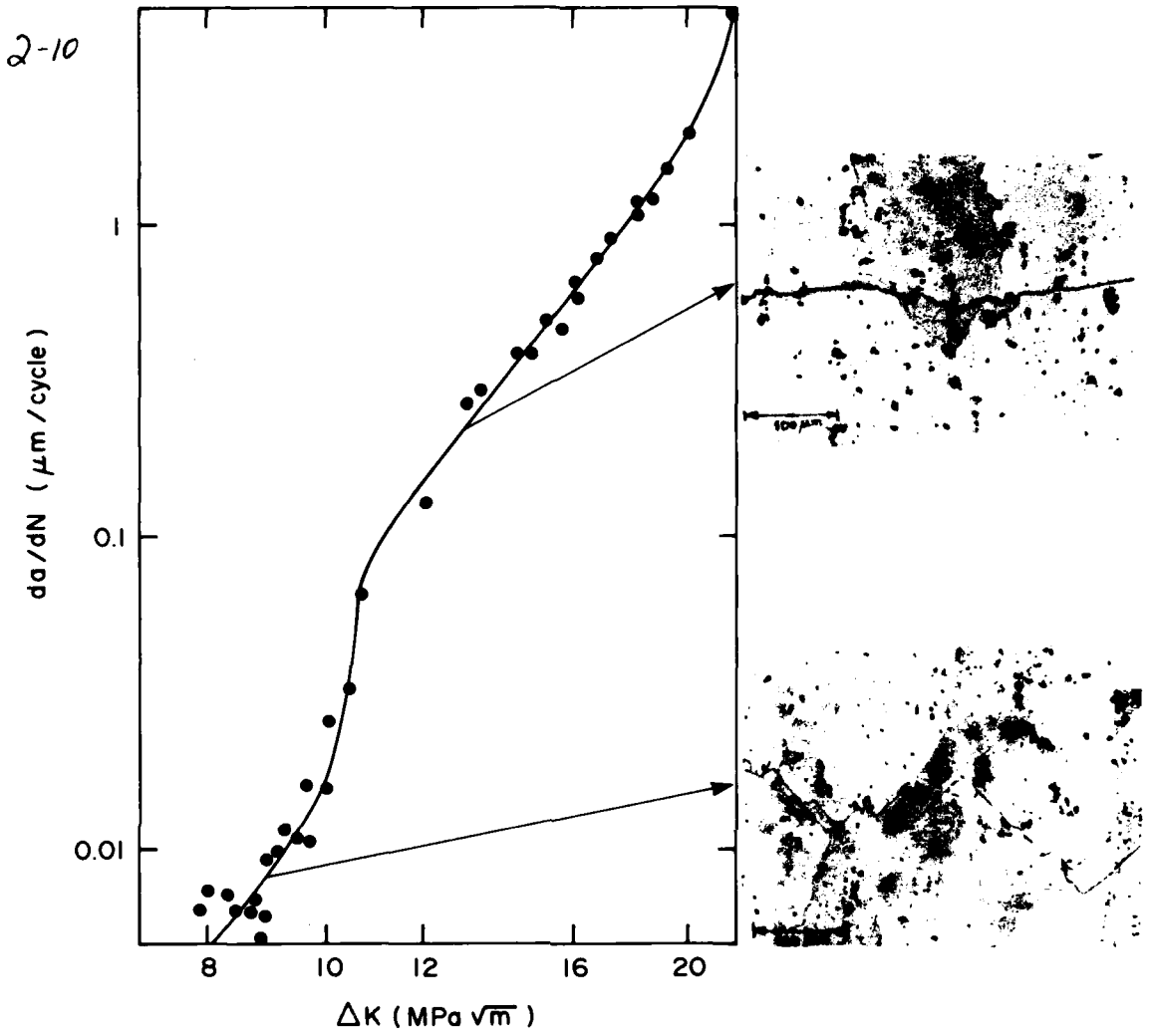

Fig. 8. Different crack growth mechanisms at low and high ΔK in coarse grained 7075-T6 aluminum tested at -100°C in vacuum. After Schijve [23].

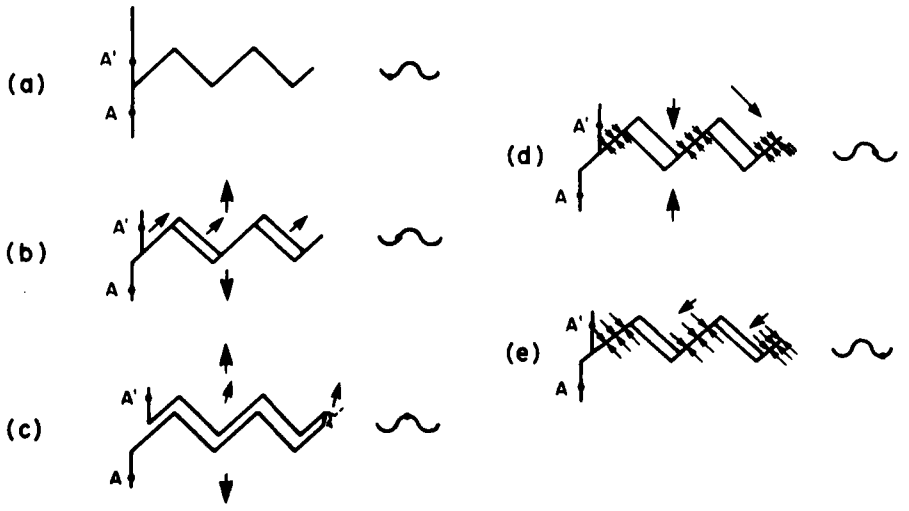

Fig. 9. Schematic illustration of combined Mode I and Mode II crack growth. After Minakawa and McEvily [24].

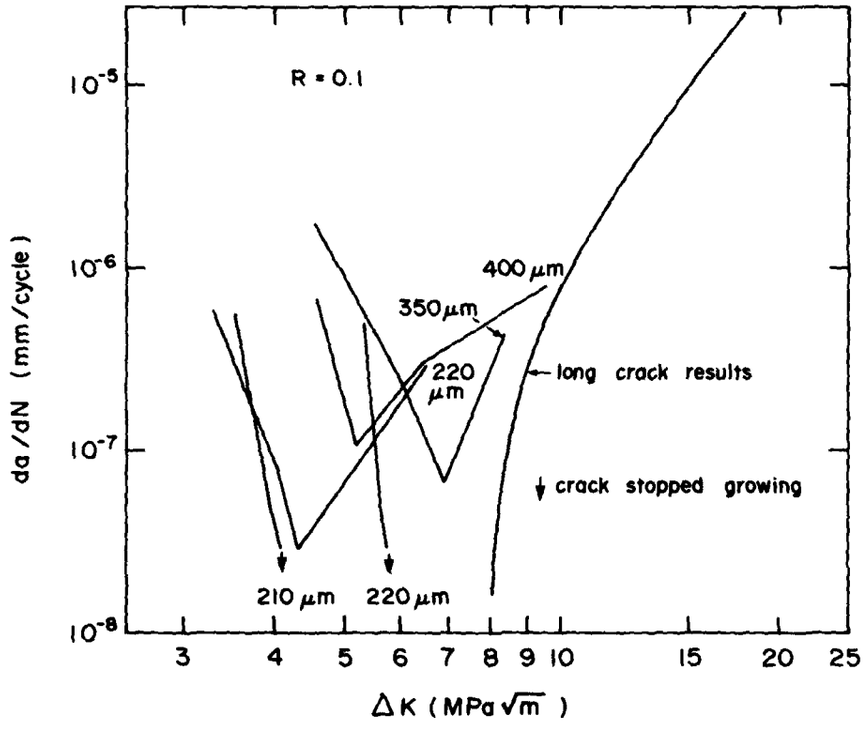

Fig. 10. Five different constant load range tests on short cracks in an aluminum bronze, the final crack length being shown for each. After Taylor and Knott [17].

AN ASSESSMENT OF THE IMPORTANCE OF SMALL CRACK GROWTH TO AIRCRAFT DESIGN

by

R F W ANSTEE

(Formerly Fatigue Research, RAE Farnborough
now
(Future Systems, Fixed Wing)
(in Directorate of Future Systems, MOD/PE)

A paper prepared for discussion at the
AGARD Conference on Small Crack Growth
- September 1982

1 INTRODUCTION

At any conference of this kind, based upon a new and potentially exciting research topic, the proceedings are inevitably dominated by research workers. This is rightly so, since the prime purpose of the meeting should be exchange of information and ideas, and generation of fresh avenues of investigation. There remains however the requirement to justify the cost of research and in this respect there are official views that the bulk of research should be aimed at a design objective, although perhaps 5-10% of research expenditure can be speculative.[1,2]

The purpose of this paper is to examine the application of small crack propagation data to the design of aircraft structures. No deliberate attempt is made to cover peculiarities of engine construction. It is intended to generate a questioning attitude within the audience to exactly how small crack data will be applied and to what benefit. It is not the intention to provide the answers! Indeed the questions asked may not be thought by some of you to be those most in need of answers. So be it. Any debate which results can only be healthy for research and design.

2 BEHAVIOUR OF SMALL CRACKS

Recent research has suggested that small cracks grow in size at a faster rate than predicted from linear elastic fracture mechanics (LEFM). However there is not universal agreement that such fast growth does occur. Some careful experimental studies have failed to show faster crack growth than would be calculated from LEFM. Naturally small cracks propagate in a regime where three dimensions are significant and at surfaces where residual stress effects may be important. Accurate stress intensity factor (SIF) solutions for three dimensional cracks are few and apply to idealised smooth crack fronts, a condition which very rarely applies for small cracks. In fact few experimental investigations are based upon a claim of an exact SIF solution, and yet it is recognised that crack growth rate is characterised as a high power function of SIF, particularly near threshold growth conditions where small crack investigations are perforce made.

Because small cracks are surface cracks the local surface stresses are important. Specimens where surface stresses were known to exist have been investigated and have been shown to correspond in a qualitative sense with what would be expected of LEFM behaviour, that is faster crack growth occurs when tensile stresses are known to be present. A closer correspondence between experiment and prediction is prohibited by a lack of detailed knowledge of the surface stresses. Edwards [3] has measured crack growth rate in fretting conditions and has shown that by accounting for the measured fretting stresses some agreement with LEFM prediction can be obtained. However even here growth rate was consistently underestimated, but by a degree which could be explained either by lack of a really accurate SIF solution or by materials crack growth data which was extrapolated down to the rates of interest. More recently he has shown [4] in tests on corner cracks propagated in bending that fast growth at short crack length is more likely to be observed under random amplitude load conditions than under constant amplitude, an observation which could be related to residual stress effects.

Most evidence of fast crack growth rate at short crack conditions has been obtained using specimens with established cracks which have been "shortened" by machining the specimen surface. In the present authors opinion this is an extremely dubious way to produce short cracks. Specimens which are left "as machined" will in all probability have unrepresentative stresses on the specimen surface. Alternatively stress relieving may affect the residual stresses at the crack tip such that the remaining condition is not that which would be experienced by a true short crack.

The volume of stretched material at the crack tip will be different between short and long cracks and it is not at all clear what effects stress relieving will have. There is also evidence that crack morphology is different between long and short cracks and what effect this has on growth rate is open to speculation. Finally machining of a specimen surface will almost inevitably alter the crack front shape. In most cases the aspect ratio will be changed by machining and also, since crack front roughness changes with increasing crack depth, the roughness of the shortened crack will not be appropriate to the new crack size.

Recent work by Lankford[5] using specimens loaded and scanned in an electron scan microscope has shown a variety of specimen behaviour. Some specimens exhibited high growth rate until becoming coincident with the curve for crack growth for long cracks. Other specimens contained cracks which grew fast initially but later reduced in crack growth rate, some stopping completely while others accelerated again to join the long crack curve (Fig 1). This data covers all the conditions previously observed and an understanding would potentially explain the so called "short crack behaviour".

The evidence on short crack behaviour has been reviewed in more detail elsewhere[6]. For our present purposes the conclusion on crack length at which short crack behaviour coincides with long crack data can be restated. The vast majority of those investigations where fast growth at short crack length was found showed also that the growth rate appropriate to a long crack had been attained at a crack length of 0.25 to 0.5 mm (0.010 to 0.020 in). The few claims to fast growth at longer lengths (up to 1.0 mm; 0.040 in) were based on evidence from remachined specimens.

3 DESIGN CONSIDERATIONS

In the previous section the evidence for short crack rapid growth effects was very briefly reviewed. It was concluded that since some investigations showed rapid growth effects while others showed none, and since the effective lengths in which short crack effects declined also varied, one interpretation was that short crack effects were specimen and test condition dependent. Further the length at which long crack growth rate was attained was unlikely to be more than 0.50 mm, and apparently never more than 1.0 mm. In order to assess the importance of short crack effects in design a number of aircraft conditions are now considered.

3.1 Safe Life Design

3.1.a Initial build conditions.

It would be expected that for safe life aeroplanes which are designed using SN data rapid growth of small cracks could be neglected. It has been established for some long time that for mild stress concentrations some 80 to 90% of the total life is crack free [7]. However in practice failures more usually occur at sharp notches or where fretting occurs. It has been shown by Edwards[3] that cracks are present at fretting surfaces after only about 10% of total life. Thus any reassessment of life due to a change of role or load condition which increases the stress on a fretted component should properly concentrate not on whole life but on crack growth life. It would seem that where life is almost wholly either cracked or crack free the usual techniques of life ratio based on SN data are quite adequate, even if in practice the cycles count is dominated by crack growth life. However this will only be true if the SN data is truly representative of the service conditions. For example smooth specimen data "corrected" to allow for fretting may be quite erroneous. Problems may arise where the life is composed of substantial proportions of cracked and crack free life and also where the failure mode is dependent upon stress level or spectrum.

3.1.b Life Extension by Structural Audit.

The process of structural audit goes some long way towards a reassessment of a safe life aeroplane on damage tolerance principles. Recently civil aeroplanes have been subjected to structural audit to achieve an extension in life beyond the present certified clearance. Many military aircraft have also been cleared for further service in the same way, not necessarily to extend life but perhaps to ensure safety in Service by inspection or re-assessment of known structural "hot-spots". A clearance for further Service use must account for possible damage during previous flying, usually based upon that crack size which can be found by inspection, or perhaps more correctly that crack size which can be found with a high degree of assurance during inspection. Thus, for a pressure cabin, "eye-ball" inspection will probably be used and cracks many millimetres in length may be missed. Experience of examination of detail fittings suggests that with the very best techniques large cracks can be missed. Certainly experience suggests that many cracks of size less than 1mm can be missed. [8] Since there is as yet no suggestion that rapid growth of small cracks extends beyond this size it is concluded that these effects are not important in structural audit.

3.1.c Repair of Safe Life Aeroplanes.

It is common practice to remove damaged material at bolt holes by increasing the hole size. Experience has shown that reaming of a cracked hole can smear across the crack faces, with the result that the crack although still present cannot be detected. Because of this it is common practice to monitor the cleaning out of damage by a suitable NDT technique, with a further cut after the last crack free indication in order to remove any residual damage. Thus an apparently crack free hole would be produced. This would be expected to produce a new clean crack free surface at which if no further precautions were taken new damage could be initiated. To support further service the design authority will follow one of two courses. The life to date may be regarded as a fatigue test under realistic conditions, in which case the part will be inspected, probably at some reduced life but certainly at no more than

previously attained. In this case no further crack growth calculations need be made. Alternatively action will be taken to improve life by working the hole or by use of interference fit fasteners. In such a case a new assessment of life will be made based upon test evidence.

3-3

In some circumstances it may not be possible to take the final cut to ensure all damage is removed from the hole. Certainly if this occurred crack growth calculations would be necessary. Most probably such calculations would assume a starting crack size at the reliable limit of crack detection, perhaps near the limit for small crack effects, but more probably greater, say not less than 0.25 mm but more likely 0.5 mm or greater. Little evidence has been published on growth of small cracks in interference stress fields, but what is available suggests that LEFM can be applied with adequate safety.[9] Thus in the damage repair case it also appears that growth of small cracks is not important.

3.2 Damage Tolerant Design

3.2.a Safety

The USAF damage tolerance requirements[10] specify minimum crack sizes which must be assumed to exist in all airframe structures. The most critical of these is specified from safety considerations as a minimum flaw size of 0.050" (ie 1.27 mm) which is represented as a semi circular or quarter circular crack in the most critical location. There is no data to suggest the possibility of more rapid growth of 1.27 mm cracks than for longer cracks at equivalent SIF. It must be concluded from the present evidence that the safety considerations of damage tolerant design are unaffected by small crack growth conditions.

3.2.b Durability

The USAF damage tolerance requirements specify small crack sizes which must be assumed to apply at every location in the structure. The smallest size so specified is 0.005" (0.127 mm). The purpose of this minimum crack size is to provide, in the less critical locations, some minimum life for growth from a starter crack to a crack length at which strength drops to a minimum acceptable level. Secondly, in combination with a growing crack which enters a hole, the minimum flaw size provides a convenient and realistic means for carrying crack growth calculation forward without involving considerations of crack re-initiation.

A crack length of 0.127 mm is within the limits in which small crack growth enhanced rate can be expected. The effects cannot be readily anticipated from the present evidence. It does appear that LEFM would over estimate the crack growth life, possibly by a substantial amount. Without further investigation which defines more exactly the limits of small crack effects and the change in rate with various conditions, an attempt to quantify lives would be speculative.

There are two factors which reduce the seriousness of the deficiency in calculation of crack growth lives from small cracks of 0.127 mm. The first of these is the way in which the starter crack size has been derived. At least part of the justification for choice of starter crack has been based upon read back of crack growth from crack surfaces found in fatigue test structures and Service aeroplanes. The degree to which this has been amalgamated with other data is not clear to those outside of the council tasked with formulating the requirements. If such read-back data has dominated the derivation of the 0.127 mm starter crack size, then because the data available at the time the requirements were formalised were all long crack data applied to LEFM it must apply that small crack effects have been inadvertently taken into account in the durability requirements. It would appear therefore that provided the same techniques are used in crack propagation calculations and also provided no great changes are made (by implication) in load spectrum, future calculations based on LEFM will result in life predictions which cause no greater risk to the structure or difficulty in repair than intended by the specification. This is not to say that such calculations are correct, but that the initial crack length has been "corrected" to produce the life which corresponds to the specification intentions. If this somewhat speculative interpretation of the specification derivation and application is correct then small crack effects can be ignored until such time as propagation calculation techniques account for small crack effects, at which stage the MIL Spec 83444 may need to be changed!

The second factor of importance is the type of structure. Structures which are based upon inspectability have considerably larger crack sizes imposed after the inspection has been performed. These sizes can be expected to dominate all post-inspection crack propagation calculations. The small crack considerations would then be of concern only during the first quarter of design life or less. By definition non inspectable structures are slow crack growth and small crack behaviour can occur at any time throughout the life. However the 1.27 mm safety-dominant crack will usually control the stress level to the extent that the importance of small crack growth is diminished.

4 THE IMPORTANCE OF SMALL CRACK GROWTH OUTSIDE THE DESIGN PROCESS

In the preceding section the importance of the growth characteristics of small cracks in aircraft design has been considered. The conclusion which must be reached is that the current design specifications and considerations are such that small crack behaviour will not normally be a dominant factor. But there are other reasons for studying the behaviour of small cracks.

The work of Edwards[4], Lankford[5] and Morris[11] suggests the stress cycle dependence, possible residual stress/strain effects, and the statistical nature of small crack growth. The most probable benefits of future small crack investigations are likely to be in the understanding of the physical behaviour during crack initiation and subsequent early growth, and through this a better appreciation of the fatigue process. That this topic as an entity is important is illustrated not only by the conferences and books devoted to the subject but far more graphically by the cost of research teams and the full scale experiments devoted to establishing fatigue lives which cannot be calculated accurately.

3-4

The advantages of an improved understanding of fatigue could be of greatest benefit in development of future fatigue resistant materials. Such development will be of benefit in increasing periods between inspections and total life potential, driving down the cost of ownership.

5 RESEARCH TOPICS

Future research should be directed towards the following topics;

1 Accurate modelling of observed effects:

a. Extremely accurate measurement of crack size and front, combined with precise load control.

b. Measurement or accurate prediction of surface stresses.

c. Accurate three dimensional stress intensity factor solutions which are not constrained to idealised (and often unreal) crack front shapes.

d. High quality base line data for long cracks obtained on the same batch of material as the small crack specimens.

e. Care that time dependent effects (eg stress - relaxation) do not confuse the results.

f. Experiments on a variety of specimens to explore specimen geometry effects.

2 Development of an understanding of elastic-plastic fracture mechanics, realising that this work is interactive with 1 above.

3 Development of statistical models to explain crack initiation, perhaps extendable to crack propagation.

6 CONCLUSIONS

1 Small cracks do not greatly affect either inspection periodicity or total fatigue life of aircraft designed to current design specification rules.

2 The application of small crack data is confined to only a few design conditions.

3 The MIL Spec 83444 may well account for small crack effects in the way the durability crack size has been derived. A more accurate understanding of small crack growth behaviour applied to propagation calculations should also be applied to a revision of the MIL Spec derivation, which would result in the same cycle count to attain the long crack condition as the present specification would demand.

4 Benefits in the understanding of the fatigue process are likely to be developed from small crack investigations.

5 Potentially large benefits in life cycle costs could be derived from an improved understanding of fatigue.

6 Accurate interpretation of small crack behaviour will depend upon a number of advances in experiment and analysis. Such advances are unlikely to come about without a deliberate attempt to bring together the component parts in a well designed and properly progressed investigation.

7 Closure

The paper presented is a highly personal interpretation of both the data available and the application of data to design. If the views expressed are the cause of discussion one of the major objectives of the paper will have been achieved. The importance of small crack growth to design has often been stated but usually has not been justified. The paper has (hopefully) demonstrated that small cracks are not important in this context given the current design rules; consideration against different revised design rules may result in different conclusions.

Future research on small crack growth can be well justified on the basis of much wider benefits which would flow from an improved understanding of the fatigue process. The author offers the view that such a basis for research is indeed stronger than unfounded statements on application to current design.

REFERENCES

1	Rothschild N M V	A framework for Government Research and Development. Presented to Parliament by the Lord Privy Seal. HMSO Command Paper 4814 - 1971
2	Strathcona and Mount Royal, Lord	Ministry of Defence Steering Group on Research and Development Establishments. Consultative Document /issued/ under the chairmanship of Lord Strathcona. London MOD 1980.
3	Edwards P R Cook R	Fracture Mechanics Prediction of Fretting Fatigue under Constant and Variable Amplitude Loading. 11th ICAS Lisbon 1978.
4	Cook R Edwards P R Anstee R F W	Crack Propagation at Short Crack Length Under Variable Amplitude Loading 17th ICAF Conference 1981.
5	Lankford	Presentation at the Euromech Colloquium on Short Crack Growth - Sheffield University - England. January 1982.
6	Anstee R F W Edwards P R	A Review of Crack Growth Threshold and Crack Propagation Rates at Short Crack Lengths. - To be published as an AGARP CP.
7	Schijve J	Significance of Fatigue Cracks in Micro Range and Macro Range. In "Fatigue Crack Propagation". ASTM STP 415.
8	Lewis W H Sproat W H Dodd B D Hamilton J M	Reliability of Non-Destructive Inspections. SA-ALC/MME 76-6-38-1 Lockheed, Georgia. December 1978.
9	Chandawanich N Sharpe W N	An Experimental Study of Fatigue Crack Initiation and Growth from Coldworked Holes. Eng Fracture Mech 11 p609 (1979).
10	Anon	Aircraft Damage Tolerance Requirements. Military Specification MIL-A-83444 (USAF). 1974.
11	Morris W L James M R Buck O	Growth Rate Models for Short Surface Cracks. Metallurgical Transactions A. 12A, p57, 1981.

RESEARCH EXPENDITURE %

90–95 Devoted to design objectives

5–10 Available for speculative research

Machining of long crack specimens to make small cracks introduces error sources

1 Surface stresses

2 Stress relief affects crack tip as well as surface

3 Differences between natural long and small cracks should exist

4 Aspect Ratio is changed

Account for surface stresses

e.g. due to machining or other treatment

fretting

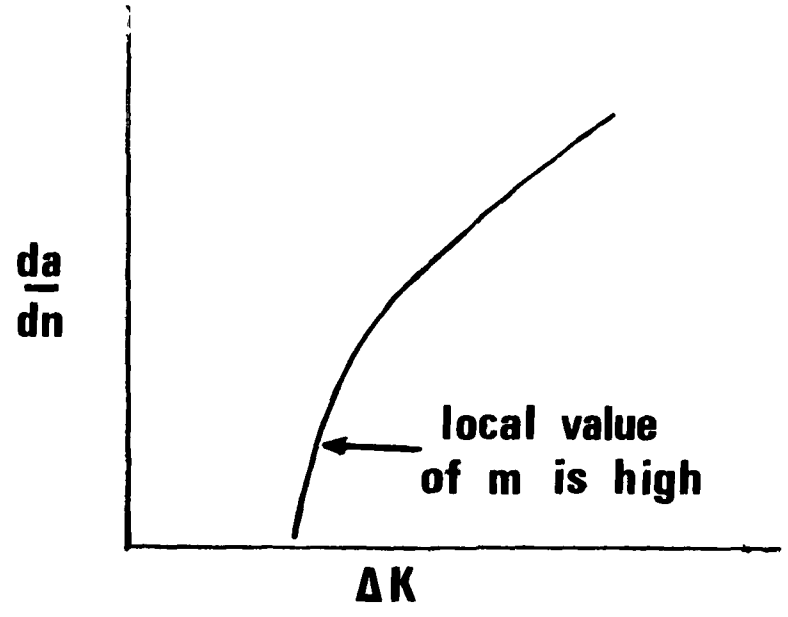

$\frac{da}{dn} = C(\Delta K)^m$.

K calculation must be accurate to predict $\frac{da}{dn}$

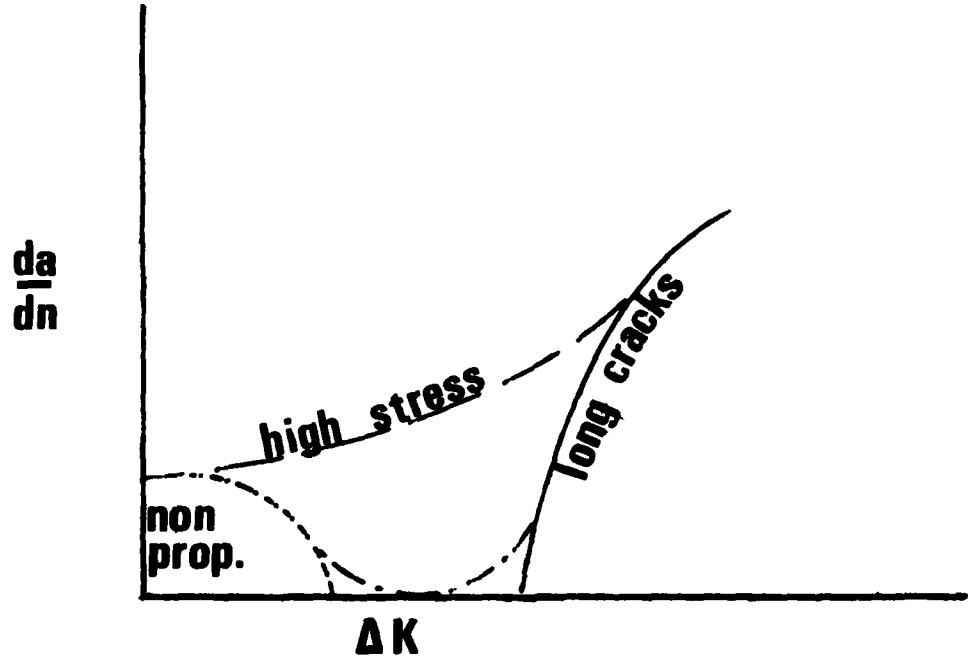

Lankford's hypothesis

Figure 1

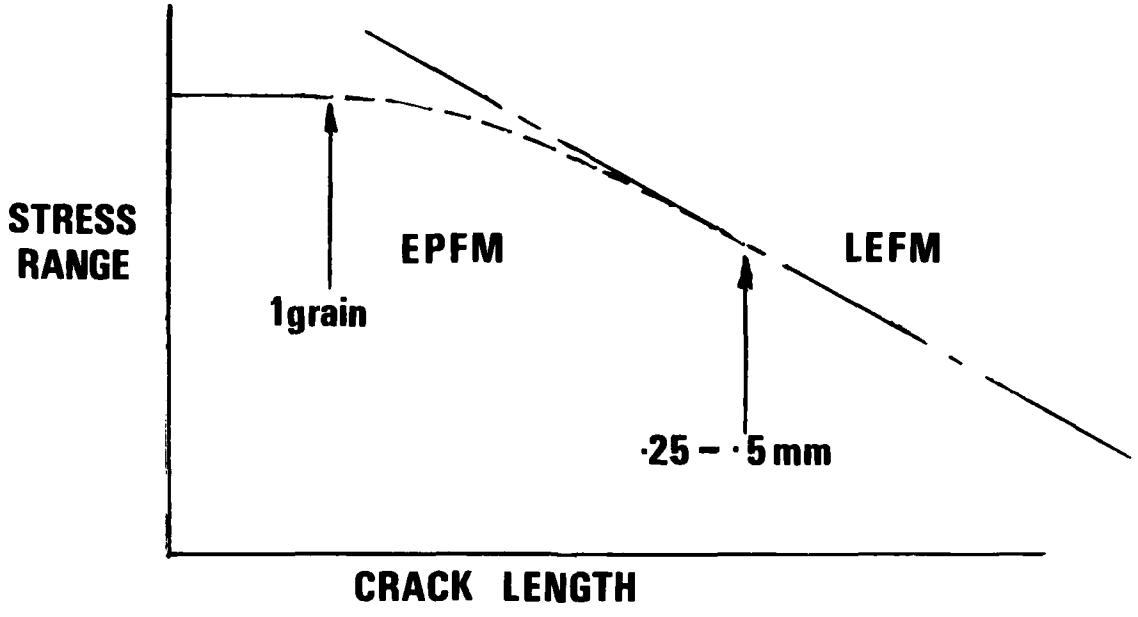

Structural audit ; crack sizes will be larger than small crack limit

Repair (1) Aim is to be crack free

(2) Working of cracked holes can improve life beyond simple LEFM prediction

Damage Tolerance

Safety 0·05" — greater than small crack size

Durability 0·005" — account for small cracks

But: Is durability a design stress condition

Does durability crack size include small crack effects (by derivation)

Post inspection cracks are beyond small crack size

Benefits of small crack research

1 Understand initiation

2 Idenify cracking processes

3 Improved materials for longer life

Work Needed

1 Higher quality experimental data

2 3D SIF solutions for real crack shapes

3 Good quality long crack data (same material batch)

4 Elastic—Plastic analysis

5 Initiation models

4-1

Use of Small Crack Data to Bring About and Quantify Improvements to Aircraft Structural Integrity

by
J. M. Potter
Aerospace Engineer
Air Force Wright Aeronautical Laboratories(FIBE)
Wright-Patterson Air Force Base
Dayton, Ohio 45433 USA
and
B. G. W. Yee
Chief, Materials Research Laboratory
General Dynamics Corporation
P.O. Box 748
Fort Worth, Texas 76101 USA

SUMMARY

Crack growth information has been used in many ways to quantitatively evaluate and predict damage tolerance and slow crack growth life limits of structures. Recent advances in the area of crack growth at small crack sizes (less than one millimeter) has enabled increasingly quantitative studies into the specific mechanisms that affect initiation and growth at structural details. As an example, through the use of small crack data the USAF/General Dynamics study on "Fastener Hole Quality" was able to identify a manufacturing-related problem causing short structural lives, propose a modification to shop equipment, and quickly and specifically evaluate the resultant flaw growth improvement. This change to shop equipment has been subsequently adopted by several other major airframe manufacturers.

The purpose of this paper is to describe the general procedures used in the derivation of small crack data and to present growth data for different structural manufacturing methods. The data will be presented in terms of equivalent initial flaw size populations, crack growth rate, and initiation life to a specific length for fractographically measured cracks within the range of .01 to 1 millimeter in length. Procedures will be discussed to utilize the small crack data for developing and verifying changes in fastener systems and manufacturing methods for improving the fatigue performance of aircraft structures.

1. INTRODUCTION

A major application of fracture mechanics is in the design and verification of a structure's safe life assuming pre-existing flaws at highly stressed locations. In fact, pre-existing flaw sizes are mandated in some industries to insure safety and reliability, and to establish liability. For damage tolerance purposes, flaw sizes for initial damage assumptions are on the order of 1000 microns (0.04 inch). In damage tolerance, a relatively few locations in a structure are designed for a full service life with the presumption of this size initial flaw. Study of the behavior of the smaller crack sizes has not been emphasized but with the maturation of the damage tolerance discipline, the subject of durability and reliability has become of greater significance.

In structural durability and reliability, the study of crack growth at small sizes (10 to 1000 microns) is of primary importance since this level of cracking defines the structural life prior to generalized cracking problems (where the number of structural flaws is too great for economical repair). In order to define the onset of generalized cracking it is important to know the crack growth behavior of the flaw geometries of interest and a measure of the initial flaw sizes and their statistical variations.

For many structures, fastener holes serve as the major location of generalized cracking. These fastener holes provide a complex stress field that makes analysis difficult at crack lengths of 10 to 1000 microns. Because of this difficulty and the problems with obtaining crack growth at small flaws, there is virtually no data on crack growth in this regime.

A significant set of data on small cracks recently became available from the study of initial quality in fastener holes by Noronha, Henslee, Gordon, Wolanski, and Yee (ref.1). The data set contained statistically significant numbers of specimens with detailed fractographic crack length measurements. The crack length measurements generally range upward from ten microns (0.0004 inches) relative to the bore of a fastener hole. The purpose of the reference study was to characterize the quality of production fastener holes in terms of the equivalent initial flaw size. Fractographic crack length data and design flaw growth analysis were combined to determine an equivalent initial flaw size level and compare data from different hole preparation methods. This study produced excellent fracture-design-level data on hole quality, but did not address the

reliability and definition of the measured crack growth data.

The purpose of this specialist's paper is to present the fractographic crack growth data obtained in reference 1 to better define crack growth behavior in the small crack regions and to discuss its application to the general improvement of structural integrity. While many individual observations and uses can be made with this data in parallel with the classical application of fracture mechanics, this will not be accomplished in this paper. The goal of this paper is to discuss the larger aspects of the unique definition (or resolution) of small crack data and its application to bringing about and quantifying significant improvements to the structural integrity. To accomplish this purpose, the fractographic data from a set of specimens made with conventional hole preparation methods were analyzed, first to evaluate repeatability, and then to define the actual behavior of flaws in the short crack length regimes. To do this, the fractographic crack length data were plotted to define the growth behavior. Following this comparison, the specific flaw origins in each specimen were identified, and means to eliminate the initial damage were proposed. The success of fatigue tests from another set of specimens where the initial damage was eliminated was verified through small crack techniques.

This specialist's paper is written as three separate chapters covering small crack measurements, interpretation of the measurements, and the applications of small crack data to structural integrity. The Rudd, Yang, Manning, and Yee(ref 2) paper in these proceedings is a companion paper which will further investigate the ref 1. and other data using a classical application of fracture mechanics to develop a durability based design methodology.

2. CHAPTER 1 -- SMALL CRACK MEASUREMENT

2.1 Introduction-Measurements

The majority of the reported studies of crack growth in the small crack regime have involved measurement of surface cracks by either direct observation or replication techniques(refs. 4 to 9). These approaches lead to significant information relating to crack growth in surface cracks. A more common situation in structural applications is the crack at fastener holes or other structural stress concentrations. These structural crack geometries often preclude the use of direct observation or periodic replication since a fastener is normally placed in its hole for the duration of life testing. Complicating the problem is the observation that many of the hole fastener cracks are embedded within the bore of the hole (ref. 10). This characteristic alone ensures that surface crack measurement of the data of interest (.1 to 1.0 mm) will not be possible since the head of virtually any fastener will cover this size crack. Thus, only means of measuring growth of embedded cracks are applicable in this regime. The available means are thus confined to either NDI/NDE during test or fractography following test completion. Unfortunately, NDE/NDI thresholds of detection are much larger than the size of fastener flaws of interest herein leaving only fractography as a means of measuring crack growth of small cracks at fastener holes.

The US Air Force completed a study in 1978 of equivalent initial flaw sizes at fastener holes. This program obtained large amounts of fractographic data on the growth of naturally occurring cracks in fastener holes for the purpose of comparing different methods of hole preparation. The data were obtained and documented (ref. 1,3) but not specifically presented as small crack data even though there were over 600 fastener cracks tracked to sizes of typically less than .05 mm. Therefore, this body of information will be presented and utilized here to demonstrate the type of data obtainable and to describe the potential application for the data.

2.2 Test and Analysis Procedure

Figure 1 shows the design of the 7475-T7651 aluminum alloy specimens used in the study. This specimen is similar to that used in the AGARD Critically Loaded Holes Program(ref. 11). The hole preparation equipment used was that specified for high quality production holes identified as fracture critical. None of the fastener holes were preflawed, or otherwise marked intentionally, during hole preparation and fastener installation; each was treated as a production fastener hole. Following hole preparation, each hole was inspected and a NAS-6204-7 straight shank, protruding head fastener was installed and tightened to 60 inch-pound torque in accordance with factory specifications. The fasteners had a maximum diameter of 0.250 inches. The specimens were fatigue tested to two lifetimes (16,000 design usage flight hours) of projected tactical fighter lower wing skin usage. The maximum gross section stress in the load history was 34 Ksi (235 MPa). Specimens that survived the 16,000 hour testing were broken apart. The load spectra applied was a blocked flight-by-flight history that was identically repeated every 400 equivalent flight hours. The exceedance curve is shown in Figure 2.

Following the completion of testing, the specimen failure surfaces were examined with a low power (10-30X) light microscope. In the case of these two piece specimens, each with two fastener holes, there were a maximum of eight possible failure surfaces to investigate. That is, two surfaces at each side of each hole multiplied by two holes in each plate and two plates. The microscopist was instructed to make observations of each potential failure surface but to fractographically follow and report only the flaw that grew to be the largest for each specimen. As a result, the data reported herein are

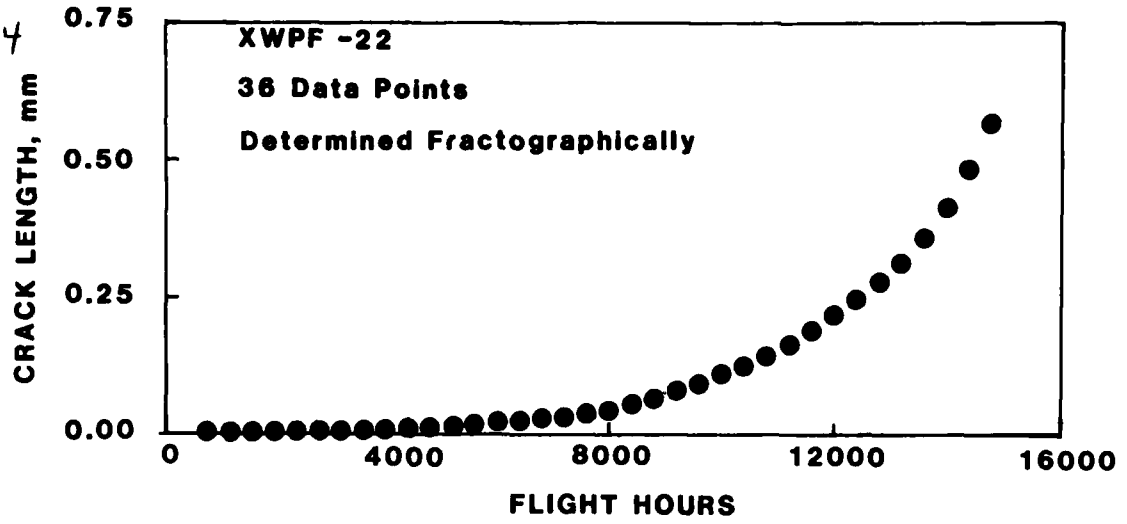

Fig. 3 FRACTOGRAPHIC CRACK GROWTH DATA FOR A TYPICAL SPECIMEN (XWPF-22)

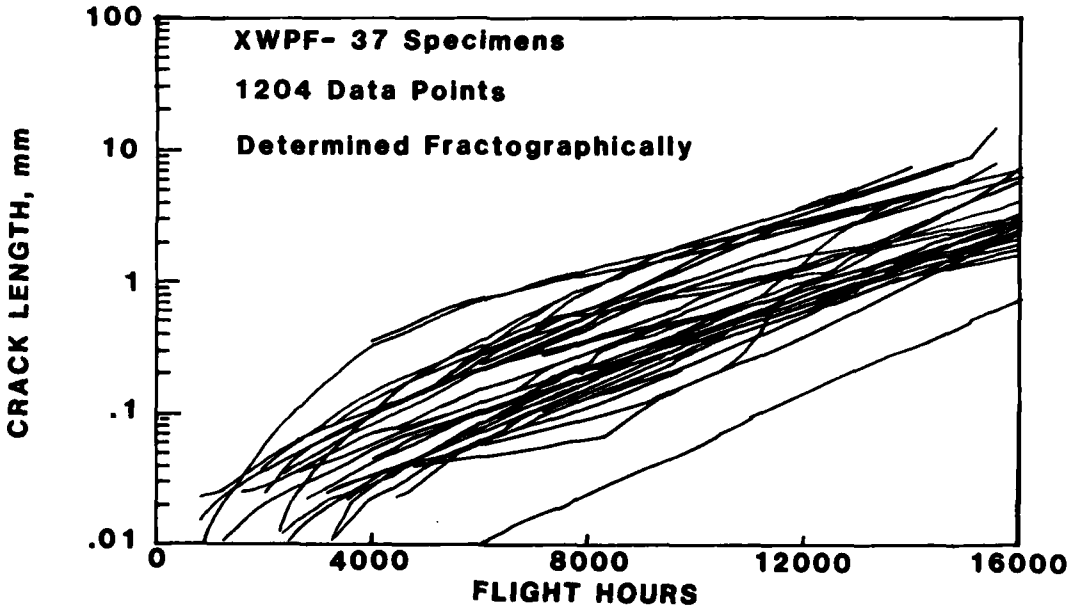

Fig. 4 FRACTOGRAPHIC CRACK GROWTH DATA FOR CONVENTIONAL QUALITY SPECIMENS

no generally recognized stress intensity solution for crack lengths of this small magnitude at a fastener hole. Again, the data show a well defined set of crack growth rate measurements which indicate that the growth process is continuous and repeatable.

Figure 6 shows the mean and one standard deviation for the crack growth rate data plotted as a function of crack length. The data has a standard deviation which averages 32% of the mean value. This variation in crack growth rate is consistent with that of the very careful surface crack measurements by Virkler, Hillberry, and Goel (ref. 13).

With the consistency in crack growth rate shown here it is possible to quantitatively identify the initiation life for these specimens. For instance, if the initiation crack sizes were assumed to be 0.2 mm(0.008 inches) then the initiation life from the XWPF data (Fig. 4) would be seen to vary from 3000 to 13,000 flight hours. This initiation crack size is significantly smaller than any the primary author has ever seen published. While other initiation flaw sizes can be used to determine a range of scatter in initiation life, the significance of this figure is that specific time-to-crack-initiation populations can be easily derived from this data because of the large number of measurements and the consistency of the crack growth data.

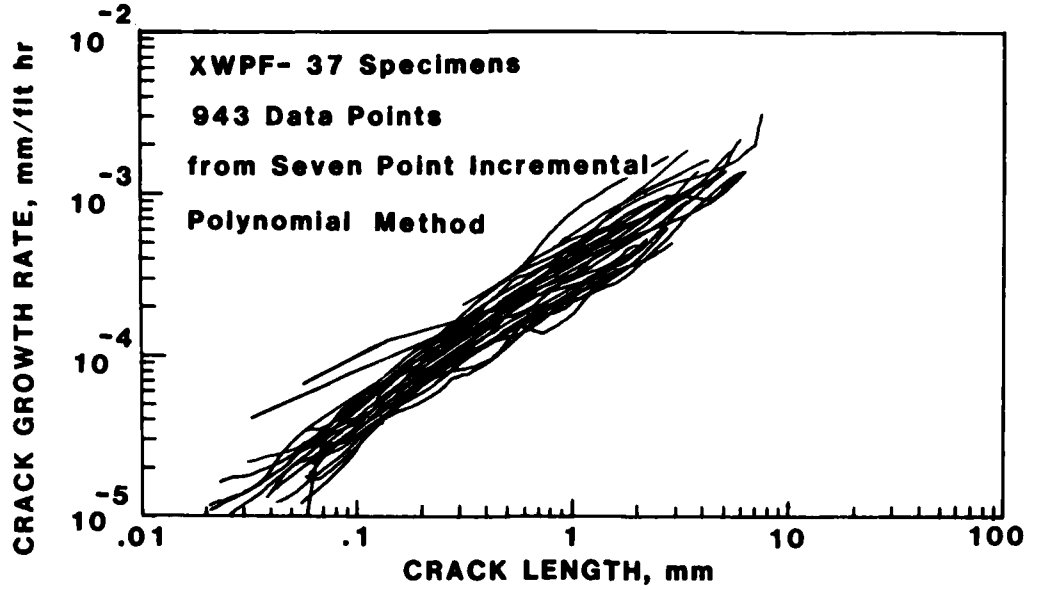

Fig. 5 CRACK GROWTH RATE DATA FOR CONVENTIONAL QUALITY SPECIMENS

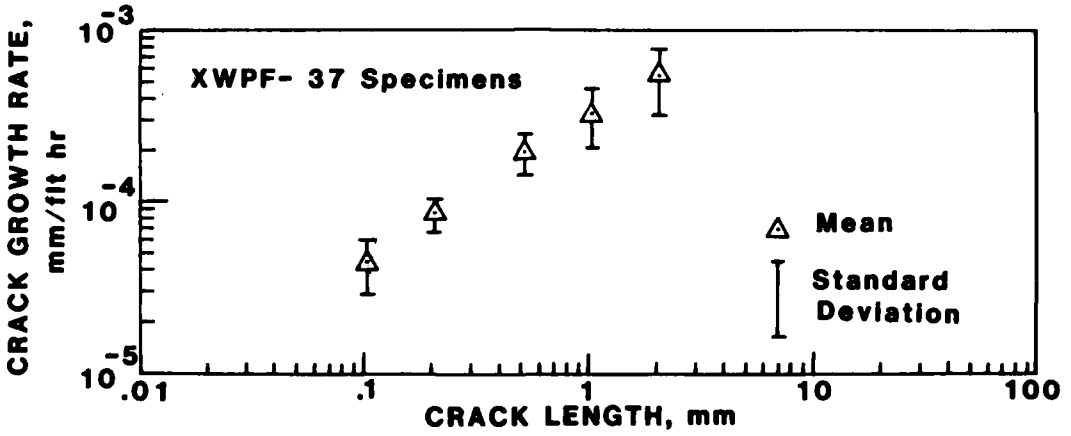

Fig. 6 MEAN AND ONE STANDARD DEVIATION OF CRACK GROWTH RATE

Many other comparisons can be made which are beyond the scope of this Chapter. The significance of this data is that information can be obtained on structures provided that the conditions are enhanced for fractographic examination. In the case of the tactical fighter load spectrum used herein, the history itself marked distinctively without changes to its content. Of primary importance is the repeated nature of the history which provided a clear pattern to the fractographic microscopist allowing him to track growth features to within 0.005 mm. The quantification of this approach made it possible to directly compare small crack growth data for different drilling techniques and quickly determine stress level and spectrum variation effects(ref. 1, 14, 15, 16, and 17).

As an added benefit, this approach saves considerable expense in testing and prospectively can save analysis costs as well. With reliance on fractographic data, there is no need for periodic crack length monitoring during the test. Thus, testing can go on unattended except for removal and replacement of broken specimens. After development of familiarity with the load spectrum marking patterns, the microscopist can fully track the flaw growth to its initiation in less than one hour per specimen. As a benchmark, the total cost of planning, manufacturing, testing, analyzing, fractographically backtracking, and documenting the ref. 1 data was under $300. (US) per specimen. This value is extraordinary considering that each 16,000 flight hour specimen was subjected to over 750,000 cycles of load.

2.4 Summary-Measurements

The results of this study indicate that consistent and significant crack growth data can be obtained simply and inexpensively in the small crack regime. The type of fastener hole growth data obtained was possible by the application of a load spectrum that distinctively marked the front of the surface. This allowed detailed fractography to be accomplished to crack sizes of less than .1 mm in length. With the detailed crack growth data, it was possible to determine crack growth rates and time to crack initiation, as well as providing the ability to estimate the significance of initiation versus crack growth life.

3. CHAPTER 2 -- INTERPRETATION AND ANALYSIS OF SMALL CRACK MEASUREMENTS

3.1 Introduction-Interpretations

One feature often missing in the field of structural integrity is quantitative flaw growth data significant to the structure. Structural analysts need data of sufficient volume and accuracy to make definitive statements of the safety and reliability of their structures. Currently, safety and durability criteria are designed into USAF structures by utilizing conservative initial flaw assumptions (MIL-A-83444, ref. 18). As an example, damage tolerance initial flaw sizes of 1.25 mm are required at fasteners for design. Initial flaws of 0.125 mm in size must be assumed at every fastener hole for the purpose of durability or economic life. The military specification is written such that these durability initial flaw size assumptions can be reduced or made less conservative if data become available indicating that smaller sizes are appropriate for a given structure, manufacturing process, or configuration.

Small crack data, if it can be obtained copiously and inexpensively, can serve to define the actual initial flaw size population of a given structure. With the definition of structural small cracks as shown in Chapter 1, further analyses can be accomplished that will answer many questions associated with materials, structural configuration, manufacturing technology, and their effect on the durability.

The purpose of this chapter is to expand on the interpretations possible with the small crack data obtained in chapter 1. To be discussed are small crack populations, initial flaw size representations, populations of flaw sizes as a function of usage or life, and time to a given initial size crack.

3.2 Small Cracks and the Flaw Size Population

Figure 4 shows a large amount of data on continuously growing cracks. These cracks were fractographically traced back as far as optically possible. The fractographic data procedure used provided 1204 crack length measurements from the 37 specimens of the XWPF test series. Given this amount of data, it is possible to construct cumulative probability distributions which represent the flaw size population at any given time in the projected usage of a structure.

Figure 7 shows the flaw size data of Fig. 4 plotted as a function of cumulative probability at the 4000, 8000, 12000, and 16000 flight hour intervals. These data reflect the actually measured flaw population of these test samples at different times during the life of a structure. Other population representations are possible because of the quantification possible in the small crack data. The mean as well as plus and minus one standard deviation in flaw growth behavior are plotted as a function of flight hours in fig. 8. These data show a flaw population that increases monotonically with a slope of approximately 1.5 decades of flaw size per each 8000 flight hours (one design lifetime) of usage. This power law relation indicates that these XWPF flaws increase by a factor of 30 for each design lifetime of usage. This data can have many uses including design and extrapolation to long term reliability. Rudd, et. al., present the statistical aspects of small crack data in a separate paper (Ref. 2) given in this document.

3.3 Small Cracks and the Initiation Life

In the last section, the small crack data from fig. 4 were examined to determine the flaw size population at a given usage period. This was done by making a vertical slice through the crack size data at a given number of flight hours. If, instead, a horizontal slice were taken at a given crack size, it would produce the population of the flight hours to reach that crack size; a sort of a time-to-crack-size or crack-initiation population. Figure 9 shows the mean time to crack size populations for the XWPF data for the crack sizes of 0.25, 0.5, 1.0 and 2.0mm length.

These data have tremendous potential for making quantitative comparisons of diff - ent structures, materials, and manufacturing methods on the basis of the amount of usage necessary to grow a crack to a given size. For instance, it may be of interest to quantitatively know the latest time when a structure may be subjected to an inspection allowing a clean-up size drill to remove a defined flaw. In the USA, cleanup drills are conveniently available at 1/64 th inch intervals. Therefore, it may be of interest to know when a one, two, or three 64 th oversize drill will be expected to clean up any crack. A one 64 th inch oversize would remove 0.008 inch or 0.2 mm of hole wall during

a clean-up. Figure 9 could be used to determine the limit of the time to expect success with a given drill size. The companion paper by Rudd, et. al., will also discuss the subject of time-to-crack-initiation in greater detail.

4-7

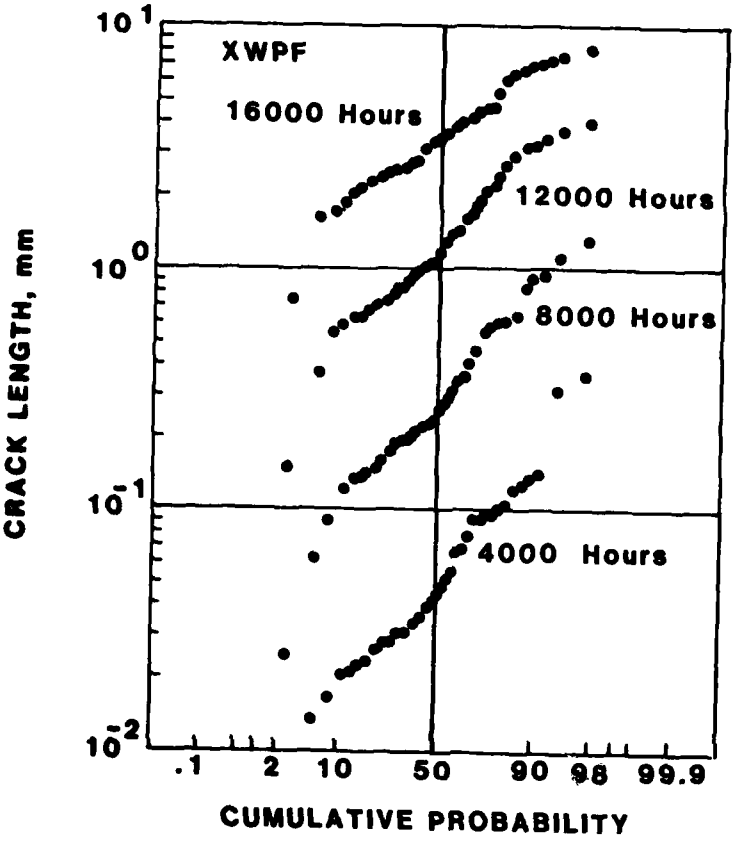

Fig. 7 FLAW SIZE DISTRIBUTIONS

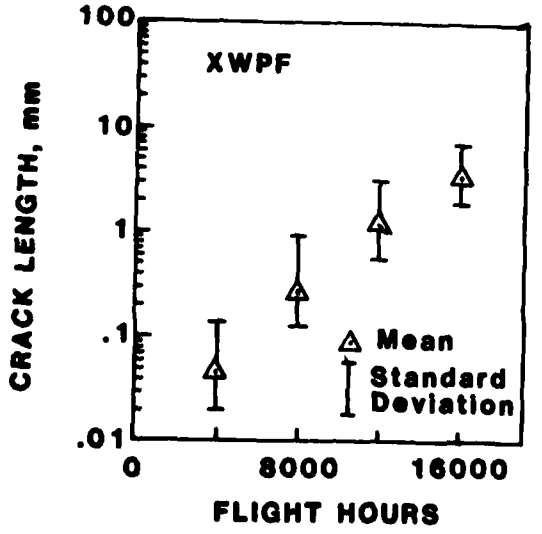

Fig. 8 MEAN AND ONE STANDARD DEVIATION OF CRACK LENGTH AT A GIVEN USAGE

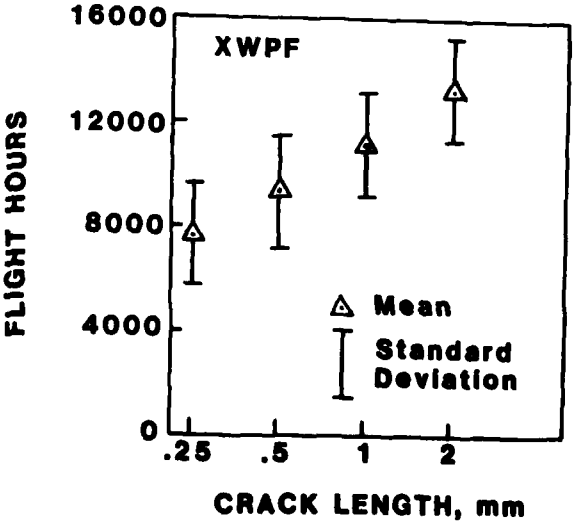

Fig. 9 MEAN AND ONE STANDARD DEVIATION OF FLIGHT HOURS TO REACH A CERTAIN SIZE CRACK

4-8

3.4 Small Cracks and the Equivalent Initial Flaw Size

The data from fig. 4 do not allow for a direct determination of the actual initial flaw size since the fractographic data do not extend to the actual origin. The concept of an equivalent initial flaw size can be utilized to extrapolate from the existing data to the apparent flaw which would be of the appropriate size to cause the observed cracking. The Equivalent Initial Flaw Size (EIFS) is a function of both the flaw growth analysis method and the data obtained. For purposes of this paper, the EIFS is used as a simple representation of the quality of these fastened joints.

The data from fig. 4 indicate a simple exponential relationship between fastener flaw depth and the usage (flight hours) for flaw sizes larger than 0.1 mm. Also, the data from fig. 5 indicate a simple power law (exponential) relationship exists between crack growth rate and the crack length for these specimens. In order to extrapolate to the apparent initial flaw, it is reasonable to extend the fig. 4 data to the zero-flight-hours axis using a continuous, power law function. This extrapolation must be consistant with the requirements of the design analysis in order for the EIFS flaw to accurately project to the observed flaw growth. In order to assure this consistency, the average growth rate data from fig. 5 were combined with a flaw growth integration methodology to determine an analytical "master curve" of crack growth from an extremely small crack size. This master curve was then "placed over" the data of fig. 4 and "best fit" using a computer program to provide an unique EIFS for each individual specimen. The "best fit" criterion was based on the desire to determine an EIFS which would most accurately depict the flaw sizes below "clean-up" sizes (less than 1 mm); that is, the EIFS approach was chosen to assure a representation which would most accurately describe the amount of usage to equate to the clean-up crack size.

The resultant EIFS population is shown in fig. 10. These data indicate that the 90 percentile EIFS for the XWPF specimens is approximately 0.02 mm (0.0008 inches). Obviously, higher reliability percentiles will result in larger EIFS values. The significance of this figure is that it is possible to quantitatively represent the apparent "quality" of a set of specimens. Other, more complicated representations can be possible by varying the assumptions for the best-fit criteria. As examples, Rudd, et al.(ref. 2), Manning, et al. (ref. 15), Shinozouka (ref. 16), and Yang (ref. 17) have labored to provide generic EIFS interpretations of this same data for the purpose of durability design.

The EIFS values determined from the XWPF specimens are very much smaller than those specified in Mil-A-83444 for durability design considerations. It may be possible for a fracture analyst to utilize these smaller demonstrated initial flaw sizes to justify a less conservative design while retaining safety and durability instead of accepting a specified initial flaw size.

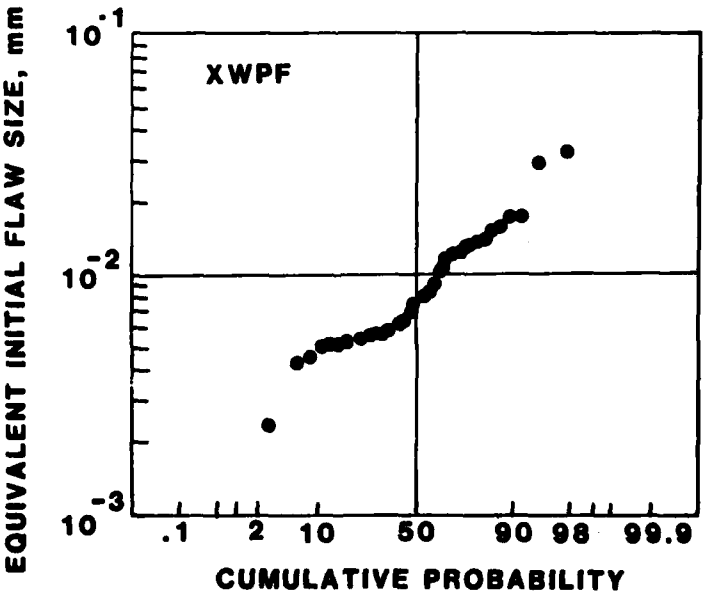

Fig. 10 EQUIVALENT INITIAL FLAW SIZE POPULATION

3.5 Small Cracks and the "Short Crack Effect"

A "short crack effect" has been identified by Pearson(ref. 5), and el Haddad, Smith, and Topper(ref. 6) and discussed by Hudak(ref. 7) and Ritchie and Suresh(ref. 19) and others(see Compilation of short crack reports, ref. 9). The short crack effect has been observed in some specimens as either a faster than "normal" flaw growth rate at small crack sizes or by an initially fast growth rate at small crack sizes followed by a transitional slowdown and a return to some steady-state condition at larger flaw sizes. Many mechanisms have been hypothesized to explain this data since, if it is consistently present, this would constitute a considerable problem for the fracture mechanics analyst.

The data obtained for test series XWPF, as shown in fig. 4 and 5, indicate no effect of short cracks in spite of meeting all of the criteria discussed by Ritchie and Suresh(ref. 19). These data exhibit a smooth, continuous, monotonically increasing flaw growth rate for all specimens. The reason that the Noronha, et al.(ref. 1 and 3) data did not show a short crack effect is not known. One possible difference between the specimens with short crack effects and those of fig. 4 and 5 are the means of initiating the cracks; those of Noronha, et al., were naturally occurring cracks whereas the specimens with the short crack effect had been preflawed. It may be possible that the preflaw procedure was responsible of the "short crack" effect.

3.6 Summary-Interpretations

The fractographic techniques utilized produced an average of thirty-two (32) crack length measurements for each specimen. These data on the large number of specimens of test series XWPF lead to the generation of statistically significant data for defining the flaw size population at any given usage, time-to-a-given-crack size, and equivalent initial flaw sizes.

This data indicates that the flaw size is seen to increase in accordance with a power law relationship fully in accordance with engineering fracture mechanics analyses practices. No "short crack effect" was apparent in any of the specimens.

For these stress-and-load spectrum conditions, the flaws were seen to increase by a factor of 30 for each design service lifetime. The equivalent initial flaw size for the XWPF test series was shown to be .008mm (0.00032 inches) which is much shorter than that specified in the military standards for durability.

4. CHAPTER 3 -- APPLICATIONS OF SMALL CRACK DATA TO IMPROVING STRUCTURAL INTEGRITY

4.1 Introduction-Improvements to Structural Integrity

Fracture Mechanics has evolved over the past 30 years to a stage where it is primarily used to evaluate a structure's capability to withstand projected usage. Since a given damage tolerance flaw size must be assumed, the fracture analyst has become a checking station during design. In durability design, the opportunity exists for the fracture analyst to provide an active input to the design process. The durability design process allows for a variation in the initial flaw size by demonstration. This provides the cognizant analyst an opportunity to apply his skills in observation to define and verify mechanisms leading to poor structural performance, hypothesize changes to eliminate these mechanisms, and later specifically determine if improvements have The analyst must be able to specifically and quantitatively define the original condition and any resultant change in structural integrity in order to be able to play this active role in design and manufacturing.

The purpose of this chapter is to discuss the application of data obtained in small crack investigations to the enhancement of structural integrity. Discussed are determination and verification of means to improve the structural integrity for the structure of interest, and extrapolation to long term life cycle costs and maintenence costs.

4.2 Determination of a Source of Early Life Failures

The data presented in Chapters 1 and 2 serve to definitively and quantitatively describe the flaw growth behavior of the XWPF test series specimens. In order to improve on the durability of a similar structure, we must determine where there are problems and try to eliminate these deficiencies. A review of the data of ref. 3 from XWPF specimens revealed that 28 of 37 specimens had failure origins at the hole surfaces with frequent references to scratches as the source. A detailed microscopic evaluation of these specimens revealed that the initiation sites were, in actuality, small axial scratches in the bore of the hole. The significant scratches found in the fastener holes were of a size on the order of 25 microns in depth making them difficult or impossible to detect by manufacturing inspection or by the unaided eye. Because of the existance of these scratches, the metal removal processes were examined in detail.

High speed motion pictures were taken of the drill operation. These indicated that the drill bit had the tendency to stop rotation in the hole during retraction. The drill equipment is a complicated air-powered device. The air-powered rotating drill bit is driven into the workpiece by an integral air-operated piston. During the retraction

cycle, the air supply is completely diverted from the motor, and directed to the retraction piston. In this case, it is hypothesized that friction between the drill and the hole was sufficient to stop the drill bit from rotating during retraction. Further, it was hypothesized that the retraction of the stopped drill bit was responsible for the scratches which coincided with shorter fatigue lives.

4-10

4.3 Hypothesis and Verification of a Solution

Since it appeared that the damaging scratches were caused by the problem in the retraction phase, positive steps were taken to modify the drill motor such that the bit rotated continuously during retraction. The air logic port system of the drill motor was changed to insure that the drill bit rotated continuously during retraction. Secondly, the extraction rate was reduced making the bit turn many times during the retraction phase. An additional 30 specimens were manufactured using the drill equipment with this trial modification to the retraction mechanism. These specimens were designated as series YWPF and are referred to as "Improved Drilling" specimens. The 30 YWPF specimens were subjected to fatigue testing and analysis just as in the XWPF series. The result of these tests was an improvement in the number of initiation origins at the hole surface as postulated; for the XWPF series, 28 of 37 had started at the hole but only 5 of 30 started there for the YWPF series. The mean flaw size at 16,000 flight hours was reduced marginally from 3.4 to 3.1 mm as a result of these modifications.

The flaw growth data for this test series is shown in Figure 11. The data of fig. 11 appears to be consistent with that of fig. 4 except that there are more specimens with longer initiation lives. A comparison of crack growth rates for the XWPF and YWPF specimen sets is shown in fig. 12. These data indicate that the growth rates did not change significantly, though there was the change in initiation site. The YWPF data also, does not support a "short crack effect" observation. The data indicate that, even though the improved drilling has resulted in fewer flaw origins at the hole, the final flaw size populations are similar with little likely improvement in structural integrity. Thus, with little effort and in a short span of time, it has been possible to specifically determine that the failure initiation mechanism can be altered by a change in the drilling process.

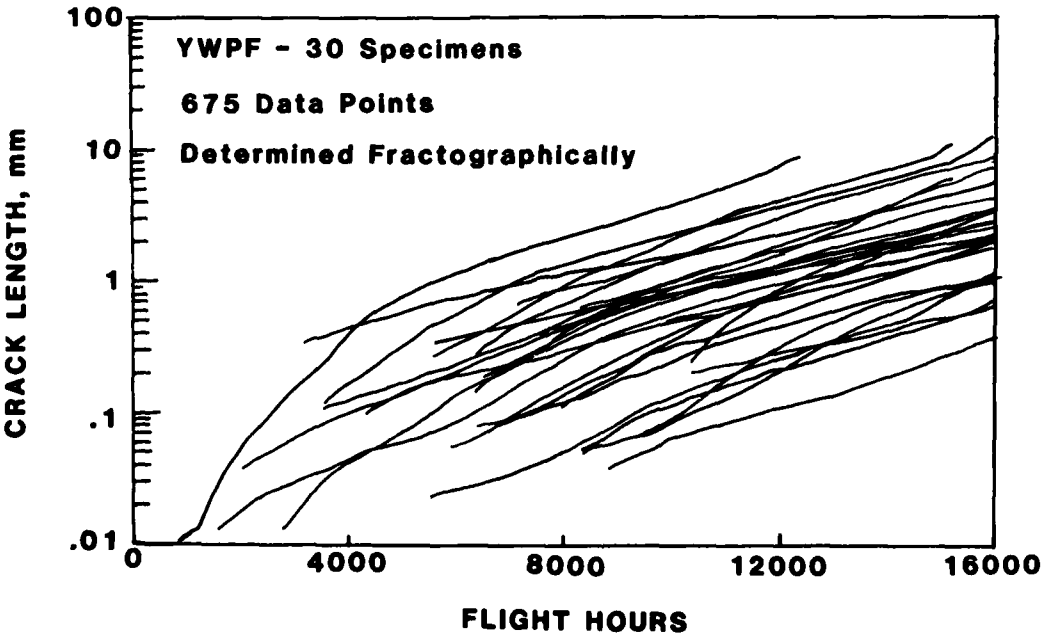

Fig. 11 FRACTOGRAPHIC CRACK GROWTH DATA FOR IMPROVED DRILLING SPECIMENS

4.4 Refinement of the Observations

The bolt hole initiation failure mechanism had been reduced in significance by the changes to the drilling equipment. Because the new dominant failure mechanism had shifted to the faying surface, a decision was made to change the specimen manufacture to reduce faying surface contact in the area of the fastener. This modification was referred to as "Improved Drilling and Assembly." A test series designated as VWPF was developed which consisted of 36 specimens. Fastener holes for each specimen were made using the improved Winslow drill and, in addition, the faying surface was spot-faced to approximately 0.005 inches in depth by 0.5 inches in diameter. The theory behind the spot-facing procedure was that it would alleviate bearing forces and thereby reduce the tendency to fretting.

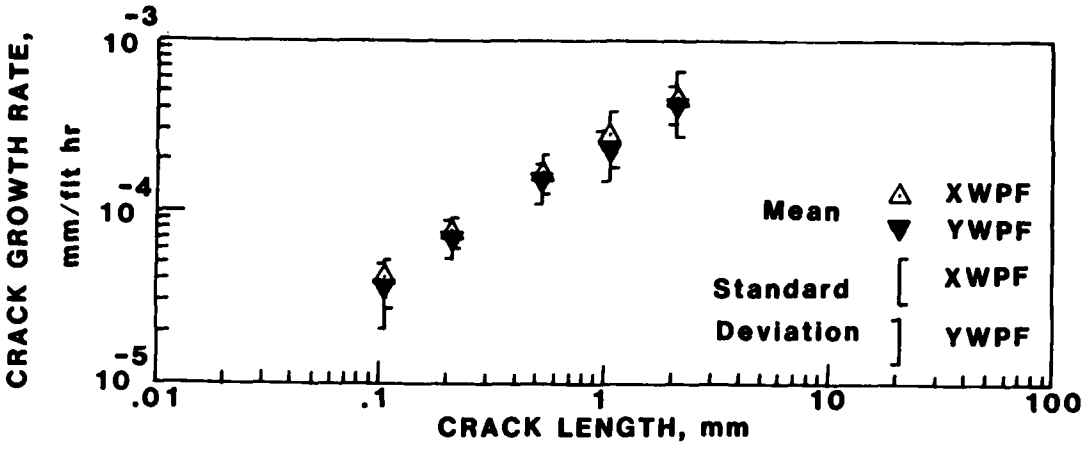

Fig. 12 COMPARISON OF CRACK GROWTH RATES FOR CONVENTIONAL AND IMPROVED DRILLING SPECIMENS

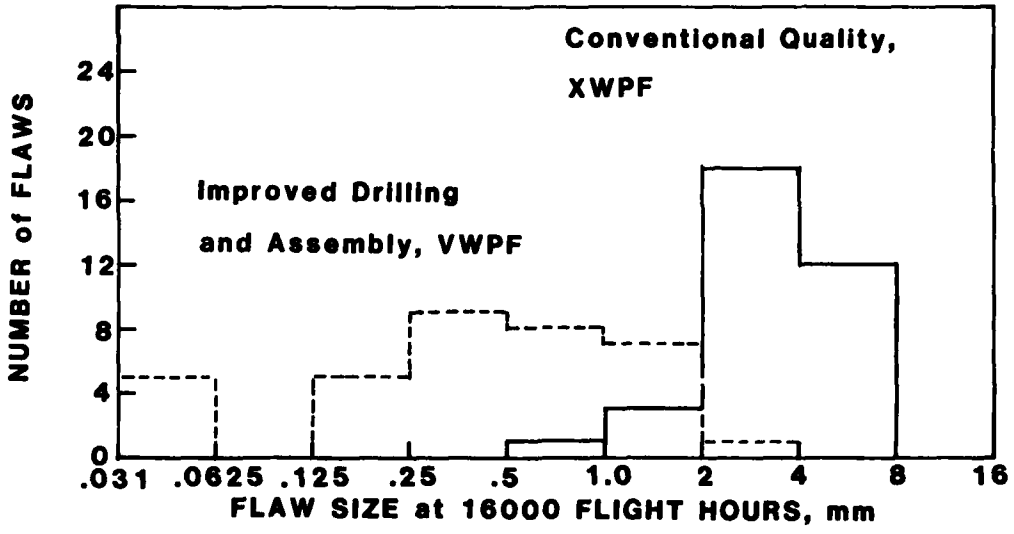

Fig. 13 COMPARISON OF FINAL FLAW SIZES FOR CONVENTIONAL AND IMPROVED DRILLING AND ASSEMBLY SPECIMENS

4.5 Extrapolation to Long Term Benefits

The improvements made to the "Improved Drilling and Assembly" test series (VWPF) compared to the conventional drilling (XWPF) shows almost an order of magnitude decrease in flaw size after 16,000 flight hours. In fig. 8, it was determined that approximately 8000 flight hours (or one design lifetime) was required in these specimens to give a factor of thirty (30) increase in flaw size. Extrapolating from fig. 8, it is possible to infer that the Improved Drilling and Assembly specimens would reach similar flaw populations as the XWPF series but at a usage of approximately 5000 flight hours. In the case of this typical fighter usage, it could mean that after 13,000 flight hours the Improved Drilling and Assembly airframe would have a flaw population equivalent to an 8000 flight hours vehicle manufactured with Conventional Quality. Alternatively, these trends could be viewed as saying that, for the same usage, the flaw population would be significantly reduced. The implications to the reduction in cost of repair due to structural cracking could be enormous. If the trends in these small cracks could be extended to actual aircraft structures, significant money could be saved through a reduction in the amount of repair necessary in a given system.

TABLE 1 -- Effect of Manufacturing Method Variations on Location of Flaw Origin and Flaw Sizes

4-12

	TEST SERIES		
	XWPF	YWPF	VWPF
Number of specimens	37	30	36
No. of initiation origins at the hole surface	28	5	n/a
No. of initiation origins at faying surface or corner	9	25	n/a
No. of specimens failing before 16,000 flight hours	5	2	0
50 Percentile flaw size at 16,000 flight hours	3.4 mm	3.1 mm	0.46 mm
No. of flaws exceeding 2 mm in length at 16,000 flight hours	33	21	1

4.6 Summary-Improvements to Structural Integrity

Small crack technology has been utilized to determine the specific flaw growth behavior of conventionally manufactured and assembled fastened structures. The information has been used to define procedures which could result in improvements to structural integrity of these coupons. Subsequent fatigue tests and small crack evaluation techniques indicated that the Improved Drilling and Assembly approach resulted in almost an order of magnitude reduction in the flaw population at equivalent usage.

The relative ease of defining the improvements is indicative of the power of the fractographic technology in providing quantitative information even in the most challenging small crack regime.

5.0 CONCLUSIONS

1. Small crack technology provides a uniquely definitive mechanism for determining the durability of actual structures. Only small crack technology can provide the crack propagation data necessary to define durability and structural integrity at structurally significant geometric details in the flaw size range of less than 1mm.

2. The crack growth rates for naturally occurring small flaws from fastener holes are exponentially related to the crack length.

3. No evidence was found to support a "short crack effect" for these naturally occurring cracks at fastener holes.

4. Small crack growth behavior as measured by fractography has a variation in crack growth rate that is consistent with that of conventional measurement techniques for much larger size flaws.

5. Details of the drill bit retraction process and interface surface preparation following hole manufacture appear to be responsible for variations in fatigue life; increased fatigue life was obtained when taking positive measures to assure continuous rotation during retraction and to reduce interfacial contact stresses at holes.

REFERENCES

1. Noronha, P.J., Henslee, S.P., Gordon, D.E., Wolanski, Z.R., and Yee, B.G.W., "Fastener Hole Quality", AFFDL-TR-78-206, Vol. 1, Air Force Flight Dynamics Laboratory, Dayton, Ohio, December 1978 (AD-A077859).

2. Rudd, J.L., Yang, J.N., Manning, S.D., and Yee, B.G.W., "Probabilistic Fracture Mechanics Analysis Methods of Structural Durability", AGARD Specialists Meeting on Behavior of Short Cracks in Airframe Structures", Toronto, Canada, 1982.

3. Noronha, P.J., Henslee, S.P., Gordon, D.E., Wolanski, Z.R., and Yee, B.G.W., "Fastener Hole Quality", AFFDL-TR-78-206, Vol. II, Air Force Flight Dynamics Laboratory, Dayton, Ohio, December 1978, (AD-A074730)

4. Lankford, J., "Initiation and Early Growth of Fatigue Cracks in High Strength Steel", Engineering Fracture Mechanics, Vol. 9, pp 617-624, 1977, Pergamon Press.

5. Pearson, S., "Initiation of Fatigue Cracks in Commercial Aluminum Alloys and the Subsequent Propagation of Very Short Cracks", Engineering Fracture Mechanics, Vol. 7, pp 235-247, 1975, Pergamon Press.

6. el Haddad, M.H., Smith, K.N., and Topper, T.H., "A Strain Based Intensity Factor Solution for Short Fatigue Cracks Initiating from Notches", Fracture Mechanics, ASTM STP 677, C.W. Smith, Editor, American Society for Testing and Materials, pp 274-289, 1979.

7. Hudak, S.J., "Small Crack Behavior and the Prediction of Fatigue Life", Journal of Engineering Materials and Technology, Transactions of the ASME, Vol. 103, p. 26, Jan. 1981.

8. Smith, R.A., and Miller, K.J., "Fatigue Cracks at Notches", International Journal of Mechanical Science, Vol. 19, pp. 11-22, Pergamon Press, 1977.

9. Potter, J.M., "A Compilation of Publications Concerning the Study of the Growth of Small Cracks", AFWAL-TM-81-71-FIBE, Air Force Wright Aeronautical Laboratories, Dayton, Ohio, Mar. 1981.

10. Wood, H.A., Rudd, J.L., and Potter, J.M., "Evaluation of Small Cracks in Airframe Structures", AGARD Pilot paper on Small Cracks, Cesme, Turkey, 1981.

11. Coombe, T., and Urzi, R.B., "Critically Loaded Hole Technology-Pilot Collaborative Test Programme", AGARD-R-678, Nov. 1980.

12. Hudak, S.J., Saxena, A.M, Bucci, R.J., and Malcolm, R.C., "Development of Standard Methods of Testing and Analyzing Fatigue Crack Growth Rate Data", AFML-TR-78-40, Air Force Materials Laboratory, Dayton, Ohio, May 1978.

13. Virkler, D.A., Hillberry, B.M., and Goel, P.K., "The Statistical Nature of Fatigue Crack Growth Propagation", AFFDL-TR-78-43, Air Force Flight Dynamics Laboratory, Dayton, Ohio, April 1978.

14. Potter, J. M., "Advances in Fastener Hole Quality through the Application of Solid Mechanics", in Proceedings of the Army Symposium on Solid Mechanics, 1978 - Case Studies on Structural Reliability, AMMRC-MS-78-3, Army Materials and Mechanics Research Center, Watertown, MA, September 1978.

15. Manning, S.D. et al.,"Durability Methods Development, Phase 1 Summary", AFFDL-TR-79-3118, Vol. I, Air Force Flight Dynamics Laboratory, Dayton, Ohio, Sept., 1979.

16. Shinozouka, M., "Durability Methods Development, Initial Quality Representation", AFFDL-TR-79-3118, Vol. IV, Air Force Flight Dynamics Laboratory, Dayton, Ohio, Sept. 1979.

17. Yang, J. N., "Statistical Estimation of Economic Life for Aircraft Structures", Journal of Aircraft, AIAA, Vol. 17, No. 7, July 1980, pp. 528-535.

18. Anon, "Airplane Damage Tolerance Requirements", Mil-A-83444(USAF), Department of Defense, Washington, D.C., 1972.

19. Ritchie, R. O., and Suresh, S., "Mechanics and Physics of the Growth of Small Cracks", AGARD Specialists' Meeting on Behavior of Short Cracks in Airframe Structures, Toronto, Canada, 1982.

ACKNOWLEDGEMENT

The data discussed in this memo resulted from the "Fastener Hole Quality" report. The authors of this report are acknowledged for their efforts in obtaining data of outstanding detail and quality. Special thanks go to Z. R. Wolanski of General Dynamics Corp/Fort Worth Division for his diligence and professionalism in fractographically tracking all cracks in the tes program. Dr. P. J. Noronha is acknowledged for his analytical skill and enthusiasm which aided immeasurably in the accomplishment of the effort and implementation of the recommendation into production changes. S.P. Henslee and D. Gordon are acknowledged for their leadership and diligence in completing the efforts. Lt. Jacqueline M. Pearson-Smith is acknowledged for her efforts to organize the "Fastener Hole Quality" data into the small crack format.

A NONLINEAR FRACTURE MECHANICS APPROACH TO THE GROWTH OF SMALL CRACKS

6-1

J. C. Newman, Jr.
NASA Langley Research Center
Hampton, Virginia 23665, U.S.A.

SUMMARY

Using linear-elastic and nonlinear fracture mechanics, many investigators have tried to explain the growth of small cracks in plates and at notches. These studies have concentrated on the growth of small cracks ranging in length from 10^{-2} to 1 mm. On the basis of linear-elastic fracture mechanics, the small cracks grew much faster than would be predicted from large crack data. Nonlinear fracture mechanics, in particular the J-integral concept, and an empirical length parameter have been used to correlate small and large crack-growth rate data. The physical interpretation of the length parameter, however, is unclear.

Recently, some investigators have suggested that crack closure may be a major factor in causing differences between growth of small and large cracks. The purpose of the present paper is to use an analytical model of crack closure to study the crack growth and closure behavior of small cracks in plates and at notches. The calculated crack-opening stresses for small and large cracks, together with elastic and elastic-plastic fracture mechanics analyses, are used to correlate crack-growth rate data. At equivalent elastic stress-intensity factor levels, calculations predict that small cracks in plates and at notches should grow faster than large cracks because the applied stress needed to open a small crack is less than that needed to open a large crack. These predictions agree with observed trends in test data. The calculations from the model also imply that many of the stress-intensity factor thresholds that have been developed in tests with large cracks and with load-reduction schemes do not apply to the growth of small cracks.

The current calculations are based upon continuum mechanics principles and, thus, some crack size and grain structure exist where the underlying fracture mechanics assumptions become invalid because of material inhomogeneity (grains, inclusions, etc.). Admittedly, much more effort is needed to develop the mechanics of a noncontinuum. Nevertheless, these results indicate the importance of crack closure in predicting the growth of small cracks from large crack data.

NOMENCLATURE

A_k	coefficients in stress-intensity factor equation (k = 1,2)
b	location of concentrated force, m
b_k	dimensions for partially-loaded crack (k = 1,2), m
c	half length of crack, m
c_i	half length of initial crack in load-reduction scheme, m
c_n	half length of crack-starter notch, m
d	half length of crack plus tensile plastic zone, m
E	Young's modulus of elasticity, MPa
F	boundary-correction factor on stress-intensity factor
K	stress-intensity factor, MPa-$m^{1/2}$
N	number of cycles
n	number of bar elements in crack-closure model
P	applied load, N
P_i	applied load at initiation of load-reduction scheme, N
P_{max}	maximum applied load, N
P_o	crack-opening load, N
R	stress ratio (S_{min}/S_{max})
r	radius of circular hole, m
S	applied stress, MPa

S_c	crack-closure stress, MPa
S_i	applied stress at initiation of load-reduction scheme, MPa
S_{max}	maximum applied stress, MPa
S_{min}	minimum applied stress, MPa
S_o	crack-opening stress, MPa
t	specimen thickness, m
V	crack-surface displacement, m
V_c	displacement of crack-tip element, m
w	half width of specimen, m
w_j	half width of bar element at point j, m
x,y	Cartesian coordinates
x_i	coordinate location of element i, m
α	constraint factor, $\alpha = 1$ for plane stress and $\alpha = 3$ for plane strain
ΔK	stress-intensity factor range, MPa-$m^{1/2}$
ΔK_{eff}	effective stress-intensity factor range, MPa-$m^{1/2}$
$\Delta \tilde{K}_{eff}$	plastic-zone corrected effective stress-intensity factor range, MPa-$m^{1/2}$
ΔK_{th}	threshold stress-intensity factor range, MPa-$m^{1/2}$
ΔS_{eff}	effective stress range, MPa
η	material constant, $\eta = 0$ for plane stress and $\eta = \nu$ for plane strain
ν	Poisson's ratio
ρ	length of tensile plastic zone, m
σ_j	stress on segment of crack surface, MPa
σ_o	flow stress, MPa
σ_u	ultimate tensile strength, MPa
σ_{ys}	yield stress (0.2 percent offset), MPa
ω	length of compressive plastic zone, m

INTRODUCTION

Most experimental and analytical studies on fatigue-crack growth have been conducted on "large" cracks with lengths in excess of 2 mm. However, in many engineering structures, crack growth from "small" pre-existing flaws is a major portion of the component's fatigue life. Numerous investigators [1-11] have observed that the growth characteristics of small fatigue cracks in plates and at notches differ from those of large cracks in the same material. These studies have concentrated on the growth of small cracks ranging in length from 10^{-2} to 1 mm. On the basis of linear-elastic fracture mechanics (LEFM), the small cracks grew much faster than would be predicted from large crack data. This behavior is illustrated in Figure 1, where the crack-growth rate is plotted against the linear-elastic stress-intensity factor range, ΔK. The solid (sigmoidal) curve shows a typical result for a given material and environment under constant-amplitude loading. The solid curve is usually obtained from tests with large cracks. At low growth rates, the threshold stress-intensity factor range, ΔK_{th}, is usually obtained from load-reduction (K-decreasing) tests. Some typical experimental results for small cracks in plates and at notches are shown by the dashed curves. These results show that small cracks grow faster than large cracks at the same ΔK level and that they also grow at ΔK levels below threshold.

Using nonlinear fracture mechanics, some investigators have tried to explain the growth of small cracks in plates and at notches. In particular, the J-integral concept and an empirical length parameter [3,4] have been used to correlate small-crack and large-crack growth rate data. The physical interpretation of the length parameter, however, is unclear. More recently, several investigators [5-11] have suggested that crack closure [12,13] may be a major factor in causing the differences between the growth of small and large cracks.

Many of the comparisons between growth rates for small and large cracks have been made in the low crack-growth rate region associated with threshold (ΔK_{th}) for large cracks. Measurement of ΔK_{th}, using load-reduction schemes [14-17], establishes a regime of crack sizes and applied stress levels where crack growth would not occur. But small cracks and cracks from pre-existing flaws have been observed to grow [1-3,10] at stress-intensity factor levels below ΔK_{th}, as shown in Figure 1. Here again, several investigators [18-20] have experimentally shown that crack closure is causing the stress-intensity factor threshold under load-reduction schemes. On the basis of these results, an important question concerning the growth of large cracks at extremely low stress levels arises. Is the ΔK-rate relationship for large cracks under constant-amplitude loading given by the dash-dot curve in Figure 1? Admittedly, a threshold could exist for large cracks due to material inhomogeneities and environmental factors, such as oxide or corrosion products on the crack surfaces [21,22]. But these thresholds must be obtained in tests without any load-interaction effects.

To adequately resolve the differences between the growth of small and large cracks, crack-closure effects must be considered. This paper is concerned with the analytical treatment of crack closure. A simple strip-yield model of crack closure was developed in Reference 23, but a more useful model was developed in References 24 and 25. There have also been several other attempts to develop simple analytical models of crack closure, but a review here is beyond the scope of the present paper (see Ref. 25).

The purpose of the present paper is to use an analytical closure model [25] to study the crack growth and closure behavior of small cracks in plates and at holes, and to study the closure behavior of large cracks under load-reduction schemes used in threshold testing. The model used here simulates the influence of plane-stress and plane-strain conditions on yielding at the crack tip. The model is based on the Dugdale model [26], but modified to leave plastically deformed material along the crack surfaces as the crack grows. Two configurations are analyzed: (1) a center-crack tension specimen and (2) two symmetric cracks emanating from a circular hole. A surface-crack configuration is also considered, but it is analyzed as a center-crack specimen with a modified stress-intensity factor solution. The crack-opening stresses for these configurations are calculated as a function of crack length for constant-amplitude loading and for the load-reduction schemes used for threshold testing. An improved method of calculating crack-opening stresses, using crack-surface displacements, is also presented. The calculated crack-opening stresses are compared with experimental measurements made under a load-reduction scheme.

Because specimens with small cracks are usually subjected to high stress levels, Elber's effective stress-intensity factor range [13] is modified herein for plasticity. Crack-growth rates under constant-amplitude loading are correlated with the plastic-zone corrected effective stress-intensity factor range, ΔK_{eff}, over a wide range of stress ratios. Using the crack-growth rate and ΔK_{eff} correlations for large cracks in several materials, predicted growth rates for small cracks in plates and at circular holes are compared with experimental rates.

FATIGUE CRACK-CLOSURE ANALYSIS

The following sections include a brief description of the analytical crack-closure model [25] and of the assumptions made in the application of the model to the growth of small cracks. These sections also include a description of the plastic-zone corrected effective stress-intensity factor range and its correlation with crack-growth rates.

Analytical Crack-Closure Model

To calculate crack-closure and crack-opening stress during fatigue crack growth, the elastic-plastic solution for stresses and displacements in a cracked body must be known. Because there are no closed-form solutions to elastic-plastic cracked bodies, simple approximations must be used when finite-element solutions [23] are inappropriate. The Dugdale model [26] is one such approximation. The crack-surface displacements, which are used to calculate contact (or closure) stresses under cyclic loading, are influenced by plastic yielding at the crack tip and residual deformations left in the wake of the growing crack. The applied stress level at which the crack surfaces become fully open (no surface contact) is directly related to contact stresses.

The analytical closure model developed in Reference 25 is for a central crack in a finite-width specimen subjected to uniform applied stress (Fig. 2(a)). This model is extended herein to cracks emanating from a circular hole in a finite-width specimen subjected to uniform applied stress (Fig. 2(b)). The model is based on the Dugdale model, but modified to leave plastically deformed material in the wake of the crack. The primary advantage in using this model is that the plastic-zone size and crack-surface displacements are obtained by superposition of two elastic problems--a crack in a plate subjected to a remote uniform stress, S, or to a uniform stress, σ, applied over a segment of the crack surface. The stress-intensity factor and crack-surface displacement equations for these loading conditions on a plate with a central crack are given in Reference 25. The corresponding equations for cracks emanating from a circular hole are given in Appendix A.

Figure 3 shows a schematic of the model at maximum and minimum applied stress. The model is composed of three regions: (1) a linear-elastic region containing a circular hole with a fictitious crack of half-length $c + \rho$, (2) a plastic region of length ρ,

and (3) a residual plastic deformation region along the crack surface. The physical crack is of length $c - r$, where r is the radius of the circular hole. The compressive plastic zone is ω. Region 1 is treated as an elastic continuum; the crack-surface displacements under various loading conditions are given in Reference 25 for a central crack and in Appendix A for cracks emanating from a hole. Regions 2 and 3 are composed of rigid-perfectly plastic (constant stress) bar elements with a flow stress, σ_o. The flow stress is taken as the ultimate tensile strength (σ_u) herein because some tests were conducted at very high applied stress levels. (If a nonlinear stress-strain curve had been incorporated into the model [27], the need for an assumed flow stress would have been eliminated.) The shaded regions in Figures 3(a) and 3(b) indicate material that is in a plastic state. At any applied stress level, the bar elements are either intact (in the plastic zone) or broken (residual plastic deformation). The broken elements carry compressive loads only, and then only if they are in contact. The elements yield in compression when the contact stress reaches $-\sigma_o$. Those elements that are not in contact do not affect the calculation of crack-surface displacements. To account for the effects of state of stress on plastic-zone size, a constraint factor α was used to elevate the tensile flow stress for the intact elements in the plastic zone. The effective flow stress $\alpha\sigma_o$ under simulated plane-stress conditions was σ_o and under simulated plane-strain conditions was $3\sigma_o$. The constraint factor is a lower bound for plane stress and an approximate upper bound for plane strain [25]. The constraint factor was assumed to be 1, 1.73 (Irwin's plane-strain constraint [28]), or 3, depending upon the test conditions. Plane-stress conditions were assumed for high applied stress levels and for crack-growth rates higher than the rate at transition (flat to slant crack growth) [29] because the plastic-zone size would be of the order of the plate thickness. Plane-strain conditions were assumed for crack-growth rates lower than the rate at transition because the plastic-zone size would be small compared to plate thickness. Where the constraint conditions were unknown, such as a small surface crack, plane-stress and plane-strain conditions were both tried.

The analytical closure model was used to calculate crack-opening stresses as a function of crack length and load history. The applied stress level at which the crack surfaces are fully open is denoted as S_o, the crack-opening stress. These stresses have been calculated by two methods. One method was based on the stress-intensity factor due to contact stresses at the minimum applied stress; the other was based on crack-surface displacements. Under constant-amplitude loading, the crack closes first and opens last at the crack tip, so the stress-intensity factor method was used to calculate S_o [24,25]. However, under some variable-amplitude loading conditions and the load-reduction schemes used for threshold testing, the crack closes first and opens last away from the tip. Under these conditions, the stress-intensity factor method was inadequate. The crack-surface displacement method was more accurate in calculating the applied stress level at which the crack surfaces open completely under general cyclic loading. In this paper, the displacement method was used to calculate S_o and is presented in Appendix B.

The closure model was only used to calculate crack-opening stresses. In turn, the crack-opening stress was used to calculate the plastic-zone corrected effective stress-intensity factor range and then the crack-growth rate.

Plastic-Zone Corrected Effective Stress-Intensity Factor Range

Elber's effective stress-intensity factor range [13] is based on linear-elastic stress-intensity factors. For small cracks and high stress levels, the plastic-zone sizes are no longer small compared to crack size, and linear-elastic analyses are inadequate. To correct the analyses for plasticity, the Dugdale plastic-zone length (ρ) is added to crack length (c), like Irwin's plastic-zone correction [28]. Thus, the plastic-zone corrected stress-intensity factor range is

$$\Delta\bar{K} = \left(S_{max} - S_{min}\right) \sqrt{\pi d}\, F\left(\frac{r}{d}, \frac{r}{w}, \frac{d}{w}\right) \tag{1}$$

where $d = c + \rho$ and ρ is calculated at the maximum applied stress, S_{max}, using the equations given in Appendix C. The boundary-correction factor F accounts for the influence of hole radius and specimen width, and is given by the product of the functions F_h^s and F_w^s. These functions are given in Appendix A, by Eqs. (6) and (22), respectively. (This parameter, $\Delta\bar{K}$, is similar to Barenblatt's cohesive modulus [30] under cyclic loading.)

The plastic-zone corrected effective stress-intensity factor range was obtained from Eq. (1) by replacing S_{min} by S_o, like Elber's modification, and is given by

$$\Delta\bar{K}_{eff} = U\,\Delta\bar{K} = \frac{S_{max} - S_o}{S_{max} - S_{min}}\,\Delta\bar{K} \tag{2}$$

Fatigue Crack Growth Rates

Instead of using an equation to relate the crack-growth rates to $\Delta\bar{K}_{eff}$, a table-lookup procedure was used in this paper. The primary advantage in using a table is that the baseline crack-growth rate data can be described more accurately than with a

multi-parameter equation, especially in the transitional region (flat to slant crack growth). To illustrate the construction and use of the table, an example is shown. 6-5

Center-crack tension (CCT) specimens (w = 80 mm) were used to obtain crack-growth rate data on 2024-T3 Alclad aluminum alloy sheet (t = 2 mm) material [5]. The tensile strength (σ_u) and the assumed flow stress (σ_o) of the material were 475 MPa. The maximum applied stress level S_{max} was 77.5 MPa at an R ratio of 0.01. A plot of log dc/dN against log ΔK was constructed. The ΔK values at selected crack-growth rates are listed in the following table:

$\frac{dc}{dN}$, mm/cycle	ΔK, MPa-$m^{1/2}$	$\Delta\bar{K}$, MPa-$m^{1/2}$	$\frac{S_o}{S_{max}}$	$\Delta\bar{K}_{eff}$, MPa-$m^{1/2}$
7.6E-06	6.59	6.70	0.571	2.90
3.0E-05	8.79	8.95	.596	3.65
4.3E-05	12.64	12.86	.597	5.23
6.8E-05	14.29	14.58	.596	5.95
1.2E-04	17.58	18.06	.600	7.30
3.8E-04	19.78	20.20	.599	8.18
1.3E-03	25.28	25.88	.594	10.61
7.6E-03	36.27	38.25	.578	16.30

The rates were selected so that straight lines between each adjacent data point would describe the ΔK-rate data using a visual fit.

Next, the plastic-zone corrected stress-intensity factor, $\Delta\bar{K}$, was computed from Eq. (1) with the plastic-zone size given by Eq. (31). The constraint factor (α) was assumed to be unity because most of the data had rates higher than the rate at transition (about 3 x 10^{-5} mm/cycle). For small ΔK levels, $\Delta\bar{K}$ is given approximately by

$$\Delta\bar{K} \approx \Delta K \sqrt{\sec\left(\frac{\pi S_{max}}{2\alpha\sigma_o}\right)} \qquad (3)$$

A closure analysis was then conducted on a CCT specimen subjected to a maximum applied stress (S_{max}) of 77.5 MPa with an R ratio of 0.01. The initial crack length was 1.5 mm. Crack-opening stresses were calculated as a function of crack length from the model. The crack-opening stress for each value of ΔK is listed in the table. Values of $\Delta\bar{K}_{eff}$ were computed from Eq. (2). The table of dc/dN against $\Delta\bar{K}_{eff}$ forms the crack-growth rate data used in all predictions made on this material and thickness. The crack-growth rates at intermediate values of $\Delta\bar{K}_{eff}$ were obtained by assuming a power-law equation, $C_1\,\Delta\bar{K}_{eff}^{C_2}$, between the two adjacent data points. For $\Delta\bar{K}_{eff}$ values outside of the table, the power-law equation between the two closest data points was extrapolated.

APPLICATION OF THE CRACK-CLOSURE ANALYSIS

The analytical closure model is used to calculate crack-opening stresses under constant-amplitude loading and under the load-reduction schemes used for threshold testing. Some comparisons are made between calculated and experimental crack-opening stresses for these loading conditions on a steel and an aluminum alloy.

Crack-growth rates under constant-amplitude loading for large cracks (c > 2 mm) in a steel, an aluminum alloy, and a cast (nickel-aluminum-bronze) alloy are correlated with the plastic-zone corrected effective stress-intensity factor range. Using these correlations, the growth rates for small cracks in plates or at circular holes are predicted and compared with experimental growth rates.

Constant-Amplitude Loading

To show how the crack-opening stress influences the local crack-tip displacements under constant-amplitude loading, and consequently the crack-tip damage or crack growth, the applied stress (S) is plotted against the displacement (V_c) of the crack-tip element in Figure 4. The maximum applied stress was $0.4\sigma_o$ and the specimen was cycled at an R ratio of zero. Recalling that the elements in the plastic zone are rigid-perfectly plastic, no change in displacement occurs until the element yields. The calculated crack-opening stress from the displacement method (Appendix B) is shown as the solid symbol on the loading branch. These results demonstrate the significance of crack closure, in that all cyclic loads below S_o would cause no plastic deformation at the crack tip and, presumably, no crack growth. These results also show that the crack opens before the crack-tip element yields. This was caused by the finite stress concentration

in the model (elastic stress concentration was about 30). If the model had had an infinite stress concentration, like an ideal crack, then the element would have yielded when the crack tip opened. Likewise, compressive yielding occurred only after some unloading. The crack-closure stress (S_c) is shown as the solid symbol on the unloading branch. S_c is the stress level at which the first crack-surface element at the crack tip closes. In this example, the crack was not allowed to grow during the loading branch. If the crack had been allowed to grow, then closure would have occurred over the newly created crack surface after a smaller amount of unloading.

The closure model was exercised under simulated plane-stress and plane-strain conditions for constant-amplitude loading. The calculated S_o values for the CCT specimen remained nearly constant over a very wide range of crack lengths [25]. This constant value is called the "stabilized" crack-opening stress. The stabilized crack-opening stresses, normalized by S_{max}, are plotted against stress ratio for various stress levels in Figure 5. The calculations were made on CCT specimens made of an aluminum alloy, but the results also apply for steels and titanium alloys when the material behavior is elastic-perfectly plastic. At any R ratio, the S_o/S_{max} values are lower for higher values of α and for higher values of stress level (S_{max}/σ_o). The influence of stress level was more pronounced under plane-stress conditions (solid curves) than under plane-strain conditions (dashed curves).

Threshold Testing

Because many of the comparisons between the growth of small and large cracks have been made in the crack-growth rate region associated with thresholds for large cracks, it is important to know whether the threshold is a material behavior or is caused by the load-reduction scheme. Some load-reduction schemes used to obtain ΔK_{th} are shown in Figure 6. The ratio of current load (or stress) to the initial load (or stress) is plotted against crack length. The crack length at initiation of the load-reduction scheme was 20 mm in a CCT specimen (w = 100 mm). The solid curve from Bucci [17] (proposed ASTM test method) is based on a constant rate of change in normalized plastic-zone size with crack extension and is independent of the R ratio. The normalized K-gradient, $(dK/dc)/K$, was -0.08 mm^{-1}, as recommended. The dashed curves show the load-reduction scheme proposed by Ohta et al. [19] for R = 0 and 0.8. Their scheme is based on a constant ΔK-gradient, $d(\Delta K)/dc$. The ΔK-gradient ranged from -20 to -100 MPa/$mm^{1/2}$. The smallest ΔK-gradient was used in Figure 6. The step function was proposed by Robin and Pluvinage [16]. The load was reduced by 10 percent after 0.2 mm of crack extension. The crack extension was large enough for the crack to traverse the plastic zone created by the previous load.

As previously mentioned, several investigators [18-20] have experimentally shown that the stress-intensity factor threshold under load-reduction schemes can be explained by the crack-closure behavior. Some typical results on an aluminum alloy are shown in Figure 7. Minakawa and McEvily [31] conducted a threshold test on a compact specimen and measured the crack-opening loads as the ΔK level approached ΔK_{th}. The crack-opening loads were determined from a displacement gage at the edge of the compact specimen. This location was remote from the crack tip. For high ΔK levels, the P_o/P_{max} values ranged from 0.15 to 0.35. The horizontal line is the calculated P_o/P_{max} ratio from the closure model under constant-amplitude loading with plane-strain conditions (α = 3). The calculated ratio agreed fairly well with the experimental values. As ΔK approached ΔK_{th}, the P_o/P_{max} ratio rapidly rose and the ratio was nearly unity at threshold. Thus, the rise in crack-opening load explains why the threshold developed. But what caused the rise in crack-opening loads? A number of suggestions have been advanced to explain this behavior. Among these are the mismatch of crack-surface features observed by Walker and Beevers [32] in a titanium alloy; the corrosion product formation on the crack surfaces, as observed by Paris et al. [33] and Ritchie et al. [34]; and the variation in the mode of crack growth with stress-intensity factor level as reported by Ohtsuka et al. [35], and Minakawa and McEvily [31]. The mismatch of crack-surface features and corrosion products on the crack surfaces could cause the surfaces to come into contact at a higher load than the load for a crack without the mismatch or corrosion products. The mode of crack growth near threshold is a combination of Mode I and Mode II (tensile and shear) instead of pure Mode I. The mixed-mode crack growth causes an irregular crack surface profile and, consequently, the possibility of crack-surface mismatch. The analytical treatment of crack closure due to crack-surface mismatch or corrosion products on the crack surface is beyond the scope of the present paper.

However, now consider the influence of the load-reduction scheme on crack closure. Using the closure model, a simulated threshold test was conducted on a CCT specimen made of steel using Bucci's load-reduction scheme [17]. The material flow stress was 800 MPa and the constraint factor was assumed to be unity. The applied load (or applied stress) against crack length is shown by the solid curve in Figure 6 at an R ratio of zero. The crack length at initiation of the load-reduction scheme (c_i) was 20 mm. As the applied stress was reduced with crack extension, the closure model predicted a rise in crack-opening stress. To find out why the crack-opening stress rose, the crack-tip displacements during a single cycle are shown in Figure 8. The figure shows applied stress normalized by the maximum applied stress plotted against displacement of the crack-tip element, similar to that shown in Figure 4 for constant-amplitude loading. Again, the crack-opening stress is shown by the solid symbol on the loading branch. Here, the crack-opening stress is higher than the value calculated for constant-amplitude loading (shown by the dashed line). In contrast to the closure behavior under constant-amplitude loading, in the threshold test the crack did not close near the crack tip but did close

away from the crack tip, as illustrated in the insert. The insert shows a schematic of the crack-surface displacements near threshold. The shaded region around the crack depicts the residual plastic deformations left in the wake of the growing crack. The largest residual deformations occur along the crack at about c_i and, consequently, the crack-opening stress is controlled by the displacements in this region. These displacements tend to prop the crack open at the tip. Figure 8 shows that the crack-tip element does not change in displacement until after the crack surfaces are fully open. During unloading, S_c' shows the applied stress level at which the crack surfaces close away from the tip and S_c shows the applied stress level at which the crack tip closes.

Ohta et al. [19] tested CCT specimens made of HT80 steel (t = 10 mm) over a wide range of R ratios (-1 to 0.8) to determine crack-growth rates down to threshold and to measure crack-opening stresses. They used the Ohta-Sasaki load-reduction scheme (dashed curves shown in Fig. 6) and a small crack-tip displacement gage to measure S_o values. Some typical results on crack-opening stresses for R = 0 are shown in Figure 9. The S_o/S_{max} ratio is plotted against ΔK level during the load-reduction scheme. The crack-opening ratio was constant down to a ΔK level of about 15 MPa-$m^{1/2}$. Near this level, the ratio rapidly rose as the applied loads were reduced and a threshold developed at about 7 MPa-$m^{1/2}$. The solid curves show calculations from the closure model with α = 1 and 1.73. The plane-stress calculations are in good agreement with the experimental data down near threshold. Because their crack-closure measurements were made on the surface of the specimen, their results should be close to those for plane-stress conditions. Similar comparisons at R = 0.8 and -1 show similar agreement between plane-stress calculations and measurements (not shown).

But crack closure near the free surfaces of a specimen may not control the overall growth rate through the thickness of a specimen. In fact, the crack-opening stresses vary through the thickness of a specimen [36]. Thus, the overall growth rate at low ΔK values may be controlled by a higher constraint factor than that of plane stress. To determine the proper constraint factor, a three-dimensional analysis would be required. However, the correlation of crack-growth rate data at various stress ratios could also be used to experimentally determine an approximate constraint factor [37]. Using a plot of ΔK and rate for various R ratios, as shown in Figure 10(a) for the HT80 steel, the spread in the data as a function of R can be used to find the crack-opening stresses needed to correlate the R-ratio data on a $\Delta\bar{K}_{eff}$ and rate plot. Because crack-opening stresses are a function of constraint factor (see Fig. 5), an approximate constraint factor can be found to correlate the data. For the 10-mm-thick steel specimens at low ΔK levels, plane-strain conditions were expected to exist under constant-amplitude loading. Figure 10(b) shows a plot of $\Delta\bar{K}_{eff}$ and rate for the same HT80 steel data using a closure analysis under plane-strain conditions (α = 3). Curves were drawn through the data for each R ratio. Growth rates above 5 x 10^{-6} mm/cycle, basically generated under constant-amplitude loading, correlated quite well under plane-strain conditions even for high ΔK values. But the threshold data showed systematic variations with $\Delta\bar{K}_{eff}$. Recalling how well the closure analysis under plane-stress conditions (α = 1) predicted threshold behavior under a load-reduction scheme (see Fig. 9), the growth rate data on the HT80 steel were replotted in Figure 11 using a closure analysis with α = 1 (Fig. 11(a)) and α = 3 (same as Fig. 10(b)). These results show that plane-stress closure is controlling the growth rates near threshold under a load-reduction scheme.

Apparently, the plane-stress regions near the free surfaces of a specimen play an important role on crack-closure effects under load-reduction schemes and variable-amplitude loading. McEvily [38] conducted experiments to confirm the importance of crack closure near the free surfaces. He found, in a test on a 6061 aluminum alloy specimen (t = 12.7 mm), that a spike load caused significant crack-growth delay. In a second test, he carefully machined 25 percent of the thickness from each surface of the specimen after the application of the spike load and found very little crack-growth delay. Thus, the crack-closure effect under spike loading is predominantly a surface phenomenon.

As shown by Figures 7 through 11, the threshold behavior observed in load-reduction schemes [15-17] is caused by a rise in the crack-opening stresses, and the rise is caused by residual plastic deformations left in the wake of the growing crack. Thus, load-reduction schemes create artifically high values of stress-intensity factor thresholds, and the crack-growth rate data generated under these load-reduction schemes cannot be used in an LEFM analysis to predict the growth of small cracks. To obtain crack-growth rate data at low ΔK levels using large cracks, the threshold testing procedures must be changed. The residual deformations on the crack surfaces near the beginning of a threshold test must be eliminated (see insert in Fig. 8). The deformations could be machined away during the test or large compressive loads could be applied to the specimen to remove this deformation. The specimen could also have been side-grooved to eliminate plane-stress conditions at the crack front.

Growth of Small Cracks

In the following sections, the crack-growth rates measured in specimens with large cracks (c > 2 mm) are correlated with the plastic-zone corrected stress-intensity factor range, $\Delta\bar{K}_{eff}$. This correlation, a table of $\Delta\bar{K}_{eff}$ against dc/dN, provides the crack-growth rate data for the particular material and thickness. Using the closure model with an assumed constraint factor, the crack-growth rates for small cracks in plates and from holes are predicted and compared with experimental rates. All initial cracks are assumed to have no previous load history (no residual deformations).

6-8

CSA G40.11 Steel.- El Haddad [3] tested CCT and single-edge-crack tension (SECT) specimens made of the CSA G40.11 steel under cyclic loading at an R ratio of -1. The material yield stress was 370 MPa and the ultimate tensile strength was 510 MPa. All specimens were 2.54 mm thick. These tests were conducted to study the growth characteristics of small and large cracks.

The ΔK-rate data for the SECT specimens with large cracks are shown in Figure 12 as solid symbols. Because the closure model has not been developed for SECT specimens, the data were assumed to be equivalent to data generated on CCT specimens. (El Haddad's data on CCT specimens, to be shown later, were in good agreement with the SECT specimen data.) The solid lines through the SECT specimen data in Figure 12 show the baseline (ΔK-rate) data. To determine $\Delta\bar{K}_{eff}$, a closure analysis on a CCT specimen (S_{max} = 135 MPa; α = 1) was conducted. The corresponding crack-growth table is:

$\frac{dc}{dN}$, mm/cycle	$\Delta\bar{K}_{eff}$, MPa-$m^{1/2}$
2.24E-06	6.53
1.02E-05	7.69
4.70E-05	9.78
1.02E-04	12.62
1.93E-04	17.29
3.18E-04	22.46
6.60E-04	34.20
1.52E-03	58.31

This table was used in all predictions made on the CSA G40.11 steel.

El Haddad [3] tested CCT specimens with small cracks at high stress levels (207 and 240 MPa). The crack-starter notch was a very small hole (r = 0.19 mm), but no details were given on how the crack was initiated. These results are shown as the open symbols in Figure 12 and show that small cracks grow much faster than large cracks at the same ΔK level.

In the closure analysis, an extremely small through crack (0.01 mm) was assumed to exist at the edge of the starter notch. The constraint factor was assumed to be unity because the specimens were subjected to high stress levels. The predicted growth rates are shown as solid curves in Figure 12. The predictions are in fair agreement with the experimental results. Both experimental and predicted results show a minimum rate at a particular ΔK level. In the analysis, this behavior was caused by the transient behavior of the crack-opening stresses shown in Figure 13. Here the calculated S_o/S_{max} ratios are plotted against crack length for the two tests. The calculated crack-opening stress was initially the minimum applied stress, but the opening stress rapidly rose and then tended to level off as the crack grew under cyclic loading. Truyens [39] has experimentally shown a similar trend in S_o with crack length in a ship steel. The effective-stress range (ΔS_{eff}), indicated in the figure, was $S_{max} - S_o$. Crack-growth rates are directly related to ΔS_{eff}. As the crack grew, the decrease in ΔS_{eff} and the increase in crack length (increase in stress-intensity factor) combined to cause the unusual behavior shown in Figure 12. Truyens [39] also observed a similar trend in crack-growth rates.

El Haddad [3] also tested specimens with cracks emanating from larger holes than that used in the previous example. The hole radii were 4.76 and 7.94 mm in 70-mm-wide specimens. The maximum applied stress was 135 MPa at an R ratio of -1. His experimental data on the cracked-hole specimens are shown as open symbols in Figure 14. The solid symbols show his results from CCT specimens also tested at an applied stress level of 135 MPa. These results show that small cracks from holes grow much faster than would be predicted from using LEFM analyses with large crack data.

In the analysis, the baseline (ΔK-rate) data were obtained from large cracks in CCT and SECT specimens. The solid lines through the CCT specimen data in Figure 14 show the baseline data. Here again, no details on the crack-starter notch were given in Reference 3. Therefore, it was assumed that a very small through-crack (0.01 mm) was at the edge of the holes. The solid curves in Figure 14 show predictions from the closure analysis with α = 1. The predicted rates were in reasonable agreement with the experimental data. For cracks emanating from holes, the transient behavior of the crack-opening stresses (similar to that shown in Fig. 13) and the plastic-zone corrected stress-intensity factor range combined to cause the trends shown in Figure 14.

Alclad 2024-T3 Aluminum Alloy.- Broek [5] tested center-crack and cracked-hole specimens made of 2024-T3 Alclad aluminum alloy subjected to tensile loading at an R ratio of 0.01. The yield stress of the material was 375 MPa and the ultimate tensile strength was 475 MPa. All specimens were 2 mm thick. The ΔK-rate data are shown in Figure 15 for the CCT specimens and for specimens with small cracks emanating from holes of various radii, ranging from 2.5 to 20 mm. Again, these results show that small cracks from holes grow faster than would be predicted using an LEFM analysis with large crack data on CCT specimens.

In the closure analysis, the constraint factor was assumed to be unity because most of the rates were above the rate at transition (flat to slant growth). The rate at transition was estimated to be about 3×10^{-5} mm/cycle (first knee in baseline data at about 9 MPa-$m^{1/2}$). The development of the crack-growth rate table was discussed and was included in the section on "Fatigue Crack Growth Rates." The predicted results for small cracks at holes are shown as solid curves in Figure 15. Solid and open symbols of the same type denote corresponding predictions and experiments. For small radii, the analysis underpredicted the growth rates; for the larger radii, the analysis overpredicted the rates. In all cases, the predicted rates were within about a factor of 2 of the experimental rates.

Cast Nickel-Aluminum-Bronze Alloy.- Taylor and Knott [10,40] tested through-cracks and small surface cracks under three-point bending at an R ratio of 0.1. The material yield stress was 250 MPa. The ultimate tensile strength was not reported in References 10 or 40, and the strength was estimated to be 550 MPa [41]. Most of the surface-crack tests were conducted with a maximum outer fiber stress of 330 MPa [40]. The small surface cracks were naturally-occurring cracks from casting defects on the surface of the specimens. Some of the largest defects shown on photomicrographs [10,40] had lengths (2c) ranging from 0.05 to 0.15 mm. The ΔK-rate data for the surface-crack specimens are shown as open symbols in Figure 16. Reference 10 did not give the particular test conditions for each surface-crack test, but the test conditions were assumed to be identical. Thus, the data show a lot of scatter which is undoubtedly due to the cracks growing through different microstructure.

The solid curve showing the threshold at about 7.5 MPa-$m^{1/2}$ was obtained from bend specimens with large through-cracks. The results on large cracks and small surface cracks show that small cracks grow at ΔK levels well below the threshold established from large crack tests. (Again, the details of the large crack tests were not reported in References 10 or 40.)

Because crack-growth rate data generated under load-reduction schemes (see comments in section on "Threshold Testing") cannot be applied to the growth of small cracks [2], the dash-dot curve was assumed to be the baseline data. In the closure analysis, the constraint factor was assumed to be either 1 (plane stress) or 3 (plane strain). The crack-growth rate table for the corresponding constraint factors is:

$\frac{dc}{dN}$, mm/cycle	$\Delta\bar{K}_{eff}(\alpha = 1)$, MPa-$m^{1/2}$	$\Delta\bar{K}_{eff}(\alpha = 3)$, MPa-$m^{1/2}$
2.54E-09	1.62	2.55
2.77E-06	5.88	9.28
6.59E-06	6.84	10.78
1.31E-05	7.71	12.18
3.19E-05	9.23	14.58
7.59E-05	11.07	17.46

The closure analysis has only been developed for through-the-thickness crack configurations. To analyze the growth of a small surface crack under bending, the analysis for the CCT specimen was used with modification. In the analysis, the CCT specimen was subjected to an applied stress level equal to the outer fiber bending stress. For small surface cracks, this assumption is adequate [42]. The crack-depth-to-crack-length (a/c) ratios for the experiments were reported to be about 0.8 [10]. For this a/c ratio and for small surface cracks (a/t nearly zero), the average stress-intensity factor around the crack front is about

$$\Delta K = \Delta S \sqrt{\pi c}\ 0.7 \qquad (4)$$

Thus, the stress-intensity factor for the CCT specimen was multiplied by 0.7 to convert the equation to a small surface crack under bending. The crack-opening stresses calculated for a center-crack specimen were also assumed to apply for the surface-crack configuration.

The predicted results for small surface cracks are shown as solid curves in Figure 16 for the respective values of α. The plane-strain predictions were closer to the experimental results than the plane-stress predictions. However, under plane-strain conditions, the initial high growth rate (solid symbol) was considerably lower than the experimental rates. This discrepancy may be due to the crack growing in some "weak" direction in the microstructure in the early stages [10].

CONCLUSIONS

An analytical fatigue crack-closure model was used to study the crack growth and closure behavior of small cracks in plates and at circular holes, and to study the closure

behavior of large cracks under load-reduction schemes used in threshold testing. Some comparisons were made between calculated and experimental crack-opening stresses for these loading conditions on a steel and an aluminum alloy.

Crack-growth rates under constant-amplitude loading for large cracks (lengths greater than 2 mm) in a steel, an aluminum alloy, and a cast nickel-aluminum-bronze alloy were correlated with the plastic-zone corrected effective stress-intensity factor range. Using these correlations, the growth rates for small cracks in plates and at circular holes were predicted and compared with experimental growth rates.

The following conclusions were obtained:

1. Under load-reduction schemes used in threshold testing, the rise in crack-opening stresses near threshold is caused by residual plastic deformations. Thus, load-reduction schemes create artificially high values of stress-intensity factor thresholds.

2. Near threshold, the calculated crack-opening stresses under plane-stress conditions agreed well with experimental measurements on steel specimens.

3. Crack-growth rate data generated under load-reduction schemes for large cracks cannot be used with linear-elastic fracture mechanics analyses to accurately predict the growth of small cracks.

4. Small cracks (less than 1 mm) in plates and at holes grow faster than large cracks (greater than 2 mm) at equal stress-intensity factor ranges because the applied stress needed to open a small crack is less than that needed to open a large crack and, consequently, the effective stress range for small cracks is greater than that for large cracks.

5. Closure analyses based on plastic-zone corrected effective stress-intensity factor ranges and crack-growth rate data from large cracks predicted the growth of small cracks in plates and at holes reasonably well.

APPENDIX A--EQUATIONS FOR STRESS-INTENSITY FACTORS AND CRACK-SURFACE DISPLACEMENTS

The analytical closure model for a crack in a finite plate [25] and for cracks emanating from a circular hole in a finite plate requires the stress-intensity factor and crack-surface displacement equations for the two elastic configurations shown in Figure 17. The equations for stress-intensity factors and crack-surface displacements for a crack subjected to various loading in an infinite plate ($r = 0$) were obtained from the literature [43]. These equations are modified herein for cracks emanating from a circular hole in a finite plate. Some of the approximate equations are verified with boundary-collocation [44,45] and conformal-mapping [46,47] analyses.

Stress-Intensity Factors for Cracks Emanating from a Circular Hole in an Infinite Plate

Remote Uniform Stress.- The stress-intensity factor equation for the configuration shown in Figure 17(a), with w equal to infinity, was obtained by fitting to the results from References 45 and 47. The equation is

$$K_h^s = K_\infty^s F_h^s = S\sqrt{\pi d}\, F_h^s \tag{5}$$

where K_∞^s is for a crack in an infinite plate without a hole and F_h^s is the boundary-correction factor for the circular hole. The equation for F_h^s is

$$F_h^s = \sqrt{1 - \frac{r}{d}}\, f_n \tag{6}$$

where $n = 1$ is for a single crack and $n = 2$ is for two symmetric cracks. The functions f_n are

$$f_1 = 0.707 + 0.765\lambda + 0.282\lambda^2 + 0.74\lambda^3 + 0.872\lambda^4 \tag{7}$$

and

$$f_2 = 1 + 0.358\lambda + 1.425\lambda^2 - 1.578\lambda^3 + 2.156\lambda^4 \tag{8}$$

where $\lambda = r/d$ and $0 \le \lambda < 1$. Eq. (5) is within 0.2 percent of the results in References 45 and 47.

Concentrated Force.- The stress-intensity factors for two cracks emanating from a circular hole subjected to a symmetric pair of concentrated forces in an infinite plate,

Figure 18, were obtained from a boundary-collocation analysis by Newman (unpublished). An equation was fitted to the results and is 6-11

$$K_h^P = K_\infty^P F_h^P = \frac{2Pd}{\sqrt{\pi d\left(d^2 - b^2\right)}} F_h^P \tag{9}$$

where K_∞^P is for a crack in an infinite plate without a hole and F_h^P is the boundary-correction factor for the circular hole. The equation for the correction factor is

$$F_h^P = 1 + A_1\left(\frac{1 - \gamma}{1 - \lambda}\right) + A_2\left(\frac{1 - \gamma}{1 - \lambda}\right)^2 \tag{10}$$

$$A_1 = -0.02\lambda^2 + 0.558\lambda^4 \tag{11}$$

$$A_2 = 0.221\lambda^2 + 0.046\lambda^4 \tag{12}$$

where $\gamma = b/d$ and $\lambda = r/d$ for $\lambda \le \gamma \le 1$ and $0 \le \lambda < 1$. Eq. (9) is within ±1 percent of the boundary-collocation results.

Partially-Loaded Crack.- The stress-intensity factors for the configuration and loading shown in Figure 17(b), with $w = \infty$, were obtained by using Eq. (9) as a Green's function and integrating over the segment b_1 to b_2. The resulting equation is

$$K_h^\sigma = \frac{2\sigma}{\pi}\sqrt{\pi d}\, G(\gamma,\lambda) \tag{13}$$

where

$$G(\gamma,\lambda) = \left\{\left[1 + \frac{A_1}{1 - \lambda} + \frac{3A_2}{2(1 - \lambda)^2}\right]\sin^{-1}\gamma + \left[\frac{A_1}{1 - \lambda} + \frac{(4 - \gamma)A_2}{2(1 - \lambda)^2}\right]\sqrt{1 - \gamma^2}\right\}\Bigg|_{\gamma = b_1/d}^{\gamma = b_2/d} \tag{14}$$

A_1 and A_2 are given by Eqs. (11) and (12), respectively. To get Eq. (13) into the same form as Eqs. (5) and (9), Eq. (13) is rewritten as

$$K_h^\sigma = K_\infty^\sigma F_h = \frac{2\sigma}{\pi}\sqrt{\pi d}\left[\sin^{-1}\left(\frac{b_2}{d}\right) - \sin^{-1}\left(\frac{b_1}{d}\right)\right] F_h^\sigma \tag{15}$$

where K_∞^σ is for a crack in an infinite plate without a hole and F_h^σ is the circular hole correction factor. The function F_h^σ is given by

$$F_h^\sigma = \frac{G(\gamma,\lambda)}{\sin^{-1}\left(\frac{b_2}{d}\right) - \sin^{-1}\left(\frac{b_1}{d}\right)} \tag{16}$$

where $G(\gamma,\lambda)$ is given by Eq. (14).

Crack-Surface Displacements for Cracks Emanating from a Circular Hole in an Infinite Plate

The exact crack-surface displacements for the configurations shown in Figure 17, with w equal to infinity and hole radius equal to zero, were obtained from Westergaard stress functions given in Reference 43. These equations are modified herein for cracks emanating from a circular hole. The following sections given approximate displacement equations for remote uniform stress and for the partially-loaded crack.

Remote Uniform Stress.- The approximate crack-surface displacements for the configurations shown in Figure 17(a), with $w = \infty$, are

$$v_h^s = \frac{2\left(1 - \eta^2\right)s}{E}\sqrt{d^2 - x^2}\, F_h^s \tag{17}$$

for $|x| \le d$, where $\eta = \nu$ for plane strain and $\eta = 0$ for plane stress. F_h^s is given by Eq. (6). In the region near the crack tip, Eq. (17) is very accurate.

Partially-Loaded Crack.- The approximate crack-surface displacements for the configuration and loading shown in Figure 17(b), with $w = \infty$, are

6-12

$$V_h^\sigma = [V_\infty(x) + V_\infty(-x)] F_h^\sigma \tag{18}$$

where

$$V_\infty(x) = \frac{2(1 - \eta^2)\sigma}{\pi E}\left[(b - x)\cosh^{-1}\left(\frac{d^2 - bx}{d|b - x|}\right) + \sqrt{d^2 - x^2}\sin^{-1}\left(\frac{b}{d}\right)\right]\Bigg|_{b = b_1}^{b = b_2} \tag{19}$$

for $|x| \le d$, and F_h^σ is given by Eq. (16). Again, the equation is very accurate in the region near the crack tip.

Finite-Width Corrections

The equations given in the preceding sections for stress-intensity factors and crack-surface displacements (Eqs. (5) to (19)) are for cracks emanating from a circular hole in an infinite plate. But these quantities are influenced by the finite width of the plate. Therefore, some approximate finite-width corrections are developed herein. The stress-intensity factor for a crack in a finite-width plate is

$$K = K_\infty F_w \tag{20}$$

where K_∞ is the stress-intensity factor for cracks emanating from a circular hole in an infinite plate and F_w is the finite-width correction for the particular loading condition. Noting that the elastic crack-surface displacements in the region of the crack tip are directly related to the stress-intensity factor, it is proposed that the same correction factor be used for displacements:

$$V = V_\infty\left(\frac{K}{K_\infty}\right) = V_\infty F_w \tag{21}$$

where V_∞ is the displacement for cracks emanating from a circular hole in an infinite plate, again subjected to the particular loading condition. Eq. (21) gives very accurate crack-surface displacements in the region near the crack tip.

Remote Uniform Stress.- The approximate boundary-correction factor for two symmetric cracks emanating from a circular hole in a finite-width plate subjected to uniform stress [48], as shown in Figure 17(a), is

$$F_w^s = \sqrt{\sec\left(\frac{\pi r}{2w}\right)\sec\left(\frac{\pi d}{2w}\right)} \tag{22}$$

for $r/w \le 0.5$ and $d/w \le 0.7$. Eq. (22) is within ±2 percent of boundary-collocation results [45]. The equation accounts for the influence of width on stress concentrations at the edge of the hole [49] and the influence of width on stress-intensity factors. The crack-surface displacements given by Eqs. (17), (21), and (22) for $r = 0$ were compared with results from Reference 44, which used the boundary-collocation method. The displacements were within 2 percent of each other for any value of x for $d/w \le 0.7$. The displacements near the crack tip were very accurate, as expected.

Partially-Loaded Crack.- The approximate boundary-correction factor for two symmetric cracks emanating from a circular hole in a finite-width plate subjected to partial loading on the crack surface (Fig. 17(b)) was obtained from the infinite periodic array of cracks ($r = 0$) solution [43]. The correction factor is modified herein, as was done in Reference 25, and is given by

$$F_w^\sigma = \left[\frac{\sin^{-1} B_2 - \sin^{-1} B_1}{\sin^{-1}\left(\frac{b_2}{d}\right) - \sin^{-1}\left(\frac{b_1}{d}\right)}\right]\sqrt{\sec\left(\frac{\pi d}{2w}\right)} \tag{23}$$

where

$$B_k = \sin\left(\pi b_k/2w\right)/\sin\left(\pi d/2w\right) \tag{24}$$

for $r/w \le 0.25$ and $d/w \le 0.7$.

APPENDIX B--CALCULATION OF CRACK-OPENING STRESS

6-13

The following section describes the method used to calculate the crack-opening stresses in the analytical closure model. To find the applied stress level needed to open the crack surface at any point, the displacement at that point due to an applied stress increment $(S_o - S_{min})$ is set equal to the displacement at that point due to the contact stresses at S_{min}. This calculation is made at the centroid of all elements in contact along the crack surface. The maximum value of $(S_o - S_{min})$ gives the applied stress level at which the last element (in contact) separates (or opens). This approach is possible because the stresses on the elements are elastic until the crack-tip element yields. Crack-tip element yielding occurs only after the crack surfaces open (see Figs. 4 and 8).

The displacement at point i, along the crack surface, due to an applied stress increment is

$$V_i^S = (S_o - S_{min}) f(x_i) \tag{25}$$

where

$$f(x_i) = \frac{2(1 - \nu^2)}{E} \sqrt{c^2 - x_i^2}\, F_h^S F_w^S \tag{26}$$

F_h^S and F_w^S are given by Eqs. (6) and (22), respectively, with d replaced by c. The displacement at point i due to contact stresses is

$$V_i^\sigma = \sum_{j=11}^{n} \sigma_j g(x_i, x_j) \tag{27}$$

where

$$g(x_i, x_j) = G(x_i, x_j) + G(-x_i, x_j) \tag{28}$$

$$G(x_i, x_j) = \frac{2(1 - \nu^2)}{\pi E} \left\{ (b_2 - x_i) \cosh^{-1}\left(\frac{c^2 - b_2 x_i}{c|b_2 - x_i|}\right) - (b_1 - x_i) \cosh^{-1}\left(\frac{c^2 - b_1 x_i}{c|b_1 - x_i|}\right) + \sqrt{c^2 - x_i^2}\left[\sin^{-1}\left(\frac{b_2}{c}\right) - \sin^{-1}\left(\frac{b_1}{c}\right)\right] \right\} F_h^\sigma F_w^\sigma \tag{29}$$

$b_1 = x_j - w_j$ and $b_2 = x_j + w_j$ (w_j is the half width of bar element at point j). (In the closure model, 10 elements were used in the plastic zone and elements 11 to n were residual plastic deformation elements along the crack surface (see Ref. 25 for details).) F_h^σ and F_w^σ are given by Eqs. (16) and (23), respectively, again with d replaced by c. Equating Eqs. (25) and (27), and solving for $(S_o)_i$, gives

$$(S_o)_i = S_{min} + \sum_{j=11}^{n} \sigma_j g(x_i, x_j) \Big/ f(x_i) \tag{30}$$

for i = 11 to n. The maximum value of $(S_o)_i$ gives the crack-opening stress, S_o.

APPENDIX C--CALCULATION OF PLASTIC-ZONE SIZE

Center-Crack Tension Specimen

The plastic-zone size (ρ) for a crack in a finite-width specimen (Fig. 2(a)) was obtained from Rice [50] and rederived by Newman [25] as

$$\rho = c\left\{\left(\frac{2w}{\pi c}\right)\sin^{-1}\left[\sin\left(\frac{\pi c}{2w}\right)\sec\left(\frac{\pi S_{max}}{2\alpha\sigma_o}\right)\right] - 1\right\} \tag{31}$$

For $\alpha = 1$, the equation reduces to the expression derived by Rice from an infinite periodic array of cracks solution. Newman derived the equation from approximate stress-intensity factor equations for finite-width specimens.

Cracked-Hole Specimen

The plastic-zone size for cracks emanating from a circular hole in a finite-width specimen (Fig. 2(b)) was determined by requiring that the finiteness condition of Dugdale [26] be satisfied. This condition states that the stress-intensity factor at the tip of the plastic zone is zero and is given by

$$K_h^s + K_h^\sigma = 0 \tag{32}$$

where

$$K_h^s = S_{max}\sqrt{\pi d}\, F_h^s F_w^s \tag{33}$$

and

$$K_h^\sigma = -\frac{2\alpha\sigma_o}{\pi}\sqrt{\pi d}\left[\frac{\pi}{2} - \sin^{-1}\left(\frac{c}{d}\right)\right] F_h^\sigma F_w^\sigma \tag{34}$$

F_h^s and F_w^s are given by Eqs. (6) and (22), respectively. F_h^σ and F_w^σ were obtained from Eqs. (16) and (23), respectively, by setting $b_1 = c$ and $b_2 = d$. Substituting Eqs. (33) and (34) into Eq. (32) and simplifying gives

$$S_{max}F_h^s F_w^s - \alpha\sigma_o\left[1 - \frac{2}{\pi}\sin^{-1}\left(\frac{c}{d}\right)\right] F_h^\sigma F_w^\sigma = 0 \tag{35}$$

For a given applied stress S_{max}, constraint factor α, flow stress σ_o, specimen width w, hole radius r, and crack length c, Eq. (35) was solved for d by using an iterative technique. Noting that ρ is equal to $d - c$ gives the plastic-zone size.

The plastic-zone sizes for cracks emanating from a circular hole in an infinite plate subjected to remote uniform stress are shown in Figure 19. The plastic-zone size normalized by c is plotted against $S/(\alpha\sigma_o)$. The dashed curve ($r = 0$) shows the Dugdale model [26]. The solid curves show the normalized plastic-zone sizes for various c/r ratios. For c/r equal to unity, yielding does not occur for $S/(\alpha\sigma_o)$ ratios less than one-third or $1/K_T$, where K_T is the stress concentration for the circular hole.

REFERENCES

1. Pearson, S.: Initiation of Fatigue Cracks in Commercial Aluminum Alloys and the Subsequent Propagation of Very Short Cracks. Engineering Fracture Mechanics, Vol. 7, No. 2, 1975, pp. 235-247.

2. Kitagawa, H.; and Takahashi, S.: Applicability of Fracture Mechanics to Very Small Cracks or the Cracks in the Early Stage. Proceedings of the 2nd International Conference on Mechanical Behavior of Materials, Boston, MA, 1976, pp. 627-631.

3. El Haddad, M. H.: A Study of the Growth of Short Fatigue Cracks Based on Fracture Mechanics. Ph.D. Thesis, University of Waterloo, Waterloo, Ontario, Canada, 1978.

4. El Haddad, M. H.; Dowling, N. E.; Topper, T. H.; and Smith, K. N.: J Integral Applications for Short Fatigue Cracks at Notches. International Journal of Fracture, Vol. 16, No. 1, 1980, pp. 15-30.

5. Broek, D.: The Propagation of Fatigue Cracks Emanating from Holes. National Aerospace Laboratory, NLR Technical Report 72134U, 1972.

6. Morris, W. L.; James, M. R.; and Buck, O.: Growth Rate Models for Short Surface Cracks in Al 2219-T851. Metallurgical Trans. A, Vol. 12A, January 1981, pp. 57-64.

7. Hudak, S. J., Jr.: Small Crack Behavior and the Prediction of Fatigue Life. Journal of Engineering Materials and Technology, Vol. 103, 1981, pp. 26-35.

8. Nisitani, H.; and Takao, K. I.: Significance of Initiation, Propagation, and Closure of Microcracks in High Cycle Fatigue of Ductile Materials. Engineering Fracture Mechanics, Vol. 15, No. 3-4, 1981, pp. 445-456.

9. Schijve, J.: Difference Between the Growth of Small and Large Fatigue Cracks--The Relation to Threshold K-Values. Proceedings of the International Symposium on Fatigue Thresholds, Stockholm, Sweden, June 1981. (Also: Delft University of Technology Report LR-327, 1981.)

10. Taylor, D.; and Knott, J. F.: Fatigue Crack Propagation Behavior of Short Cracks--The Effects of Microstructure. Fatigue of Engineering Materials and Structures, Vol. 4, No. 2, 1981, pp. 147-155.

11. Leis, B. N.; and Forte, T. P.: Fatigue Growth of Initially Physically Short Cracks in Notched Aluminum and Steel Plates. Fracture Mechanics: Thirteenth Conference, Richard Roberts, ed., American Society for Testing and Materials, ASTM STP 743, 1981, pp. 100-124.

12. Elber, W.: Fatigue Crack Closure Under Cyclic Tension. Engineering Fracture Mechanics, Vol. 2, No. 1, 1970, pp. 37-45.

13. Elber, W.: The Significance of Fatigue Crack Closure. Damage Tolerance in Aircraft Structures, American Society for Testing and Materials, ASTM STP 486, 1971, pp. 230-242.

14. Paris, P. C.: Testing for Very Slow Growth of Fatigue Cracks. Closed Loop Magazine, MTS Systems Corporation, Vol. 2, No. 5, 1970.

15. Ohta, A.; and Sasaki, E.: A Method for Determining the Stress Intensity Threshold Level for Fatigue Crack Propagation. Engineering Fracture Mechanics, Vol. 9, No. 3, 1977, pp. 655-662.

16. Robin, C.; and Pluvinage, G.: Fatigue Threshold in a 2618A Aluminum Alloy. Fatigue of Engineering Materials and Structures, Vol. 3, 1980, pp. 147-157.

17. Bucci, R. J.: Development of a Proposed ASTM Standard Test Method for Near-Threshold Fatigue Crack Growth Rate Measurement. Fatigue Crack Growth Measurement and Data Analysis, S. J. Hudak, Jr., and R. J. Bucci, eds., American Society for Testing and Materials, ASTM STP 738, 1981, pp. 5-28.

18. Frandsen, J. D.; Inman, R. V.; and Buck, O.: A Comparison of Acoustic and Strain Gauge Techniques for Crack Closure. International Journal of Fracture, Vol. 11, No. 2, 1975, pp. 345-348.

19. Ohta, A.; Kosuge, M.; and Sasaki, E.: Fatigue Crack Closure Over the Range of Stress Ratios from -1 to 0.8 Down to Stress Intensity Factor Threshold Level in HT80 Steel and SUS 304 Stainless Steel. International Journal of Fracture, Vol. 14, No. 3, 1978, pp. 251-264.

20. Minakawa, K.; and McEvily, A. J.: On Crack Closure in the Near-Threshold Region. Scripta Metallurgica, Vol. 15, 1981, pp. 633-636.

21. Ritchie, R. O.: Effects of Strength and Grain Size on Near-Threshold Fatigue Crack Growth in Ultra-High Strength Steel. Proceedings of the Fourth International Conference on Fracture, Waterloo, Ontario, Canada, 1977, pp. 1325-1331.

22. Nordmark, G. E.; and Fricke, W. G.: Fatigue Crack Arrest at Low Stress Intensities in a Corrosive Environment. Journal of Testing and Evaluation, Vol. 6, No. 5, 1978, pp. 301-303.

23. Newman, J. C., Jr.: Finite-Element Analysis of Fatigue Crack Propagation--Including the Effects of Crack Closure. Ph.D. Thesis, Virginia Polytechnic Institute and State University, Blacksburg, VA, May 1974.

24. Hardrath, H. F.; Newman, J. C., Jr.; Elber, W.; and Poe, C. C., Jr.: Recent Developments in Analysis of Crack Propagation and Fracture of Practical Materials. Fracture Mechanics, N. Perrone, ed., University Press of Virginia, 1978, pp. 347-364.

25. Newman, J. C., Jr.: A Crack-Closure Model for Predicting Fatigue Crack Growth Under Aircraft Spectrum Loading. Methods and Models for Predicting Fatigue Crack Growth Under Random Loading, J. B. Chang and C. M. Hudson, eds., American Society for Testing and Materials, ASTM STP 748, 1981, pp. 53-84.

26. Dugdale, D. S.: Yielding of Steel Sheets Containing Slits. Journal of Mechanics, Physics, and Solids, Vol. 8, No. 2, 1960, pp. 100-104.

27. Newman, J. C., Jr.: Fracture of Cracked Plates Under Plane Stress. Engineering Fracture Mechanics, Vol. 1, No. 1, 1968, pp. 137-154.

28. Irwin, G. R.: Plastic Zone Near a Crack and Fracture Toughness. Proceedings of the 7th Sagamore Conference, 1960, p. IV-63.

29. Newman, J. C., Jr.: Discussion on Cyclic Crack Growth Transitional Behavior. Fatigue Crack Propagation, American Society for Testing and Materials, ASTM STP 415, 1967, pp. 380-383.

6-16

30. Barenblatt, G. I.: Mathematical Theory of Equilibrium Cracks in Brittle Fracture. Advances in Applied Mechanics, Vol. 7, 1962.

31. Minakawa, K.; and McEvily, A. J.: On Near-Threshold Fatigue Crack Growth in Steels and Aluminum Alloys. Proceedings of the International Conference on Fatigue Thresholds, Vol. 2, Stockholm, Sweden, 1981, p. 36.

32. Walker, N.; and Beevers, C. J.: A Fatigue Crack Closure Mechanism in Titanium. Fatigue of Engineering Materials and Structures, Vol. 1, No. 1, 1979, pp. 135-148.

33. Paris, P. C.; Bucci, R. J.; Wessel, E. T.; Clark, W. G.; and Mager, T. R.: Extensive Study of Low Fatigue Crack Growth Rates in A533 and A508 Steels. Stress Analysis and Growth of Cracks, American Society for Testing and Materials, ASTM STP 513, 1972, pp. 141-176.

34. Ritchie, R. O.; Suresh, S.; and Moss, C. M.: Near-Threshold Fatigue Crack Growth in 2.25Cr-1Mo Pressure Vessel Steel in Air and Hydrogen. Journal of Engineering Materials and Technology, Vol. 102, 1980, pp. 293-299.

35. Ohtsuka, A.; Mori, K.; and Miyata, T.: The Condition of Fatigue Crack Growth in Mixed Mode Condition. Engineering Fracture Mechanics, Vol. 7, No. 3, 1975, pp. 429-439.

36. Ewalds, H. L.; and Furnee, R. T.: Crack Closure Measurement Along the Fatigue Crack Front of Center Cracked Specimens. International Journal of Fracture, Vol. 14, No. 2, 1978, pp. R53-R55.

37. Newman, J. C., Jr.: Prediction of Fatigue Crack Growth Under Variable-Amplitude Loading Using a Closure Model. Design of Fatigue and Fracture Resistant Structures, P. R. Abelkis and C. M. Hudson, eds., American Society for Testing and Materials, ASTM STP 761, 1982, pp. 255-277.

38. McEvily, A. J.: Current Aspects of Fatigue. Metal Science, August/September 1977, p. 284.

39. Truyens, P.: Crack Growth Under Variable Loads in Ships. Ph.D. Thesis, University of Gent, Gent, Belgium, 1976.

40. Taylor, D.; and Knott, J. F.: Growth of Fatigue Cracks from Casting Defects in Nickel Aluminum Bronze. Proceedings of the Metal Society Conference on Defects and Crack Initiation in Environment Sensitive Fracture, University of Newcastle-on-Tyne, 1981.

41. Metals Handbook, Properties and Selection of Metals. Vol. 1, 8th Ed., American Society for Metals, 1961.

42. Newman, J. C., Jr.; and Raju, I. S.: An Empirical Stress-Intensity Factor Equation for the Surface Crack. Engineering Fracture Mechanics, Vol. 15, No. 1-2, 1981, pp. 185-192.

43. Tada, H.; Paris, P. C.; and Irwin, G. R.: The Stress Analysis of Cracks Handbook. Del Research Corporation, 1973.

44. Newman, J. C., Jr.: Crack-Opening Displacements in Center-Crack, Compact, and Crack-Line Wedge-Loaded Specimens. NASA Technical Note D-8268, 1976.

45. Newman, J. C., Jr.: An Improved Method of Collocation for the Stress Analysis of Cracked Plates with Various Shaped Boundaries. NASA Technical Note D-6376, 1971.

46. Bowie, O. L.: Analysis of an Infinite Plate Containing Radial Cracks Originating at the Boundary of an Internal Circular Hole. Journal of Mathematics and Physics, Vol. XXXV, No. 1, 1956, pp. 60-71.

17. Shivakumar, V.; and Forman, R. G.: Green's Function for a Crack Emanating from a Circular Hole in an Infinite Sheet. International Journal of Fracture, Vol. 16, No. 4, 1980, pp. 305-316.

48. Newman, J. C., Jr.: Predicting Failure of Specimens with Either Surface Cracks or Corner Cracks at Holes. NASA Technical Note D-8244, 1976.

49. Howland, R. C. J.: On the Stresses in the Neighbourhood of a Circular Hole in a Strip Under Tension. Philosophical Transactions of the Royal Society of London, Series A, Vol. 229, 1930, pp. 49-86.

50. Rice, J. R.: The Mechanics of Crack Tip Deformations and Extension by Fatigue. Brown University Technical Report NSF GK-28613, May 1966.

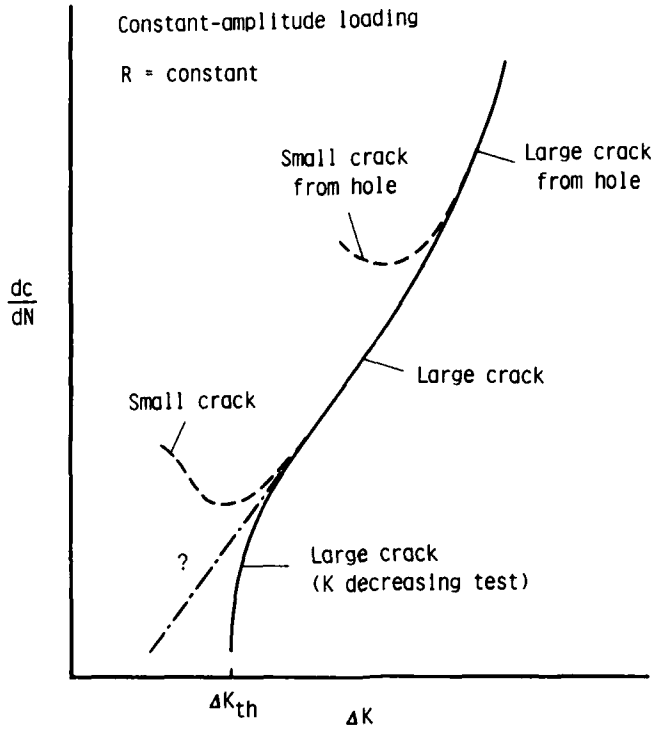

Figure 1.- Typical fatigue-crack growth rate data for small and large cracks.

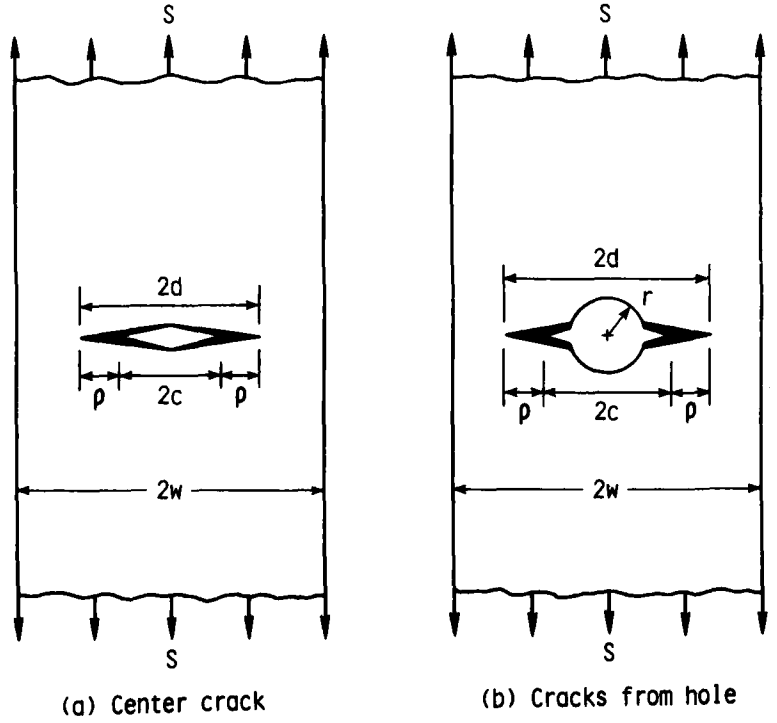

Figure 2.- Center-crack and cracks from circular hole specimens with Dugdale plastic zones and residual plastic deformations.

6-18

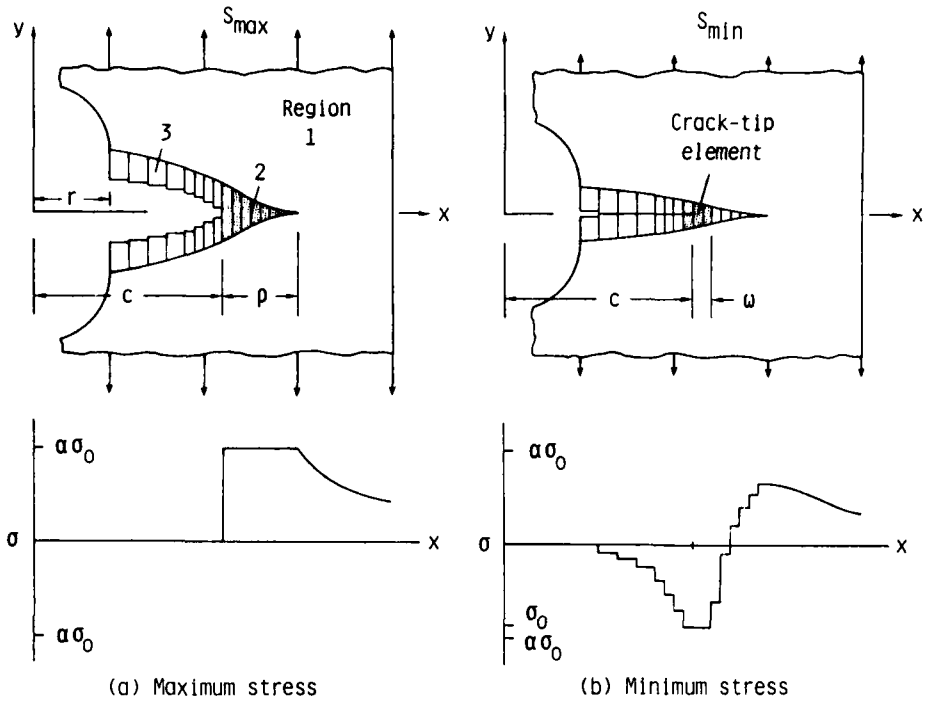

Figure 3.- Crack-surface displacements and stress distributions along crack line.

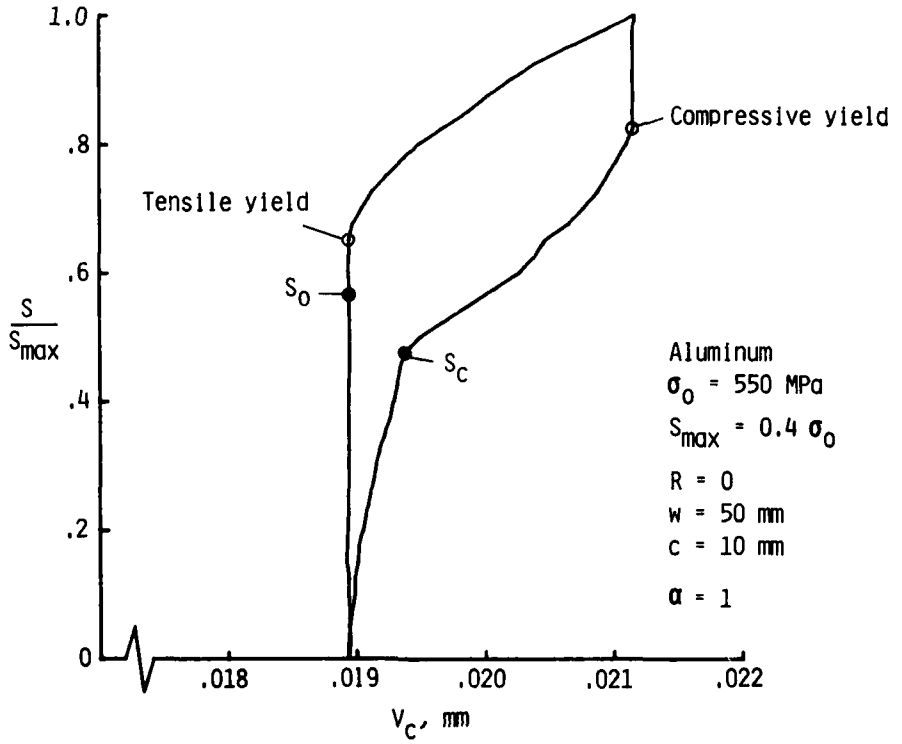

Figure 4.- Calculated displacement of crack-tip element under constant-amplitude loading.

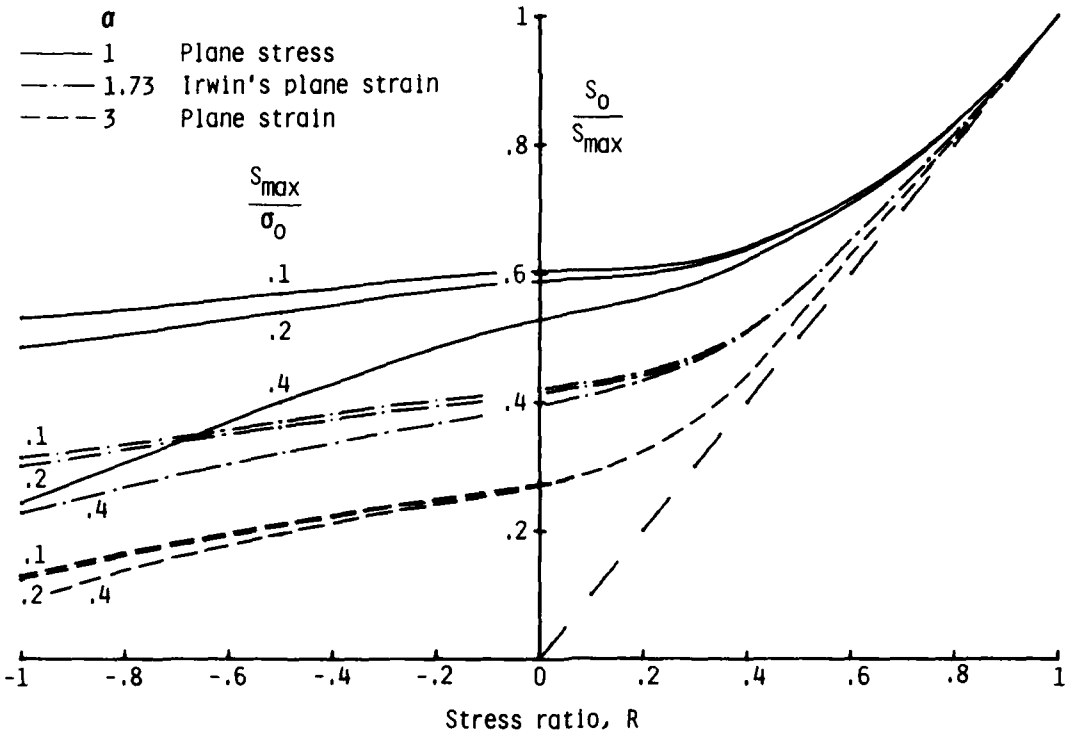

Figure 5.- Normalized crack-opening stresses as a function of R ratio under constant-amplitude loading for simulated plane-stress and plane-strain conditions.

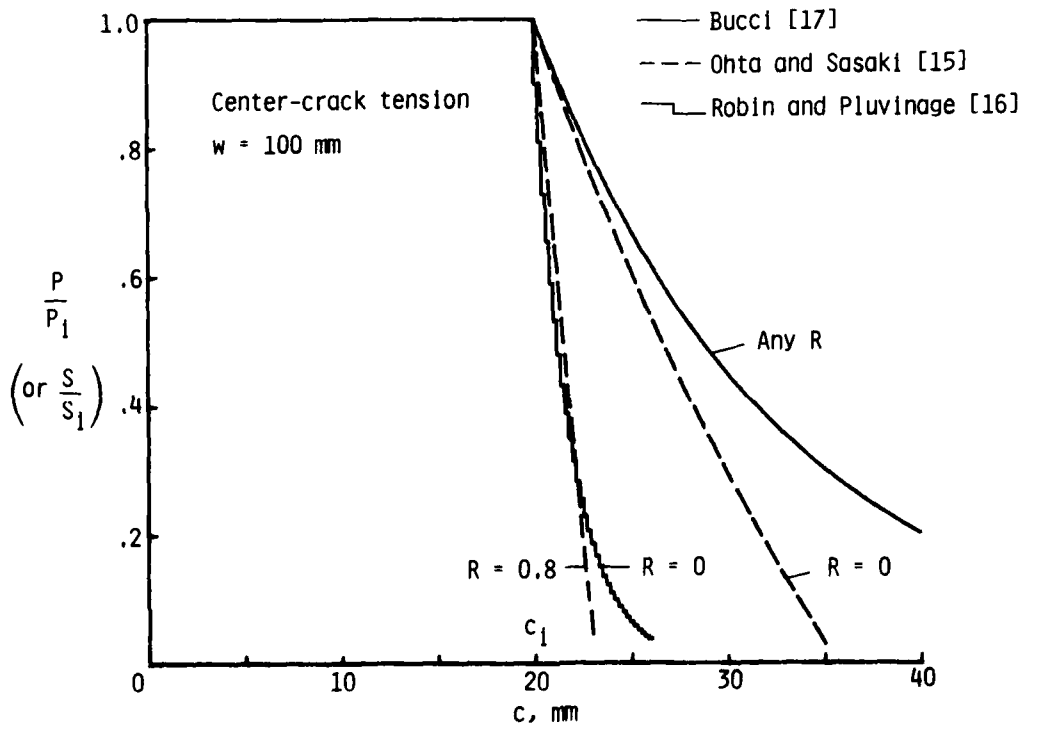

Figure 6.- Various load-reduction schemes used in ΔK threshold testing.

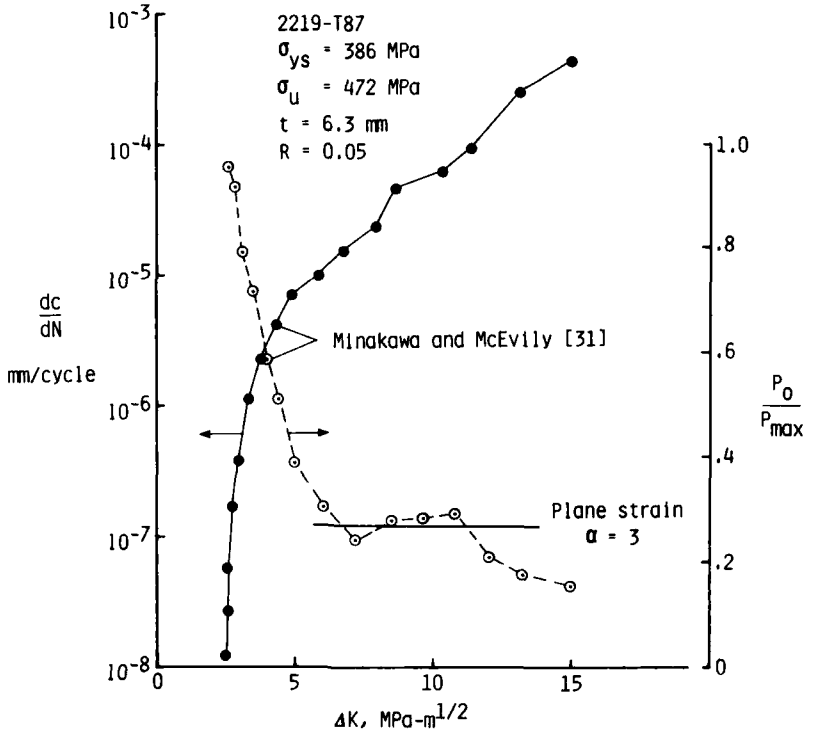

Figure 7.- Comparison of experimental growth rates and crack-opening stresses on a 2219-T87 aluminum alloy compact specimen [31].

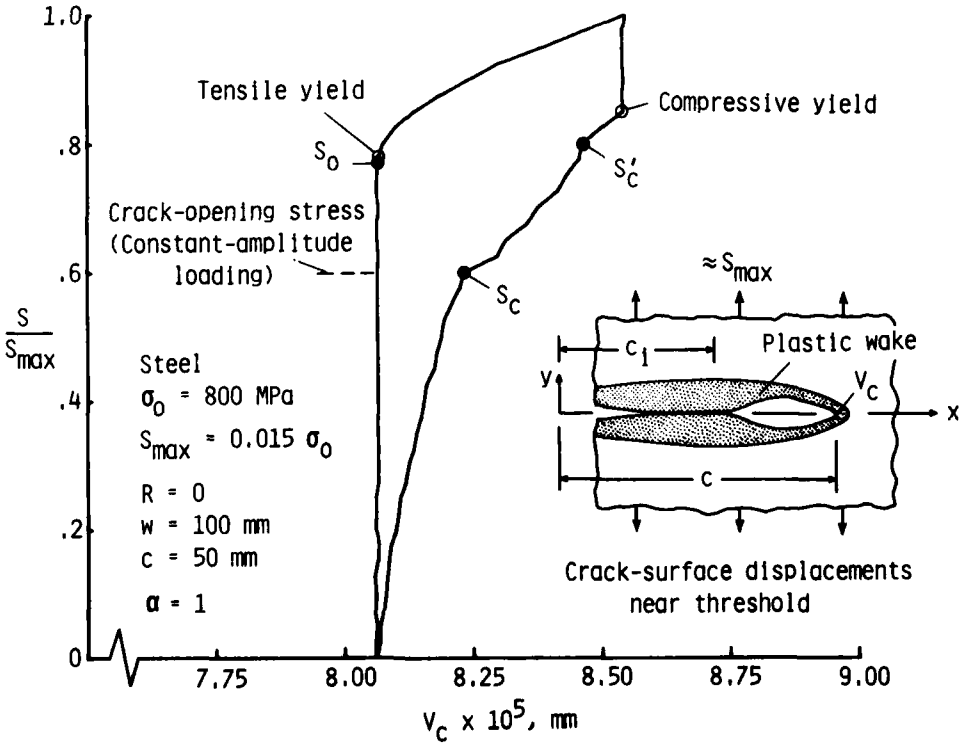

Figure 8.- Calculated displacement of crack-tip element for a ΔK-threshold test using Bucci's load-reduction scheme [17].

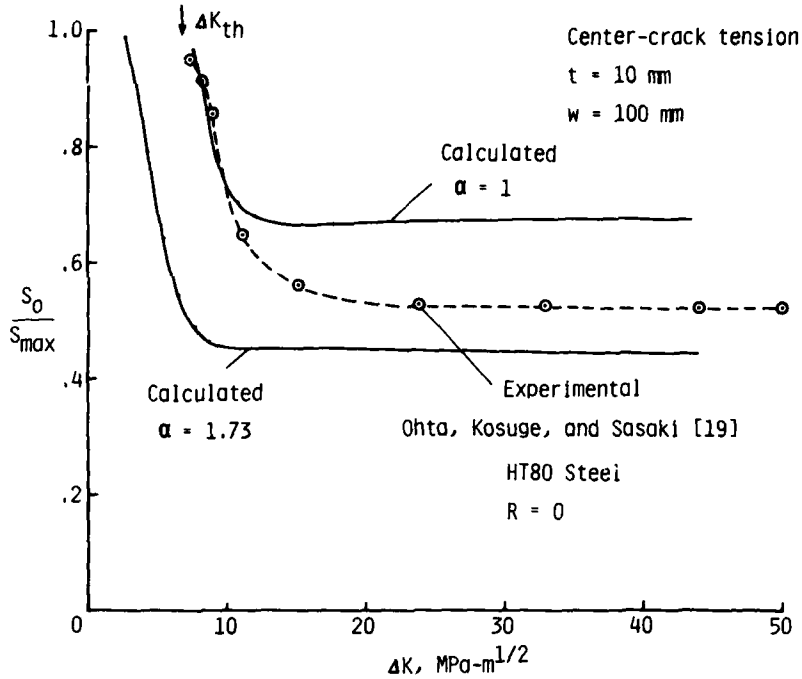

Figure 9.- Comparison of experimental and calculated crack-opening stresses for a ΔK-threshold test using Ohta-Sasaki load-reduction scheme [15].

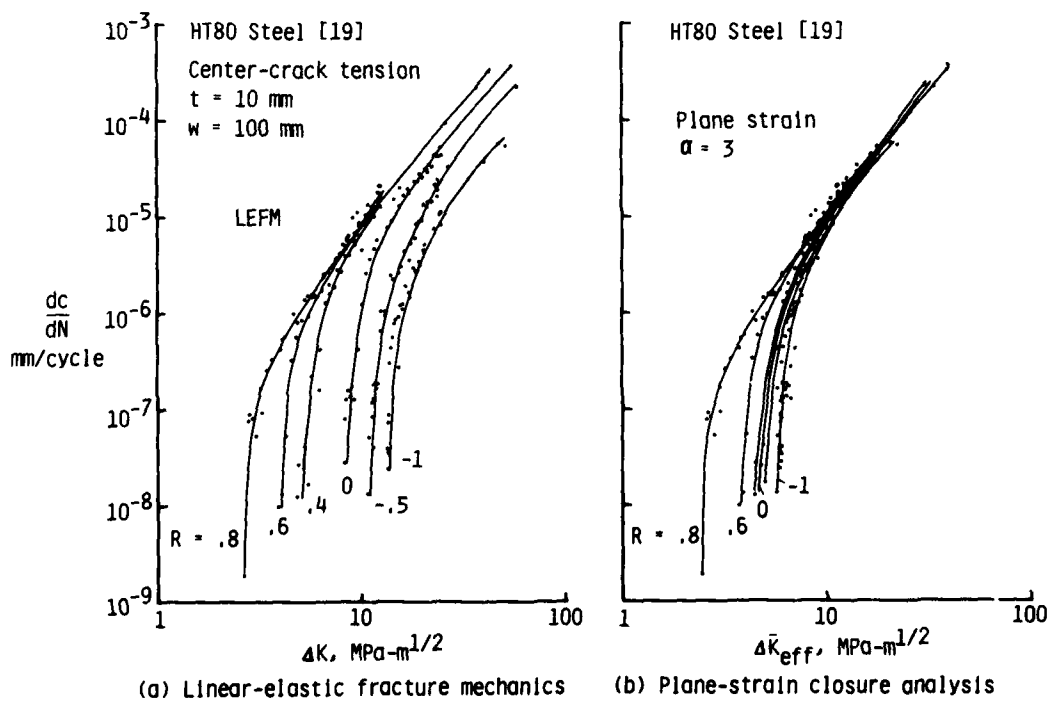

(a) Linear-elastic fracture mechanics (b) Plane-strain closure analysis

Figure 10.- Crack-growth rates as a function of stress-intensity factor range for various R ratios using LEFM and closure analysis for simulated plane-strain condition.

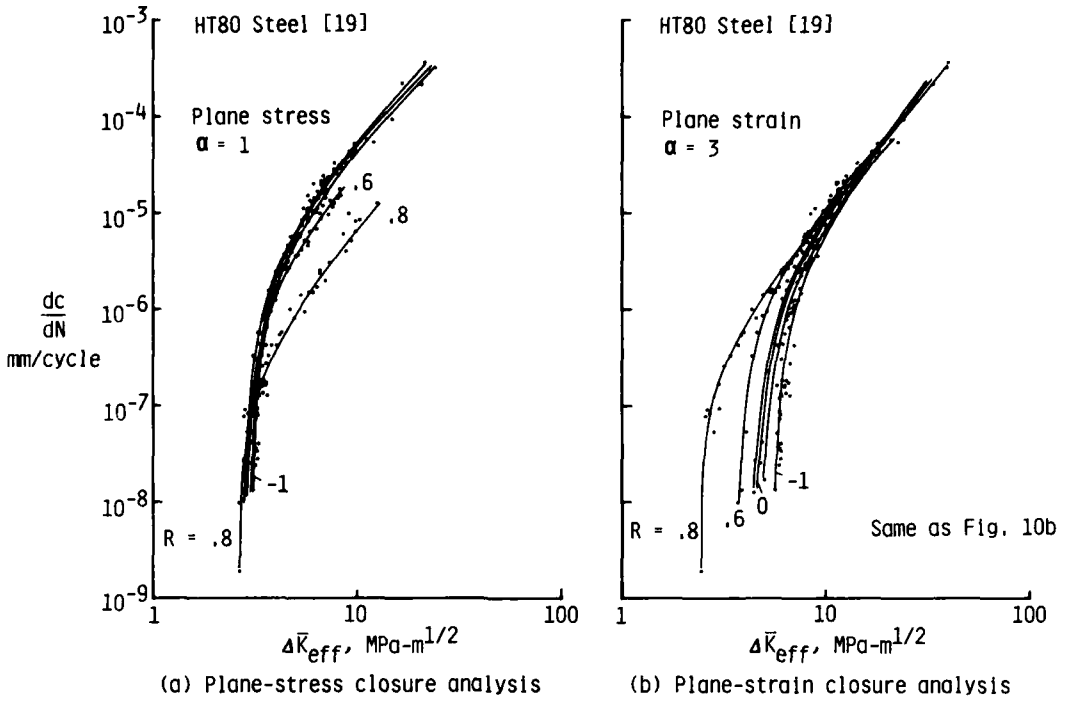

(a) Plane-stress closure analysis (b) Plane-strain closure analysis

Figure 11.- Crack-growth rates as a function of stress-intensity factor range for various R ratios using closure analyses for simulated plane-stress and plane-strain conditions.

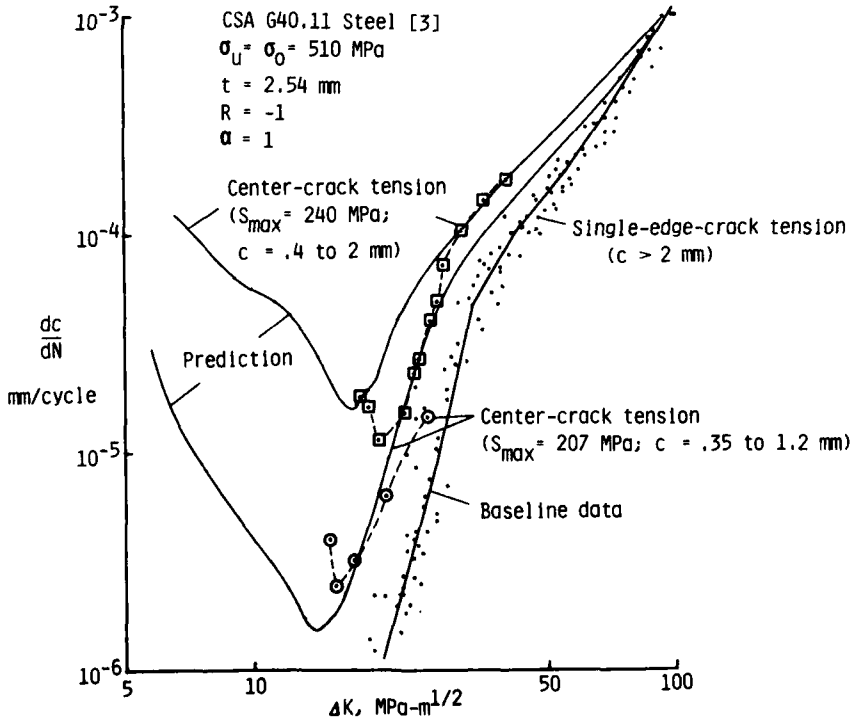

Figure 12.- Comparison of experimental and predicted crack-growth rates for small cracks in center-crack tension specimens subjected to high stress levels.

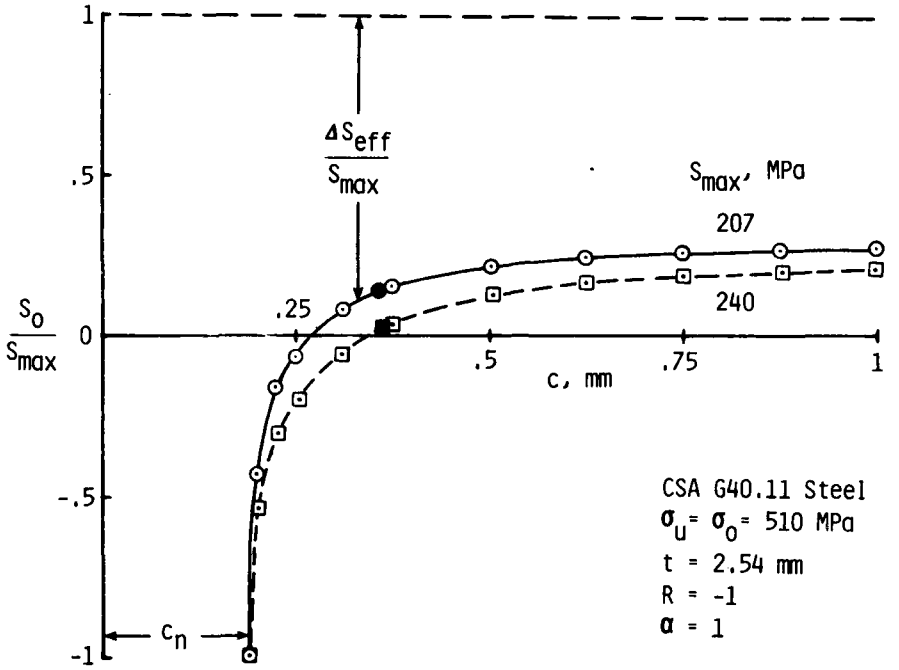

Figure 13.- Calculated crack-opening stresses as a function of crack length under constant-amplitude loading (solid symbol denotes crack length at minimum crack-growth rate).

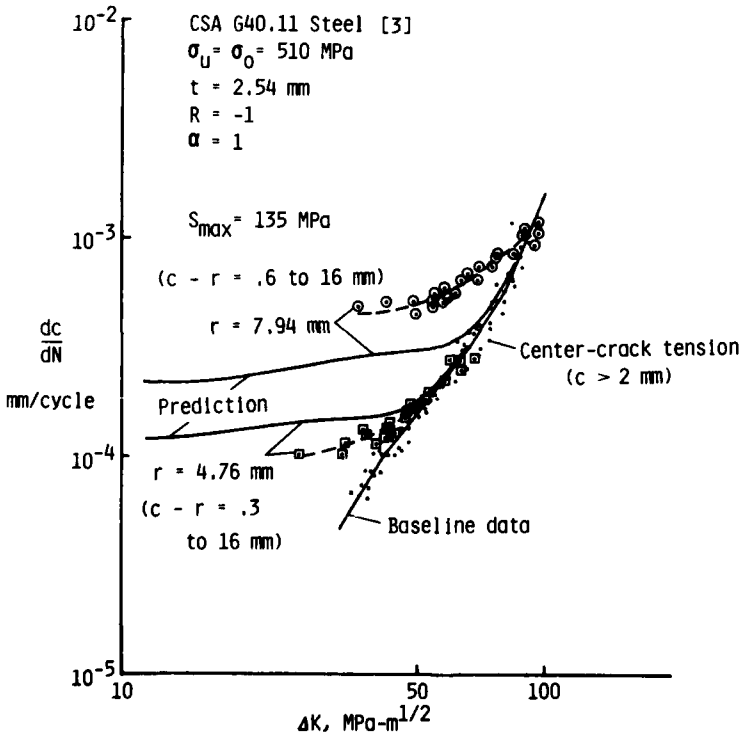

Figure 14.- Comparison of experimental and predicted crack-growth rates for small cracks emanating from a circular hole in steel specimens.

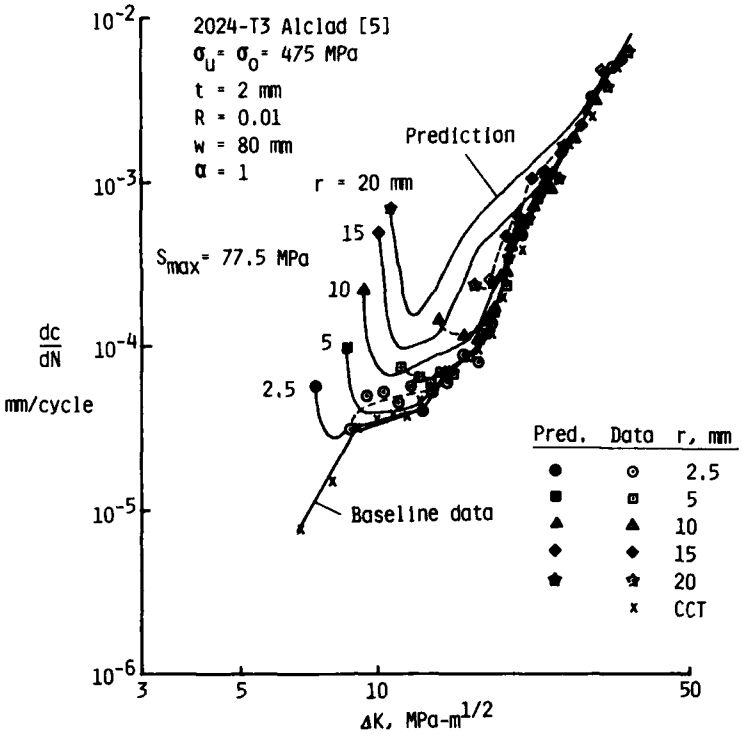

Figure 15.- Comparison of experimental and predicted crack-growth rates for small cracks emanating from a circular hole in aluminum specimens.

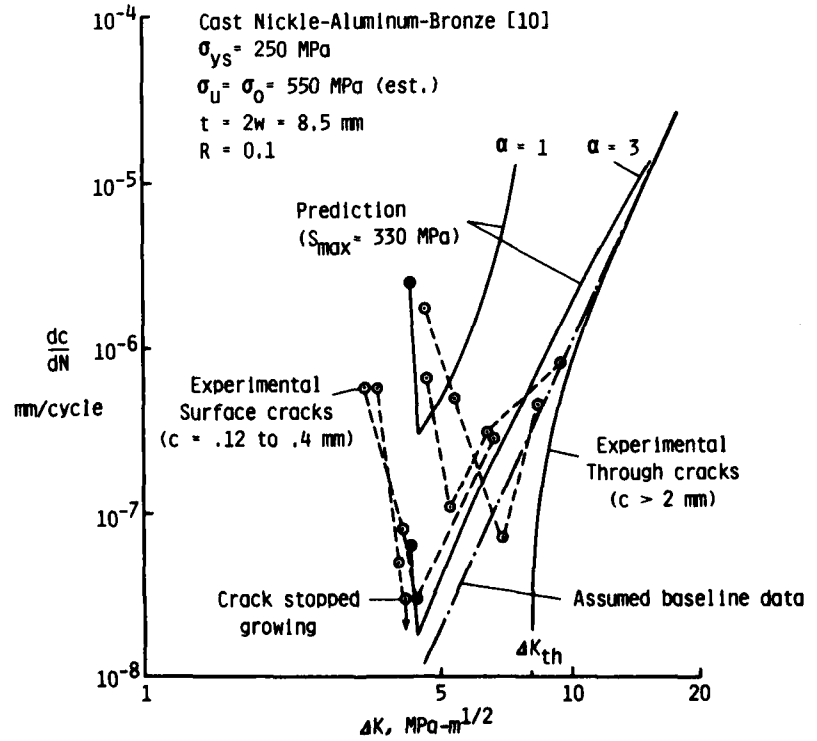

Figure 16.- Comparison of experimental and predicted crack-growth rates for small surface cracks in specimens subjected to a high stress level.

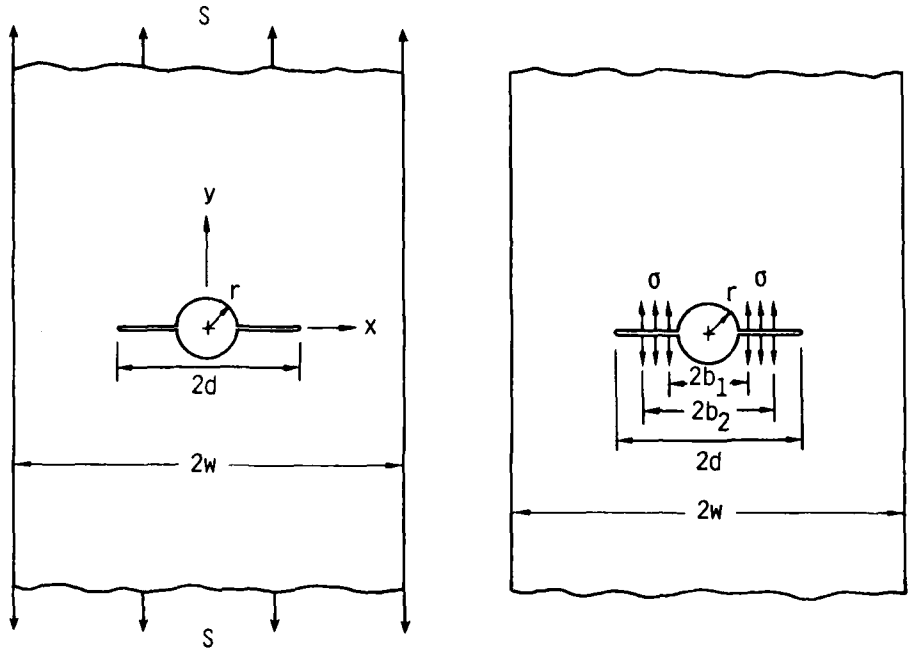

(a) Uniform stress (b) Partially-loaded crack

Figure 17.- Cracks from a hole in finite-width plate subjected to various loading.

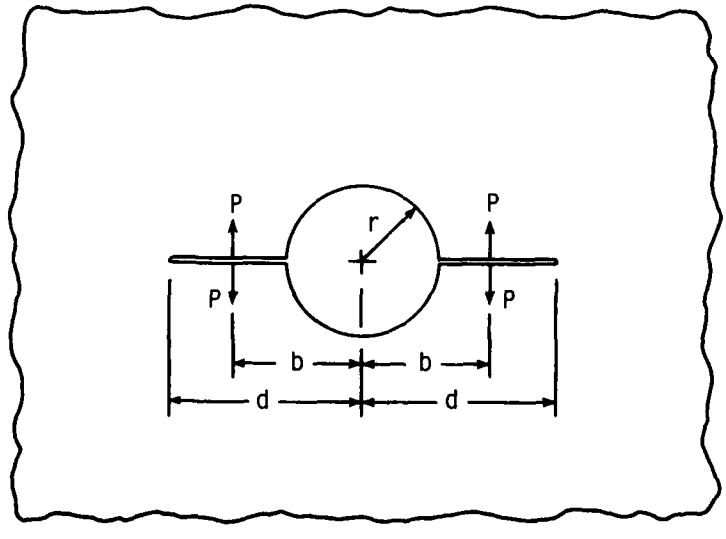

Figure 18.- Cracks from circular hole in infinite plate subjected to concentrated forces on crack surface.

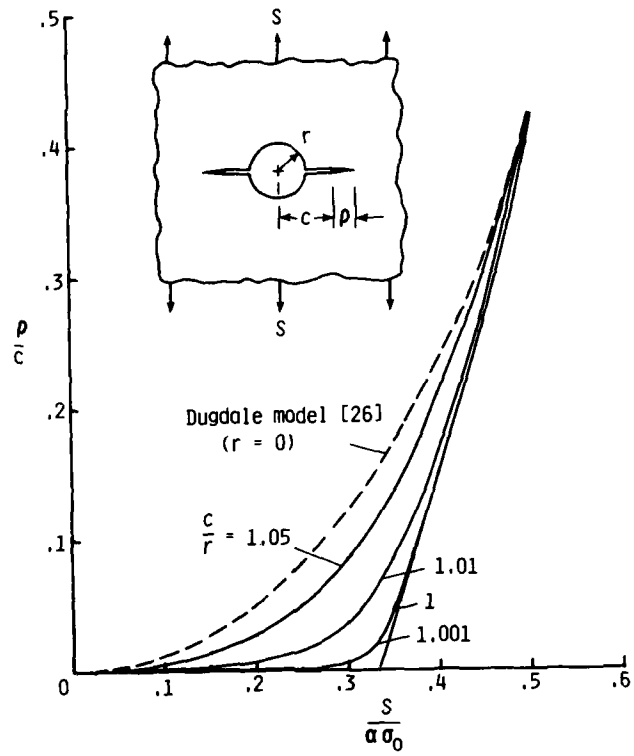

Figure 19.- Dugdale plastic-zone sizes for cracks from hole in an infinite plate subjected to remote uniform stress.

DAMAGE TOLERANCE EVALUATION OF STRUCTURES WITH SMALL CRACKS

by

Lüder Schwarmann
VFW/MBB GmbH
Postfach 10 78 45
2800 Bremen 1
Federal Republic of Germany

SUMMARY

This paper deals with the analytical determination of the linear-elastic stress intensity factor (SIF) for structures with small cracks. Two different cases are considered : a) through-the-thickness-cracks emanating from a circular hole, b) semi-elliptical surface cracks. The analytical methods studied herein are : the WEIGHT-FUNCTION METHOD by GRANDT for the case a) and the ENGINEERING METHOD by NEWMAN for the case b). Results obtained from analyses are compared with corresponding test results. The comparisons show good agreement. Analyses show that a cracked pin-loaded hole is the most critical case as compared with other crack-configurations. Furthermore, analyses indicate the degree of conservative assessment when assuming a through-crack instead of a surface crack as far as the crack propagation behaviour is concerned. Both methods studied herein are recommended for practical application in aircraft design.

LIST OF SYMBOLS

Symbol	Notation
x,y	Cartesian coordinates, mm
d	Diameter of circular hole, mm
w	Width of cracked plate, mm
t	Thickness of cracked plate, mm
E	Young's modulus of plate material, MPa
S	Remote uniform tensile stress, MPa
S_U	Upper level of S during a load cycle, MPa
S_L	Lower level of S during a load cycle, MPA
S_R	Residual strength (gross-sectional failure stress), MPa
σ	Local stress distribution near circular hole in the plate, MPa
F	Applied tension load, N
F_P	Pin-load, N
a	Length of through-crack and surface crack, respectively, mm
a_i	Initial crack length, mm
a_f	Final crack length, mm
da/dN	Crack propagation rate, mm/cycle
c	Depth of surface crack, mm
v_B	Crack opening displacement of the BOWIE-Problem, mm
K	Stress Intensity Factor (SIF), $N/mm^{3/2}$
K_B	Value of SIF for the BOWIE-Problem, $N/mm^{3/2}$
ΔK	Range of SIF during a load cycle, $N/mm^{3/2}$
K_c	Critical value of SIF (fracture toughness), $N/mm^{3/2}$
Y	Correcting function of SIF, -
N	Crack life, number of applied load cycles

1. INTRODUCTION

The damage tolerance evaluation of airframe structures is part of the fatigue-certification and specified in corresponding documents /1/. The basic assumption is that cracks are present in the load-carrying structures during the operational life of aircraft. Therefore, it is the main task of the design engineer to guarantee that cracked structural components do not fail and cause catastrophic loss of the aircraft.

It is well-known that the total fatigue life of a airframe structure consists of the crack-free life and the so-called crack life. Since the major part of the crack life is achieved when the cracks originate and increase to a certain size, it is evident that the case of small cracks dominates during the crack life.

2. PROBLEM AERAS

Damage tolerance analyses deal with the evaluation of the crack propagation and of the residual strength behaviour of the structure. It is common use in aircraft industry to apply the concept of the linear-elastic stress intensity factor for damage tolerance analyses. From this concept following equations have been derived :

a) crack propagation analyses, i.e. crack length = f (applied load cycles)

$$a(N) = a_i + \int_{N(a_i)}^{N(a_f)} (da/dN)\,dN \qquad da/dN = f(\Delta K) \qquad \Delta K = (S_U - S_L)\sqrt{\pi a}\,Y \qquad (1)$$

b) residual strength analyses, i.e. failure stress = f (crack length)

7-2

$$S_R = \frac{K_c}{\sqrt{\pi a}\, Y} \qquad (2)$$

It is assumed that the following data is known prior to damage tolerance analyses :

- geometry and stiffness of the structural component considered
- loads and stress spectra being expected during service life
- initial crack length being detected by corresponding inspection methods
- material data, i.e. crack propagation and fracture toughness data.

The main task to assess the crack propagation and the residual strength behaviour, respectively, is to determine the correcting function Y of the stress intensity factor as can be seen from eqns. (1) and (2).

For two different cases, i.e. through-cracks emanating from a hole and surface cracks in a plate, two methods to determine the correcting function Y will be discussed in the following sections. For both cases only the range of small cracks are considered.

3. THROUGH-CRACKS EMANATING FROM A CIRCULAR HOLE

The case of cracks emanating from holes are of high interest in aircraft design as far as fatigue problems are concerned. It is known that most failures in airframe structures originate from fastener holes /2/. Since built-up structures are designed to be thin-walled the assumption that possible damages are through-the-thickness-cracks is evident.

The classical solution for a sheet containing a circular hole, from which through-cracks emanate, loaded by remote uniform tension has been derived by BOWIE /3/. His solution shows that the case of two cracks is more critical than the case of one crack; therefore only the case of two cracks is considered herein. Taken BOWIE's solution into consideration GRANDT has developed a special mathematical model to determine SIF for cracks emanating from a circular hole /4/ based on the so-called WEIGHT-FUNCTION-TECHNIQUE /5/. A brief description of GRANDT's model is given in fig.1.

If the local stress distribution near the uncracked hole is known, say from Finite Element Analyses, then the SIF, and thus the required correction function, can be calculated from eqn.(3). This procedure seems to be advantegeous for a lot of practical problems, e.g. holes with installed interference-fit-fasteners, cold-worked holes.

The application of eqn.(3) will be demonstrated herein for a strip of finite width containing a central hole and being loaded by a remote uniform tensile stress or by a pin-load, respectively. Since the local stress distribution is known for these two cases /6,7/, the correcting function has been calculated; the results are given in fig.2, especially for very short crack lengths. In fig.2 results from extensive residual strength tests /8/ are added for comparisons purpose. The comparison shows good agreement.

Bearing in mind GRANDT's own results one can conclude that the method given in fig.1 gives sufficient results as far as the accuracy with respect to practical applications is concerned. Furthermore, it is evident from fig.2 that for very short crack lengths the pin-loaded hole ($F_P/F = 1$) gives higher values for the correcting function of SIF than the hole loaded by remote tension ($F_P/F = 0$) and is therefore more critical as far as the damage tolerance performance is concerned.

4. SEMI-ELLIPTICAL SURFACE CRACKS

Many fatigue-critical airframe components are thick-walled, e.g. fittings etc. It is known that possible damages in thick-walled structures originate as surface cracks.

The analyses of these cracks is difficult, since the SIF varies at the boundary of the crack-front. Due to these difficulties NEWMAN developed an ENGINEERING METHOD from corresponding test results /8/.His formulas give an approximate value for the maximum SIF, which is present at the minor axis of the assumed semi-elliptical surface crack. The crack configurations, for which NEWMAN's method can be applied, are given in fig.3.

For the crack configurations shown in fig.3 some calculations to determine the correcting functions of the SIF have been carried out using NEWMAN's method; the results of these calculations are given in fig.4 and indicate that -especially for small crack sizes- the pin-loaded hole is the most critical crack configuration.

Since NEWMAN's method has been derived from extensive residual strength tests, the following question arises : "How can NEWMAN's method predict the crack propagation behaviour of components with surface cracks ?". In order to answer this question some comparisons between prediction using a corresponding computer-program /9/ and tests /10/ have been carried out. The specimen used is a plate containing a central semi-circular surface crack and being loaded by constant-amplitude fatigue-loads. The results of this comparison are given in fig.5 and show good agreement for all cases considered.

Another problem of high practical interest will be discussed next. It is assumed that a certain crack length (on the surface of a structural component) is detected by appropriate inspection methods. However, no information about the shape of the crack in direction of the depth can be given unequivocally. Thus the question to be answered is: "How great is the error in assuming a through-crack instead of a semi-elliptical surface crack of different shape as far as the achieved crack life is concerned ?". In order to answer this question some calculations have been carried out taken the following conditions into consideration :

- material, loading conditions, geometry of the structure considered, initial and final crack length are the same for all calculations,
- the shape of the assumed semi-elliptical surface crack, i.e. the ratio of the major axis to the minor axis (a/c) is kept constant during the crack propagation phase.

The results of these calculations are given in fig.6. From this figure it is evident that a surface crack has a greater crack life than a through-crack of the same crack length.

5. CONCLUSION

Two different methods for damage tolerance evaluation of airframe structures with small cracks are investigated. These methods are : WEIGHT-FUNCTION METHOD by GRANDT for through-the-thickness cracks emanating from a circular hole and ENGINEERING METHOD by NEWMAN for semi-elliptical surface cracks.

Both methods give sufficient results as far as the comparison with corresponding test results is concerned. Therefore both methods are recommended for practical applications in aircraft design concerning damage tolerance evaluation.

As shown in this paper, a cracked pin-loaded hole is the most critical crack configuration, especially for small cracks, as compared with other cases. Therefore the degree of pin-load, i.e. the load-tranfer by a bolt or by a rivet, has to be determined very thoroughly in order to avoid overestimations of the damage tolerance performance of the airframe structure.

Analyses based on through-cracked configurations are pessimistic as compared with surface-cracked configurations and should therefore be the first (safe) step of damage tolerance evaluation procedure.

REFERENCES

/1/ N.N. : "Damage Tolerance and Fatigue Evaluation of Structures", 14 FCR, Part 25, Paragraph 25.571, FAA, 1977.

/2/ H.HUTH, D.SCHÜTZ : "Sammlung und Analysen von im Betrieb von Luftfahrzeugen aufgetretenen Ermüdungsschäden (in German)", Report BMVg-FBWT 7910, LBF, 1979.

/3/ O.L.BOWIE : "Analysis of an infinite Plate containing radial Cracks originating at the Boundary of an internal circular Hole", Journal of Mathematics and Physics, Vol. 35, pp. 60-71, 1956.

/4/ A.F.GRANDT : "Stress Intensity Factors for some through-cracked Fastener-Holes", International Journal of Fracture, Vol. 11, No. 2, pp. 283-293, 1975.

/5/ H.F.BUECKNER : "A novel Principle for the Computation of Stress Intensity Factors", ZAMM 50, No, 9, pp. 529-546, 1970.

/6/ G.N.SAWIN : "Spannungserhöhung am Rande von Löchern (in German)", VEB Verlag Technik, Berlin, 1956.

/7/ P.S.THEOCARIS : "The Stress Distribution in a Strip loaded in Tension by Means of a central Pin", Journal of Applied Mechanics, Trans. ASME, pp. 85-90, 1956.

/8/ J.C.NEWMAN : "Predicting Failure of Specimens with either Surface Cracks or Corner Flaws at Holes", Report TN D-8244, NASA, 1976.

/9/ L.SCHWARMANN, J.BAUER : "DAMTOL - Computerprogram for DAMage TOLerance Evaluation of Airframe Structures", VFW/MBB, Bremen, unpublished.

/10/ W.GEIER : "Investigations of Surface Cracks and Through-Cracks in thick-walled Components", Report STR-P-0032, MBB, Munich, 1977.

7-4

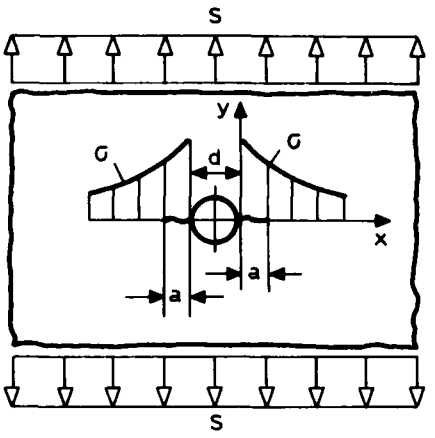

$$K = S\sqrt{\pi a}\,Y = \frac{E}{K_B}\int_0^a \left(\sigma\,\frac{\partial v_B}{\partial a}\right)dx \qquad (3)$$

(Solution from GRANDT[4])

σ = Local Stress Distribution (uncracked)

$$v_B = \frac{4K_B}{E}\sqrt{\frac{a-x}{2\pi}}$$

K_B = SIF for BOWIE-Problem

E = Young's Modulus

FIG. 1 DETERMINATION OF SIF FOR THROUGH-CRACKS EMANATING FROM A CIRCULAR HOLE

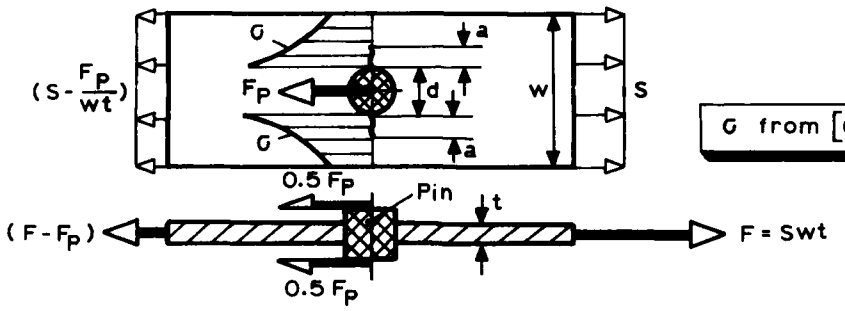

σ from [6] [7]

d/w = 0.2
pin with net-fit

$\frac{a}{d/2}$	$Y = K/S\sqrt{\pi a}$					
	$F_P/F = 0$			$F_P/F = 1$		
	Eqn.(3)	[8]	Δ(%)	Eqn.(3)	[8]	Δ(%)
0.1	2.91	2.92	-0.3	5.57	5.69	-2.1
0.2	2.59	2.53	+2.4	4.46	4.63	-3.7
0.3	2.36	2.28	+3.5	3.76	3.94	-4.6
0.4	2.17	2.11	+2.8	3.29	3.45	-4.6
0.5	1.99	1.99	0	2.97	3.10	-4.2
0.6	1.86	1.89	-1.6	2.73	2.83	-3.5
0.7	1.78	1.82	-2.2	2.55	2.61	-2.3
0.8	1.71	1.76	-2.8	2.39	2.44	-2.0
0.9	1.65	1.72	-4.1	2.26	2.30	-1.7
1.0	1.60	1.69	-5.3	2.14	2.19	-2.3

FIG. 2 CORRECTING FUNCTION Y FOR TWO THROUGH-CRACKS EMANATING FROM A CIRCULAR HOLE

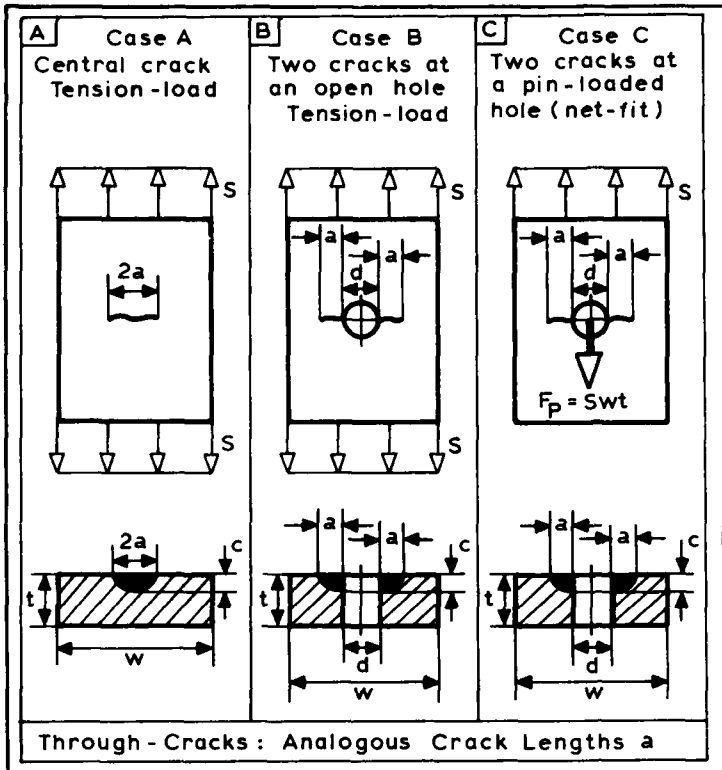

Through-Cracks: Analogous Crack Lengths a

$$K = S\sqrt{\pi a}\, Y$$

Case A : $Y = f(\frac{a}{c}; \frac{a}{w}; \frac{c}{t})$

Case B : $Y = g(\frac{a}{c}; \frac{a}{w}; \frac{c}{t}; \frac{d}{w})$ (4)

Case C : $Y = h(\frac{a}{c}; \frac{a}{w}; \frac{c}{t}; \frac{d}{w})$

(Solution from NEWMAN[8])

FIG. 3 DETERMINATION OF SIF FOR SEMI-ELLIPTICAL SURFACE-CRACKS

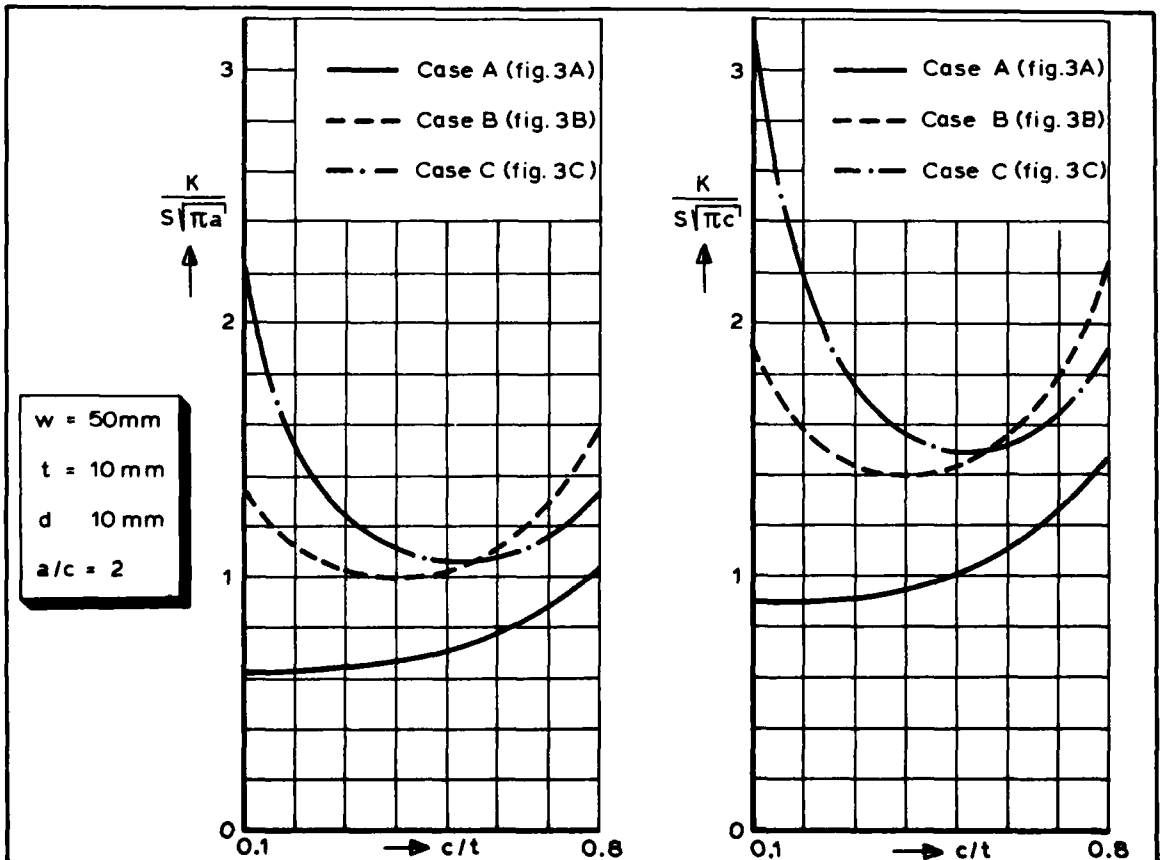

FIG. 4 CORRECTING FUNCTIONS FOR SEMI-ELLIPTICAL SURFACE-CRACKS

Case A (w=160mm; a/c=1), s. fig. 3A Plate-Material : Alum. 7075T7351

Constant-Amplitude-Loading : S_U = 160MPa ; S_L = 20MPa

Calculation : Eqns. (1), (4) Test : Mean Values of 3 Test-Results per t [10]

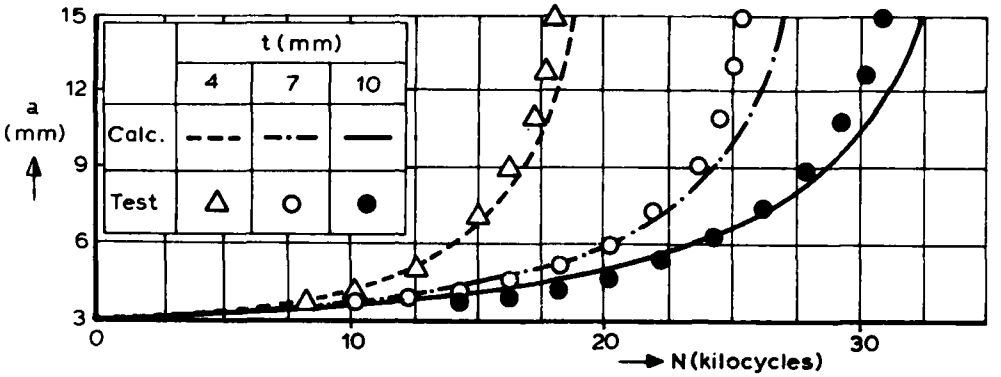

FIG. 5 CRACK PROPAGATION INVESTIGATIONS OF PLATES CONTAINING CENTRAL SEMI-CIRCULAR SURFACE-CRACKS

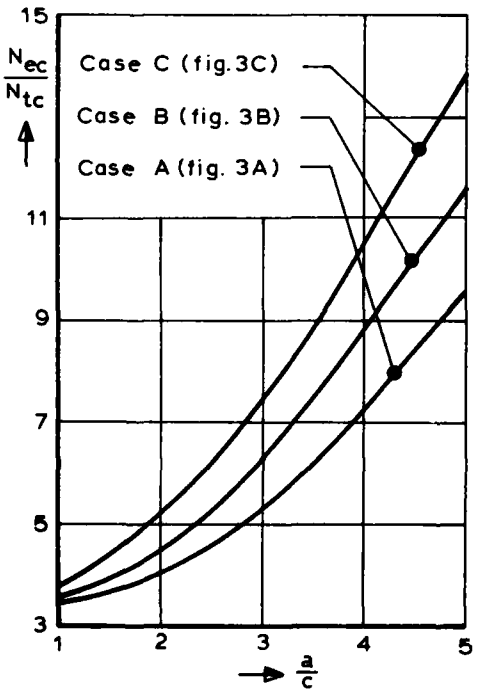

- Constant - Amplitude - Loading
  S_U = 100 MPa , S_L = 0
- Material = ALUM 7075T7351
- Configuration of plate (w=50mm, t=10mm)
  - Central crack, tension-load, s. fig. 3A
  - Two cracks emanating from an open hole (d=10mm), tension-load, s. fig. 3B
  - Two cracks emanating from a hole (d=10mm), pin-load, s. fig. 3C
- Crack-geometry
  - a = crack length of through-crack and of elliptical crack, s. fig. 3
  - c = depth of elliptical crack, s. fig. 3
  - a_i = initial crack length = 2mm
  - a_f final crack length = 10mm
  - Assumption : a/c = const.
- Crack-life from a_i to a_f
  - N_{tc} through-crack
  - N_{ec} elliptical crack
- Results in diagram show tendencies

FIG. 6 INFLUENCE OF RATIO a/c OF SEMI-ELLIPTICAL SURFACE-CRACKS ON THE CRACK-LIFE COMPARED WITH THROUGH-CRACKS

FRACTURE MECHANICS ANALYSIS OF SHORT CRACKS AT LOADED HOLES

D. P. Rooke
Royal Aircraft Establishment,
Farnborough,
Hants, GU14 6TD,
United Kingdom

SUMMARY

In a predominantly tensile field the time for a fatigue crack to grow to a critical length is dominated by the time spent when the crack is short. Cracks frequently start in the vicinity of a stress concentrator such as a hole, and the stress intensity factor which controls crack growth-rate is largely determined by the local stress field. If the hole is loaded on its perimeter, the stress intensity factor for short cracks is strongly dependent on the actual distribution of load on the perimeter. In a cracked pin-loaded lug load is, in general, transmitted from the pin to the lug by both normal and shear forces; the shear forces arise from the friction (fretting) between the pin and the lug. It is shown, by using a Green's function technique, that the presence of friction increases the stress intensity factor and hence increases the rate of growth of fatigue cracks which reduces the fatigue lifetime. The magnitude of these effects depends on the coefficient of friction and how it varies round the hole.

1 INTRODUCTION

Cracks frequently occur in aircraft structures and, in order to assess structural reliability, it is necessary to know both the strength of the cracked component and the rate at which cracks grow under in-service fatigue loads. Both strength and crack-growth depend upon the stress field at the tip of the crack, which is characterized by the stress intensity factor K.

Because holes are stress concentrators, cracks frequently start at their edges. When the holes are loaded, for example, holes in pin-loaded lugs, the value of K depends upon the particular distribution of loads around the perimeter of the hole. It has been shown by Rooke and Tweed[1] that the influence of the radial load distribution on K is especially strong when the crack is short because of the closeness of the crack tip to the applied forces. This must be taken into account in order to obtain reliable estimates of the fatigue life of an aircraft structure since most of the lifetime is spent while the crack is short; accurate values of K are therefore needed for short cracks.

In practice, the load from a pin is transmitted to the edge of the hole by both normal (radial) and shear (tangential) forces. Edwards[2] has shown, that under fatigue loading, in the presence of fretting (friction between the pin and the edge of the hole), the shear forces can be comparable in magnitude to the radial forces. A Green's function technique developed by Rooke and Hutchins[3] can be used to evaluate both opening-mode and sliding-mode factors for any distribution of radial and shear loads acting on the perimeter of the hole.

In a pin-loaded lug, the most likely site for a crack is at the edge of the hole along a radial line perpendicular to the direction of the applied load. The fretting will be a maximum in the region of the perimeter close to the root of the crack. For short cracks radial forces in this region tend to close the crack and shear forces to open it[3]. If the total load is kept constant, then some of these beneficial radial forces will be replaced by shear forces when fretting is present. A larger crack tip opening will result, which implies an increase in the stress intensity factor and hence an increase in fatigue growth-rate with a consequent decrease in lifetime. It is therefore important that the effects of shear forces be included in assessments of structural reliability.

In section 2 of this paper, the stress intensity factor is first evaluated for a crack at the edge of a hole subjected to a given radial pressure when there is no friction between the pin and the edge of the hole, then the factor is evaluated if friction is present. The models chosen for the radial force distribution and the variation of friction around the hole are based on the experimental evidence of 'fretting fatigue' experiments by Edwards[2] and Moon[4]. It is shown that the transfer of some of the load from the pin to the edge of the hole by shear forces increases K and the resulting increase in crack growth-rates is evaluated in section 3.

Only the opening-mode stress intensity factor K_I is evaluated and used in the calculation of the growth-rates of fatigue cracks. Since the sliding-mode factor K_{II} will be much less than K_I and the law governing crack growth under mixed mode conditions is not known.

2 ANALYSIS

In this section a cracked pin-loaded lug is modelled by a sheet containing a circular hole of radius R with a distribution of load acting on the perimeter of the hole; in r, θ coordinates, the crack of length ℓ lies along $\theta = 0$ (see Fig 1). If there is no friction between the pin and the edge of the hole the load P will be transmitted from the pin to the sheet by radial forces only; these are represented by a normal stress (pressure) distribution around $r = R$. If there is friction, then the load will be transmitted by a combination of radial and tangential forces; these are represented by a normal stress and a shear stress distribution acting around $r = R$. At any given point on the perimeter the shear force is proportional to the radial force; the constant of proportionality is the coefficient of friction which will be a function of position.

The above model does not include effects resulting from the remote stress required for equilibrium which acts in the opposite direction to P or those due to the presence of the lug edges. These effects can be included by a combination of superposition and the use of the compounding technique developed by Rooke[5] for evaluating the stress intensity factor for a crack at the edge of a loaded hole in the presence of boundaries.

2.1 Load transfer by normal and shear forces

Consider the configuration given in Fig 1 with a pressure distribution $p(\beta)$ given by

$$p(\beta) = p_0 \cos \beta \quad , \qquad -\tfrac{\pi}{2} \leq \beta \leq \tfrac{\pi}{2} \quad , \tag{1}$$

which acts on the perimeter of the hole. This distribution has been shown[4] to be a good representation of the load for some lug configurations in the absence of friction. The force per unit thickness acting in a direction perpendicular to the crackline on an arc of the perimeter between β and $\beta + d\beta$ is $p(\beta) \cos \beta \, R d\beta$; therefore the total force per unit thickness P_0, acting in that direction is given by

$$P_0 = R \int_{-\pi/2}^{\pi/2} p_0 \cos^2 \beta \, d\beta = \tfrac{\pi}{2} R p_0 \quad . \tag{2}$$

If there is friction between the pin and the edge of the hole, then shear stresses will act on the perimeter; they are given by

$$\tau(\beta) = \mu p(\beta) \tag{3}$$

where μ is the coefficient of friction and $p(\beta)$ is the distribution of pressure. In general μ will be a function of position round the hole. Edwards[2] has shown that the coefficient of friction increases with the amount of slip under fretting conditions; thus μ will be a maximum at $\beta = \pm\pi/2$ and zero at $\beta = 0$. The distribution of pressure $p(\beta)$ will be modified from that given by equation (1). The shear stress $\tau(\beta)$ changes direction (and hence sign) at $\beta = 0$; it acts in a counter-clockwise direction for $0 < \beta \leq \pi/2$ and clockwise for $-\pi/2 \leq \beta < 0$.

The force perpendicular to the crackline acting on an arc of the perimeter of length $Rd\beta$ is given by $[p(\beta) \cos \beta + \tau(\beta) \sin \beta] Rd\beta$ therefore the total force P_T is after substitution of equation (3), given by

$$P_T = R \int_{-\pi/2}^{\pi/2} p(\beta)(\cos \beta + \mu \sin \beta) d\beta \quad . \tag{4}$$

In order to evaluate P_T both $p(\beta)$ and μ must be known as functions of β. It is assumed that the angular dependence of the pressure is the same as that given in equation (1) but the amplitude is reduced, that is

$$p(\beta) = p_\mu \cos \beta \quad , \tag{5}$$

where $p_\mu < p_0$. It is assumed that the coefficient of friction is given by

$$\mu = \mu_m |\sin \beta| \quad , \tag{6}$$

which satisfies the conditions given above when μ_m is a positive constant.

Substitution of equations (5) and (6) into equation (4) and integrating leads to

$$P_T = \frac{R p_\mu}{6} (3\pi + 4\mu_m) \quad . \tag{7}$$

Since the total load transmitted from the pin to the sheet will be the same with or without friction, it follows that $P_T = P_0$. Thus from equations (2) and (7), 8-3

$$\frac{p_\mu}{p_0} = \frac{3\pi}{3\pi + 4\mu_m} \quad . \tag{8}$$

Edwards[2] has shown that μ_m may be as large as unity, and two values $\mu_m = 0.5$ and 1.0 will be considered in this paper. From equation (8) it follows that $p_\mu = 0.825p_0$ for $\mu = 0.5$ and $p_\mu = 0.702p_0$ for $\mu = 1.0$. Since from equation (2) the load transmitted by the normal forces due to the pressure is proportional to the amplitude of the pressure, it follows that the proportion of the load transmitted by the shear forces (P_s say) is given by

$$\frac{P_s}{P_0} = \frac{p_0 - p_\mu}{p_0} \quad . \tag{9}$$

That is, 17.5% of the load is transmitted by shear if $\mu_m = 0.5$, and 29.8% if $\mu_m = 1.0$. Moon[4] has measured the radial strains next to the hole at $\beta = 0$ and shown that after many fretting cycles, reductions of ~30% occurred in the strain, which implies a similar reduction in the normal stress and hence in the load transmitted by that stress.

By combining equations (3), (5), (6) and (8) the shear stress is given by

$$\tau(\beta) = \mu_m p_0 \left(\frac{3\pi}{3\pi + 4\mu_m}\right) \sin\beta \cos\beta \quad . \tag{10}$$

This is plotted in Fig 2 for $\mu_m = 0.5$ and 1.0 . The pressure

$$p(\beta) = p_0 \left(\frac{3\pi}{3\pi + 4\mu_m}\right) \cos\beta \tag{11}$$

is also plotted for $\mu_m = 0.0$, 0.5 and 1.0 .

2.2 Stress intensity factors

The stress intensity factors for a crack at the edge of a hole can be obtained from the stress distributions around the perimeter by using the Green's function technique developed in Ref 3. In general the opening-mode stress intensity factors are of the form

$$K_I^n = K_1^n + \alpha K_2^n \quad \text{and} \quad K_I^s = K_1^s + \alpha K_2^s \ , \tag{12}$$

where the superscripts n and s denote normal stresses and shear stresses respectively, and α is a function of Poisson's ratio. If the normal stress distribution $p^n(\phi)$ on the perimeter is given by

$$p^n(\phi) = p_0^n h^n(\phi) \quad , \tag{13}$$

where ϕ is the angle measured counter-clockwise from the crackline, and the shear stress distribution $p^s(\phi)$ is given by

$$p^s(\phi) = p_0^s h^s(\phi) \quad , \tag{14}$$

then K_i^n and K_i^s (i = 1,2) are given[1] by

$$K_i^n = \tfrac{1}{2} p_0^n \sqrt{\pi \ell} \sum_{m=1}^{N} h^n(\phi_m) G_i^R(\phi_m) \Delta\phi_m \tag{15}$$

and

$$K_i^s = \tfrac{1}{2} p_0^s \sqrt{\pi \ell} \sum_{m=1}^{N} h^s(\phi_m) G_i^T(\phi_m) \Delta\phi_m \quad . \tag{16}$$

The Green's functions $G_i^R(\phi_m)$ and $G_i^T(\phi_m)$ are tabulated in Ref 3 for fixed values of ϕ_m at intervals $\Delta\phi_m$ (measured in radians).

The stress distributions to be used in equations (15) and (16) are those given in the previous section; that is

8-4

$$p^n(\phi) = p(\beta) \quad \text{and} \quad p^s(\phi) = \tau(\beta) , \qquad \beta = \frac{\pi}{2} - \phi . \tag{17}$$

The functions $h^n(\phi)$ and $h^s(\phi)$ are thus given by

$$h^n(\phi) = \cos \beta = \sin \phi \tag{18}$$

and

$$h^s(\phi) = \sin \beta \cos \beta = \sin \phi \cos \phi . \tag{19}$$

Since $h^n(\phi)$ is symmetric about $\phi = \pi/2$ and $G_2^R(\phi)$ is antisymmetric[1], it follows that K_2^n is zero; and since $h^s(\phi)$ is antisymmetric about $\phi = \pi/2$ and $G_2^T(\phi)$ is symmetric it follows that K_2^s is also zero. Therefore

$$K_I^n = \frac{1}{2}\left(\frac{3\pi}{3\pi + 4\mu_m}\right) p_0 \sqrt{\pi \ell} \sum_{m=1}^{N} \sin \phi_m \, G_1^R(\phi_m) \Delta\phi_m \tag{20}$$

and

$$K_I^s = \frac{\mu_m}{2}\left(\frac{3\pi}{3\pi + 4\mu_m}\right) p_0 \sqrt{\pi \ell} \sum_{m=1}^{N} \sin \phi_m \cos \phi_m \, G_1^T(\phi_m) \Delta\phi_m . \tag{21}$$

Equations (20) and (21) together with the tabulated[3] values of $G_1^R(\phi_m)$ and $G_1^T(\phi_m)$ have been used to evaluate K_I^n and K_I^s for various crack lengths. Curves of the opening-mode stress intensity factor K_I $(= K_I^n + K_I^s)$ are shown in Fig 3 for $\mu_m = 0.0$, 0.5 and 1.0; also shown separately are the normal and shear contributions K_I^n and K_I^s for $\mu_m = 0.5$ and 1.0. It is seen from Fig 3 that although the presence of friction reduces the stress intensity factor arising from the normal stresses, the factor arising from the shear stresses more than compensates and the total K_I increases as μ_m increases.

At the shortest crack lengths, K_I is increased by a maximum of 26% for $\mu_m = 1.0$ and by 15% for $\mu_m = 0.5$. The increase is shown as a function of crack length in Fig 4 where $K_I/K_I(0)$ *vs.* ℓ/R is plotted; $K_I(0)$ is the stress intensity factor in the absence of friction. Also plotted are the ratios $K_I^n/K_I(0)$ and $K_I^s/K_I(0)$. It is seen, for $\mu_m = 1.0$, that at the shortest cracks K_I^n is reduced to ~70% of the original K_I without friction, but K_I^s is ~55% of the original K_I . The reduction in K_I^n is less for smaller values of μ_m and K_I^s is smaller.

3 FATIGUE CRACK GROWTH

The increase in the stress intensity factor, calculated in the previous section, implies that fatigue cracks will grow faster if shear forces are present at the edge of the hole. The magnitude of the increase in growth rate can be deduced by considering a simple crack growth law such as that suggested by Paris[6]. He postulated that the growth of the crack per cycle of stress $(d\ell/dN)$ was proportional to the stress intensity factor raised to a power p , that is,

$$\frac{d\ell}{dN} \propto K_I^p ; \tag{22}$$

for many materials p is in the range 2 to 4.

If $(d\ell/dN)_\mu$ is the growth rate in the presence of frictional shear forces, and $(d\ell/dN)_0$ the rate in the absence of friction, then it follows from equation (22) that

$$\frac{(d\ell/dN)_\mu}{(d\ell/dN)_0} = \left(\frac{K_I}{K_I(0)}\right)^p . \tag{23}$$

The ratio of stress intensity factors, in the above equation, was obtained in the previous section, hence the increase in crack growth rate can be determined. Plots of $(d\ell/dN)_\mu/(d\ell/dN)_0$ are shown as a function of ℓ/R in Fig 5 for $p = 2$, 3 and 4 and $\mu_m = 0.5$ and 1.0.

It can be seen from Fig 5 that the presence of frictional forces causes significant increases in crack growth rates, particularly at short crack lengths. The magnitude of the increases depends on both the friction constant and the power p in the crack growth law. The biggest effects occur at the largest values of both μ_m and p ; for instance,

for $\mu_m = 1.0$ and $p = 4$, the crack grows more than twice as fast for $\ell/R < 0.4$. These large increases in crack rate mean that the lifetime of a cracked structure will be substantially reduced; for example, if the crack rate for short cracks is doubled, then the lifetime will be approximately halved since the crack is short during most of the lifetime.

8-5

4 DISCUSSION

In order to illustrate the effects of frictional forces on the fatigue lifetime of a cracked pin-loaded lug, simple models were chosen to represent the radial load distribution and the variation of the coefficient of friction around the hole. For some pin-loaded lugs other distributions of radial load may be more appropriate[4] and the variation of the coefficient of friction will probably need modification when experimental evidence becomes available. Nevertheless, the essential feature remains the presence of frictional shear forces near the root of the crack increases the crack opening thereby increasing the stress intensity factor and hence reducing the lifetime in fatigue.

It was assumed in section 2.1 that the transfer of some load by shear stresses reduced the magnitude of the load transferred by normal stresses (pressure) but not its distribution. This assumption also may require modification in the light of experimental evidence. In practice the transfer of load by friction with a coefficient that varies with position will probably lead to a change in the distribution in the normal stress subject to the condition of constant total load as defined by equation (4). Changing the distribution of normal stress will change the contribution to the stress intensity factor in a more complex way[1,3] than the simple scaling factor assumed above. Various assumptions regarding both the distribution of pressure round the hole and the distribution of the coefficient of friction can be examined theoretically using the same Green's function approach as in this paper.

Large increases in the value of the crack growth rate, due to fretting, have been measured[4] for some lugs. The magnitude of the measured increases is similar to that shown in Fig 5, but rises more rapidly at very short cracks. This suggests that the shear forces between the pin and the edge of the hole may be larger than assumed in this paper. A model in which the coefficient of friction μ varied more slowly than $|\sin\beta|$ in the region of $\beta = \pm\pi/2$ would give larger shear stresses and hence larger stress intensity factors leading to increased growth rates.

Only the opening-mode stress intensity factor K_I has been considered in this paper. The sliding-mode K_{II} can be evaluated using similar techniques[3]; however insufficient is known about crack growth in the presence of mixed modes for the effects of K_{II} to be included in lifetime calculations. These effects would, in this case, be small since for the configuration studied $K_{II} \ll K_I$ for all crack lengths.

5 CONCLUSIONS

When fretting occurs in a pin-loaded lug, some load will be transmitted, due to friction, by shear forces from the pin to the perimeter of the hole; the presence of these shear forces will cause an increase in the stress intensity factor of a crack at the edge of the hole. This increase which is most significant at short cracks, leads to a substantial reduction in fatigue lifetime. The magnitude of these effects depends strongly on the actual distribution of loads around the hole and the coefficient of friction between the pin and the lug.

REFERENCES

1 D.P. Rooke and J. Tweed: 'Stress intensity factors for a crack at the edge of a pressurized hole.' Int. J. Eng. Sci., 18, (1980), 109-121

2 P.R. Edwards and R. Cook: 'Fracture mechanics prediction of fretting fatigue under constant and variable amplitude loading.' Proceedings of 11th ICAS Conference, Lisbon, 1978, pp.505-517

3 D.P. Rooke and S.M. Hutchins: 'Stress intensity factors for cracks at loaded holes - effect of load distribution.' (1982) RAE Technical Report 82054

4 J.E. Moon: 'Crack growth in pin-loaded lugs.' In Aircraft Fatigue in the 80's. Eds. J.B. de Jonge and H.H. van der Linden, 11th ICAF Symposium, Noordwijkerhaut (1981), pp 2.9/1 to 2.9/54

5 D.P. Rooke: 'Stress intensity factors for cracks at fastener holes.' (1981) RAE Technical Report 81144

6 P.C. Paris: 'The fracture mechanics approach.' In Fatigue - an interdisciplinary approach. Eds. J.J. Burke, N.L. Reed and V. Weiss, New York, Syracuse University Press, (1964) pp.107-132

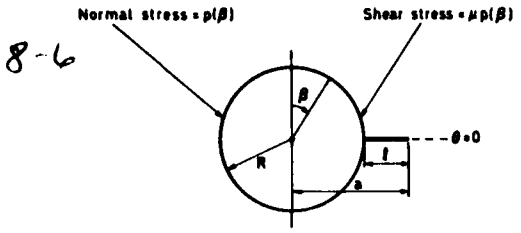

Fig 1 Loaded hole with radial crack

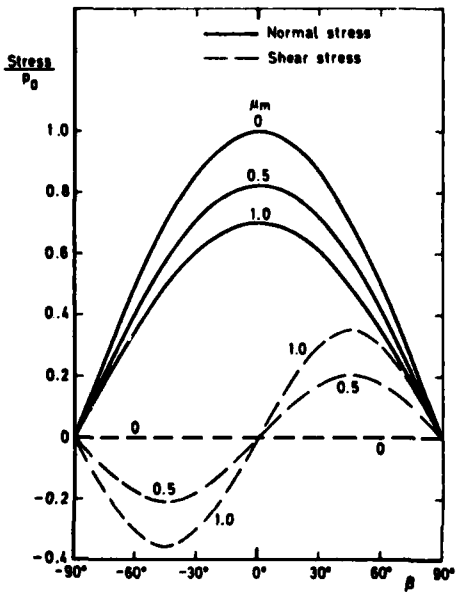

Fig 2 Stress distributions around the perimeter of the hole

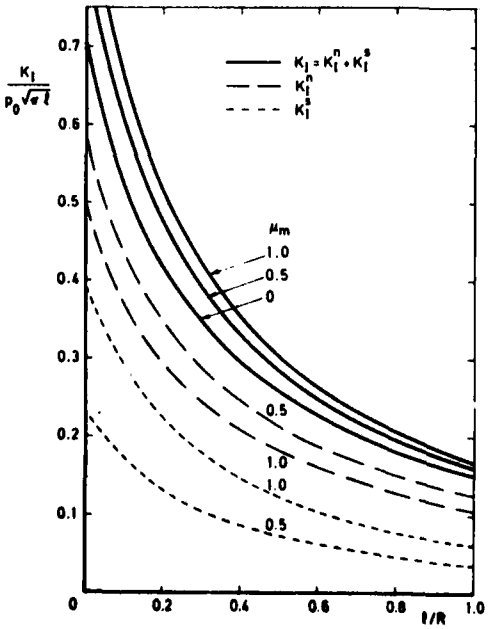

Fig 3 Stress intensity factors in the presence of frictional forces

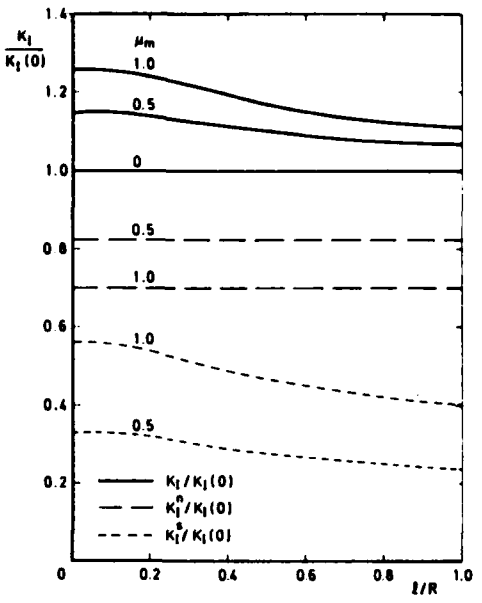

Fig 4 Effect of frictional forces on the stress intensity factor

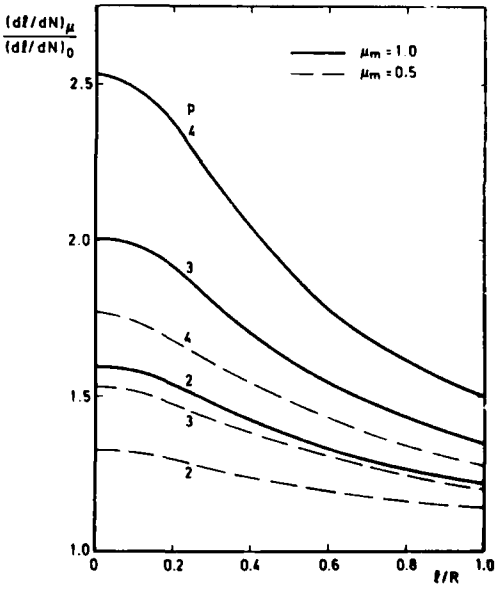

Fig 5 Effect of frictional forces on the crack growth rate

LIFETIME PREDICTION METHODS FOR CORNER CRACKS AT HOLES

by
C.J. Lof
National Aerospace Laboratory NLR
1059 CM Amsterdam, The Netherlands

9-1

SUMMARY

An application of linear elastic fracture mechanics to 3-dimensional crack growth prediction was developed in two phases. In the first phase finite element techniques for accurate stress intensity calculation were evaluated. In the second phase, treated in the underlying paper, corner flaw growth during constant-amplitude fatigue testing was studied. A lifetime prediction algorithm was developed based on investigated crack behaviour as a function of calculated instantaneous stress intensity distribution along the crack boundary. Finally, as an example lifetime predictions are given. Comparison of such results with other data, both from experiments and from the literature showed very acceptable agreement.

1. INTRODUCTION

Cracks emanating from holes in aircraft structural components mostly start at the intersection of a surface and a bore wall. Cracks of this type develop both in size and shape under fatigue load. It is stated that during a considerable part of its total fatigue lifetime, the crack is small with respect to the local thickness of the plate or structural component. In the present paper corner cracks are considered with sizes between 0.1 and 1.0 times the local thickness. The cracked structure is treated as a three-dimensional configuration with plane cracks. The cracks have curved boundaries and the shape of the boundary is described by more than two free parameters essentially.

The characteristics of the stress intensity (K-) distributions of such cracks are studied using the Finite Element technique (1,2) or, if available, data from the literature (3,4).

Concerning crack growth prediction, and using Paris' law application, the variation in local K-values causes various local crack growth velocities and, consequently, the crack size and shape changes during its growth. It appeared that K-distributions change instantly by crack shape variation. An algorithm is developed making allowance for the change in K-distribution during each crack growth prediction step.

2. THE ΔK-CRACKGROWTH RELATIONSHIP FOR CONSTANT-AMPLITUDE LOADS

For considered low constant Amplitude loads Linear Elastic Fracture Mechanics can be applied, using the stress intensity amplitude ΔK as a calibrated measure for crack growth velocity da/dN. The influence of crack tip plasticity effects is incorporated in the calibration data obtained using the same stress amplitude ratio $R = \sigma_{max}/\sigma_{min}$.

Also for short cracks, described in 3-d, available or obtained calibration data appeared to be valid however, within restrictions, as mentioned by Schijve (5) and Hodulac (6).
Calibration tests have to be performed using thick-walled specimens with a central crack and crack fronts having a slight curvature (no shear lips).

In general, a proper regression to a number of ln da/dN - lnΔK data is not adequately described by a single straight line (Fig.1). However, for prediction application one may consider the regression line sectioned into parts with constant gradients. So, within such parts an equation like Paris/law can be applied easily for purposes of numerical integration of life time during incremented steps in crack size.

3. CALCULATION OF LOCAL ΔK-VALUES ON THE BOUDNDARY OF A PLANE CRACK

It is very essential for proper lifetime prediction that instantaneous K-distributions along subsequent crack boundaries can be derived with high accuracy. In practice, K is calculated on a discrete number of nodes of each subsequent (incremental) crack front variant. For simple configurations with a crack, the K-values on quarter elliptical boundaries can be derived from data published (3,4). Data are available for a few discrete values of plate thickness, bore diameter, and crack size parameters. The K-distribution is given for a number of discrete points at such boundaries (figure 2). K-values for arbitrary parameters are derived by linear interpolation. Accuracies obtained are within 2-4%.

For arbitrary configurations and, or arbitrary crack shapes, no "databank" is available. K-values then have to analysed by e.g. the finite element technique.

Special techniques are developed for application to Fracture Mechanics purposes, namely the use of crack tip elements and the application of virtual crack extensions.

Special crack tip elements can be used, or if possible, crack tip situated elements can be deformed (by quarter node positioning) so that a local strain field singurarity is obtained at the crack boundary.

The virtual crack extension method (7) can be applied to accurate energy release rate calculations. Several crack front virtual variants can be treated within only one solution.

Lokal K-values are found using the equation:

$$K_i^2 = \frac{E}{1-\nu^2} \frac{\delta V_i}{\delta a_i} \qquad (1)$$

for plane strain, in which

$$\delta V_i = (U^T \{\delta S_i\} U)/2 \qquad (2)$$

Here, δS_i is the so-called stiffness derivative calculated for each local virtual variations δa_i of the crack boundary.

K-values at local positions can also be derived using the known relationship between K and the local Crack Opening Displacement (C.O.D.) value. This method appeared to be somewhat less accurate for coarse meshes, as applied for the 3-d configurations.

(ΔK values are in the same proportion to K-values as the applied remote stress amplitude is to a remote constant load of the finite element model).

4. THE MECHANISM OF THE BOUNDARY SIZE AND SHAPE DEVELOPMENT

9-2

Calculated ΔK-values of discrete points at one instantaneous crack front may differ considerably. Therefore, because of the assumed relationship between the local ΔK-value and local crack growth velocity, the crack shape may change rapidly during crack growth. However, cracks in practice show rather stable crack shape development. It is shown (Fig.11) that crack shapes reproduce very well if no conditions that may cause local delay are present (5,6).

The stability of crack shapes may be explained as follows. The occurrence of local deviations from the stable crack shape causes a re-distribution of ΔK, resulting in a shape correction towards the stable one. This is depicted in figure 3, showing the effect of local crack shape exceedance on ΔK-distributions.

During crack growth the local stress intensity (ΔK_i), as a function of a local crack size parameter (a_i) can be described along a "path" intersecting subsequent crack boundaries perpendicularly (figure 4). These ΔK_i (a_i)-functions, however appear to be interdependant. The rule of crack growth towards stable shapes effects a shallower increase of relatively higher ΔK_i-values and a steeper increase of the relatively lower ones. ΔK-values tend to converge towards a narrow band on the ΔK(a) diagram (figure 5). The rules mentioned above are successfully applied in a prediction algorithm which reckons with effects of shape development,

5. A PREDICTION ALGORITHM BASED ON PREVIOUSLY DESCRIBED CRACK GROWTH BEHAVIOUR

5.1 Numerical integration of lifetime steps

For accurate prediction of crack behaviour the change of local ΔK-values during a prediction step has to be taken into account. So, a set of local ΔK_i (a_i)-functions have to be estimated in accordance with crack growth behaviour as described before. A global ΔK(a)-function is estimated as:

$$\Delta K(a) = \Delta K(a_0) \sqrt{a} / \sqrt{a_0} \qquad (3)$$

for a node being positioned centrally at the crack front (i.e. node 2 of figure 4). The gradients of other $\Delta K_i(a_i)$ - functions are estimated towards an assumed point of convergence in the ΔK(a)-diagram (figure 6). Lifetime increments δN are related to constant finite cracksize increments δa by:

$$\delta N_{ij} = \delta a \, (C \, \Delta K^n \, (a_{ij}) \,)^{-1} \qquad (4)$$

where C and n are the Paris' law constants derived from calibration, and $\Delta K(a_{ij})$ is the local ΔK-value at node i after the j th cracksize increment δa and

$$a_{ij} = a_{io} + (j - .5) \, \delta a \qquad (5)$$

Local crack extension values da_i are obtained by numerical integration of equation 4 until a certain value dN:

$$dN_i = \sum_{j=1}^{k} \delta N_{ij} \equiv dN \qquad (6)$$

and simultaneously, along the local "path" (figure 7):

$$a_{ij} = a_{io} + j \cdot \delta a \qquad (7)$$

until: $da_i \approx a_{ik} - a_{io}$ (7a)

Crack size increments δa are taken very small ($a_o . 10^{-3}$). The value of the counter K will in general be different for each node i after dN cycles.

It is noticed that da_i-values are calculated for internal nodes only. The prediction of crack growth velocity for crack front intersections at free surfaces is avoided.

Experience showed that the 3d-relation between derived ΔK and da/dN is not valid in a narrow zone along free surfaces (see also ref.6). For relatively low stress maxima however, the 3-d crackgrowth behaviour appeared to be dominant with respect to crack shape development control.

5.2 Stepwise verification of the predicted growth

A verification of ΔK-values is needed for the predicted new curve. If discrepancies between local verified values and estimated values are within an accepted range (e.g.5%), the prediction can be continued starting from the new boundary. Otherwise, shorter incremental steps have to be defined;this is not a real problem if a databank is available for effective verifications of the ΔK_i-values.

If no databank is available for the configuration at hand, and a finite element calculation is needed for stepwise verification of the K-distribution, a better estimate of local ΔK_i-a_i gradients is urgent . This better "estimate" is obtained after a second prediction from the original boundary. This second prediction uses updated $\Delta K_i(a_i)$-gradients as found after the first verification (see line 1-4 on figures 8,9). Newly verified ΔK values on this second predicted curve are in general not closer to estimated gradients (point 5, fig. 8,9). A very accurate ΔK gradient estimate is found now by interpolation between two verified ΔK-values and two estimated values for corresponding a_i (crossing intersection lines on the ΔK (a) diagram, fig. 8,9).

This method necessitates two ΔK verification calculations per step, but relatively large steps can be made (up to 50% of the instantaneous crack size).

6. PROGRAMS FOR EASY CRACK GROWTH PREDICTION

The availability of reliable and detailed stress intensity data from Raju and Newman's databank (3,4) was the basis for some very practical Fortran routines fot quick lifetime calculation of surface and corner cracks.The principles of crack growth controlled by internal nodes were applied successfully. Three

basic cracked configurations are involved: (figure 10)

The surface crack;

Corner cracks at an unloaded hole;

Corner cracks at a pin-loaded hole.

Application of a correction factor β for finite width of the plate by Bowie (8) is involved:

$$\beta = \sqrt{\frac{1}{\cos \frac{\pi}{2} \left(\frac{D+C}{D-C}\right)}} \qquad (8)$$

where $C = \pi ac/4t$

Also crack growth at one side of a hole can be considered, or even unequal crack sizes on both sides, using a correction factor CF supplied by Shah (9):

$$CF = \sqrt{(D + C + C^1)/(D + 2C)} \qquad (9)$$

where $C = \pi ac/2t$ and $C^1 = \pi a^1 c^1/2t$ (Fig.10).

Calculations may be started at any initial crack shape. During crack growth prediction, all initial shapes develop towards stable shapes that belong to the specific configuration and load.

For applied pin-loads at a hole, the real load distribution in the bore during crack growth is not known exactly and, thus, predictions based on the pin load databank are uncertain. Application to a lug configuration demands a correction on S.I. data for the lug head shape instead of the long strip.

Correction of the databank values for both load distribution effects and shape effects may be derived through restricted finite element calculations.

7. EXAMPLES

Many experimental lifetime measurement results are "checked" by application of the prediction routine described, A useful reliability test of applied algorithm's is supplied using surface crack testing data and crack shape markings (Fig.11) available from former investigations. K data from finite element analysis and from Newman's databank agreed within 2 percent. Predicted crack shapes agreed within marking line thicknesses, so, the program reproduces stable shapes in the right way.
The lifetime of the short crack between crack initiation and the first marking was calculated as 145 kc against 169 kc needed in the experiment. The lifetime between the first and the last marking (almost-thru crack) was predicted as 152 kc against 164 kc needed in the experiment.

Examples of cornercrack predictions at one side and at both sides of the hole are shown in figures 12 and 13.(11) . Experimental crack sizes and shapes shown some scattering (with respect to corresponding values of the lifetime). Predicted crack sizes appear to lie reasonably between the extremes. Also predicted shapes are reasonable however, in some cases crack shapes deviate from predicted elliptic shapes.

Available former calculated K-values for a lug configuration (10) were used for the derivation of correction factors for the pin-loaded configurations, the third configuration of figure 9. Cronological mapping of predicted crack fronts up to 25 kc is shown in figure 14. The corresponding specimen showed similar crack sizes after 18-24 kc.

8. CONCLUSIONS

-The knowledge of instantaneous ΔK distributions is indispensable for proper numerical prediction of crack-size and -shape development. Reliable ΔK-values can be derived within 3-4% from a databank or by a Finite Element technique.

-The accuracy of numerically predicted lifetimes is highly dependent on the reliability of calibration data; material and load condition have to be the same for applied calibration tests.

-Reliable predictions of crack life during constant-amplitude loading within some restrictions can be made within 10-15%. This level of accuracy can be seen as very acceptable for life-time prediction calculation.

9. RECOMMENDATIONS

Since the method offers the possibility to predict using S.I. data at internal points on the crack boundary, arbitrary shapes can be treated by using sufficient nodes. Predictions using K-data on the surface points, and 3-d calibration supplied wrong results in crack shapes.

10. REFERENCES

1. Bartelds, G and de Koning, A.U., "Application of finite element methods to the analysis of cracks"- Phase I- evaluation of method", NLR TR 78138 U, 1978.

2. Lof, C.J. "Lifetime prediction methods for corner cracks at holes". NLR TR 81077. 1981

3. Raju, I.S. and Newman, J.C.Jr "Stress Intensity Factors of two symmetric corner cracks". ASTM STP 677 (1979)

4. Newman J.C.Jr. and Raju, I.S. "Analysis of surface cracks". NASA T.P. 1578. dec.'79.

5. Schijve, J. "Differences between the growth of small and large fatigue cracks.....Report LR-327 Delft University of Technology july 1981.

6. Hodulak, L, Kordisch, H. , Kunzellmann, S., Sommer, E. " Growth on Part-Through Cracks". ASTM STP 677, 1979, pp 399-410.

7. Parks, D.M., "Stiffness derivative finite element technique for determination of elastic crack tip stress intensity factors", Int. Journal of Fracture, Vol.10, No.4, 1974.

8. Bowie, O.L. "Analysis of an Infinite Plate Containing Radial Cracks Originating from the Boundary ...." J of Mathematics and Physics, Vol.35, 1956, pp.60-71.

9. Shah, R.C. in "Mechanics of Crack Growth, ASTM STP 590, 1976, pp.429-459.

10. Wanhill, R.J.H. and Lof, C.J. "Calculation of Stress Intensity Factors for corner cracking in a lug". AGARD Conference Proceedings no 221, 1976.

11. Minderhoud, S. "Fatigue Crack Growth of corner cracks" (Thesis) Delft University of Techn.Dep of Aerospace Eng. june 1982.

AD-A131 159 BEHAVIOUR OF SHORT CRACKS IN AIRFRAME COMPONENTS CONFERENCE PROCEEDINGS O..(U) ADVISORY GROUP FOR AEROSPACE RESEARCH AND DEVELOPMENT NEUILLY.. APR 83 2/3

UNCLASSIFIED AGARD-CP-328 F/G 1/3 NL

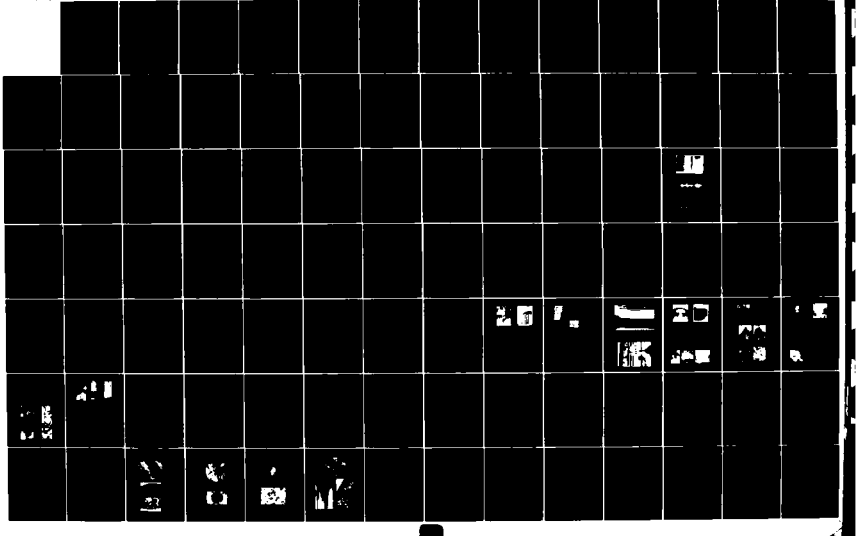

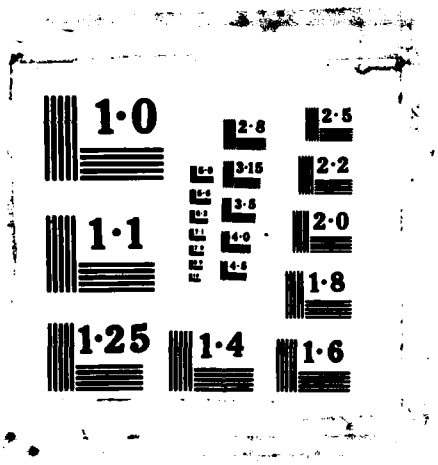
1·0
1·1
1·25
1·4
1·6
1·8
2·0
2·2
2·5
2·8
3·15
3·5
4·0
4·5

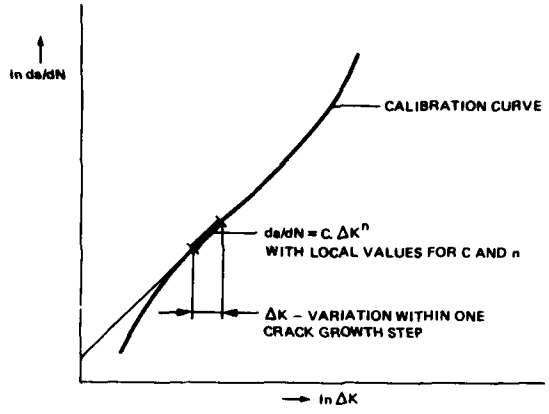

Fig. 1 Local approximation of crack growth calibration curve

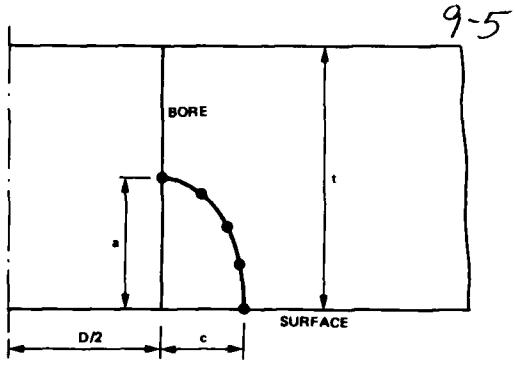

Fig. 2 Discrete points at a crack boundary

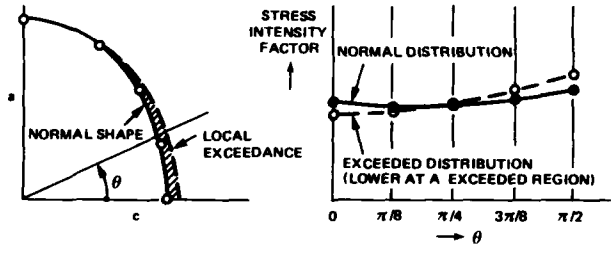

Fig. 3 The effect of local crack variation on the stress intensity distribution

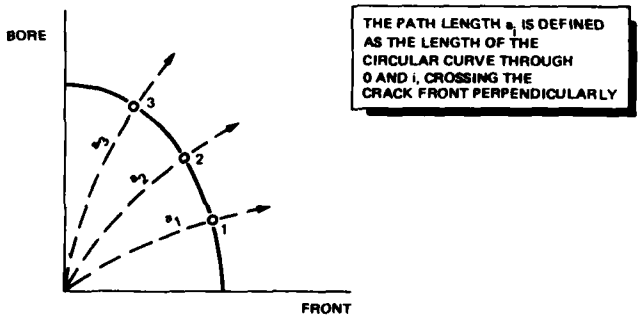

Fig. 4 Definition of a path length

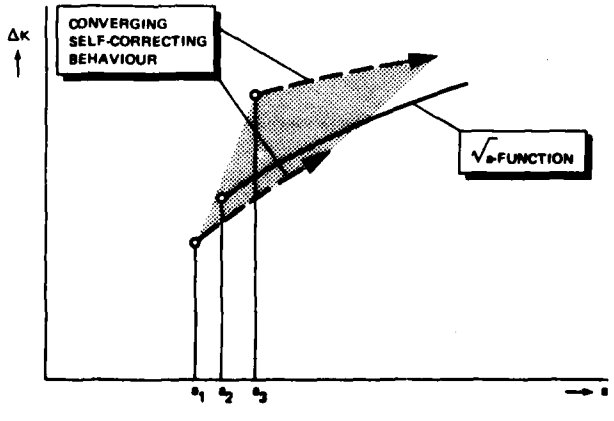

Fig. 5 Convergence of local ΔK,a-functions

9-6

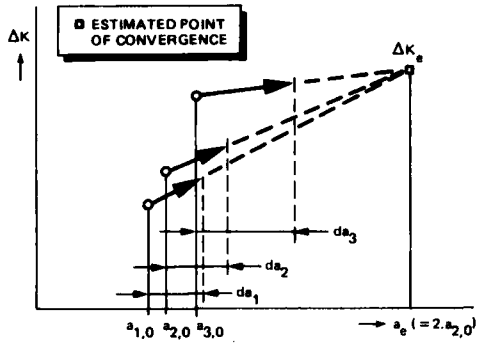

Fig. 6 Estimated local ΔK,a-gradients

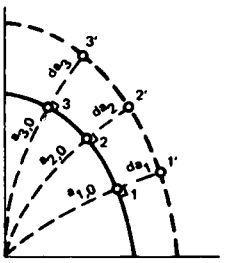

Fig. 7 Fitting a new predicted crackfront

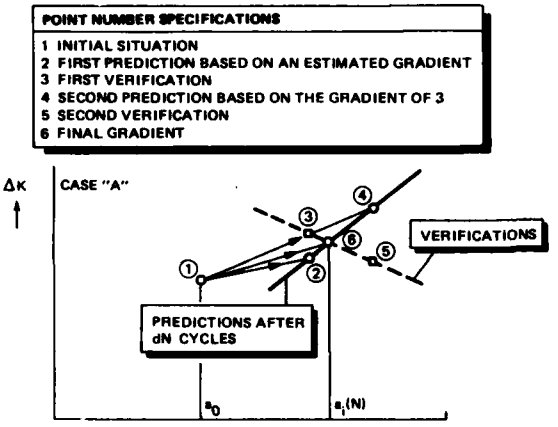

Fig. 8 The behaviour of ΔK versus a at a crack growth location for which the ΔK-gradient was underestimated initially

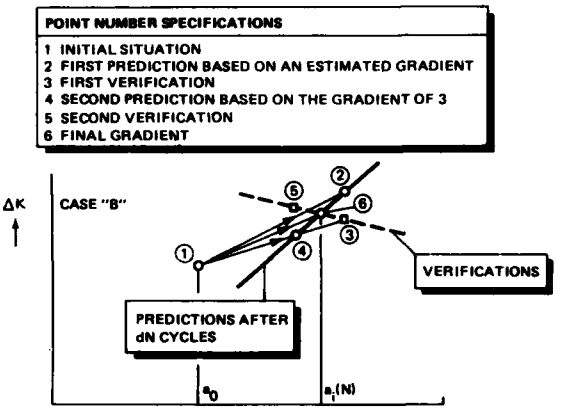

Fig. 9 The behaviour of ΔK versus a at a crack growth location for which the ΔK-gradient was overestimated initially

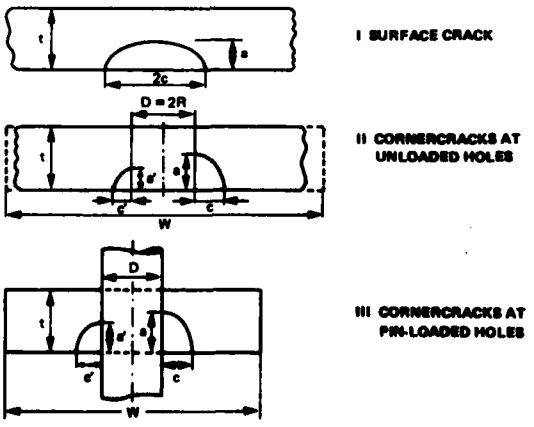

Fig. 10 Prediction programs for the standard configurations

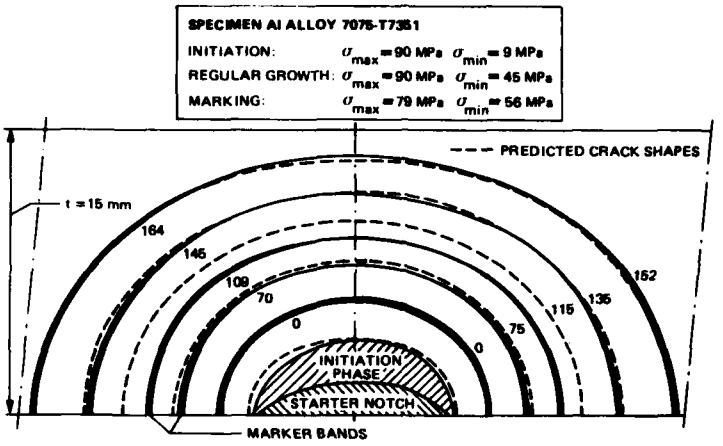

Fig. 11 Comparison of experimental and predicted crack shapes

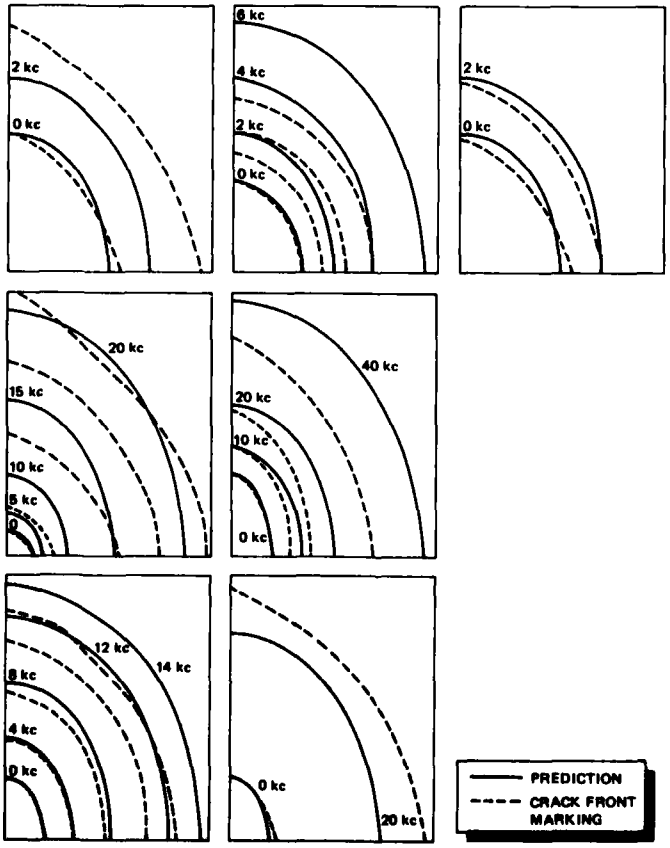

Fig. 12 Predictions and test results for a single corner crack at a hole (R/t = 0.5)
(Experiments by S. Minderhoud, Delft university)

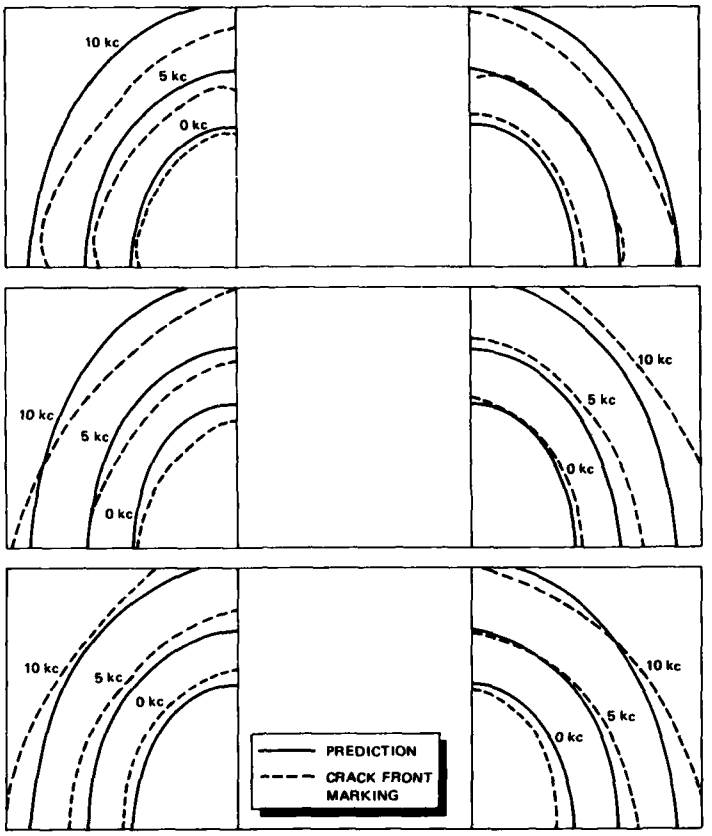

Fig. 13 Predictions and test results for two corner cracks at a hole (R/t = 0.5)
(Experiments by S. Minderhoud, Delft university)

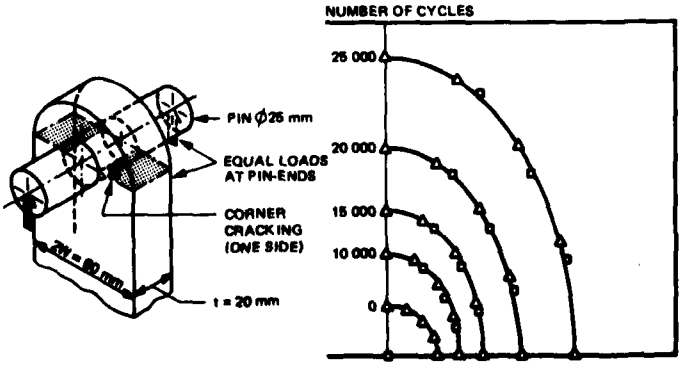

Fig. 14 Predicted crack shapes for a lug

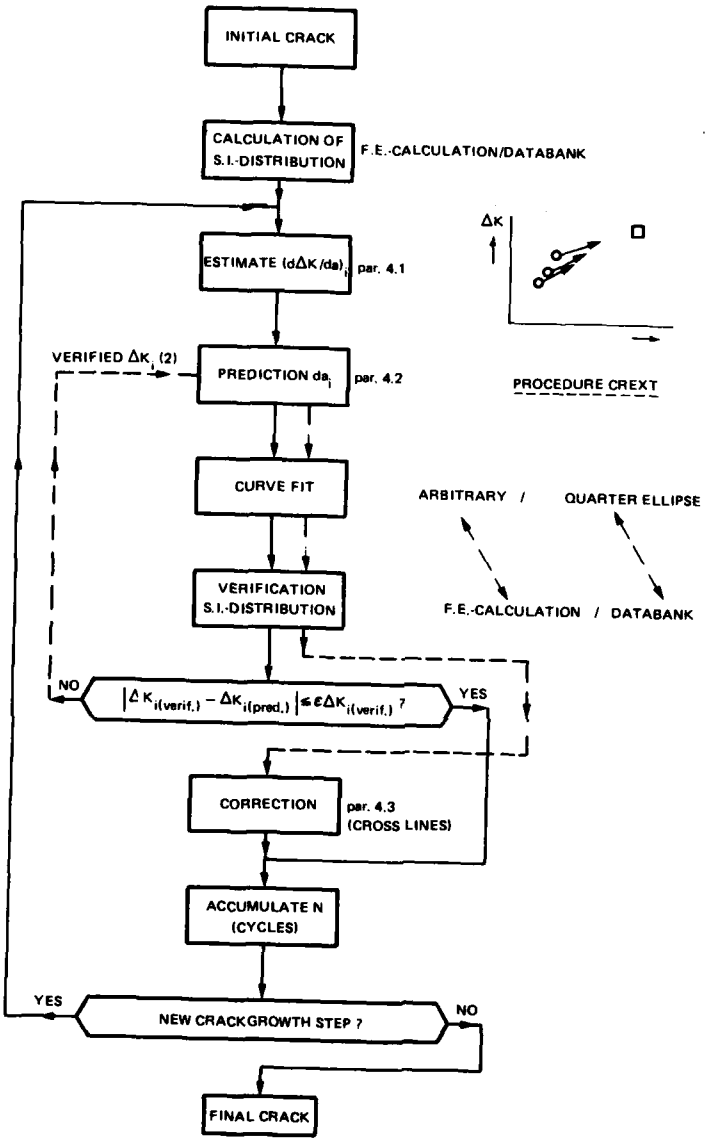

Fig. 15 Flow diagram of the prediction procedure

PROBABILISTIC FRACTURE MECHANICS ANALYSIS METHODS FOR STRUCTUPAL DURABILITY

JAMES L. RUDD
Aerospace Engineer

Air Force Wright Aeronautical Laboratories (FIBEC)
Wright-Patterson AFB, Ohio 45433, USA

JANN N. YANG
Professor

George Washington University
School of Engineering and Applied Science
Washington, D.C. 20052, USA

SHERRELL D. MANNING
Engineering Specialist Sr.

BILL G.W. YEE
Chief of Materials Research Laboratory

General Dynamics Corporation
Fort Worth Division
P.O. Box 748
Fort Worth, Texas 76101, USA

The United States Air Force requires that Air Force aircraft be designed to be durable. This requirement necessitates an analytical demonstration that excessive cracking within the airframe will not occur during the aircraft's design service life. In order to predict the time at which excessive cracking occurs, an analysis is needed which is capable of predicting the distribution of crack sizes within the airframe at any point in time. Such an analysis was recently developed and is presented in this paper. The durability analysis is based on a fracture mechanics philosophy, combining a probabilistic format with a deterministic crack growth rate relationship. Essential elements of the methodology are presented, with emphasis on the statistical representation of the initial fatigue quality of the structure. The accuracy of the durability analysis is demonstrated by correlating analytical predictions with experimental results of a fighter full-scale test article as well as complex-splice specimens subjected to a bomber load spectrum.

I INTRODUCTION

The United States Air Force structural integrity requirements for metallic airframes are specified in Reference 1. Of particular importance are the damage tolerance (Refs. 2 and 3) and durability (Refs. 3 and 4) requirements. The damage tolerance requirements ensure aircraft safety while the durability requirements minimize structural maintenance costs and functional impairment problems. Both sets of requirements are necessary to ensure the operational readiness of Air Force aircraft.

This paper addresses the durability aspects of structural integrity. The durability damage mode considered is fatigue cracking in fastener holes. This was found to be a very prevalent form of degradation in aircraft structures (Ref. 5). Aircraft structural durability involves many fastener holes in various components which are susceptible to cracking in service. The associated structural maintenance costs are proportional to the number of fastener holes requiring repair. Therefore, to assess the durability of the structure or the extent of damage as a function of time, the entire population of fastener holes must be considered. Thus, a statistical approach is best suited for quantifying the extent of damage as a function of time.

Various aspects of structural durability have been considered in the literature (Refs. 6-27). Structural durability can be defined in many different ways. The most appropriate definition is dependent on the particular aircraft considered. The crack sizes of interest are a function of the definition used. This paper considers relatively small subcritical crack sizes which often affect durability. For example, 0.76 mm - 1.27 mm (0.03 inch - 0.05 inch) radial cracks in fastener holes can affect functional impairment, structural maintenance requirements, and life-cycle costs. Such cracks do not pose an immediate safety problem. However, if the fastener holes containing such cracks are not repaired, economical repairs cannot be made when these cracks exceed a limiting crack size. For example, a 0.76 mm - 1.27 mm radial crack in a fastener hole can be cleaned up by reaming the hole to the next nominal hole size. When the crack sizes exceed this economical repair limit, excessive maintenance and repair costs can occur. Hence, an analysis is needed for predicting the extent of damage present at any particular point in time. Such an analysis was recently developed (Refs. 11-16 and 18-27) and evaluated for load transfer coupon specimens (Refs. 11, 12, 15, 21, 22, and 27).

This paper presents the recently developed durability analysis methodology. The methodology is based on a probabilistic fracture mechanics approach. The initial
10-2 fatigue quality of a structure is represented in a statistical manner by a distribution of equivalent initial flaw sizes. These equivalent initial flaw sizes are grown forward in time using a deterministic crack growth rate relationship. An evaluation is made of the accuracy of the analysis by correlating analytical predictions with test data for a fighter full-scale test article (Refs. 21 and 22) and complex splice specimens subjected to a bomber load spectrum (Ref. 27).

II DURABILITY DESIGN REQUIREMENTS

Air Force durability design requirements for metallic airframes are presented in References 1, 3 and 4. According to these requirements, the airframe must be designed to have an economic life greater than the design service life. Furthermore, the economic life must be demonstrated by analysis and test. The economic life analysis must account for the effects of initial quality variations, material property variations and the design loads/environments.

The economic life of a structure is currently defined in only qualitative terms: "... the occurrence of widespread damage which is uneconomical to repair and, if not repaired, could cause functional problems affecting operational readiness" (Ref. 1). There is no universal quantitative definition of "widespread damage" or acceptable structural maintenance cost limits. Such limits are currently determined by the contractor and the Air Force for the particular aircraft of interest. Durability compliance standards are defined based on the results of the full-scale durability test article.

III DURABILITY ANALYSIS CRITERIA

A. Durability Critical Parts Criteria

Criteria must be developed for determining which parts of an aircraft are durability critical (i.e., which parts must be designed to meet the durability design requirements). The durability critical parts criteria vary from aircraft to aircraft. They are especially dependent on the definition of economic life for the particular aircraft involved. A more detailed discussion of the durability critical parts criteria is presented elsewhere (Ref. 12). A typical flow diagram for selecting which parts are durability critical is presented in Fig. 1. In Fig. 1, durability refers to the ability of an airframe to resist cracking whereas damage tolerance refers to the ability of an airframe to resist failure due to the presence of such cracks.

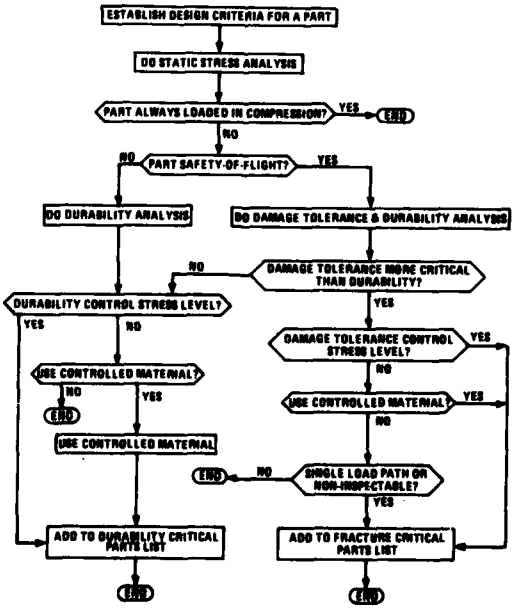

Figure 1 - Flow diagram for selecting durability critical parts

B. Economic Life Criteria

Criteria must be developed for determining the economic life of the particular aircraft of interest. Similar to the durability critical parts criteria, economic life criteria vary from aircraft to aircraft. They may be based on fastener hole repair (e.g., reaming the damaged fastener hole to the next nominal hole size), functional impairment (e.g., fuel leakage), residual strength, etc. Two promising analytical formats for quantifying the economic life of an airframe are (1) the probability of crack exceedance, and (2) cost ratio: repair cost/replacement cost. Both formats require a durability analysis methodology capable of quantifying the extent of aircraft structural damage as a function of service time. For example, assume the economic life criteria are based on the number of fastener holes which cannot be economically repaired (i.e., number of fastener holes with crack sizes equal to or greater than specified size X_1). Then an analytical format for quantifying economic life is presented in Fig. 2. In Fig. 2, P is the exceedance probability. More detailed discussions of economic life criteria are presented elsewhere (Refs. 11, 12, 15, and 18).

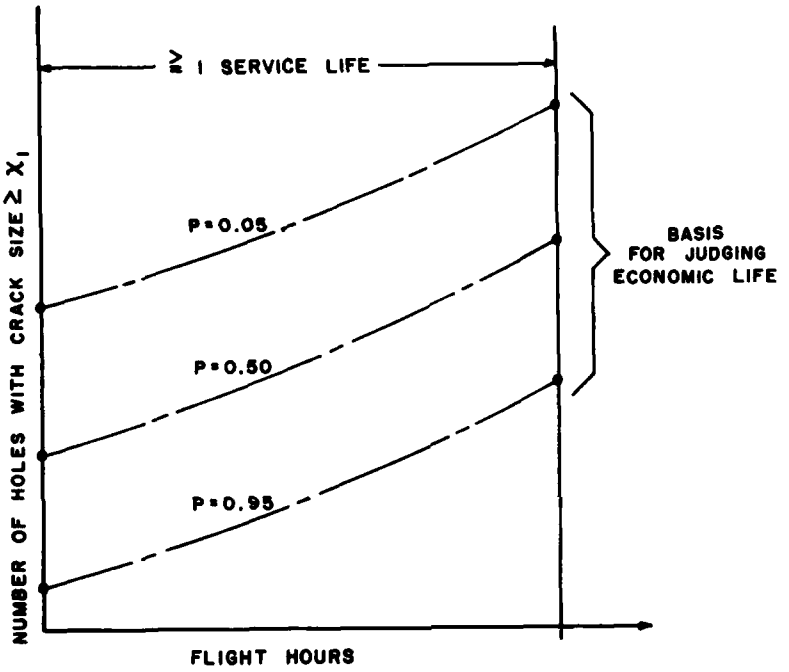

Figure 2 - Analytical format for economic life

IV DURABILITY ANALYSIS METHODOLOGY

A. General Description

The basic objective of the durability analysis methodology is to quantify the extent of damage as a function of service time for a given aircraft. The extent of damage is measured by the number of structural details (e.g., fastener holes, cut-outs, fillets, lugs, etc.) expected to have a crack size greater than a specified size at a given service time. Hence, the extent of damage is represented by the probability of crack exceedance. The durability analysis results provide a quantitative description of the extent of damage and a basis for analytically assuring that the economic life of the structure will exceed the design service life.

The durability analysis includes two essential steps: (1) the quantification of the initial fatigue quality of the structural details considered, and (2) the prediction of the probability of crack exceedance based on the initial fatigue quality and the applicable design conditions (e.g., load spectrum, stress levels, percent load transfer, etc.).

B. Initial Fatigue Quality

10-4

1. Initial Fatigue Quality Description

Initial fatigue quality (IFQ) defines the initial manufactured state of a structural detail or details with respect to initial flaws in a part, component or airframe prior to service. The IFQ for a group of replicate details is represented by an equivalent initial flaw size (EIFS) distribution. An equivalent initial flaw is a hypothetical crack assumed to exist in a detail prior to service. An equivalent initial flaw size is the initial size of a hypothetical crack which would result in an actual crack size at an actual point in time. An arbitrary crack size, a_0, is selected which can be readily detected or which can be reliably observed fractographically following testing. The time required for an initial defect, of whatever type, to become a fatigue crack of size a_0 is defined as the time-to-crack-initiation (TTCI). Test results of TTCI and crack growth rates using coupon specimens are employed to define the EIFS distribution. A conceptual description of the initial fatigue quality model is shown in Fig. 3 (Refs. 11, 12, 15, 21). Once the EIFS distribution has been defined for a group of details, a deterministic crack growth analysis is used to grow the entire EIFS population to any service time τ; thus determining the time-varying crack size distribution in service (Fig. 4).

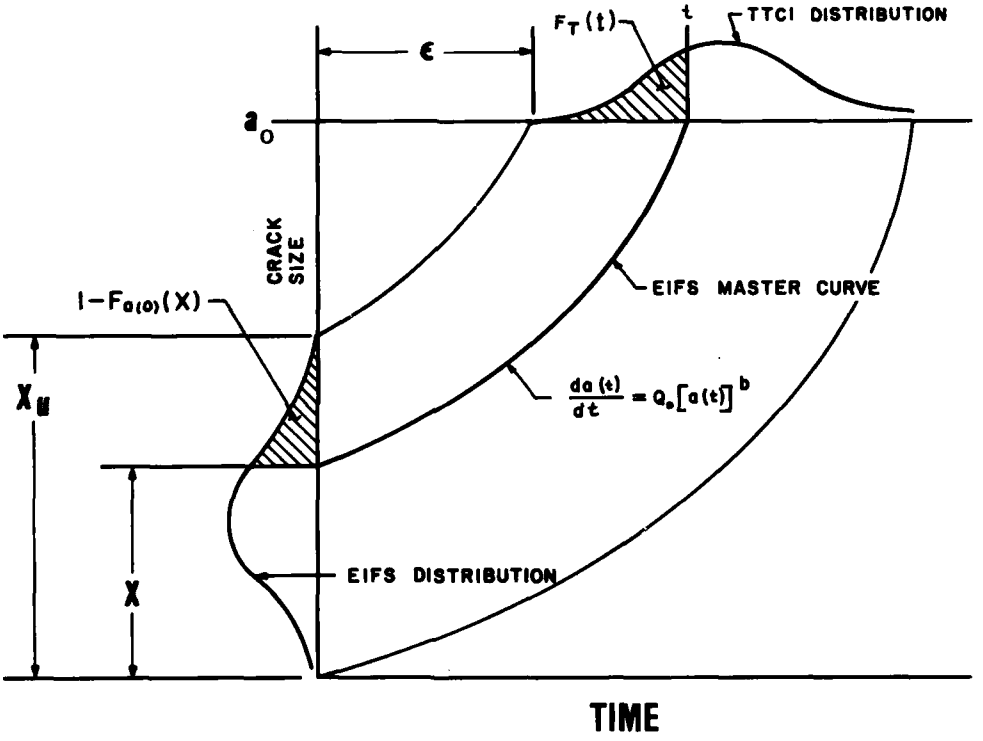

Figure 3 - Initial fatigue quality model

2. Initial Fatigue Quality Model

A prototype initial fatigue quality (IFQ) model has been previously described for quantifying the EIFS distribution for structural details, such as fastener holes (Refs. 11, 15, and 16). Such a model is conceptually described in Fig. 3. IFQ model refinements and EIFS distributions for two model variations are summarized in the following.

The TTCI distribution for coupon specimens is represented by the three-parameter Weibull distribution, $F_T(t)$ (Refs. 11, 15 and 16).

$$F_T(t) = P[T \leq t] = 1 - \exp\left[-\left(\frac{t-\epsilon}{\beta_0}\right)^{\alpha_0}\right], \quad t > \epsilon \tag{1}$$

where T = TTCI, α_0 = shape parameter, β_0 = scale parameter and ϵ = lower bound TTCI. The three Weibull parameters (i.e., α_0, β_0, ϵ) are determined from fractography for coupon specimens or other suitable test results.

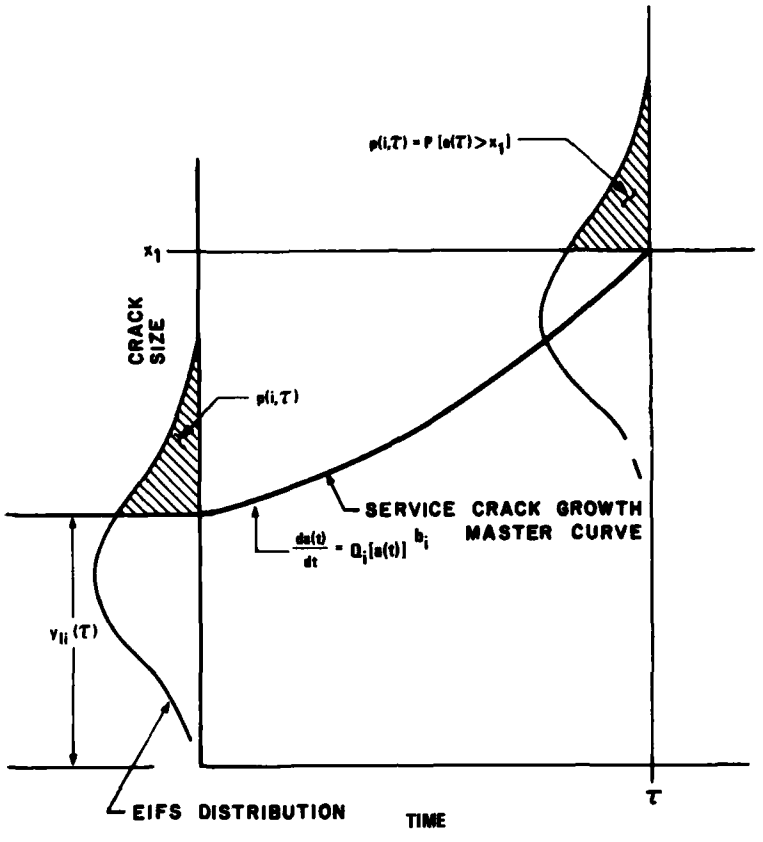

Figure 4 - Growth of EIFS distribution as function of time

The crack growth rate in the small crack region is assumed to be of the following form

$$\frac{da(t)}{dt} = Q_0[a(t)]^b \qquad (2)$$

where Q_0 and b are parameters depending on loading spectra, structural and material properties, etc.; a(t) is the crack size at time t. Other functional forms for the crack growth rate could also be used. Equation 2 is used because of its simplicity and general applicability for matching the crack growth data. A crack growth rate equation, such as Eq. 2, is used to obtain the EIFS distribution through a transformation of the TTCI distribution; hence both EIFS and TTCI are statistically compatible. EIFS distributions are obtained using Eq. 2 for $b \neq 1$ (case I) and $b = 1$ (case II). The resulting EIFS distribution for both cases are described below.

a. Case I ($b \neq 1$)

Integrating Eq. 2 from t = 0 to t = T, the relationship between the initial crack size, a(0), and the reference crack size, $a_0 = a(T)$ for TTCI (flight hours), is obtained,

$$\text{EIFS} = a(0) = [a_0^{-c} + cQ_0T]^{-1/c} \qquad (3)$$

where c = b - 1.

The EIFS cumulative distribution, $F_{a(0)}(x)$, is obtained by combining Eqs. 1 and 3 as follows:

$$F_{a(0)}(x) = \exp\left\{-\left[\frac{x^{-c} - a_0^{-c} - cQ_0\varepsilon}{cQ_0\beta_0}\right]^{\alpha_0}\right\}, \quad x \leq x_u \qquad (4)$$

$$1, \quad x \geq x_u$$

where

10-6

$$x_u = [a_0^{-c} + cQ_0\varepsilon]^{-1/c} \tag{5}$$

is the upper bound of the EIFS distribution. The lower bound of the TTCI distribution, ε, for a given reference size, a_0, is obtained from Eq. 5 as follows:

$$\varepsilon = \frac{1}{cQ_0}\,[x_u^{-c} - a_0^{-c}]; \quad a_0 \geq x_u \tag{6}$$

Equation 4 for $F_{a(0)}(x)$ can be simplified by substituting the expression for $CQ_0\varepsilon$ from Eq. 5 into Eq. 4 as follows:

$$F_{a(0)}(x) = \exp\left\{-\left[\frac{x^{-c} - x_u^{-c}}{cQ_0\beta_0}\right]^{\alpha_0}\right\}; \quad x \leq x_u \tag{7}$$

$$= 1; \qquad x \geq x_u$$

b. Case II (b = 1)

Integrating Eq. 2 from t = 0 to t = T and considering b = 1, one obtains the relationship between the initial crack size, a(0), and the reference crack size, a_0, as follows

$$\text{EIFS} = a(0) = a_0 \exp(-Q_0 T) \tag{8}$$

The EIFS cumulative distribution. $F_{a(0)}(x)$, is obtained by combining Eqs. 1 and 3 as follows:

$$F_{a(0)}(x) = \exp\left\{-\left[\frac{\ell n(x_u/x)}{Q_0\beta_0}\right]^{\alpha_0}\right\}; \quad 0 < x \leq x_u \tag{9}$$

$$= 1; \qquad x \geq x_u$$

where X_u is the upper bound of the EIFS distribution:

$$x_u = a_0 \exp(-Q_0\varepsilon) \tag{10}$$

The lower bound of TTCI distribution, ε, for a given reference crack size, a_0, is obtained from Eq. 10 as follows:

$$\varepsilon = \frac{1}{Q_0}\,\ell n\,(a_0/x_u); \quad a_0 \geq x_u \tag{11}$$

When each test specimen consists of ℓ fastener holes equally stressed and fractography results are taken only for the fastener hole in each specimen which has the largest crack size, the exponential exponents of Eqs. 1, 4, 7 and 9 should be multiplied by a factor of $1/\ell$ (Ref. 22).

3. Generic EIFS and Discussion of IFQ Model

Intuitively, the EIFS cumulative distribution, $F_{a(0)}(x)$, should be only a function of the material and the manufacturing/fabrication processes. As such, $F_{a(0)}(x)$ (Eqs. 4, 7 and 9) should be independent of loading spectra, stress level, percent shear load transfer through the fasteners, etc. If the same EIFS cumulative distribution is valid for replicate fastener holes under different design conditions (e.g., loading spectra, stress level, % load transfer, etc.), then the resulting $F_{a(0)}(x)$ is said to be "generic". If $F_{a(0)}(x)$ is generic, then the crack growth damage accumulation can be calculated analytically or numerically for different design conditions using the EIFS distribution (Eqs. 4, 7 or 9).

The IFQ model parameters, α_0, β_0, ε, Q_0, and b depend on the fractographic results. Therefore, these parameters depend on the conditions used to generate the crack initiation and crack growth data (e.g., material, loading spectra, stress level, etc). A basic premise of the durability analysis method proposed is that $F_{a(0)}(x)$ can be determined from a given fractography data set or sets economically and the resulting EIFS distribution can be used for crack exceedance predictions for different loading spectra.

stress levels, % load transfer, etc. Encouraging results have been obtained to date which suggest that such a basic premise appears to be promising. However, further study is required to evaluate the IFQ distributions using available fractographic data generated in Ref. 23 and to assess the accuracy of the crack exceedance predictions, $p(i,\tau)$, under different design conditions.

For simplicity, suppose two sets of replicate specimens are tested using the same loading spectrum but different stress levels. Using the fractographic results for each data set, the respective TTCIs for a given a_0 can be determined for each data set as illustrated in Fig. 5. For the EIFS cumulative distribution, $F_{a(0)}(x)$, to be "generic", the TTCI distributions, $F_T(t)$, for data sets 1 and 2 should transform into the same EIFS distribution. From Eq. 9, the necessary conditions for a generic EIFS cumulative distribution are for α_0 and $Q_0\beta_0$ to be constants.

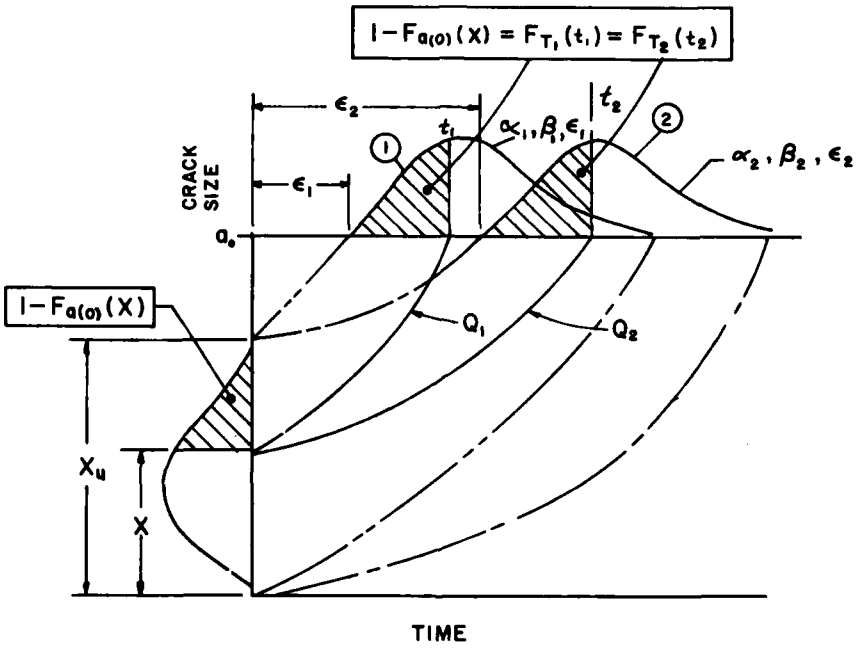

Figure 5 - Generic EIFS condition

Investigations have shown that α_0 is a material constant for a given type of fastener hole and the product $Q_0\beta_0$ appears to be the common denominator for linking different fractographic data sets together on a common baseline. Although results to date are very encouraging, futher research is required to evaluate and compare $Q_0\beta_0$ values for different fractographic data sets.

The EIFS distribution for case I ($b \neq 1$) and case II ($b = 1$) are given by Eqs. 7 and 9, respectively. In both cases, the EIFS cumulative distribution, $F_{a(0)}(x)$, is independent of the reference crack size, a_0, used to define the TTCI values. This is an important attribute of the IFQ distribution. The upper bound EIFS value in the IFQ distribution, X_u, is either selected by the user or computed from Eq. 5 or 10. The other parameters (i.e., α_0, β_0, ϵ, Q_0 and b) are determined from fractographic results for coupon specimens or other suitable test results.

In previous work, Case I ($b \neq 1$) has been considered (Refs. 11, 12, 16, 21, and 22). Fractographic results for protuding head (Ref. 33) and countersunk head (Ref. 23) fasteners resulted in b values <1. When b is < 1.0, it is possible to obtain EIFS values ≤ 0 using the original IFQ model. Mathematically, however, the original IFQ model can handle both positive and negative EIFS values, since the IFQ model is simply a "mathematical tool" for predicting the probability of crack exceedance. An explanation of the negative EIFS issue in terms of the original IFQ model and the crack initiation process is given in Ref. 22.

There are certain advantages and disadvantages associated with the use of Case I ($b \neq 1$) and Case II ($b = 1$) in Eq. 2. For example, the EIFS master curve for Case I with two parameters Q_0 and $b \neq 1$ generally fit the selected fractographic crack size range better than Case II with a single parameter (Q_0, $b = 1$). However, the resulting Q_0 and b values must be on a comparable baseline when different fractography data sets are considered. Since the resulting Q_0 and b values affect the IFQ distribution, they must be consistently defined. In Eq. 2, Q_0 and b are shown to be strongly correlated parameters (Ref. 19). Hence, for a given b there is likely to be a corresponding Q_0 and vice versa. Thus, for consistent IFQ results, the same b value may be determined using pooled fractography results for different data sets.

When the one parameter form of Case II is used in Eq. 2 (i.e., Q_0, $b = 1$), the "Q_0" value for one fractography data set is already comparable with the "Q_0" value for another data set. Nevertheless, whichever form of Eq. 2 is used (i.e., Q_0, $b \neq 1$ or Q_0, $b = 1$) the resulting $F_{a(0)}(x)$ will be statistically compatible with the TTCI distribution. Consequently, as long as the resulting $F_{a(0)}(x)$ is used in a consistent manner, the same crack exceedance prediction will be obtained.

C. Durability Analysis Procedures

The durability analysis procedures, described and discussed in detail elsewhere (Refs. 15, 21 and 22), are summarized below for Case II ($b = 1$). Similar expressions can be developed for Case I ($b = 1$) using the same procedures.

(1) Divide the durability component into m stress regions where the maximum stress in each region may be reasonably assumed to be equal for every location or detail (e.g., fastener hole).

(2) Use the model shown in Fig. 3 and suitable fractography results to define the EIFS distribution expressed in Eq. 9. Determine α_0 and $Q_0\beta_0$ (Ref. 22). The x_u selected should be consistent with Eq. 10.

(3) Determine for each stress region, the corresponding EIFS value, $y_{1i}(\tau)$, which grows to crack size x_1 at service time τ as illustrated in Fig. 4 (Ref. 22). If applicable fractography data are available for different stress levels and fractography data pooling procedures are used, the crack growth rate expression in Eq. 12, where $b_i = 1$, can be integrated from $a(0) = y_{1i}(\tau)$ to $a(\tau) = x_1$ to obtain $y_{1i}(\tau)$ in Eq. 13.

$$\frac{da(t)}{dt} = Q_i [a(t)]^{b_i} \tag{12}$$

$$y_{1i}(\tau) = x_1 \exp(-Q_i \tau) \tag{13}$$

in which

$$Q_i = \xi \sigma^{\gamma} \tag{14}$$

is assumed to be a power function of the maximum applied stress σ, and ξ and γ are constants to be determined from available fractography data.

If applicable fractographic results are not available for the desired design conditions (e.g., load spectra, % load transfer, stress level, etc.), an analytical crack growth program (e.g., Ref. 36) can be used to generate a "service crack growth master curve" to determine $y_{1i}(\tau)$ for a given x_1 (Refs. 11 and 15). When an analytical crack growth program is used, $y_{1i}(\tau)$ must be determined in a manner which is consistent with that used to determine the EIFS distribution from the fractographic test data.

(4) Compute the probability of crack exceedance for each stress region, i.e., $p(i,\tau) = P[a(\tau) > x_1] = 1 - F_{a(0)}[y_{1i}(\tau)]$, using Eq. 9.

$$p(i,\tau) = 1 - \exp\left\{-\frac{1}{\ell}\left[\frac{\ell n(x_u/y_{1i}(\tau)}{Q_0\beta_0}\right]^{\alpha_0}\right\}; \quad 0 < y_{1i} \leq x_u \tag{15}$$

$$p(i,\tau) = 0; \qquad y_{1i}(\tau) \geq x_u$$

in which $y_{1i}(\tau)$ is given by Eq. 13, and ℓ is the scaling factor described previously based on the number of fastener holes per specimen used in the fractography data base.

(5) The average number of details $\bar{N}(i, \tau)$, and the standard deviation $\sigma(i, \tau)$ in the ith stress region with a crack size greater than x_1 at service time τ are determined using the binomial distribution and are expressed as follows:

$$\bar{N}(i,\tau) = N_i p(i,\tau) \tag{16}$$

$$\sigma_N(i,\tau) = \{N_i p(i,\tau)[1 - p(i,\tau)]\}^{1/2} \tag{17}$$

in which N_i denotes the total number of details in the ith stress region. The average number of details with a crack size exceeding x_1 at the service time τ for m stress regions, $\bar{L}(\tau)$, and its standard deviation, $\sigma_L(\tau)$, can be computed using Eqs. 18 and 19.

$$\bar{L}(\tau) = \sum_{i=1}^{m} \bar{N}(i,\tau) \tag{18}$$

$$\sigma_L(\tau) = \left[\sum_{i=1}^{m} \sigma_N^2(i,\tau)\right]^{1/2} \tag{19}$$

Equations 18 and 19 can be used to quantify the extent of damage for a single detail, a group of details, a part, a component, or an airframe. Upper and lower bounds for the prediction can be estimated using $\bar{L}(\tau) \pm Z\sigma_L(\tau)$, where Z is the number of standard deviations, $\sigma_L(\tau)$, from the mean, $\bar{L}(\tau)$. Equations 16 through 19 are valid if cracks in each detail are relatively small and the growth of the largest crack in each detail is not affected by cracks in neighboring details. Hence, the crack growth accumulation for each detail is statistically independent (Refs. 11, 12, 15 and 21).

V. DURABILITY ANALYSIS DEMONSTRATIONS

A durability analysis of the lower wing skins of afighter is presented. Durability analysis results for complex-splice specimens subjected to a bomber load spectrum are also presented. Both analyses are correlated with test data.

A. Fighter Lower Wing Skins

A durability analysis of the lower wing skins of a fighter durability test article is presented to illustrate the methodology described. Analytical predictions of the extent of damage in each wing skin are presented in various formats, and results are compared with observations from the tear-down inspection of the fighter durability test article.

The fighter durability test article was tested to 16,000 flight hours (equivalent to 2 service lives) using a 500-hour block spectrum. Each wing received the same loading. Following the test, all fastener holes in the lower wing skins were inspected using eddy current techniques. Fastener holes with crack indications were confirmed by fractographic evaluation. The right hand and left hand lower wing skins were found to have twenty six and seven fastener holes, respectively, with a crack size $\geq$ 0.76 mm (0.03 inch) at τ = 16,000 flight hours.

A preliminary durability analysis for the fighter lower wing skins was presented in Ref. 21. The preliminary analysis reflected: (1) fastener hole IFQ based on fractographic results for protruding head fasteners, (2) crack growth rates for the IFQ model based on Eq. 2 ($b \neq 1$), (3) three-parameter Weibull distribution used in the IFQ model, (4) model parameters based on a single data set (one stress level, 400-hour block spectrum, Ref. 33), (5) three stress regions considered for the lower wing skin, and (6) an analytical crack growth program (Ref. 36) and the 500-hour block spectrum were used to define the "service crack growth master curve" for each stress region.

Essential features of the present analysis are: (1) fractographic results for countersunk fasteners used to quantify IFQ (countersunk fasteners were used on the fighter durability test article), (2) crack growth rates for the IFQ model based on Eq. 2 ($b = 1$), (3) three-parameter Weibull distribution used in the IFQ model, (4) model parameters based on three different data sets (three stress levels, 400-hour block spectrum) (5) lower wing skin divided into 10 stress regions, and (6) crack growth rate parameter Q_i defined for each stress region as a function of stress level σ, determined from available fractography data. There were no significant differences in the 400-hour and 500-hour spectra.

The fighter lower wing skin was divided into ten stress regions as shown in Fig. 6. Applicable stress levels and the corresponding number of fastener holes in each stress region are shown in Table 1. The stress levels for Zones I-IV were determined using strain gage data in combination with finite element analyses. The stress levels for Zones V, VII-IX were determined using a coarse grid finite element analysis and a theoretical stress distribution for a circular hole in an infinite plate under uniaxial tension. The stress levels for Zones VI and X were determined from a fine grid finite element analysis.

Fractographic results for three data sets (i.e., AFXLR4, AFXMR4, and AFXHR4) for maximum stress levels of 220.7 MPa (32 ksi), 234.5 MPa (34 ksi), and 262.1 MPa (38 ksi) were used to calibrate the IFQ model parameters. A 400-hour block load spectrum was used. The AFX series specimens were designed for 15% load transfer. The specimens were made of 7475-T7351 aluminum and contained two MS90353-08 (½ dia.) blind, countersunk rivets as shown in Fig. 7. All specimens reflect typical aircraft production quality, tolerances and fastener fits. Nine specimens were tested per data set.

10-10

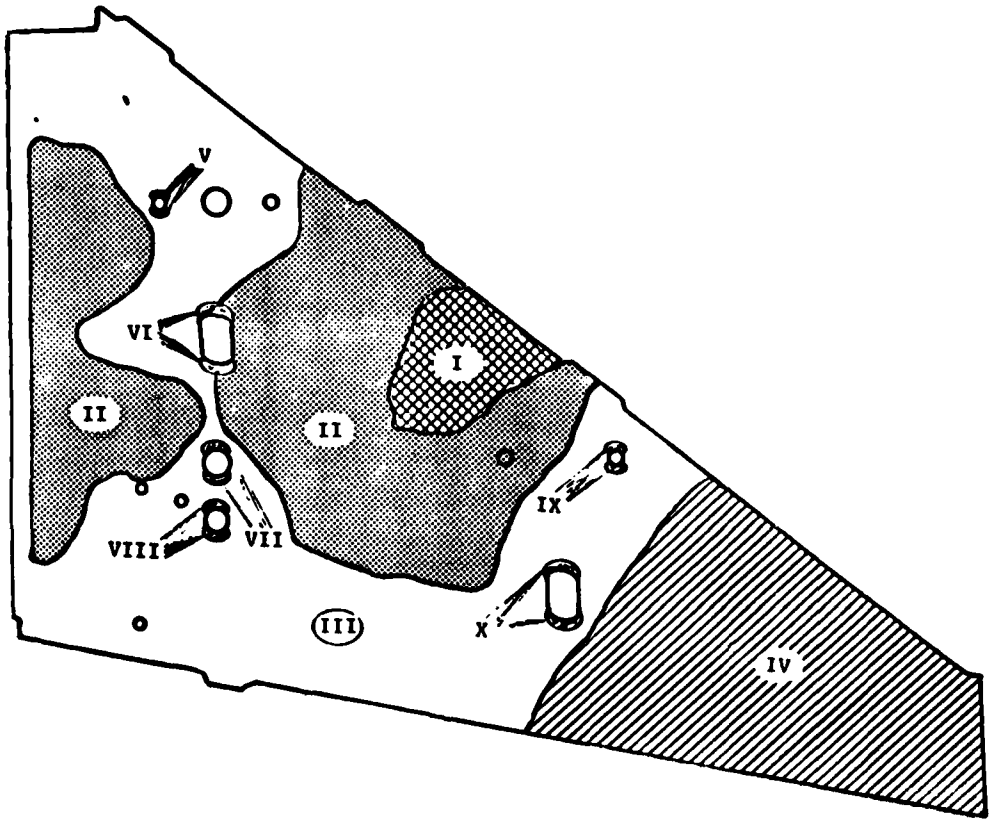

Figure 6 - Stress zones for fighter lower wing skin

Table 1 - Stress levels and number of fasteners holes for fighter lower wing skin

STRESS ZONE	LIMIT STRESS LEVEL, MPa (ksi)	NUMBER OF FASTENER HOLES
I	195.2 (28.3)	59
II	186.2 (27.0)	320
III	167.6 (24.3)	680
IV	115.2 (16.7)	469
V	195.9 (28.4)	8
VI	201.4 (29.2)	30
VII	223.5 (32.4)	8
VIII	180.7 (26.2)	8
IX	180.7 (26.2)	12
X	177.2 (25.7)	20
		1614

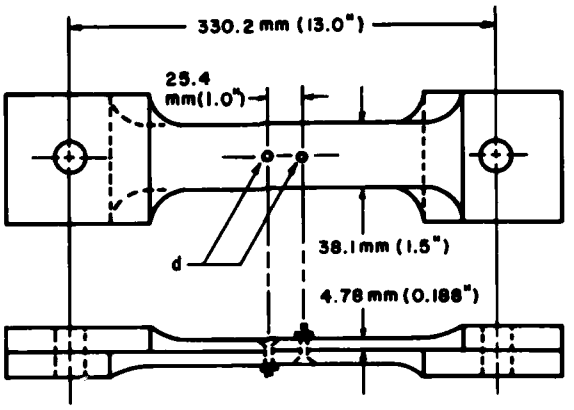

Figure 7 - IFQ specimen

The crack growth rate parameter Q_0 in Eq. 2 (b = 1) was determined for each of the three AFX data sets. Q_0 was determined from the fractographic results using a least-square fit of Eq. 2 (Ref. 22). A fractographic crack size range of 0.127 mm - 2.54 mm (0.005 inch - 0.10 inch) was used. An upper bound EIFS of X_u = 0.762 mm (0.03 inch) was assumed for the IFQ distribution. Using Eq. 11 and the estimated Q_0 values, the corresponding lower bound of TTCI value, ϵ, for each reference crack size, a_0, was determined for each data set. The results of Q_0 and ϵ are shown in Table 2.

Table 2 - Summary of IFQ model parameters for fighter spectrum

DATA SET	σ_{MAX} (MPa)	a_0 (mm)	$Q_0 \times 10^4$ (HRS^{-1})	ϵ (HRS)	α_0	β_0 (HRS)	$Q_0\beta_0$
AFXLR4	220.7	0.76	1.201	0	1.823	15,033	1.805
		1.27		4,253		12,916	1.551
		2.54		10,025		13,421	1.612
AFXMR4	234.5	0.76	2.037	0		8,721	1.777
		1.27		2,508		7,759	1.581
		2.54		5,910		9,093	1.852
AFXHR4	262.1	0.76	4.731	0		5,469	2.587
		1.27		1,079		5,098	2.412
		2.54		2,545		4,598	2.175
POOLED α_0 = 1.823, AVERAGE $Q_0\beta_0$ = 1.928							

Fractographic results for the three AFX series data sets were combined together to determine the corresponding "pooled" α_0 value using the following procedures. Time-to-crack-initiation (TTCI) results for three different reference crack sizes (a_0 = 0.762 mm, 1.27 mm and 2.54 mm) were used for each of the three data sets. The adjusted TTCI data, i.e., TTCI-ϵ data for each reference crack size for each data set were normalized using the corresponding average values ($\bar{X}$). Results for the three data sets were pooled together and the (TTCI-ϵ)/$\bar{X}$ data were ranked in ascending order. Equation 1 was transformed into a least-squares fit form for determining the pooled α_0 value (Ref. 22). The pooled value was found to be 1.823 (Table 2).

After determining α_0 for the pooled data sets, the adjusted TTCI's for each reference crack size for each data set were considered separately to determine the corresponding β_0 values (Ref. 22). These values are presented in Table 2. Also summarized in Table 2 are the $Q_0\beta_0$ values for the nine cases considered. For generic

EIFS, the α_0 and $Q_0\beta_0$ values should be constants. Average values of $Q_0\beta_0 = 1.928$ and $\alpha_0 = 1.823$ are used for the present durability analysis. A plot of Q_o versus β_o is shown in Fig. 8 for the three data sets considered (9 cases).

10-12

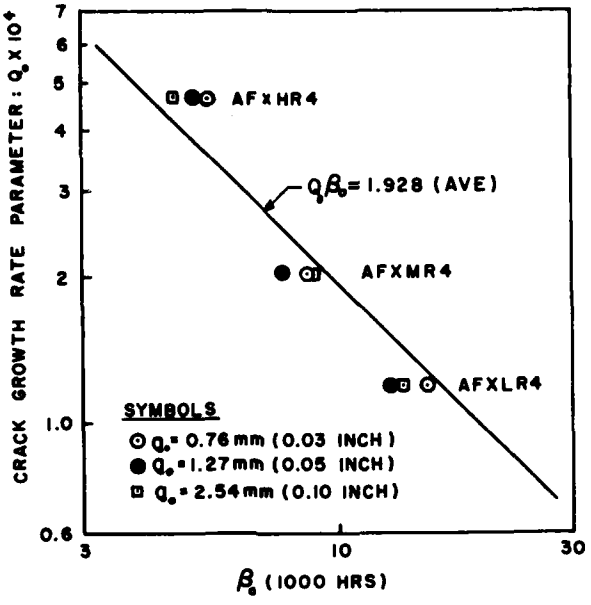

Figure 8 - Q_o versus β_o for fighter 400-hour load spectrum

The crack growth rate parameter Q_i for the three data sets is plotted against the applicable gross stress for each data set in Fig. 9. Using a least-square *fit (solid* line in Figure 9), the following expression is obtained for Q_i as a function of stress level when stress is expressed in ksi units:

$$Q_i = 1.427 \times 10^{-16} \sigma^{7.928} \quad (20)$$

When stress is expressed in MPa units, the appropriate expression for Q_i is as follows:

$$Q_i = 3.2 \times 10^{-23} \sigma^{7.928} \quad (21)$$

Equation 20 is used to estimate the Q_i value for each of the ten stress regions shown in Fig. 6.

Crack exceedance predictions for the fighter lower wing skin were determined using Eqs. 13, 15, and 20 as well as the following parameters: x_o = 0.762 mm (0.03 inch), α_o = 1.823, $Q_o\beta_o$ = 1.928 (average), ℓ = 4 and various τ values. The results are presented in various formats as described below.

The extent of damage predictions for the fighter lower wing skin are summarized in Table 3 at τ = 16000 flight hours for each of the ten stress regions shown in Fig. 6. The number of fastener holes with a crack size $\geq$0.762 mm (0.03 inch), $\bar{L}(\tau)$, and the standard deviation, $\sigma_L(\tau)$, was estimated to be 17.6 and 4.077, respectively. Based on the test results for the right hand and left hand lower wing skins, an average of 16.5 fastener holes had a crack size $\geq$0.762 mm (0.03 inch) at τ = 16000 hours. In Table 3, the predicted extent of damage results track the average test results for the individual stress regions very well.

In Fig. 10 the predicted percentages of crack exceedance versus fastener hole crack size are plotted for the fighter lower wing skin at τ = 16000 flight hours. Curves 1, 2 and 3 are based on $L(\tau) \times 100\%/N^*$, $[\bar{L}(\tau) + \sigma_L(\tau)] \times 100\%/N^*$ and $[\bar{L}(\tau) - \sigma_L(\tau)] \times 100\%/N^*$, respectively. $\bar{L}(\tau)$ and $\sigma_L(\tau)$ are defined by Eqs. 18 and 19, respectively. N^* is the total number of fastener holes in the fighter lower wing skin (i.e., 1614 holes). Since the number of fastener holes in each stress region is large, it is reasonable to approximate the binomial distribution by the normal distribution. The corresponding exceedance probabilities for curves 1, 2, 3 are shown in Fig. 10 in parentheses.

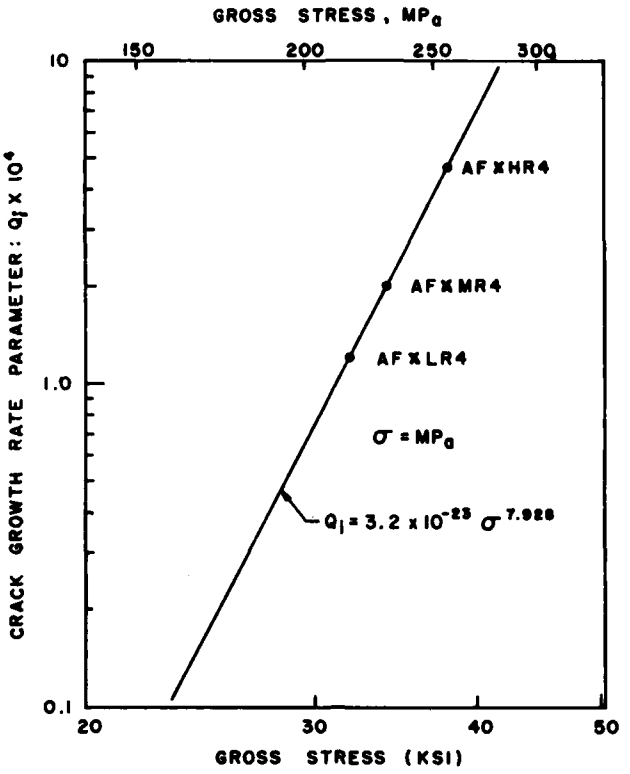

Figure 9 - Q_i versus gross stress for fighter 400-hour load spectrum

Table 3 - Durability analysis results for fighter lower wing skin

STRESS REGION	$Q_i \times 10^4$ (HRS^{-1})	p(i,τ)	NO. HOLES WITH a ≥ 0.76 mm @ τ = 16,000 HRS				
			PREDICTED		TEST		
			$\bar{N}(i,\tau)$	$\sigma_N(i,\tau)$	R.H. WING	L.H. WING	AVERAGE
I	0.4620	0.0426	2.5	1.547	7	0	3.5
II	0.3182	0.02182	6.9	2.598	7	2	4.5
III	0.1380	0.00480	3.3	1.812	4	1	2.5
IV	0.0071	0.00002	0.0		0	0	0
V	0.4751	0.0448	0.4	0.618	1	0	0.5
VI	0.5921	0.0662	1.9	1.332	5	1	3.0
VII	1.3504	0.2649	2.1	1.242	0	2	1.0
VIII	0.2507	0.0142	0.1	0.314	1	1	1.0
IX	0.2507	0.0142	0.2	0.444	1	0	0.5
X	0.2152	0.0108	0.2	0.445	0	0	0
$\bar{L}(\tau) = 17.6$, $\sigma_L(\tau) = 4.077$, TOTAL TEST AVERAGE = 16.5							

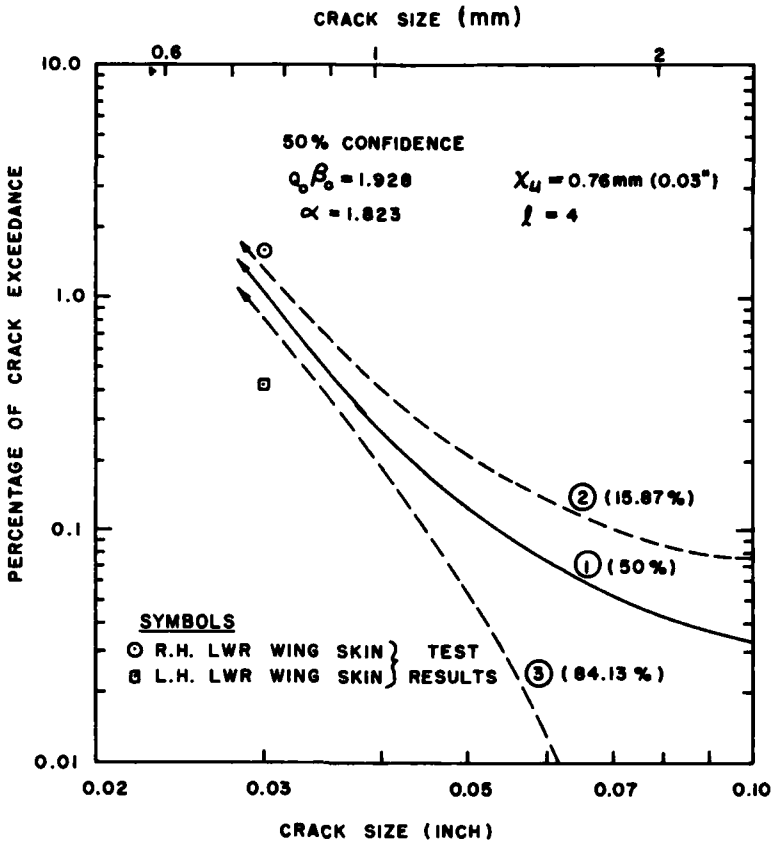

Figure 10 - Percentage of crack exceedance versus crack size at 16,000 hours for 3 probability levels (fighter)

Test results for the right and left hand lower wing skin (at X_1 = 0.762 mm and τ = 16000 hours) are plotted as a circle and a square, respectively, in Fig. 10. Approximately 1.1% of the fastener holes in the fighter lower wing skin are predicted to have a crack size $\geq$ 0.762 mm (0.03 inch) at τ = 16000 hours. This compares with an average of 1.02% based on test results for the right hand and left hand lower wing skins.

In Fig. 10, the predicted average percentage of crack exceedance decreases rapidly for larger crack sizes. For example, the average percentage of crack exceedance for the fighter lower wing skin decreases from approximately 1.1% at X_1 = 0.762 mm (0.03") to approximately 0.14% at X_1 = 1.27 mm (0.05 inch). Crack exceedance predictions are based on the service crack growth master curve defined by Eqs. 13 and 14. A single service crack growth master curve may not adequately fit the full range of desired crack sizes for all crack exceedance predictions. For example, different service crack growth master curves are required to fit two different crack size ranges as illustrated in Fig. 11. Curve 1 and Curve 2 shown in Fig. 11 apply to crack size ranges A_1 and A_2, respectively. Crack exceedance predictions based on Curves 1 and 2 of Fig. 11 will be different for the same crack exceedance size, X_1. For example, $p(i,\tau)$ predictions based on Curve 2 for X_1, τ_1, and X_2, τ_2 will be larger than those based on Curve 1.

The extrapolation of crack exceedance predictions to larger crack sizes should be consistent with the applicable crack growth process for given design conditions and the crack exceedance crack size, X_1. Further research is needed to develop a better understanding and confidence in crack exceedance predictions for different crack sizes, materials, and design conditions.

Analytical predictions of the extent of damage are presented in Fig. 12 in an exceedance probability format. In this case, the predicted number of fastener holes in the fighter lower wing skin with a crack size $\geq$ 0.762 mm (0.03 inch) are plotted as a function of flight hours for different exceedance probability values (i.e., P = 0.05, 0.50, 0.95). The plots are based on Eq. 15, x_1 = 0.762 mm (0.03 inch), α_0 = 1.823, $Q_0\beta_0$ = 1.928 (average), ℓ = 4, N_1 = 1614 fastener holes, Z = $\pm$1.65 and $\bar{L}(\tau) \pm Z\sigma_L(\tau)$. For example, at τ = 16,000 hours, $\bar{L}(\tau)$ = 17.6 fastener holes and $\sigma_L(\tau)$ = 4.077. The upper bound prediction, $\bar{L}(\tau) + Z\sigma_L(\tau)$, is approximately 24.3 fastener holes. In other words, there is a probability of 0.05 that more than 24.3 fastener holes in the fighter lower wing skin will have a crack size $\geq$ 0.762 mm (0.03 inch) at 16000 flight hours. There is a probability of 0.50 and 0.95, respectively, that more than 17.6 and 10.9 fastener holes will have a crack size $\geq$0.762 mm (0.03 inch) at τ = 16000 flight hours. The

average and upper/lower bound predictions for the fighter lower wing skin compare very well with test results for the right hand and left hand lower wing skins at τ = 16000 flight hours (Fig. 12).

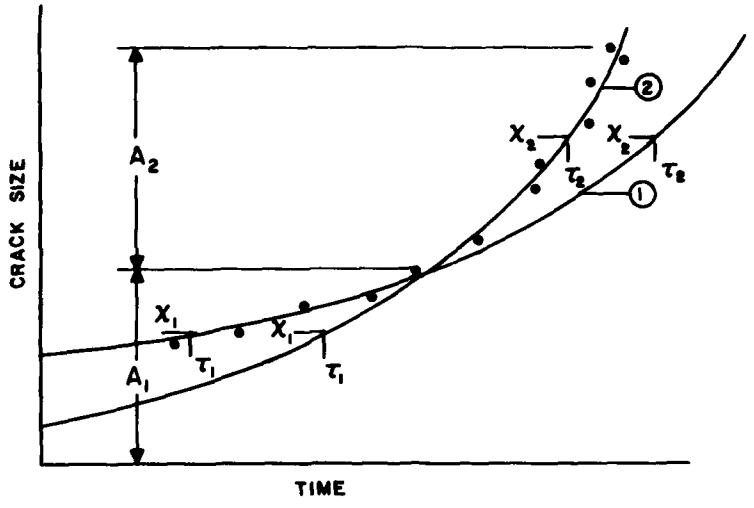

Figure 11 - Service crack growth master curves for different crack size ranges

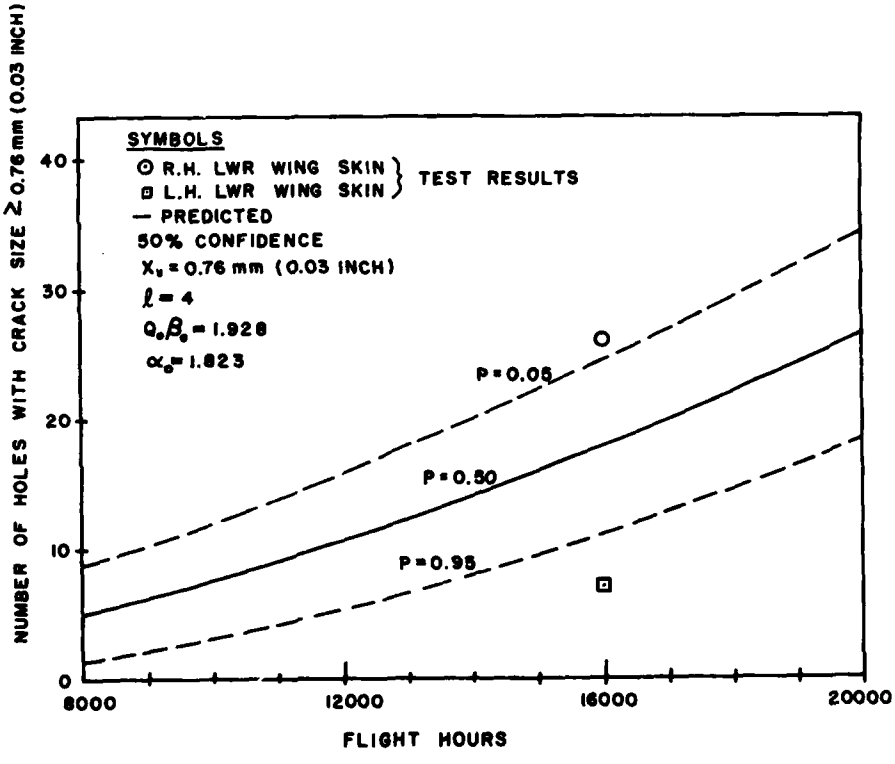

Figure 12 - Number of holes with crack size ≥ 0.76 mm (0.03 inch) versus flight hours - exceedance probability format (fighter)

The extent of damage predictions are presented in a stress level format in Fig. 13. Curves are shown for the baseline stress (σ), 1.1σ , and 1.2σ. Results are based on Eqs. 13, 15 and 20. The "baseline stress" refers to the maximum stress level for each of the ten stress zones. For prediction purposes, the baseline stresses for each

stress zone were all increased by the same percentage. The results shown in Fig. 13 can be used to assess the extent of damage as a function of stress level and flight hours. This format is particularly useful for evaluating durability design tradeoffs in terms of the extent of damage. For example, at τ = 16000 flight hours approximately 1.1% of the fastener holes in the fighter lower wing skin would be predicted to exceed a crack size of 0.762 mm (0.03 inch) for the baseline stress levels. If the baseline stresses were increased to 1.1σ and 1.2σ, the predicted average percentage of holes with a crack size $\geq$ 0.762 mm (0.03 inch) would be approximately 4% and 12%, respectively. This provides a quantitative measure of the structural durability as a function of stress level and flight hours.

10-16

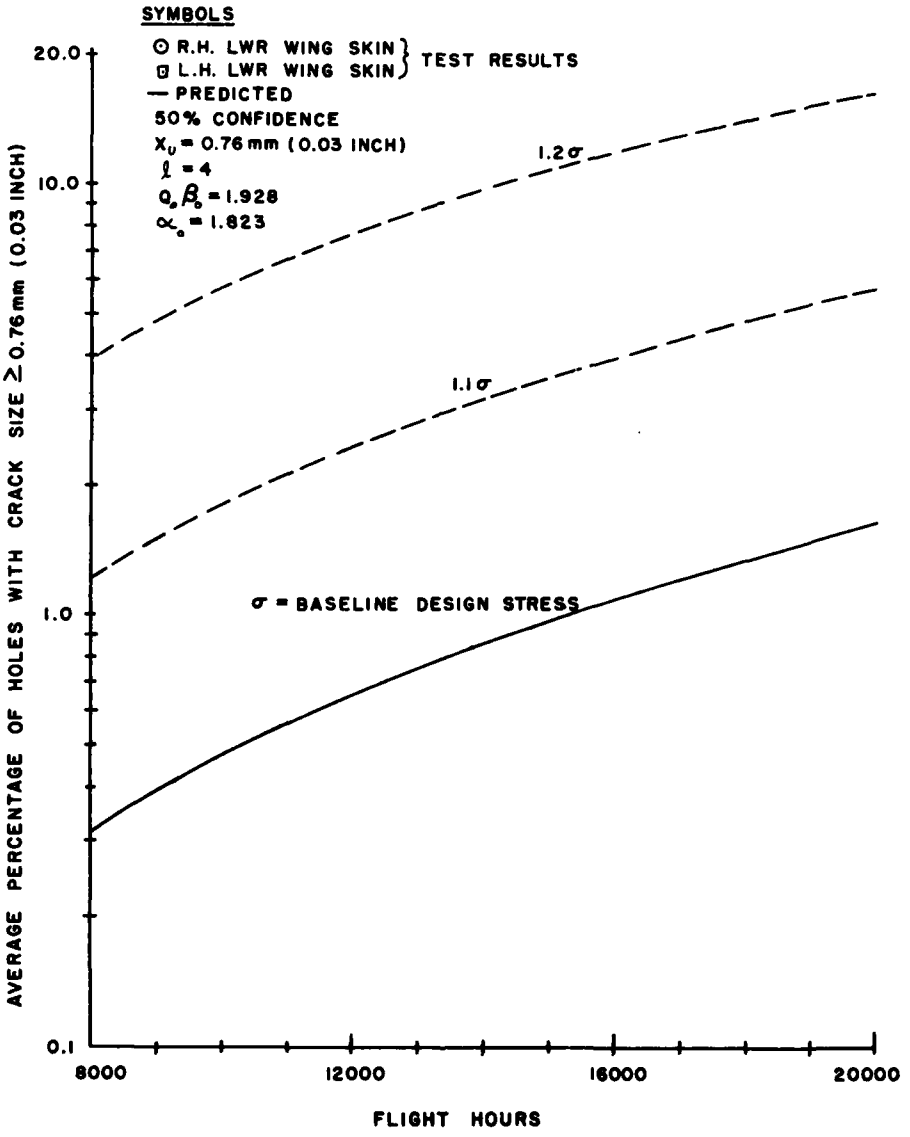

Figure 13 - Average percentage of holes with crack size $\geq$ 0.76 mm (0.03 inch) versus flight hours - stress level format (fighter)

B. Complex-Splice Specimens Subjected to Bomber Load Spectrum

A durability analysis of complex-splice specimens subjected to a bomber load spectrum is presented. Analytical predictions of the extent of damage in the specimens are presented in various formats and compared with fractographic results. The analytical/experimental results are summarized here and described in more detail in Ref. 27.

The complex-splice specimen geometry is presented in Fig. 14. The specimens were made of 7475-T7351 aluminum plate and countersunk steel rivets. A bomber load spectrum was applied. Based on a simplified stress analysis and strain gage results, the maximum gross stress in the outer row of fastener holes at the faying surface was

estimated to be 246.8 MPa (35.8 ksi). The eleven specimens were tested to two service lifetimes (27,000 flight hours) or failure, whichever came first.

10-17

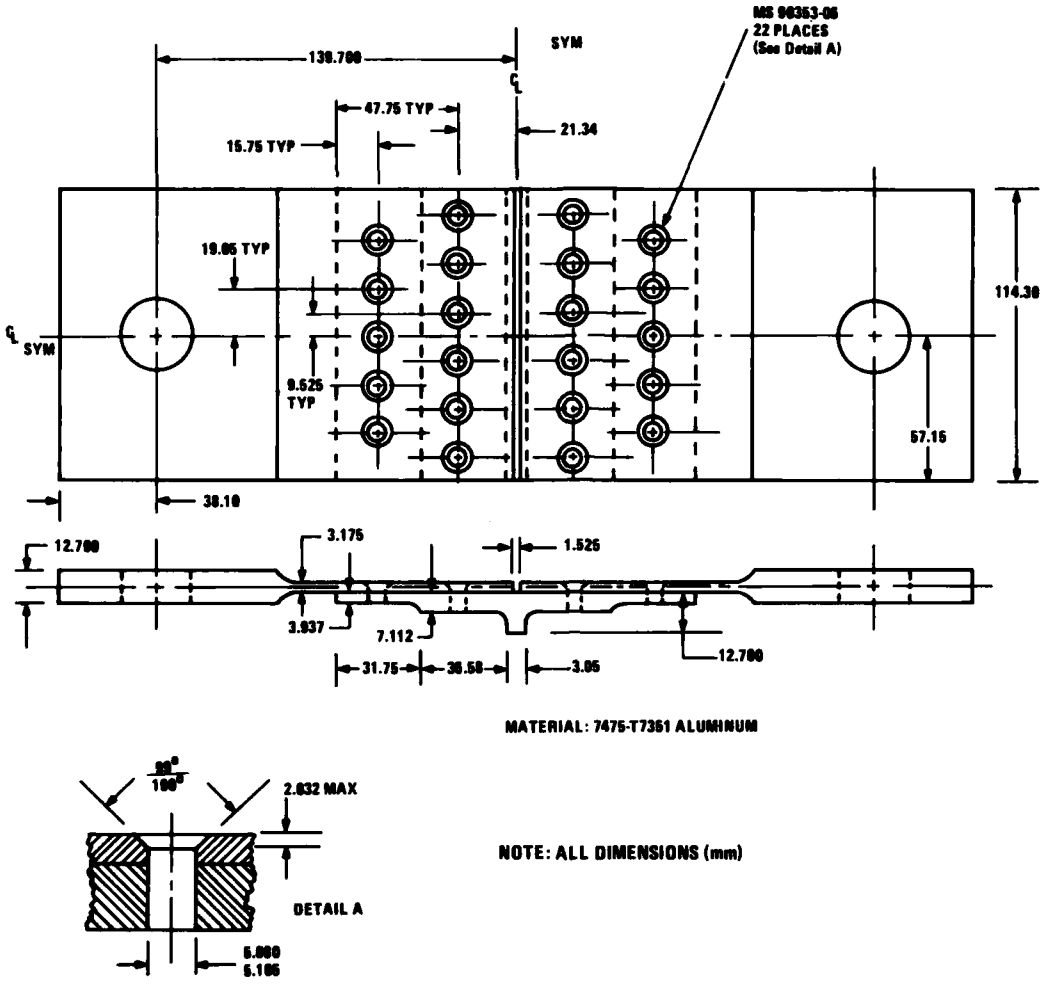

Figure 14 - Complex - splice specimen

After testing, all fastener holes in the outer rows were inspected. Fractography was performed for the largest crack in each fastener hole in the outer rows. Twenty five out of 110 fastener holes in the outer rows had a crack size $\geq$1.27 mm (.05 inch) at 13,500 hours. Hence, 22.7% of the fastener holes in the outer rows had a crack size $\geq$1.27 mm (.05 inch) at 13,500 hours.

The IFQ of the fastener holes was based on the fractographic results for nine data sets and three different reference crack sizes. The specimens were made of 7475-T7351 aluminum and contained 2 countersunk rivets. Load transfer levels of 15%, 30% and 40% were considered. All specimens had the same configuration (Fig. 7) with the same overall length and basic test section dimensions. However, the lug end dimensions varied depending on the amount of load transfer. Three maximum stress levels were considered for each load transfer level.

A fractographic crack size range of 0.127 mm - 2.54 mm (0.005 inch - 0.1 inch) was considered. An upper bound EIFS of X_u = 1.27 mm (0.05 inch) was assumed for the IFQ distribution. A fractography scaling factor of ℓ = 4 was used. The same data pooling procedures were used which were previously described for the fighter demonstration. The average α_0 and $Q_0\beta_0$ values were found to be 2.702 and 2.823, respectively.

The crack growth rate parameter Q_i for the 9 data sets is plotted against the applicable gross stress for each data set in Fig. 15. The solid line represents the least-square best fit through the plot points. The dashed lines have the same slope as the solid line and they encompass all the plot points. The corresponding best-fit equation for Q_i as a function of gross stress level when stress is expressed in ksi units is as follows:

10-18

$$Q_i = 6.151 \times 10^{-13} \sigma^{5.381} \quad (22)$$

When stress is expressed in MPa units, the appropriate expression for Q_i is as follows:

$$Q_i = 1.895 \times 10^{-17} \sigma^{5.381} \quad (23)$$

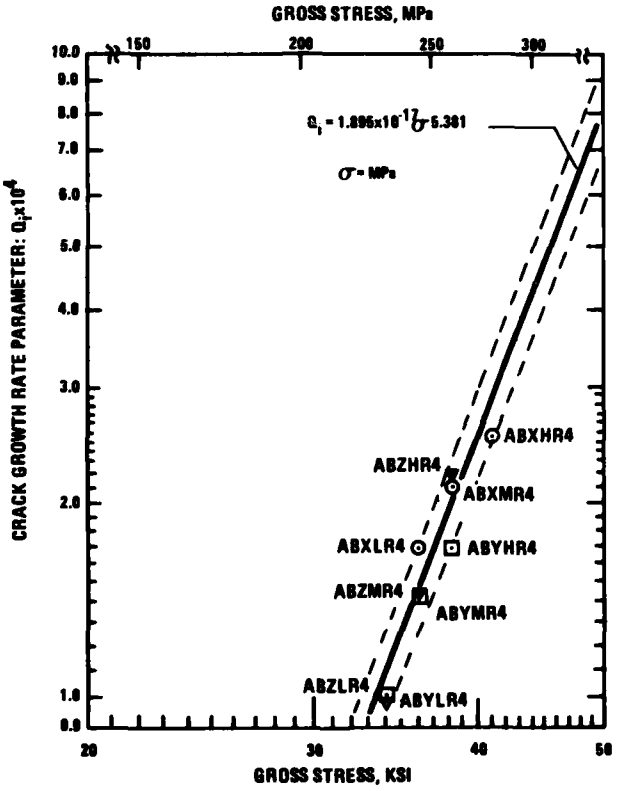

Figure 15 - Q_i versus gross stress for bomber load spectrum

Crack exceedance predictions for the complex-splice specimens were determined using Eqs. 13, 15, and 22. At τ = 13,500 hours, an average of 9 fastener holes (8.3%) were predicted to exceed a crack size of 1.27 mm (0.05 inch). The test results showed an average of 25 fastener holes (22.7%) exceeding a crack size of 1.27 mm (0.05 inch). The difference in the predicted and test crack exceedances is attributed mainly to the stress level used in the predictions. The actual stress level and distribution in the outer row of fastener holes is far more complex, due to lateral bending effects, than those considered for the damage assessment. The crack exceedance predictions are very sensitive to the gross applied stress level used. This is illustrated in Fig. 16. The solid line represents average crack exceedance predictions for the gross stress level of 246.8 MPa (35.8 ksi) obtained using the simplified stress analysis approach. The dashed lines represent average crack exceedance predictions for other gross stress levels. Also plotted as a single point is the average test crack exceedance at τ = 13,500 hours. It can be seen that if the gross applied stress level used in the predictions were 266.1 MPa (38.6 ksi) rather than 246.8 MPa (35.8 ksi), the predicted crack exceedance at τ = 13,500 hours would match the test results. Hence, a more accurate stress analysis could result in improved predictions.

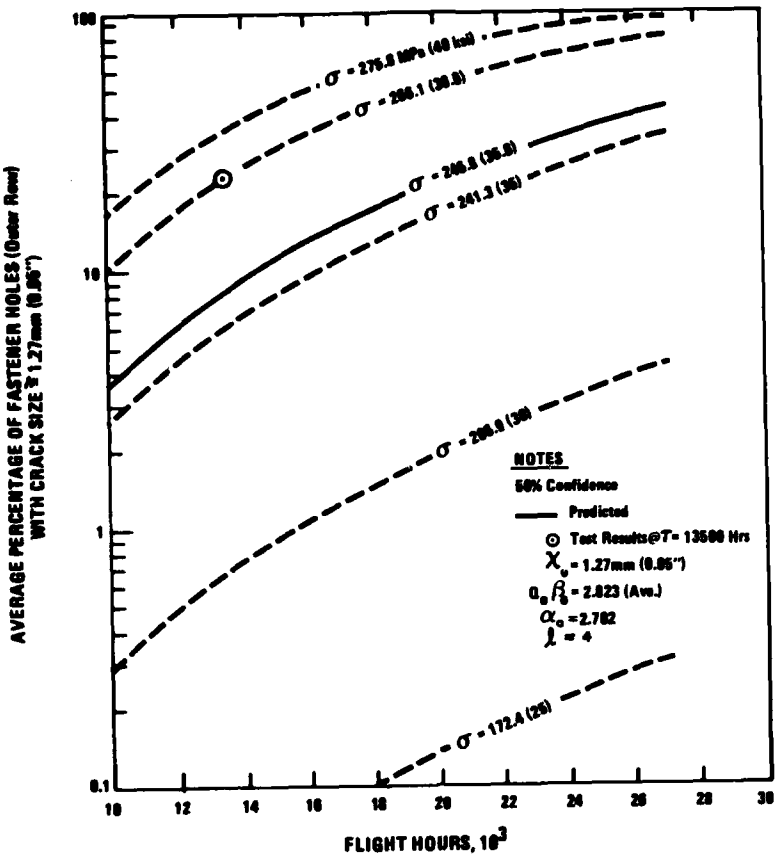

Figure 16 - Average percentage holes with crack size > 1.27 mm (0.05 inch) versus flight hours - stress level format (bomber)

Other useful crack exceedance formats, previously discussed for the fighter demonstration, are presented in Figs. 17 and 18 for the complex-splice specimens.

VI CONCLUSIONS AND DISCUSSIONS

Probabilistic fracture mechanics methods for durability analysis have been described and demonstrated for both a full-scale fighter aircraft structure and for a complex splice subjected to a bomber spectrum. These methods can be used to analytically assure compliance with the Air Force's durability design requirements. The analytical tools described can be used to quantify the extent of damage as a function of the durability design variables for structural details in a part, a component or airframe. Once the economic life and durability critical parts criteria are established, the extent of damage predictions can be used to assure design compliance with Air Force durability requirements.

An initial fatigue quality model can be used to define the EIFS cumulative distribution using suitable fractographic results. Procedures and guidelines have been developed for determining the IFQ model parameters for pooled fractographic data sets and for scaling TTCI results. The parameters α_0 and $Q_0\beta_0$ provide the basis for putting fractographic results on a common baseline for quantifying the initial fatigue quality. For generic EIFS, α_0 and $Q_0\beta_0$ should be constants for different fractographic data sets (same material, fastener type/fit, and drilling technique), loading spectra, stress levels and percent load transfer. Encouraging results have been obtained to justify the use of the same EIFS cumulative distribution for crack exceedance predictions for different design conditions. Further research is required to confirm the IFQ distributions for different materials, load spectra, stress levels, fastener types/diameters/fit, % load transfer, etc. A considerable amount of fractographic results exist which need to be evaluated using the IFQ model.

The effects of fretting, clamp-up, corrosion, size effect (scale-up from coupon to component), faying surface sealant, interference-fit fasteners, etc. on IFQ need to be investigated. Also, the feasibility of using no-load transfer specimens with multiple holes for quantifying the IFQ should be evaluated using spectrum and constant amplitude loading. This could provide an economical way to generate the fractographic results needed to quantify the IFQ.

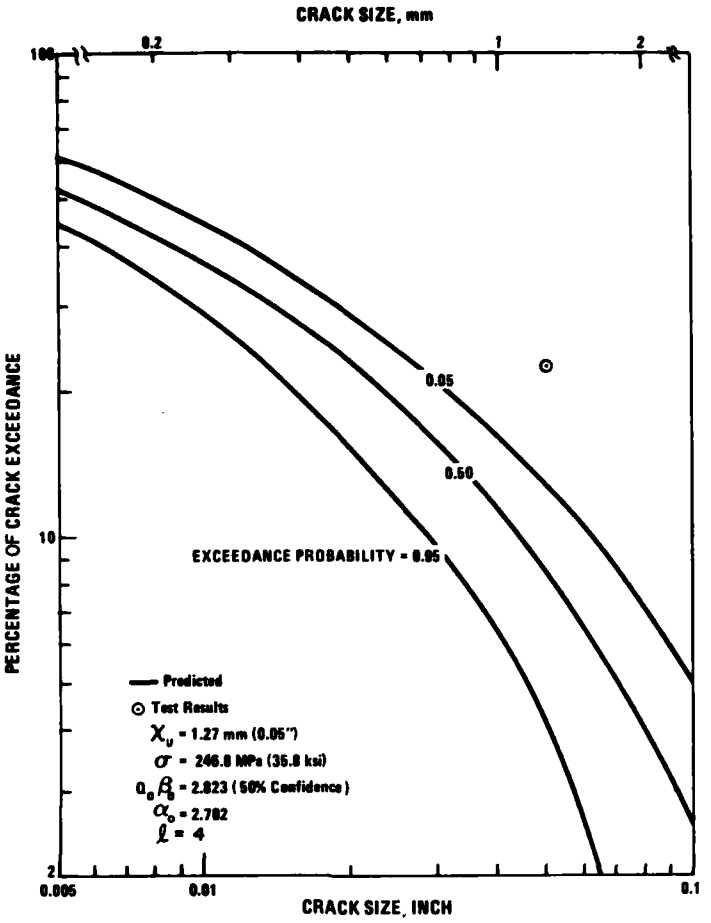

Figure 17 - Percentage of crack exceedance versus crack size and exceedance probability at 13,500 hours (bomber)

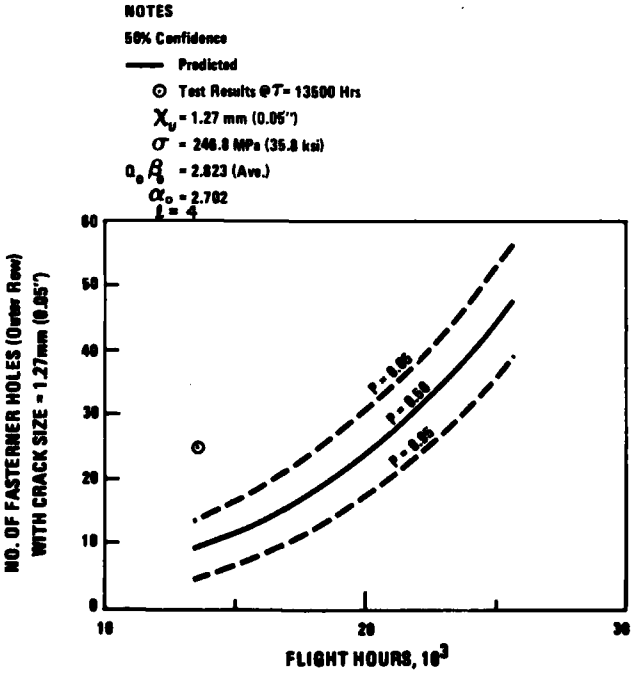

Figure 18 - Number of holes with crack size $\geq$ 1.27 mm (0.05 inch) versus flight hours - exceedance probability format (bomber)

Theoretically, the IFQ model can be used to quantify the EIFS cumulative distribution for various structural details as long as fractographic results are available for the details to be included in the durability analysis. The IFQ model has been evaluated using fractographic results for fastener holes. Suitable specimens and guidelines need to be developed for generating crack initiation and crack growth results for other details such as, cutouts, fillets, lugs, etc. Fractographic results should be developed and evaluated for such details so that the durability analysis methods described can be efficiently applied to different types of structural details in typical aircraft structures.

The accuracy of crack exceedance predictions, based on the same EIFS cumulative distribution, needs to be evaluated for different design conditions. Also, IFQ model parameter sensitivity studies need to be performed to better understand the average parameter values and variances and the impact of these parameters on the IFQ for different fractographic data sets.

The durability analysis methodology was developed for crack exceedance predictions for relatively small crack sizes (e.g., = 2.54 mm) in structural details. The largest crack in each detail was assumed to be statistically independent to justify using the binomial distribution for combining crack exceedance predictions for structural details. If the largest crack in a given detail doesn't significantly affect the growth of cracks in neighboring details, perhaps the proposed durability analysis methodology can be extended to crack sizes >2.54 mm (0.10 inch). The simplistic crack growth rate equation (Eq. 12) is not suitable for use in the crack exceedance predictions for crack sizes>2.54 mm (0.10 inch). However, a general service crack growth master curve can be generated under given design conditions which is valid for crack sizes >2.54 mm (Ref. 11, 12 15, and 22). Nevertheless, this approach has not been demonstrated in the present study and further research is required to extend the probabilistic fracture mechanics approach developed to larger crack sizes.

Two different $F_{a(0)}(x)$ equations (i.e., Eqs. 7 and 9) were presented for representing the IFQ. Either equation works but Eq. 9 is recommended for two reasons: (1) It assures all EIFS's in the IFQ distribution will be>0, and (2) the crack growth rate parameter Q_0 can be easily determined from the fractographic results and the resulting Q_0 values for different data sets will be directly comparable. If Eq. 7 is used, a common b parameter (Eq. 2) must be imposed for different fractographic data sets to put the $Q_0\beta_0$ values on a comparable baseline. As long as b > 1, all EIFS's in Eq. 7 will be ≥ 0. Further studies are needed to evaluate the accuracy of these two $F_{a(0)}(x)$ equations.

The EIFS cumulative distribution, $F_{a(0)}(x)$, is independent of the reference crack size, a_0. This is illustrated in Eqs. 7 and 9. Therefore, the TTCI distribution for different reference crack sizes will transform into a common $F_{a(0)}(x)$.

The IFQ model is simply a "mathematical tool" for quantifying the IFQ of structural details. Therefore, the resulting EIFS's must be considered in the context of the IFQ model and the fractographic results used to calibrate the model parameters. EIFS's should be considered as hypothetical cracks used for crack exceedance predictions rather than actual initial flaws per se.

Back extrapolations of fractographic data must be done consistently to put the EIFS's on a common baseline for different data sets. Inconsistent EIFS results will be obtained if the EIFS distribution is determined by back extrapolating the fractography results for individual specimens and then fitting a statistical distribution to the EIFS results for different data sets. Two problems result if this approach is used: (1) the EIFS's are not on a common baseline for different data sets, and (2) the resulting EIFS distribution is not statistically compatible with the TTCI distribution and the fatigue wear out process. The resulting EIFS distribution should be statistically compatible with the TTCI distribution. The IFQ model presented in this paper satisfies this requirement.

Several useful applications of the durability analysis methodology developed are: (1) The evaluation of durability design tradeoffs in terms of structural design variables, (2) the evaluation of structural maintenance requirements before or after aircraft is committed to service, and (3) the evaluation of aircraft user options affecting life-cycle-costs, structural maintenance requirements, and operational readiness.

ACKNOWLEDGEMENTS

This research is based on work performed under the "Durability Methods Development" program, sponsored by the Air Force Wright Aeronautical Laboratories, Flight Dynamics Laboratory, Wright-Patterson Air Force Base, Ohio (Contract F33615-77-C-3123). The authors are indebted to the following General Dynamics' personnel who supported the research effort: D.E. Gordon, J.W. Norris, S.M. Speaker, W.T. Kaarlela, A. Meder, R.O. Nay and F.C. Nordquist. Valuable discussions with Dr. Y.H. Kim, Dr. W.R. Garver, Dr. V.D. Smith and J.W. Morrow of General Dynamics and Dr. M. Shinozuka of Modern Analysis Incorporated are acknowledged.

10-22

REFERENCES

1. Anon., Aeronautical Systems Division, "Aircraft Structural Integrity Program," 1975, MIL STD 1530A.

2. Anon., Aeronautical Systems Division, "Airplane Damage Tolerance Requirements," 1974, MIL-A-83444 (USAF).

3. Anon., Aeronautical Systems Division, "Airplane Strength and Rigidity Ground Tests," 1975, MIL-A-8867B.

4. Anon., Aeronautical Systems Division, "Airplane Strength, Rigidity and Reliability Requirements; Repeated Loads and Fatigue," 1975, MIL-A-8866B.

5. Pendley, B.J., Henslee, S.P., and Manning, S.D., Air Force Flight Dynamics Laboratory, "Durability Methods Development, Volume III - Structural Durability Survey: State-Of-The-Art Assessment," 1979, AFFDL-TR-79-3118.

6. Wood, H.A., Engle, R.M., Gallagher, J.P., and Potter, J.M., Air Force Flight Dynamics Laboratory, "Current Practice on Estimating Crack Growth Damage Accumulation with Specific Application to Structural Safety, Durability and Reliability," 1976, AFFDL-TR-75-32.

7. Tiffany, C.F. et al, American Institute for Aeronautics and Astronautics, "Analysis of USAF Aircraft Structural Durability and Damage Tolerance," 1978, Proceedings of Structural Durability and Damage Tolerance Workshop.

8. Coffin, M.D., and Tiffany, C.F., "New Air Force Requirements for Structural Safety, Durability, and Life Management," Journal of Aircraft, Vol. 13, No. 2, 1976, pp. 93-98.

9. Yang, J.N., "Statistical Estimation of Service Cracks and Maintenance Cost for Aircraft Structures," Journal of Aircraft, Vol. 13, No. 12, 1976, pp. 929-937.

10. Yang, J.N., "Statistical Approach to Fatigue and Fracture Including Maintenance Procedures," Fracture Mechanics, Univ. of Virginia Press, Proc. of 2nd International Conf. on Fracture Mechanics, 1978, pp. 559-577.

11. Yang, J.N., "Statistical Estimation of Economic Life for Aircraft Structures," Journal of Aircraft, Vol. 17, No. 7, 1980, pp. 528-535.

12. Manning, S.D., Yang, J.N., Shinozuka, M., and Garver, W.R., et al, Air Force Flight Dynamics Laboratory, "Durability Methods Development, Volume I - Phase I Summary," 1979, AFFDL-TR-79-3118.

13. Manning, S.D., Flanders, M.A., Garver, W.R., and Kim, Y.H., Air Force Flight Dynamics Laboratory "Durability Methods Development, Volume II - Durability Analysis: State-Of-The-Art- Asessment," 1979, AFFDL-TR-79-3118.

14. Shinozuka, M., Air Force Flight Dynamics Laboratory, "Durability Methods Development, Volume IV - Initial Quality Representation," 1979, AFFDL-TR-79-3118.

15. Yang, J.N., Manning, S.D., and Garver, W.R., Air Force Flight Dynamics Laboratory, "Durability Methods Development, Volume V - Durability Analysis Methodology Development," 1979, AFFDL-TR-79-3118.

16. Yang, J.N., and Manning, S.D., "Statistical Distribution of Equivalent Initial Flaw Size," 1980 Proceedings Annual Reliability and Maintainability Symposium, 1980, pp. 112-120.

17. Walker, E.K., Ekvall, J.C., and Rhodes, J.E., "Design for Continuing Structural Integrity," Trans. ASME, Vol. 102, January 1980, pp. 32-39.

18. Manning, S.D., and Smith, V.D., "Economic Life Criteria for Metallic Airframes," Proceedings of 21st AIAA Structures, Structural Dynamics, and Materials Conference, Part 1, 1980, pp. 504-511.

19. Yang, J.N., "Statistical Crack Growth in Durability and Damage Tolerant Analyses," Proceedings of the AIAA/ASME/ASCE/AHS 22nd Structures, Structural Dynamics and Materials Conference, Part 1, 1981, pp. 38-49.

20. Manning, S.D., Garver, W.R., Kim, Y.H., and Rudd, J.L., "Durability Analysis - Format Requirements and Critique of Potential Approaches," 1981 Proceedings of ASME Failure Prevention and Reliability Conference, 1981, pp. 223-229.

21. Rudd, J.L., Yang, J.N., Manning, S.D., and Garver, W.R., "Durability Design Requirements and Analysis for Metallic Airframes," Design of Fatigue and Fracture Resistant Structures, ASTM STP 761, 1982, pp. 133-151.

22. Manning, S.D., Yang, J.N., et al, Air Force Flight Dynamics Laboratory, "Durability Methods Development, Volume VII - Phase II Documentation," 1982, AFFDL-TR-79-3118.

23. Speaker, S.M., and Gordon, D.E., Air Force Flight Dynamics Laboratory, "Durability Methods Development, Volume VIII - Test and Fractography Data," 1982, AFFDL-TR-79-3118.

24. Norris, J.W., Air Force Flight Dynamics Laboratory, "Durability Methods Development, Volume IX - Documentation of Durability Analysis Computer Program," to be published, AFFDL-TR-79-3118.

25. Manning, S.D., and Yang, J.N., Air Force Flight Dynamics Laboratory, "Durability Methods Development, Volume X - Final Program Summary," to be published, AFFDL-79-3118.

26. Manning, S.D., Norris, J.W., and Yang, J.N., Air Force Flight Dynamics Laboratory, "USAF Durability Design Handbook: Guidelines for the Analysis and Design of Durable Aircraft Structures," to be published.

27. Rudd, J.L., Yang, J.N., Manning, S.D., and Yee, B.G.W., "Damage Assessment of Mechanically Fastened Joints in the Small Crack Size Range," Proceedings of the Ninth U.S. National Congress of Applied Mechanics, 1982.

28. Freudenthal, A.M., "The Expected Time To First Failure," Air Force Materials Laboratory, AFML-TR-66-37, February 1966.

29. Freudenthal, A.M., Itagahi, H., and Shinozuka, M., "Time to First Failure for Various Distributions of Time To Failure," Air Force Materials Laboratory, AFML-TR-66-241, July 1966.

30. Yang, J.N., and Trapp, W.J., "Joint Aircraft Loading/Structure Response Statistics of Time to Service Crack Initiation," Journal of Aircraft, AIAA, Vol. 13, No. 4, 1976, pp. 270-278.

31. Rudd, J.L., and Gray, T.D., "Equivalent Initial Quality Method," Air Force Flight Dynamics Lab., AFFDL-TM-76-83, 1976.

32. Rudd, J.L., and Gray, T.D. "Quantification of Fastener Hole Quality," Proc. 18th AIAA/ASME/SAE Structures, Structural Dynamics and Materials Conf., 1977.

33. Noronha, P.J., et al, "Fastener Hole Quality," Vol. I & II, Air Force Flight Dynamics Lab., AFFDL-TR-78-209, 1978.

34. Potter, J.M., "Advances in Fastener Hole Quality Through the Application of Solid Mechanics," in Proceedings of U.S. Army Symposium on Case Studies in Structural Integrity and Reliability, AMMRC-MS-78-3, U.S. Army Mechanics and Material Research, Watertown, MA., 1978.

35. Wood, H.A., Rudd, J.L., and Potter, J.M., "Evaluation of Small Cracks in Aerospace Structures," AGARD Publication (In Press) CESME, Turkey, 1981.

36. Johnson, W.S., and Spamer, T., "A User's Guide to CGR-GD, A Computerized Crack Growth Prediction Program," General Dynamics, Fort Worth Division, Report FZS-241, November 1976.

37. "Test Results of Spectrum/Environmental Fatigue Testing to Determine the Crack Growth Rates of Flaws in 7475, 2124, and 2024 Aluminum Alloys and 6Al-4V-Titanium," General Dynamics, Fort Worth Division, Report 16PR925, 10 June 1978.

THE EFFECTS OF COMPRESSIVE OVERLOADS ON THE THRESHOLD STRESS INTENSITY FOR SHORT CRACKS

P. Au, T.H. Topper, and M.L. El Haddad
The University of Waterloo, Waterloo, Ontario, Canada, N2L 3G1

SUMMARY

Fatigue tests of smooth and notched specimens in which stress levels are relatively high and most of the fatigue life is spent at short crack lengths, have shown that the compressive as well as the tensile part at a load cycle causes fatigue damage and that overloads significantly reduce fatigue life. Crack propagation tests using longer cracks and lower stress levels have, on the other hand, indicated that the compressive part of the load cycle has little effect on crack growth and that tensile overloads are beneficial and delay crack growth.

In the present investigation, crack propagation specimens of an aluminum alloy are subjected to continuous and periodic cycles having compressive stresses. Results indicate that for a tension compression load cycle crack growth in the near threshold regime is controlled by the tensile peak stress intensity and the compressive peak stress. Compressive loading significantly reduces the threshold intensity and increases crack growth rate. Furthermore, periodic application of compressive overloads during zero to maximum stress intensity tests is shown to drastically reduce the threshold stress intensity for thousands of cycles following each overload application.

1. INTRODUCTION

Fatigue tests of smooth specimens in which a crack is initiated and propagated to a length associated with the fracture of small samples, indicate that both the tensile and compressive parts of the stress strain cycle affect fatigue life. On the other hand, crack growth studies concerned with the propagation of longer cracks in larger specimens usually at lower stress levels have generally shown that the compressive part of the load cycle has little effect on crack propagation rate. The latter observation is consistent with fracture mechanics concepts since cracks will close in compression and the stress intensity will be zero. In fact crack closure measurements have shown that cracks open only at a positive stress level so that part of the tension portion of the load cycle also does not contribute to crack propagation. This concept has led to the use of pulsating tension cycles in reference tests to measure crack growth rates and the use of only the tensile part of the load spectrum in fatigue crack growth analyses even if some compressive loads are present. The difference in effectiveness of compressive loads between smooth specimen tests and crack propagation tests has usually been explained by attributing the effect of the compressive loads to crack initiation only. Recent work by the authors [1-4] showing that short crack growth usually included in "crack initiation" can be predicted from long crack data using fracture mechanics concepts, however, suggests that such a distinction between crack initiation and propagation might not be valid. Several investigators [5-12] have indeed noted that the compressive portion of a load cycle can increase fatigue crack propagation rates under some conditions.

Gurney, who tested centre-cracked mild steel plate at R = -1 and R = 0 concluded that part of the compressive load in the alternating cycle was effective in crack propagation. Crooker [6] found that in the high strength steels he examined, both crack initiation and propagation were affected by the compressive portion of a fully reversed load cycle. It was observed that for the same maximum applied stress, the number of cycles to initiate a crack from a notch was less for R = -1 than for R = 0; also, the crack growth curve at R = -1 was approximately parallel to that at R = 0 and 1.5 times higher. Maddox et al [7] came to a similar conclusion while studying the stress ratio effect on crack propagation in four structural steels; the stress ratios used ranged from -4 to +0.67. Their results indicate that the crack growth rates at R = -1 varied from 1.65 to 2.5 times those at R = 0, the factor depending on the material. In all four steels, the crack propagated more slowly at R = 0 than at any of the other positive or negative R ratios investigated. These observations are similar to those obtained by Sullivan and Crooker [8] in a 5 Ni-Cr-Mo-V steel. In addition, Haigh and Skelton [9] examined the effect of compressive loading during fatigue of a 0.5% Cr-Mo-V steel at 550 C and concluded that both in air and in vacuum, crack growth rates are always increased by compressive loading. They also showed that it is possible to restart a fatigue crack stopped at R = 0 by changing the stress ratio to R = -1. Their investigation was later expanded by Haigh et al [10], who observed that the threshold stress intensity factor was lower at R = -1 than at R = 0.

Limited work has been performed to study the effect of full or partial compressive cycling on crack propagation in aluminum alloys. Hudson and Scardina [11,12] observed that in 2024-T3 aluminum alloy, a fatigue crack grew faster at R = -1 than at R = 0. However, in 7076-T6 aluminum alloy, the crack growth rate at values of R ranging from -1 to +0.8 were approximately the same, indicating that this material is relatively insensitive to compressive loads.

Recent work [13-16] has indicated that when applied continuously, the compressive part of the load cycle can increase the steady state crack growth rates and also accelerate the propagation rates for subsequent smaller load or strain cycles. Conle and Topper [13,14] and El Menoufy, Leipholz, and Topper [15] showed that in variable amplitude straining of smooth specimens, large cycles increased the damage for subsequent smaller cycles beyond that found in constant amplitude straining. They also noted in variable amplitude that cycles whose amplitude fell far below the constant amplitude fatigue limit contributed to damage. In addition, they showed that an equivalent strain-life curve which gave correct damage summations for the variable amplitude tests, continued as an approximately log linear extension of the low cycle portion of the strain-life curve to levels well below the constant amplitude fatigue limit.

Topper and Au [16] hypothesized that since tensile overloads are known to delay crack propagation, the above accelerations must be due to the compressive overloads in the load spectrum. They found that in 2024-T351 aluminum alloy, continuous application of load cycles with a compressive peak stress equal to about one half of the yield stress reduced the peak tensile stress for threshold conditions by almost an order of magnitude. At high crack growth rates, the effect of the compressive part of the load cycle diminished and there was little difference in crack growth rates between tests with a high compressive stress and those in which the compressive stress was zero.

From the results of the aforementioned investigations, it is evident that compressive loads may have an important influence on the fatigue crack initiation and propagation response of a material. Large compressive cycles can decrease the threshold stress intensity and the fatigue limit of a material. If the magnitude of these compressive cycles is sufficiently large, they may accelerate crack growth for many cycles at lower load levels. This study examines the effect of compressive loads on near-threshold crack growth behavior in 2024-T351 aluminum alloy. The crack propagation response of the aluminum subjected to periodic applications of a single compressive cycle is also noted.

2. MATERIALS, TEST EQUIPMENT AND TEST TECHNIQUES

Crack propagation specimens with the geometries shown in Figure 1 were cut and machined from 12.7 millimeter thick plates of 2024-T351 aluminum alloy. The specimen surface was hand polished for ease of crack detection. A travelling microscope with a 0.025 mm resolution was used to measure crack growth; crack growth data were recorded after the crack had grown out of the 2 mm cut and reached a length of approximately 5 mm.

Constant minimum peak stress (S_{min}) crack propagation tests were performed at room temperature in an electrohydraulic testing system [13]. In the periodic overload crack growth tests, the testing system was connected to a process control computer assisted by some simple analogue computer circuits, as outlined in Reference [9]. The test frequencies used in these tests ranged from 20 to 100 Hz, depending on the level of S_{min}. All the data were obtained using the near-threshold crack propagation test technique guideline suggested by Bucci [14]. At the end of each test, the specimen fracture surface was examined visually for crack tunnelling. A strain-gaged specimen was tested at an S_{min} of -208 MPa to determine the amount of bending induced by high compressive loads, the result showed that the induced bending stress remained negligible even when the crack was long.

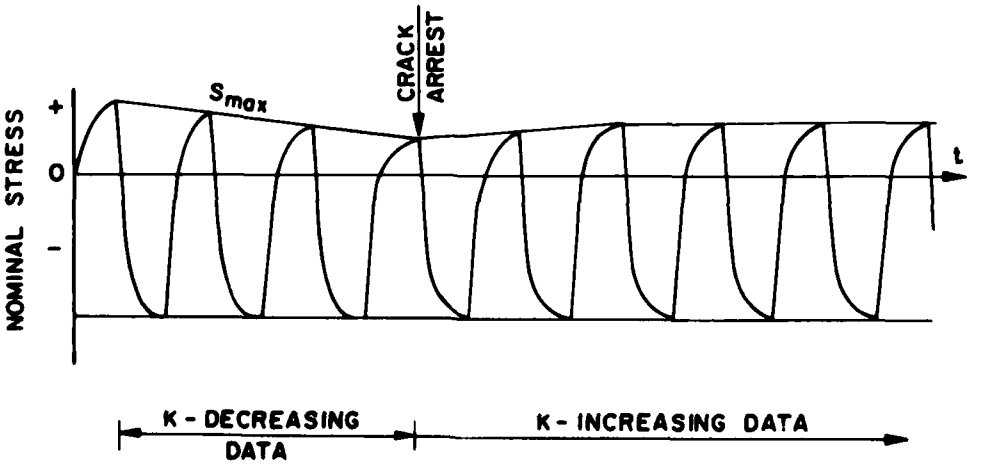

CONSTANT MINIMUM LOAD STRESS HISTORY

FIGURE 1

3. EFFECT OF COMPRESSIVE LOAD ON CRACK GROWTH RATE

Figure 2 schematically represents the load pattern used in this study to investigate the near-threshold crack growth behavior in 2024-T351 aluminum alloy under the influence of compressive cycles. In each test, the compressive peak stress in each cycle was held constant throughout, the tensile peak stress was progressively decreased and the maximum threshold value of the positive threshold stress intensity, $K_{max_{th}}$, for the chosen S_{min} established when crack arrest occurred. Then the load was increased by a small amount and K-increasing crack growth data were obtained when crack propagation resumed.

Figure 3 shows the K-increasing data for the aluminum tested at R = 0 (i.e. S_{min} = 0), and various negative S_{min} levels. All of the crack growth curves are sigmoidal in shape except that the 'knee' portion is amplified as S_{min} becomes more negative. The effect of S_{min} on K_{max} is most pronounced near the threshold region and diminishes as K_{max} increases, eventually data for all values of S_{min} closely approach the R = 0 curve at approximately the same K_{max} value of 11 MPa√m.

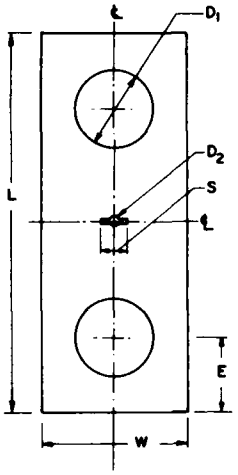

Dimension	in	mm
L	4.6	116.84
W	1.75	44.55
E	0.9	22.86
D_1	0.875	22.23
D_2	0.04	1.02
S	0.08	2.03
Thickness	0.1	2.54

SPECIMEN DIMENSIONS

DESIGN OF CRACK PROPAGATION PLATE SPECIMENS

FIGURE 2

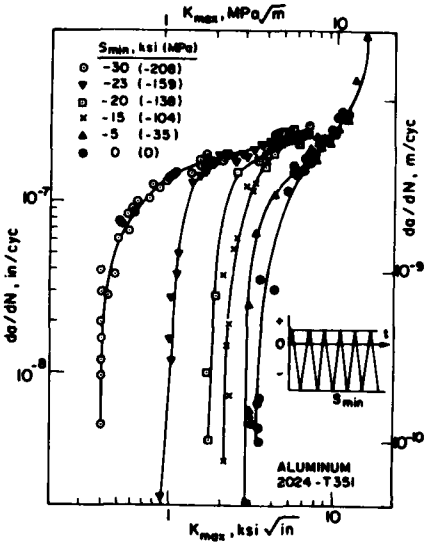

CRACK GROWTH RATE vs MAXIMUM STRESS INTENSITY AT CONSTANT MINIMUM STRESS IN 2024-T351 ALUMINUM ALLOY

FIGURE 3

Values of the threshold K_{max} taken at a growth rate of 10^{-10} m per cycle from Figure 3 are replotted versus the magnitude of minimum stress peak in Figure 4. The relationship between S_{min} and $K_{max_{th}}$ is approximately linear for the values of minimum stress investigated. This figure shows that an S_{min} of -208 MPa can reduce the $K_{max_{th}}$ from 3.5 to 0.44 MPa√m - an eight-fold decrease. It is expected that the decrease in $K_{max_{th}}$ will level off at some positive value since crack extension is not expected for a completely compressive load cycle. However, investigation of this region would require a specimen with a greater lateral stiffness than the one used in this investigation.

4. TESTS WITH A CONSTANT MINIMUM LOAD AND MAXIMUM STRESS INTENSITY

Tests were performed to determine the extent to which crack length influenced the growth rate. In these tests the minimum peak stress was held constant and the maximum stress peak was decreased as the crack grew to maintain a constant maximum stress intensity.

Figure 5 shows the results of a test at zero minimum load (R = 0) and a maximum stress intensity of 6.6 MPa√m (twice the threshold stress intensity at R = 0). A constant growth rate independent of crack length is observed. Data for a second test in which the minimum peak stress was held at -208 MPa and the maximum stress intensity at 1.65 MPa√m are also shown in the figure. Again, the crack growth rate remains constant as crack length increases. Furthermore, the crack growth rate observed corresponds to that found for the same K_{max} and S_{min} in the constant minimum load K-increasing test shown in Figure 3.

Figure 6 represents crack growth data for a specimen tested at a constant minimum peak stress in which the maximum stress intensity was successively held constant for a period of time at each of three values. No variation of growth rate with crack length is evident at any of the K_{max} levels and again the growth rates observed correspond to those found in the constant S_{min}, K-increasing test of Figure 3.

It appears then that steady crack growth rates are dependent on maximum stress intensity and minimum peak stress but not on crack length.

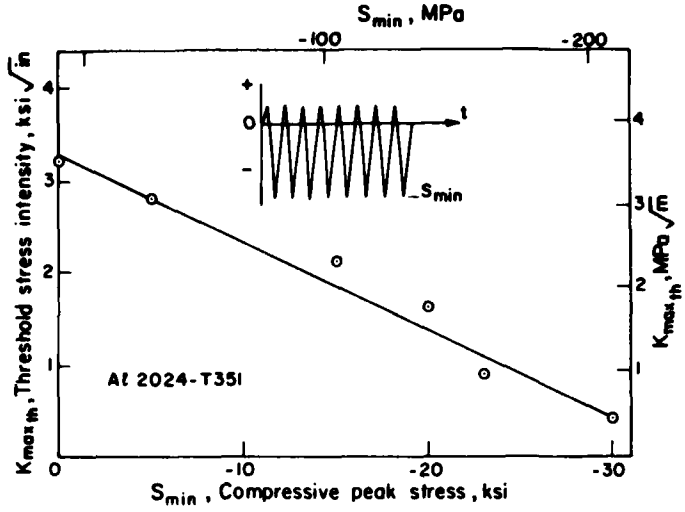

THRESHOLD MAXIMUM STRESS INTENSITY vs COMPRESSIVE PEAK STRESS IN ALUMINUM ALLOY 2024-T351

FIGURE 4

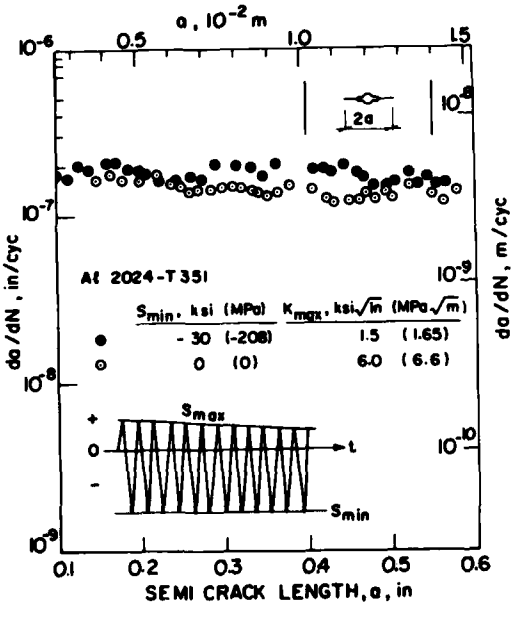

CRACK GROWTH RATE vs LENGTH AT A CONSTANT MAXIMUM STRESS INTENSITY AND CONSTANT MINIMUM STRESS IN 2024-T351 ALUMINUM ALLOY

FIGURE 5

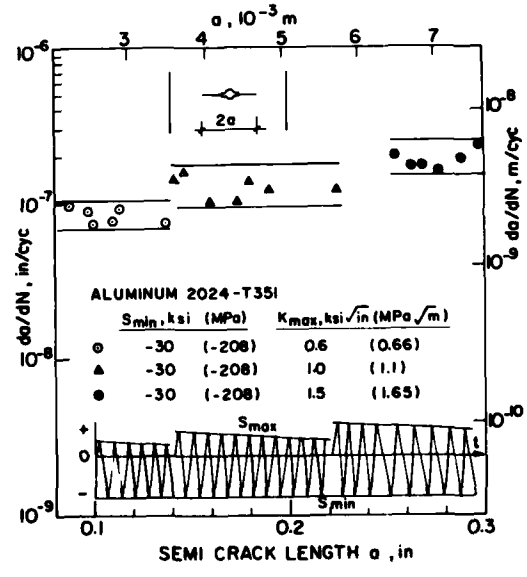

CRACK GROWTH RATE vs LENGTH AT THREE CONSTANT MAXIMUM STRESS INTENSITY LEVELS AND A CONSTANT MINIMUM STRESS IN 2024-T351 Al ALLOY

FIGURE 6

5. TESTS WITH A CONSTANT R RATIO

The two test series above indicate that when the minimum stress is held constant, the crack growth rate remains constant and independent of crack length for a given value of K_{max}. The results also imply that each value of S_{min} would yield a separate crack growth curve and that K_{max} decreasing and K_{max} increasing data would coincide if S_{min} were held constant although the crack length changes throughout the test.

Threshold and crack growth data are, however, usually obtained from tests with a constant R ratio (S_{min}/S_{max}). In these tests the magnitude of the maximum and minimum stress to yield a given K_{max} value depend on the crack length. On the basis of the above observations, it would be expected that data obtained in the constant R ratio tests would not be unique since a given K_{max} value could be combined with various minimum stress levels in different tests and at different crack lengths in the same test when a K-decreasing phase is followed by a K-increasing phase in a typical threshold test.

Figure 7 shows the crack growth data obtained from tests in which K_{max} was first decreased and then increased at a constant R ratio. During the decreasing phase maximum and minimum stresses were decreased in the same ratio until crack arrest occurred. Then both were increased slightly and held constant to obtain the K-increasing crack growth data. Note that during this second phase S_{min} also remained constant. The K-increasing and K-decreasing curves do not coincide, indicating that data obtained in this way are not unique. Unfortunately S_{min} has not generally been recognized as an important variable and test data available in the literature usually specify only stress intensity and R ratio. While this data is unique for the special case of R = 0 where the minimum stress is zero, values for other R ratios can vary from investigation to investigation, depending on the magnitude of minimum stress associated with a given stress intensity.

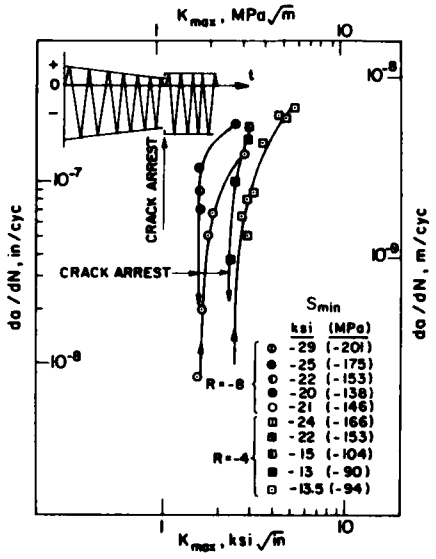

CRACK GROWTH RATE vs MAXIMUM STRESS INTENSITY AT CONSTANT R-MINIMUM STRESS DECREASING & AT CONSTANT MINIMUM STRESS

FIGURE 7

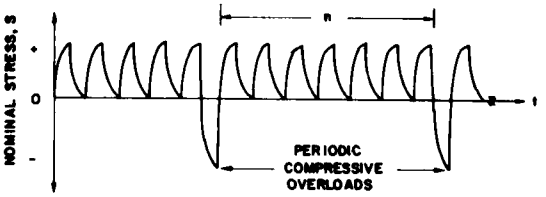

PERIODIC COMPRESSIVE OVERLOAD HISTORY

FIGURE 8

6. PERIODIC SINGLE COMPRESSIVE OVERLOADS

Results presented so far show that the threshold value of maximum stress intensity is decreased and crack growth rates increased in the near threshold region as the magnitude of continuously applied compressive stress cycles is increased. The next series of tests examines the effect of periodic applications of a compressive overload on subsequent zero to tension cycles in the near threshold region.

Aluminum alloy specimens were subjected to the intermittent overloads followed by zero to tension load cycles shown schematically in Figure 8. The load spectrum was generated by a process control computer with the assistance of some simple analog circuits. Referring to Figure 8, n pulsating zero to tension cycles were applied to the specimen between applications of each single compressive overload having a magnitude of 208 MPa. Both n and the magnitude of the periodic compressive overload were held constant throughout a test.

Figure 9 presents results from the tests on the aluminum alloy. The n = 1 curve reproduces the data of S_{min} = -208 MPa of Figure 3 in which the compressive overload accompanies each zero to tension cycle; the n = ∞ curve reproduces the R = 0 zero to maximum load test in which no overloads are applied. These define upper and lower bounds for growth rate at all other n values. Somewhat unexpectedly results for the other tests at n = 250, 500, 1000, 2000, 5000 and 50,000 fall close to one another. This indicates that the effect of a single compressive overload in accelerating crack growth persists for at least 50,000 cycles.

Attempts to detect fatigue striation differences between the various overload tests and between these tests and the zero to maximum tension test by scanning microscopy were not successful. No surface markings corresponding to the overloads could be observed on the fracture surface.

DISCUSSION

Continuous application of compressive stress cycles decreases the threshold and increases near threshold crack growth rates dramatically in the aluminum alloy examined. The amount of the decrease in the maximum stress intensity at the threshold increases with increasing compressive stress level. A compressive peak stress of 208 MPa (about 60 percent at the yield stress) results in an eightfold decrease in the threshold value of maximum stress intensity.

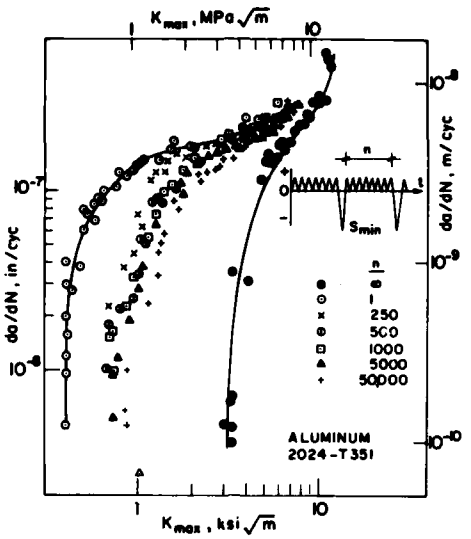

CRACK GROWTH RATE vs MAXIMUM STRESS INTENSITY WITH INTERMITTENT COMPRESSIVE OVERLOADS FOR 2024-T351 ALUMINUM ALLOY

FIGURE 9

It appears that the variables controlling crack growth are maximum stress intensity and minimum stress. When these two variables were held constant crack growth rates remained constant as crack length increased. This suggests that the effect of compressive stress should be similar for short and long cracks.

The present observations explain why previous investigations have generally found the effect of compressive stresses to be much more pronounced in crack initiation (short cracks) than in crack propagation (long cracks). In the former the stress levels necessary to initiate a crack are of endurance limit magnitude. Threshold stress levels for long cracks are much lower. Consequently, for long cracks the effect of compressive stresses which is most pronounced in near threshold crack growth will be significant only when compressive stress peaks are much greater in magnitude than the tensile stress peaks (large negative R ratios), an unusual test condition. It is not, however, that compressive stresses have less effect at greater crack lengths but that the tensile stresses, because the controlling tensile variable is stress intensity, have an effect that increases with length.

A plausible explanation for the effect of compression stress cycles on crack growth is that during the compressive overload, metal behind the crack propping open the crack and causing crack closure at positive load levels [19] is flattened and crack closure loads are decreased. Residual stresses ahead of the crack tip may also be modified. This explanation is consistent with the observation that crack growth rates remain constant with increasing crack length when compressive peak stress and tensile peak stress intensity are held constant. (Preliminary attempts to maintain constant crack growth rates below the R = 0 threshold with constant minimum and maximum stress intensities eventually resulted in crack arrest.)

The intermittent compressive overload tests show that at low growth rates, accelerated crack growth and a lowered threshold stress intensity persist for a large number of cycles following a compressive overload. Even after 50,000 cycles threshold values are still greatly reduced. If the assumption that compressive overloads decrease crack closure loads is correct, a considerable period of crack growth is necessary to re-establish steady state closure levels.

These results suggest that current methods of estimating crack growth rates in variable amplitude fatigue tests may be seriously unconservative when the load history contains large numbers of small cycles. Conditions in which short cracks grow out of notches are often accompanied by high compressive stress cycles which can accelerate crack growth during many subsequent small tensile stress cycles. Similar non conservative assumptions are included in editing of small cycles from variable amplitude load histories. The present tests indicate that small cycles well below the constant amplitude stress intensity threshold can cause crack growth following compressive overloads. The previously noted results of Conle and Topper show that fatigue damage may indeed be caused by small cycles well below the endurance limit in variable amplitude fatigue.

CONCLUSIONS

1. **Continuously applied compressive overloads significantly reduced the threshold values of peak stress intensity and accelerated near threshold crack growth rates in a 2024-T351 aluminum alloy.**

2. In the aluminum alloy tested, intermittent application of a single compressive overload reduced the threshold stress intensity and accelerated near threshold crack growth rates for up to 50,000 small zero to tension cycles following the overload's application. 11-7

3. Constant crack growth rates independent of crack length when compressive minimum stress peak and maximum tensile stress intensity were held constant indicate that the minimum stress associated with the compressive overload is the controlling variable in determining the effect of overloads, rather than for instance, the minimum stress intensity.

REFERENCES

1. Topper, T.H., and El Haddad, M.H., "Fatigue Strength of Notches Based on Fracture Mechanics", International Symposium on Fatigue Thresholds, Stockholm, Sweden, June, 1981.

2. Haddad, M.H., Topper, T.H. and Smith, K.N., "Prediction of Non Propagating Cracks", Eng. Fracture Mechanics, Vol. 11 (3), 1979, pp. 573-584.

3. El Haddad, M.H., Topper, T.H., and Topper, T.N., in WAM-ASME Symposium on Methods for Predicting Materials Life in Fatigue, American Society of Mechanical Engineers, New York, 1979, pp. 41-56. Also in Journal of Engineering Materials and Technology, Transactions of the A.S.M.E. Vol. 103, April 1981, pp. 91-96.

4. El Haddad, M.H., Smith, K.N. and Topper, T.H., "A Strain Based Intensity Factor Solution for Short Cracks Initiating From Notches", Eleventh National Symposium on Fracture Mechanics, ASTM, June 1978, Blacksburg, VA., STP 677.

5. T.R. Gurney, "The Effect of Mean and Naterial Yield Stress on Fatigue Crack Propagation in Steels", Metal Constr., 1(2)(1969) 91.

6. T.W. Crooker, "Effect of Tension Compression Cycling on Fatigue Crack Growth in High Strength Alloys", NRL Report No. 7220, January 1971.

7. S.J. Maddox, T.R. Gurney, A.M. Mummery, and G.S. Booth, "An Investigation of the Influence of Applied Stress Ratio on Fatigue Crack Propagation in Structural Steels", Welding Institute Report 72/1978/E.

8. A.M. Sullivan, and T.W. Crooker, "Analysis of Fatigue Crack Growth in Effects at Constant Amplitude", Trans. ASME J. Press Vessel Tech. (Series J), 98(2). May 1976, 179-94.

9. J.R. Haigh, and R.P. Skelton, "The Effect of Compressive Loading During Fatigue of a 0.5% Cr-Mo-V Steel at 550 C", Central Electricity Research Laboratories Note No. RD/L/N 219/75.

10. J.R. Haigh, T.C. Lindley, and R.P. Skelton, "Effects of Stress Ratio on Fatigue Crack Growth Rates and Thresholds in Cr-Mo-V Steels at 550 C", Central Electricity Research Laboratories, C.E.R.L. Note No. RD/L/N 65/78.

11. C.M. Hudson, "Effect of Stress Ratio on Fatigue-Crack Growth in 7075-T6 and 2024-T3 Aluminum Alloy Specimens", NASA Technical Note TN D-5390, August 1969.

12. C.M. Hudson, J.T. Scardina, "Effect of Stress Ratio on Fatigue Crack Growth in 7075-T6 Aluminum Alloy Sheet", Eng. Frac. Mech., 1969, Vol. 1, pp. 429-446.

13. A. Conle, and T.H. Topper, "Evaluation of Small Cycle Omission Criteria for Shortening of Fatigue Service Histories", Int. J. Fatigue, Jan. 1979.

14. A. Conle, and T.H. Topper, "Evaluation of Small Cycle Omission Criteria for Shortening of Fatigue Service Histories", Int. J. Fatigue, Jan. 1979.

15. M. El Menoufy, H. Leipholz and T.H. Topper, "Fatigue Life Evaluation, Stochastic Loading, and Modified Life Curves", presented at 52nd Shock and Vibration Symposium, New Orleans, Louisiana, Oct. 27-29, 1981.

16. T.H. Topper, P. Au, "Cyclic Strain Approach to Fatigue in Metals" AGARD lecture series 118, Fatigue Test Methodology, The Technical University of Denmark, Denmark, Oct. 19-20, 1981.

17. G.N. Butzow, R.W. Churchill, "Electrohydraulic Fatigue Test Systems Capabilities", presented at SESA Annual Meeting, Cleveland, Ohio, Oct. 29-30, 1964.

18. R.J. Bucci, "Development of a Proposed Standard Practise for Near Threshold Fatigue Crack Growth Rate Measurement", presented at ASTME-9/E-24 Symposium on Fatigue Crack Growth Measurements and Data Analysis, Pittsburgh, Pennsylvania, Oct. 29, 1979.

19. W. Elber, "The Significance of Fatigue Crack Closure", Damage Tolerance in Aircraft Structures, ASTM STP 486, 1971, pp. 230-242.

CRACK PROPAGATION AT SHORT CRACK LENGTHS UNDER VARIABLE AMPLITUDE LOADING (2ND REPORT)

R. COOK
P. R. EDWARDS

Materials and Structures Department,
Royal Aircraft Establishment,
Farnborough, Hants., England.

SUMMARY

An experimental programme was carried out to investigate short crack anomalies whereby short cracks propagate faster than long cracks at the same calculated stress intensity factor. This paper is the second to be issued on this programme and contains all results to date. Fatigue tests were carried out on notched 2L65 aluminium alloy specimens under constant and variable amplitude loading. Measurements of corner cracks growing from holes were taken down to crack lengths of 0.01mm using replicas. Under constant amplitude loading short crack anomalies were identified at zero mean stress but not at R=0 (zero to peak) loading. Under Gaussian random loading much greater anomalies were identified. A linear summation of constant amplitude crack rates to predict those under Gaussian random loading gave predictions that were too slow at short crack lengths and too fast at longer crack lengths. It is suggested that at short crack lengths, cracks remain open below zero stress, due to the relatively large plastic zone. The effect is particularly marked under variable amplitude loading; high loads lower the crack closure stress and accelerate crack growth, in contrast to long crack behaviour.

1. INTRODUCTION

Before crack growth prediction techniques based on fracture mechanics were developed, the fatigue life of aircraft structure was determined from curves of life cycles to failure related to nominal stress and stress concentration factor. Problems of durability and strength of fatigue damaged structures in service hastened the introduction of life assessment techniques based on the prediction of crack growth. The notable example of a requirement for this is MIL SPEC 83444[1]. In this document an initial flaw of ".005 (0.125mm) is assumed to exist at every hole. This flaw size is intended to take crack initiation as well as propagation into account since it is in practice an equivalent initial flaw which, using current crack prediction techniques, gives a fatigue life which is equivalent to lives typical of service experience[2].

However, there is some question as to whether conventionally-applied fracture mechanics will predict accurately crack rates at short crack lengths. In experimental investigations into crack growth rates and growth thresholds at short crack lengths a number of investigators e.g.[3-6] have concluded that an anomaly exists, typically for cracks shorter than about 0.25mm although individual investigators put this limit as low as 0.1mm or as high as 0.5mm. In nearly every case it was found that for short cracks, crack rates were higher than for long cracks at the same calculated stress intensity factor. There is, then, the possibility that, since in most cases as considerable portion of crack growth life is obtained from the growth at small crack sizes, conventionally applied fracture mechanics, between, say, 0.125mm and 0.25mm, could greatly underestimate life. An improved understanding of short crack effects could be employed either to modify crack growth prediction techniques or to provide a more certain base for the equivalent initial flaw size.

This paper describes all the results to date, with discussion, from an investigation into crack propagation at short crack lengths under constant and variable amplitude loading. Some of this work has been reported previously[7] where it was found that short crack anomalies were very marked under Gaussian random loading but not so evident under constant amplitude loading. As described later in this paper it was found that there were significant variations in the mean stresses applied in the earlier investigation. This would be expected to affect the crack rate, an effect most apparent in the constant amplitude data and could explain why the short crack anomaly was not consistently observed. Further tests under constant amplitude loading using carefully controlled conditions are reported in this paper at two different stress ratios (R=0 and R=-1). The results of these tests support the hypothesis that short crack anomalies are associated with crack closure.

2. SPECIMEN AND MATERIAL

12-2 The test specimen used in this investigation was a centre-notched specimen as shown in Fig.1. In direct tension the stress concentration factor was calculated as 2.3. However, for the work described in this paper the specimen was tested in four point bending and so the stress concentration factor was slightly lower at 1.9. The material used was to specification BS 2L65 being the fully artificially-aged version of a 4% Cu-Al alloy. Nominal chemical composition and tensile properties are given in Table 1.

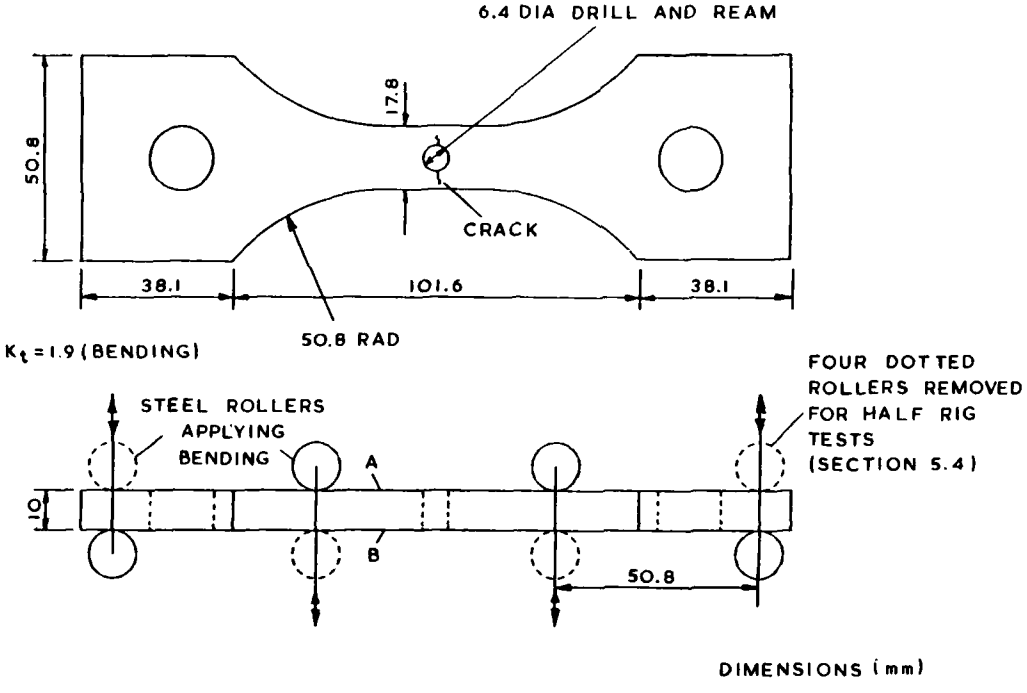

FIG 1: Notched Specimen

3. FATIGUE TEST PROCEDURE

The specimens were tested in four point bending with the loads applied by steel rollers as shown in Fig.1. By using this method fatigue cracks did not initiate down the bore of the hole. In any test up to four cracks initiated reliably at the 'corners' of the 6.4mm diameter hole, as shown, and grew across the plane faces A and/or B. The lengths of the cracks were monitored by replicas applied to the plane faces at suitable intervals. Measurement of surface cracks in this case was found to be a good method of determining the progress of the crack fronts since, as can be seen from Fig.2 subsequent fractographic examination showed that the cracks consistently approximated to quarter-circles up to crack lengths of about 2mm.

Variable amplitude loadings used were Gaussian random and FALSTAFF as illustrated in Figs.3a and 3b respectively. The constant amplitude and Gaussian random tests were carried out in a 60KN resonant fatigue machine modified for random loading, as described previously[8]. FALSTAFF testing was carried out in a 100KN electrohydraulic fatigue machine.

4. CALCULATION OF STRESS INTENSITY FACTORS

Recently a theoretical investigation into the influence of crack growth pattern on damage tolerance life prediction was carried out[9-10]. One of the configurations of structural element used for this exercise was identical to that of the test section of the specimen in the present work. A stress intensity factor solution was derived for the element under direct stress assuming quarter elliptical, including quarter circular, cracks growing from the corners of the hole. The method started with the factor for an ellipse embedded in an infinite solid, and then incorporated suitable adjustments for the presence of the hole and the boundaries of the element. For the purpose of the current investigation the solution was modified to account for the stress gradient due to the fact that the specimens were tested in bending.

12-3

FIG.2: Fracture surface of failed specimen under Gaussian random loading

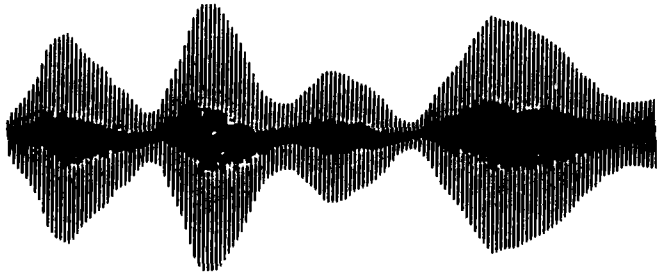

FIG.3a: Gaussian narrow band random loading

FIG.3b: Part of FALSTAFF sequence

12-4

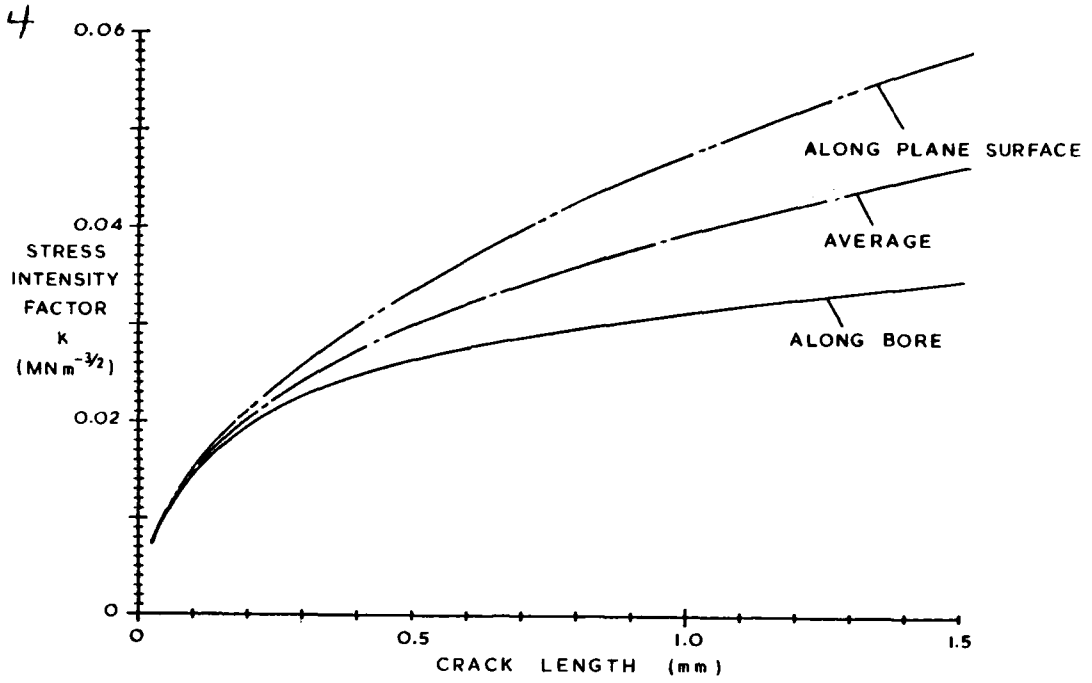

FIG.4: Calculated stress intensity factors for a maximum stress at the stress concentration of 1MN m^{-2}

Fig.4 shows the derived stress intensity factors for the edge of the crack propagating along the bore of the hole and also across the plane surface of the specimen. As can be seen the two solutions were close together at the shortest crack length but at 1.5mm crack length the stress intensity factor for the surface was calculated as about 66% greater than that down the bore. This is similar to a result obtained by Raju and Newman[11] for a similar configuration, but using finite elements. It would be expected, then, that the crack front along the surface would propagate much faster than that along the bore, in conflict with the observed quarter-circular shape of the cracks (Section 3). However, the prediction of crack growth with curved crack front is not well understood. It has been demonstrated[10] that, using calculated surface stress intensity factors at each end of corner cracks to determine crack rates, and allowing the calculated crack to develop into an ellipse, the resulting crack front shape tended to be too elongated. In the present work the cracks were, as stated above, reliably quarter-circular up to 2mm length, which implied at first sight relatively constant stress intensity factors around the crack front. It is well established, however, that stress intensity factors vary around the fronts of quarter-circular cracks. This suggests that some average value should be used in the analysis of the data although it should be appreciated that the configuration in the present work was complex and the stress intensity factor solution could probably be improved.

In analysing the data it was decided to use for this paper the average of the calculated stress intensity factors for the bore and the surface. In order to minimise errors crack rates were plotted in this paper for crack lengths up to only about 1.5mm. However, the whole analysis was repeated using first the calculated bore stress intensity factor and then that of the surface. No essential differences in the patterns of the data which could affect the conclusions of this paper were noted in either case.

5. RESULTS AND DISCUSSIONS

Sections 5.1 to 5.7 present and discuss all the test results to date. The discussion from the previous work[7] is incorporated.

In Section 5.1 test results[7] under constant amplitude loading at R=-1(zero mean stress) are presented and discussed. Some evidence for short crack anomalies was found together with considerable scatter.

In Section 5.2 a mechanism for short crack anomalies involving crack closure is suggested. A consequence of this is that such anomalies may be dependent on mean stress or residual stress. Accordingly, Section 5.2 describes the results of constant amplitude tests at R=-1 on specimens which had been subjected to a series of stress-relieving loads prior to testing. The dependence of short crack anomalies on mean stress is investigated further in Section 5.3 with the results of tests at R=0 (zero to tensile cycling).

At this point it was discovered that significant mean loads could be applied inadvertently whilst tightening the rollers on the bending rig, no matter how careful the tightening procedure. It was therefore decided to repeat the zero and tensile mean stress tests under better controlled conditions. The test procedures and results are described in Sections 5.4 and 5.5 for the cases of R=0 and R=-1 respectively. Section 5.5 also summarises the conclusions of the constant amplitude tests. Test results under Gaussian random and FALSTAFF loading are described in Sections 5.6 and 5.7 respectively.

The fatigue test results are presented in Tables 2 and 3 for the cases of constant amplitude and variable amplitude loading respectively.

5.1 Constant Amplitude Crack Propagation Results at R=-1 (from Ref.7)

The data obtained from the replicas were plotted out in terms of length vs. cycles, and crack rates were derived from these plots by drawing tangents manually and calculating the slope. Normally only one such curve was obtained for each specimen as, under constant amplitude loading, in general only one crack initiated per test. Fig.5 shows plots of crack rate vs. range of stress intensity factor ΔK. As is conventional in this type of plot the value of ΔK used was the tensile part only, the compressive part being ignored. Results are shown for the six different alternating stress levels applied to the specimens. Note that the stress values should be multiplied by the stress concentration factor 1.9 to obtain uncracked notch root stresses.

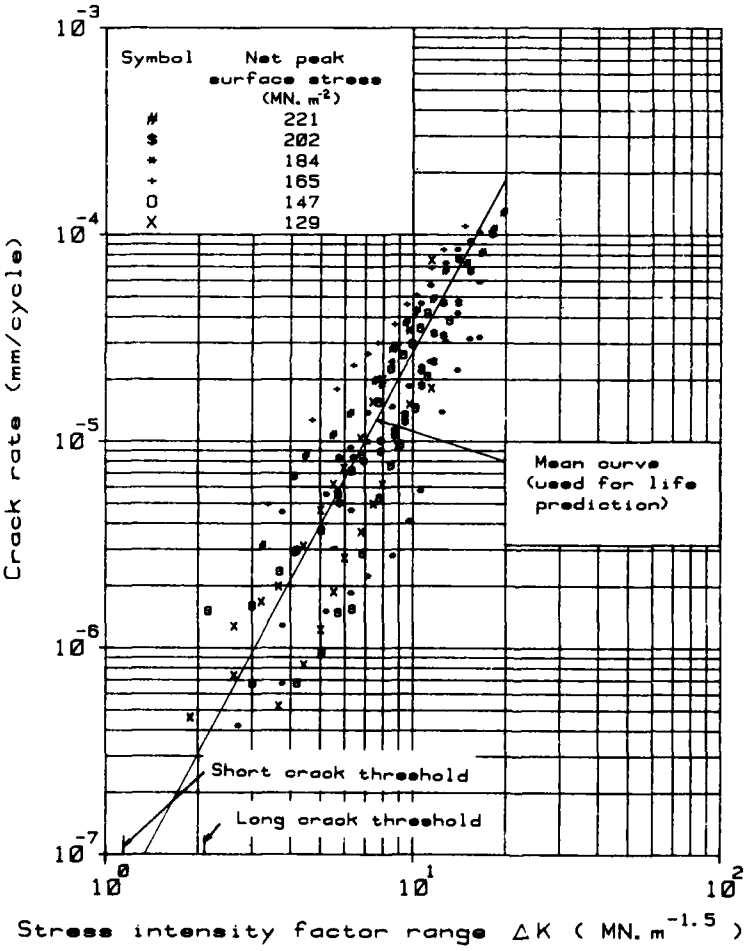

FIG.5: Constant amplitude crack rates at R=-1

It can be seen from Fig.5 that, at first sight, stress intensity factor was fairly successful in correlating crack rate curves at different applied stress levels. Although there was considerable scatter, test points from different stress levels appeared to be distributed in a relatively random fashion throughout the scatter band. However, Fig.6 which shows the same data as Fig.5 except that related test points have been joined by continuous curves, indicated evidence of anomalous behaviour at the lower ends of the individual curves. As can be seen there was a tendency for some individual curves to turn leftwards at the

lower ends. Out of the eleven curves plotted, five turned sharply to the left, three showed no great tendency to turn and the three remaining tended to turn downwards. Such leftward turns, if occurring at increasing higher crack rates for increasing net test stress values, indicate a short crack anomaly as discussed in Section 1, where short cracks propagate faster than expected.

12-6

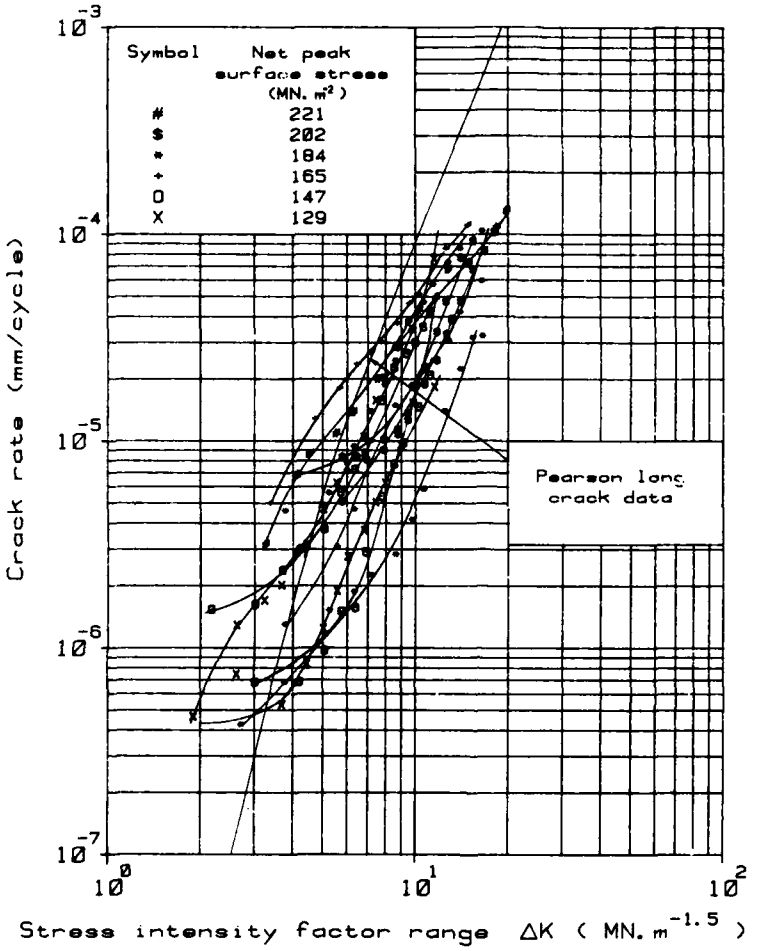

FIG.6: Constant amplitude crack rates at R=-1 with related points joined

Although it was not felt that a short crack anomaly was conclusively demonstrated from these results, it was shown to be a possibility. Some supporting evidence for this can be seen by comparing Pearson's[12] long crack data plotted in Fig.6 with the present data. As can be seen the general slope of the present data was considerably shallower than that of Pearson, and showed no tendency to turn over towards the crack growth threshold for long cracks as measured by Frost[4] and shown on Fig.5.

It was been suggested[13] that short crack anomalies under constant amplitude loading can be explained by crack closure. The closure of long cracks, tested at R=-1, when load approaches zero, is well established. It is argued that at short crack lengths the plastic zone is large compared with the crack length and props it open so that it does not close until some way into compression. Thus the effective range of stress intensity factor at short crack lengths is greater than at long and the crack propagates faster.

A consequence of the above explanation is that, under fully tensile loading, both long and short cracks are open for the greater part of the stress range, and very little short crack anomaly would be expected. Examination of Fig.6 shows that the two curves propagating fastest did not show the anomaly. If it is assumed that these curves were effectively at a tensile (residual) mean stress due to manufacture then this is consistent with the above explanation. For this reason the next two sections, 5.2 and 5.3, investigate the effect of mean stress due to residual stresses and a change in mean stress respectively.

5.2 Constant amplitude crack propagation results at R=-1 with "stress relieved"specimens

On the basis of the model discussed in Section 5.1 it would be expected that specimens without manufacturing residual stresses would show lower scatter and more consistent anomalies at R=-1 than those with residual stresses. To examine this hypothesis a number of specimens were subjected to a series of stress relieving axial alternating preloads prior to testing in the bending configuration. The preloads were applied at zero mean load and started with a load large enough to cause notch root plasticity. Subsequent loads were gradually decayed to zero in a 20 step sequence. The magnitude of the highest load was designed to cause plasticity at the notch root to a depth of 1.5mm using Howland's data[14]. The crack propagation tests were carried out under the same conditions as described in Section 5.2 and are presented in Fig.7. It can be seen from Fig.7 that all of the curves turn to the left at the short crack lengths. However, it cannot be said that this trend was any more marked in this case than in Fig.6 or that scatter was necessarily less. More data would be required for that.

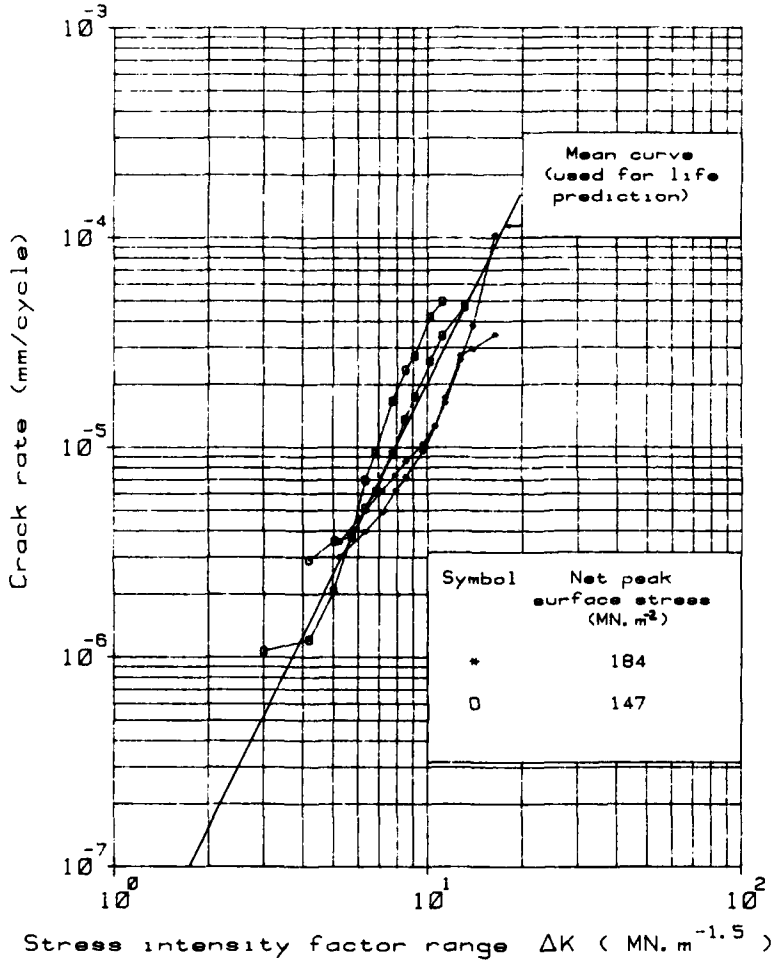

FIG.7: Constant amplitude crack rates at R=-1 Stress relieved specimens

However, as discussed in Ref.4 and Section 7 the possibility exists that the anomalies were due to residual stresses. A conclusion drawn from the tests described in this section was that residual stresses were not, in this investigation, the cause of short crack anomalies because they were found in specimens which had been cycled to be effectively stress free at and near the root of the stress concentration.

5.3 Constant amplitude crack propagation results at R=0

These tests were carried out in order to investigate the hypothesis as discussed in Section 5.1 that these under fully tensile loading would show a much reduced short crack anomaly. The test results are presented in Fig.8 and were all at R=0.

A comparison with Fig.6 shows two noteworthy differences. First, as suggested in Section 5.1, there

were no indications of any anomalous behaviour at short crack lengths. All the curves turned downwards at the bottom.

12 - 8

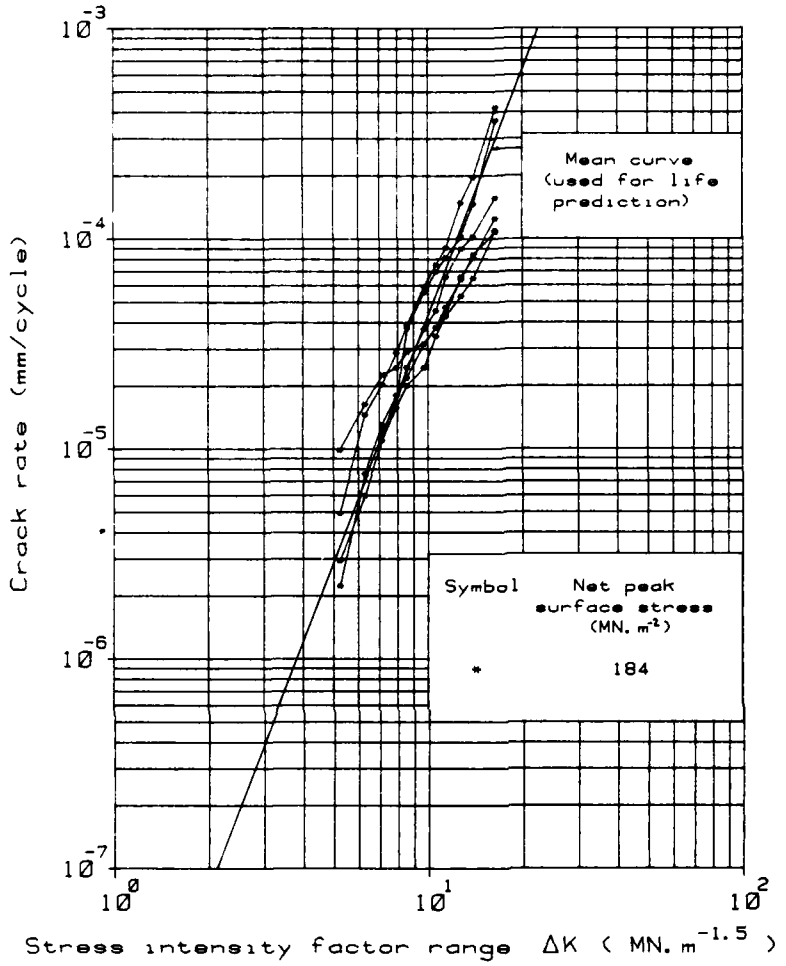

FIG.8: Constant amplitude crack rates at R=O

However, there was a noteworthy reduction in scatter. This is consistent with residual (mean) stresses giving rise to scatter because a change in mean stress for a test at R=-1 is effectively an equal change in the alternating stress range, due to crack closure at zero stress. At R=O an increase in the mean stress only changes the mean stress intensity factor. Therefore increases in mean stress for R=O loading are not as effective in changing crack rate as for R=-1 loading, and mean stress-related scatter will be greater in the latter case.

It was at this point in the investigation that variations in the mean stress were discovered due to tightening the rollers on the bending rig giving another cause of mean stress-related scatter which applied to all the results discussed so far and to all the variable amplitude tests. This was investigated as described in Sections 5.4 and 5.5.

5.4 Constant amplitude crack propagation results at R=O with "half rig"

The results described in this section are a repeat of those at R=O described in Section 5.3 but using "half rig" to ensure true R=O loading.

Four of the loading rollers were removed, as shown in Fig.1. The arms holding the remaining rollers were carefully shimmed and adjusted prior to each test to ensure that the specimen was evenly gripped. The mean load was applied to the specimen and the dynamic load gradually increased until the loading waveform was on the point of truncation at zero load side, thus ensuring a true R=O situation.

The results of these tests are presented in Fig.9. As can be seen scatter was markedly better than for

the original R=-1 results (Fig.6) but similar to that shown in Fig.8 under the same loading conditions. This probably reflects that fact that mean load control for this data in Fig.8 was fortuitously good and/or that variations in mean load are not as important at R=0 as at R=-1 (see 5.3).

Out of nine test results plotted in Fig.9 only one showed any indication of the short crack anomaly.

12-9

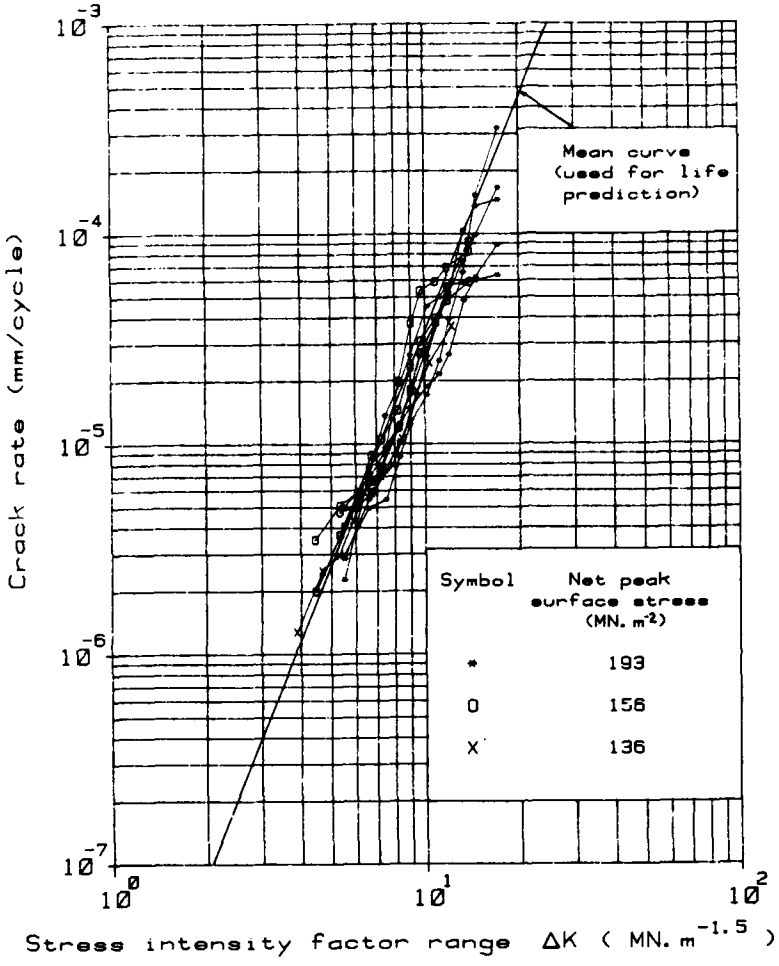

FIG.9: Constant amplitude crack rates at R=0 Half-rig tests

5.5 Constant amplitude test results at R=-1 with strain gauged specimens

The results described in this section and presented in Fig.10 should be compared with those presented in Fig.6, in that the test conditions were the same except that the mean stress was controlled better for the present tests.

For R=-1 it was found that, even with careful shimming and adjustment, when all eight rollers were used significant mean loads could still be induced during tightening. Each specimen tested in this section had a strain gauge attached to the net section away from the notch. The specimen was installed in the rig and the rollers tightened carefully, ensuring that the strain gauge output remained at zero. After the rollers were tightened, the strain gauge was removed using dimethylformamide and the surface of the specimen cleaned so that replicas could be used on the surface.

A comparison with Fig.6 shows that improving the mean stress control greatly reduced the scatter. The degree of improvement implies that better mean stress control was more important than variations in mean stress due to manufacturing residual stresses.

The overall picture of short crack anomalies under constant amplitude loading is shown by comparing all the curves nominally at R=0 (Figs.8-9) with those nominally at R=-1. Out of fifteen curves at R=0 only one (in Fig.9) showed any tendency to the anomaly and then only slightly. In contrast, twelve out of twenty-three curves in Figs.6, 7 and 10 at R=-1 showed marked anomalous behaviour. It is considered that this

difference is sufficient to verify the existence of the anomaly for constant amplitude loading. In the earlier work, with only the results presented in Fig.6, the anomaly was not identified positively because it was felt that the identified leftward turns could be due to scatter. However, the marked difference in behaviour at R=0 is sufficient to reject that possibility.

12-10

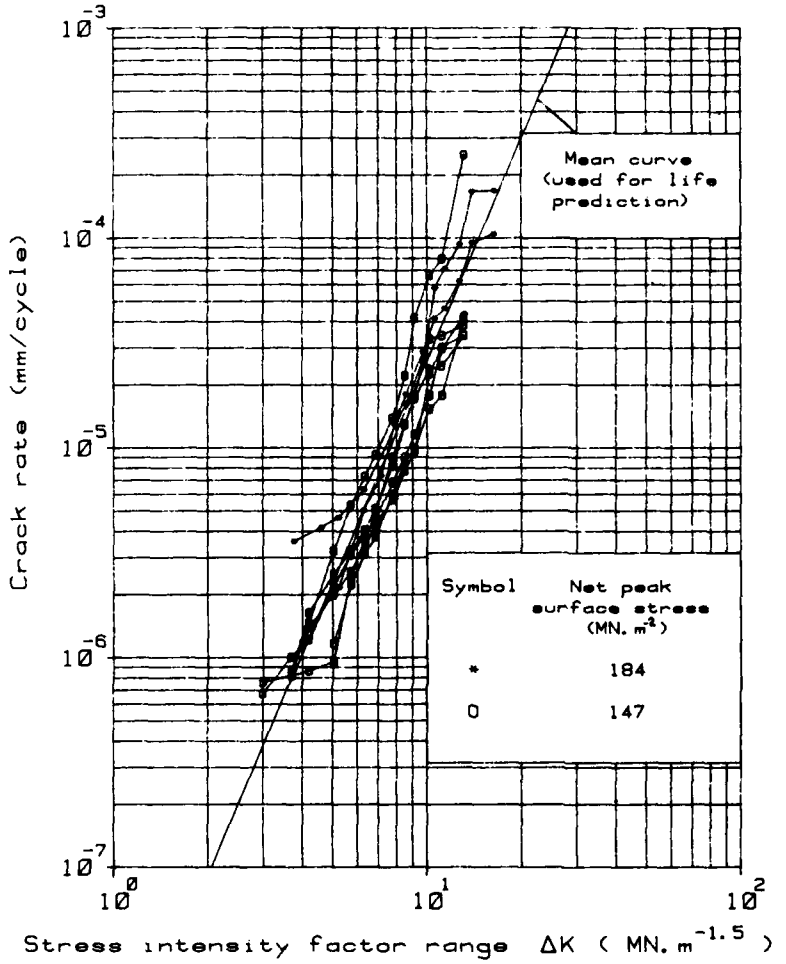

FIG.10: Constant amplitude crack rates at R=-1 Strain gauged specimens

As discussed earlier, the data was confused by the possibility of residual stresses and inaccurately applied mean stresses and it may be that if stress relieved specimens were tested at R=-1 the anomaly would be observed more consistently. However, this test condition was not investigated and is a subject for further work.

The relative absence of anomalies at R=0 was predicted in the earlier report[7] before the testing was carried out, and it is concluded that this result supports the crack closure model outlined in Section 5.1.

5.6 Gaussian random crack propagation results at R=-1 (from Ref.7)

Fig.11 shows crack rates for Gaussian random loading plotted in a fashion similar to that of the earlier data in Fig.6. In Fig.11 the stress intensity plotted is the root mean square value corresponding to the conventionally measured rms value of the waveform in the fatigue test. For the specimens under Gaussian random loading commonly four cracks were monitored in each test. Crack initiation was much more consistent than in the constant amplitude tests, a phenomenon which was attributed to reversed yielding which occurred under the highest loads in the random spectrum at the notch root, and which would tend to negate any inadvertent application of mean stresses other than zero.

As can be seen from Fig.11, the correlation of crack rate with stress intensity factor was not good for the data obtained at different stress levels. Although not completely consistent there was a strong trend for cracks in specimens at the highest stresses to propagate fastest, i.e. at a given stress intensity the shortest cracks propagate fastest.

Thus it was concluded that a much stronger short crack anomaly existed for Gaussian random loading at zero mean stress than for constant amplitude loading.

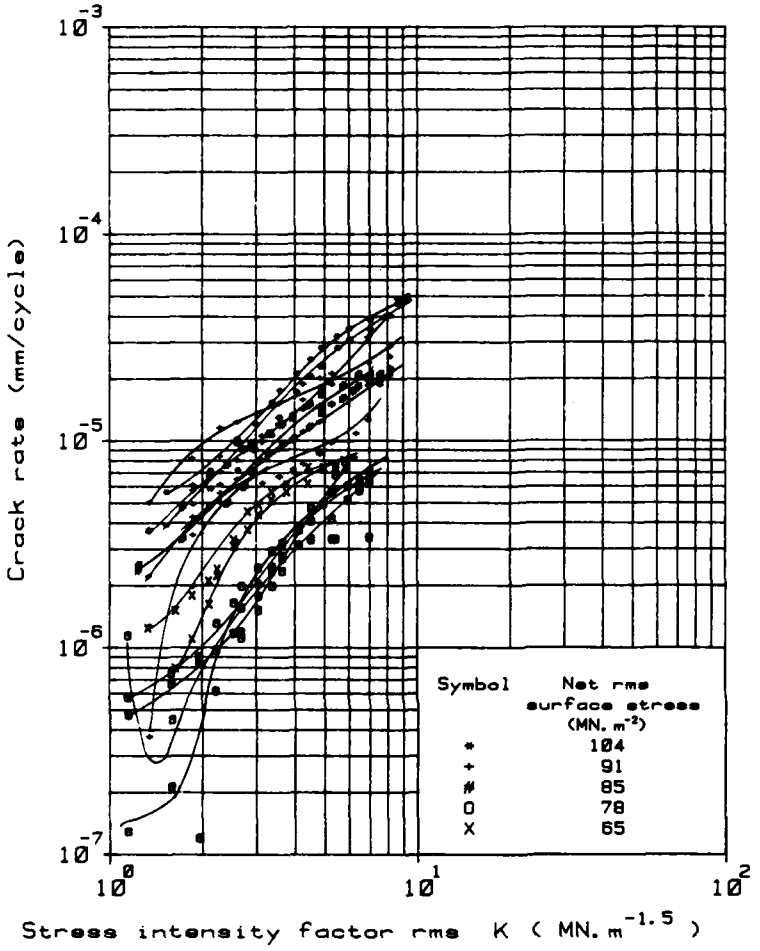

FIG.11: Gaussian random crack rates at R=-1

5.7 FALSTAFF crack propagation results (from Ref.7)

Crack propagation data under FALSTAFF loading is plotted in Fig.12. The stress intensity factor plotted is the peak value as calculated assuming no notch root plasticity. It should be appreciated that FALSTAFF loading is predominantly tensile. However, in the present tests the highest loads were high enough to give local yielding at the notch root. Therefore a residual stress would have been induced by the first application of the highest load. This would have reduced the local mean stress in the region of the notch root and hence slowed the crack growth rate. The cracks propagate through this region of lowered mean stress and the crack rate would be expected to have been affected most at the shortest crack lengths where the magnitude of the residual stress was at its greatest. This situation was in contrast to that for the Gaussian loading at zero mean stress. Since Gaussian loading is symmetrical it is to be expected that alternating plasticity occurred under the highest tensile and compressive loads. This would have a stress-relieving effect and ensure that propagation under the lower loads was, at least initially, in an effectively stress-free specimen.

As can be seen from Fig.12, the data is somewhat limited, being only the results of two tests at the same stress level. The significance of the results is best appreciated in relation to the predicted values, as discussed in Section 6.2.

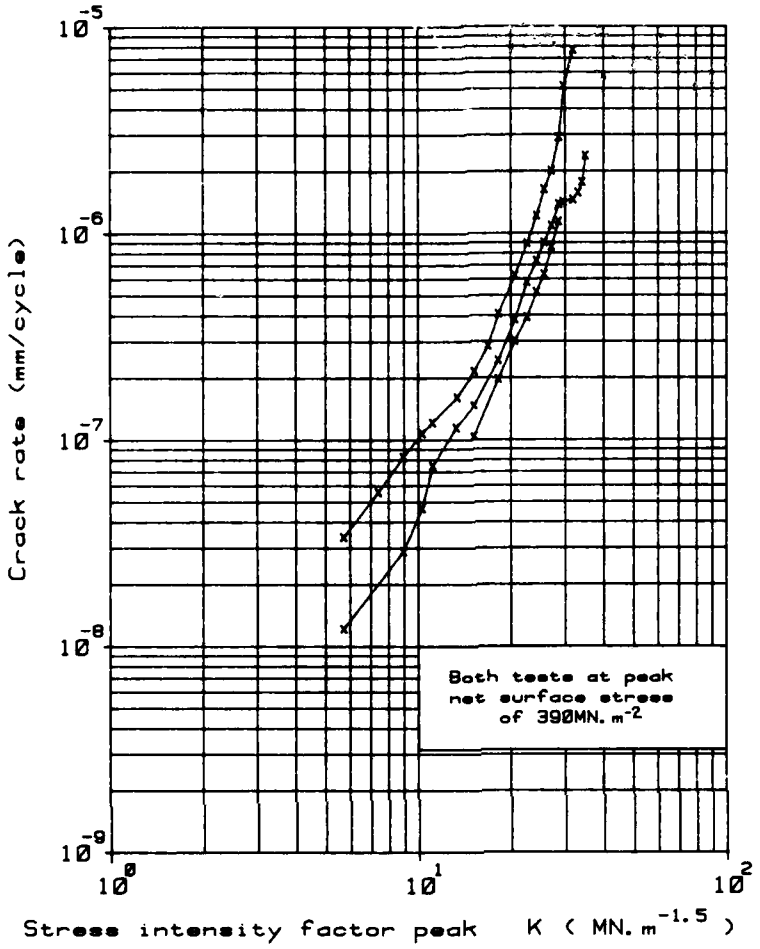

FIG.12: FALSTAFF crack rates

6. CUMULATIVE DAMAGE CALCULATIONS

6.1 Cumulative damage calculations for Gaussian random loading

The crack rate under Gaussian random loading was calculated from each set of constant amplitude data. The method used was a simple linear summation of the constant amplitude levels weighted according to the measured probability distribution of peaks in the random loading. Crack closure at zero load was assumed. The mean curves used for the predictions are plotted in Figs.5, 7-10. It was assumed that the curves cut off sharply at the crack growth threshold. Predictions were made for two assumed threshold values, the 'long crack' and 'short crack' values measured by Frost[4] (see Fig.5).

As can be seen from Fig.13 the predictions from all sets of constant amplitude data are similar. The prediction from the prestressed data has a shallower slope than the others, probably due to the limited data available. The predictions also show very little difference between the two assumed thresholds. However, at the shortest crack lengths, i.e. occurring with the lowest stress intensity factors and the highest net surface stresses, all of the predictions greatly underestimate the crack rate. Conversely, at the longer crack lengths (highest stress intensity and lowest net surface stresses) the crack rate was overestimated, as is common for variable amplitude loading at long crack lengths.

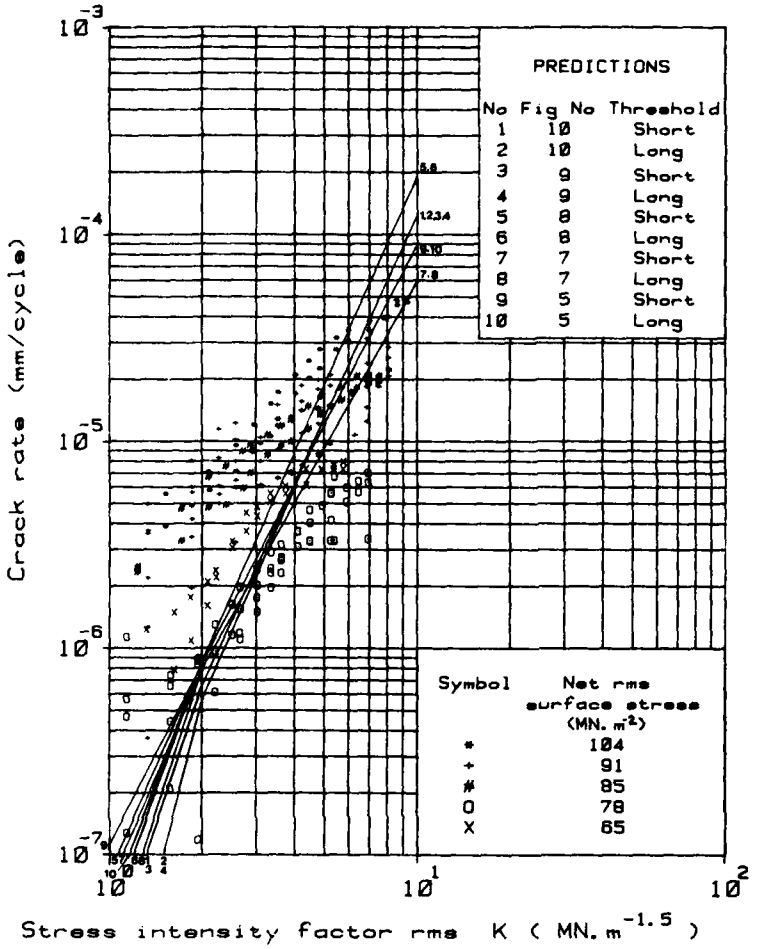

FIG.13: Gaussian random crack rates at R=-1 with cumulative damage predictions

6.2 Cumulative damage calculations for FALSTAFF

Crack rates under FALSTAFF[15] were calculated from the constant amplitude data in Figs.5, 7-10. The method used was the same as for Gaussian loading (Section 6.1) except that there were additional considerations which were due to the irregular nature of the waveform (see Fig.3b). Before the cumulative damage calculations were carried out rainflow counting[16] was used to give a logical interpretation of the loading sequence in terms of numbers of cycles at different mean and alternating stress levels. The cumulative damage calculations were then carried out as before. Crack rates for individual cycles were determined as those for the same stress intensity factor range. In Figs.5, 7-12 no extra allowance was made for mean stress intensity factor. Compressive parts of any stress intensity factor range were ignored.

The calculated crack rates under FALSTAFF loading are compared with the experimental values in Fig.14. As before, predictions were made using the rate data in Figs.5, 7-10, but with the two assumed thresholds. In this case the effect of changing the assumed threshold value was rather more marked than for Gaussian loading. However, over the entire range of the experimental data the measured rate was markedly slower than any of the predictions.

In view of the limited nature of the data it was not possible to come to any firm conclusions as to the presence, or otherwise, of short crack anomalies. The slopes of the curves suggested that any anomalies were not as marked as for Gaussian random loading. However, for both specimens the curves, in a manner similar to that for constant amplitude loading, showed no tendency to turn downward at the lower ends towards the threshold(s) as indicated by the predictions. This is particularly noteworthy in view of the fact that the early stages of crack propagation would have been expected to show slow crack rates due to the action of residual stresses.

It was concluded that more data was required to establish with some certainty the presence of a short crack anomaly under FALSTAFF for these tests. However, the limited data generally supported the existence of such an anomaly.

12-14

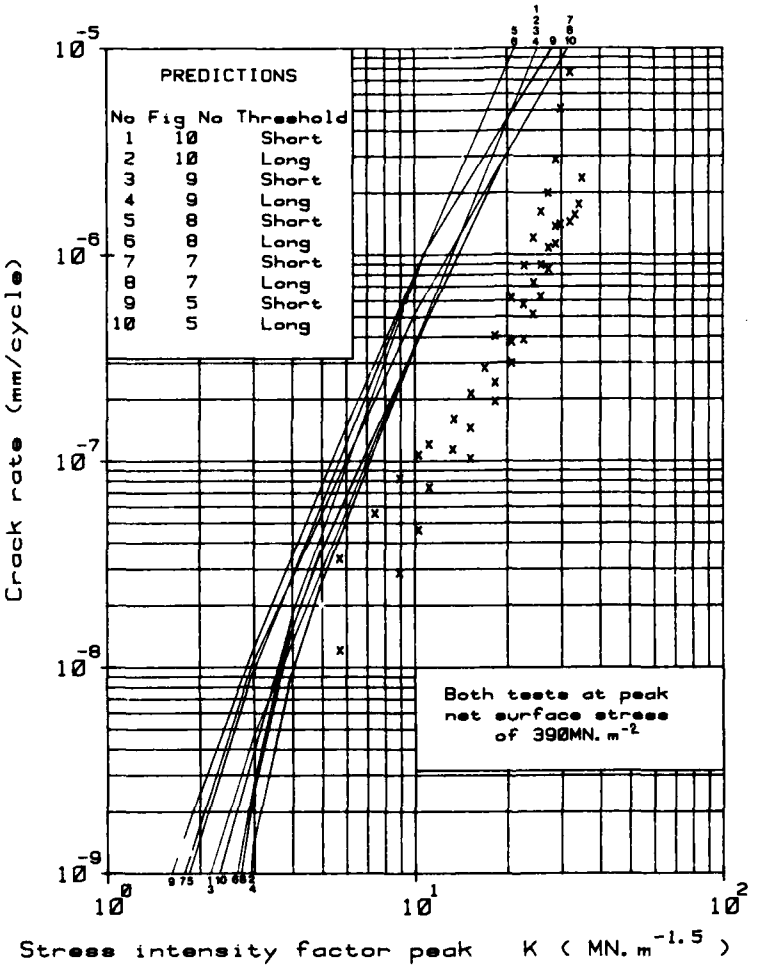

FIG.14: FALSTAFF crack rates with cumulative damage predictions

7. CONCLUDING DISCUSSION

Establishing and accounting for short crack anomalies is not a simple matter because the number of variables is so large and difficult to control in a small thickness of material near the surface. For instance, a marked short crack anomaly was found by Pearson[12] in the same material as used in the present investigation. Subsequently it was established that much, if not all, of the anomaly was due to initiation at inclusions. The inclusions provided an extra stress concentration which accelerated the crack growth at short crack lengths. Pearson's specimens, as it happened, provided a relatively large area for cracks to initiate by 'finding' suitable inclusions. Therefore his results are unlikely to apply to the present work where the position of the initiated cracks was closely controlled. This example illustrates how difficult it can be to take one investigation and apply the results generally, or even to compare the results of one investigator with another. Both Pearson's results and those in the present investigation may be applicable to structural fatigue, but in different situations.

The above provides one small example of the way the metallurgical state of metals near the point of fatigue initiation can vary greatly from situation to situation. This is rarely accounted for by investigators. Additional problems arise when residual stresses are considered, either induced by the loading or present in the specimen before testing. In most practical situations where fatigue failures are liable to occur, both aspects of residual stresses may be significant.

The question then has to be asked: how far were the results of the present investigation affected by metallurgical factors and residual stresses? Also is it possible to account for short crack anomalies by metallurgical factors and residual stresses only?

Consider first the constant amplitude results. As described in Section 5.5 anomalies were positively identified at R=-1 but not at R=0. This makes it unlikely that metallurgical state near the surface, for example a work hardened layer due to machining,[17] is responsible for the effect. If such a layer were to accelerate crack growth at R=-1 it is difficult to see how this would not happen at R=0. A similar argument applies for residual stresses. Additionally, as discussed in Section 5.2 the presence of the anomaly in specimens which had been subjected to a stress-relieving prestress confirms that residual stresses were not responsible.

12-15

Turning now to the results under Gaussian random loading, where, as discussed in Sections 5.6 and 6.1, a very large anomaly was found, the question has to be asked as to whether it arose from the same causes as the anomaly established under constant amplitude loading. This is by no means certain, particularly as the difference in crack growth behaviour was very great, as illustrated by a comparison of Fig.13 with any of the comparable sets of data obtained under constant amplitude loading. This very large difference in behaviour between the two loading actions is illustrated in a different form in Fig.15 which shows typical curves of crack length vs. cycles over the entire life of constant amplitude and Gaussian specimens. As can be seen, for both cases, cracks of about 0.5mm were reached at just over 10^5 cycles. In the Gaussian case the crack was detected first at less than 2×10^4 cycles, but in the constant amplitude case a crack was detected at more than four times that number of cycles, accelerated past the Gaussian curve and failed well before it. Returning to Fig.15 it should be noted that, as can be deduced from Fig.6, long crack fracture mechanics data would predict, for the constant amplitude loading, even quicker acceleration of growth rate with length than was measured. The same data would predict for Gaussian loading a shape of curve similar to that measured for constant amplitude loading.

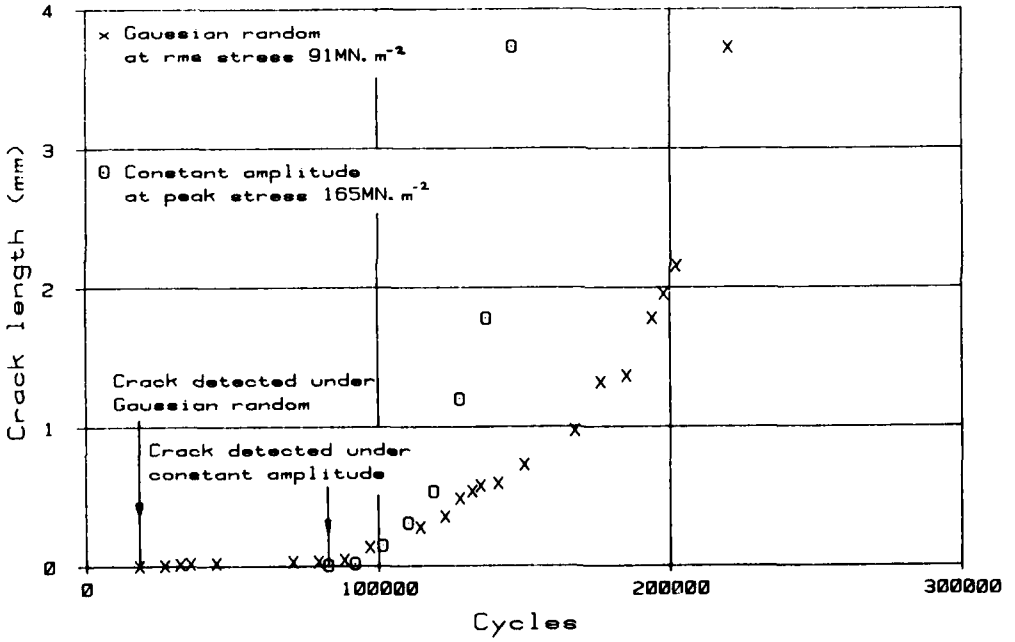

FIG.15: Comparison between shapes of crack length vs. number of cycles curves under constant amplitude and Gaussian random loading

For Gaussian random loading, metallurgical state near the surface is unlikely to have been the cause of the short crack anomaly. In this case the argument is that it is difficult to see how such an effect could have been so large for variable amplitude loading and not for constant amplitude. Residual stresses can be eliminated as a cause because under Gaussian loading the highest and lowest loads in the waveform gave rise to yielding in both directions, thus washing out any residual stresses. However, the alternating plasticity due to the highest and lowest loads could be involved since it did not occur under constant amplitude loading and could be the cause of the differences in behaviour under the two loading actions.

Having examined and rejected residual stresses and metallurgical state near the surface as possible explanations for the short crack anomalies found in this investigation, both under constant and variable amplitude loading, the model described in Section 5.1 will now be examined likewise. Essentially it suggests that crack closure occurs at stresses below zero for short cracks, because the crack is propped open by the plastic zone, which in this case is large compared with the crack length. As discussed in Section 5.5 it was deduced in an earlier paper[7] that if the above model were the correct one then anomalies would be very much less for R=0 loading than for R=-1. Virtually no such anomalies were found subsequently at R=0 in the

present investigation, thus supporting the model for constant amplitude loading. Some direct evidence[18] linking short crack anomalies with crack closure was given in a recent review[19]. In tests on 52N6 steel, where cracks were initiated from saw cuts under constant amplitude loading at R=-1, it was found that at crack lengths less than about 1mm the crack was open for about 80% of the stress range. This reduced progressively as the crack increased in length, until for a crack length of 3mm the crack was open for slightly less than 50% of the stress range. This value was maintained for crack lengths of up to 30mm. Although the material and method of initiation were very different from that in the present work and so the results are not necessarily applicable, such behaviour is entirely consistent with the model described above and could account for the anomalies found in the present work under constant amplitude loading.

Returning to the results under Gaussian random loading, it can be argued as follows that the crack closure model can explain also the large anomaly found under these conditions. Crack closure is well established as a controlling mechanism in fatigue crack propagation under variable amplitude loading[20]. Measurements have shown[21] that for long cracks, when cycling is changed from a high alternating stress level to a low one the crack closure stress first is lowered, corresponding to a momentary increase in the crack rate and then rises, giving a retardation of the crack rate. The overall effect is that of a retardation and it is believed that under variable amplitude loading the observed retardation in crack rate which occurs when larger loads are introduced into the loading sequence is due to the effect of the highest loads on the crack closure stress under subsequent loads of lower amplitude. This leads normally to variable amplitude crack rates being measured which are markedly slower than those predicted using the linear summation method as described in Section 6.1. For the short crack case, if the model described earlier for short crack anomalies is accepted, then it is likely that response of the crack to high loads will differ from that at long cracks. Under constant amplitude loading it was argued that the plastic zone, being large compared with the crack length, holds the crack open until some way into compression, i.e. lowers the crack closure stress. For the Gaussian random case, as stated above, the highest loads give general yielding at the notch root and are likely to give a much larger plastic zone than under constant amplitude loading. If this has the same effect as under constant amplitude loading then the raising of the crack closure stress and retardation of the crack rate is unlikely to occur as at longer crack lengths. As discussed in Section 6.1 and shown in Fig.13, crack rates measured tended to be faster than predicted by a linear summation of constant amplitude crack rates. This was particularly marked at the shortest crack length, i.e. lowest stress intensity factor and highest rms stress (104 MNm^{-2}). Under this condition cracks were propagating a factor of 10 faster then predicted. This is consistent with the large plastic zone created by the largest loads in the Gaussian sequence inhibiting crack closure under subsequent lower loads and hence being damaging. This extra effect of the high loads explains the greater anomaly in the Guassian case and the fact that achieved rates tended to be faster than predicted. At longer crack lengths achieved rates tended to be slower than predicted, in line with the generally accepted beneficial effect of crack closure at a higher stress.

The FALSTAFF test results shown in Fig.14 and discussed in Section 6.2 are rather more complex to analyse than those under Gaussian loading because of the existence of another variable, the redistribution of stresses near the stress concentration, due to the highest loads in the sequence. Unlike Gaussian loading FALSTAFF is predominantly tensile, so a compressive residual stress would have developed near the stress concentration. This would be expected to slow the crack at the shortest crack lengths and tend to act in opposition to any short crack anomaly. As can be seen from Fig.14 the limited data suggested that anomalies were present but not to the same extent as for Gaussian loading. Also the achieved crack rates were all slower than predicted, in marked contrast to the picture under Gaussian loading. Thus the local redistribution of stresses could explain the differences in behaviour under the two variable amplitude loading actions. However, more work will be necessary to verify this.

8. CONCLUSIONS

An experimental programme has been carried out to investigate short crack anomalies whereby short cracks propagate faster than long cracks at the same calculated stress intensity factor. Fatigue tests were carried out on notched 2L65 aluminium alloy specimens under constant amplitude, Gaussian random and FALSTAFF loading. Crack propagation measurements were taken down to crack lengths of 0.01mm using replicas. The following conclusions were drawn:

(1) Under constant amplitude loading short crack anomalies were identified positively at zero mean stress. For fully repeated loading however they were almost completely absent.

(2) Under Gaussian random loading marked anomalies were identified. A linear summation of constant amplitude crack rates predicted rates that were too slow at short crack lengths and too fast at longer crack lengths.

(3) It is suggested that the explanation for such anomalies is that at short crack lengths, cracks remain open below zero stress, due to the relatively large plastic zone. The effect is particularly marked under variable amplitude loading; high loads lower the crack closure stress and accelerate crack growth, in contrast to long crack behaviour.

REFERENCES

1 Airplane damage tolerance requirements. Military Specification MIL-A-83444 (USAF) (1974) 12-17

2 R.C. Rice, D. Broek. Evaluation of equivalent initial flaws for damage tolerance analysis. NADC-77250-30 (1978)

3 B.C. Fisher, F. Sherratt. A fracture mechanics analysis of fatigue crack growth data for short cracks. Fracture Mechanics in Engineering Practice, Applied Science Publishers (1977)

4 N.E. Frost, L.P. Pook, K. Denton. A fracture mechanics analysis of fatigue crack growth data for various materials. NEL/A2/1/69 (1969)

5 M.H. El Haddad, K.N. Smith, T.H. Topper. Fatigue crack propagation of small cracks. Trans. ASME Vol.101 (1979)

6 J.T. Barnaby, R. Holder. Fatigue from notches in cast steels. Metal Science 11, 5-10 (1977)

7 R. Cook, P.R. Edwards, R.F.W. Anstee. Crack propagation at short crack lengths under variable amplitude loading. Proc. ICAF Noordwijkerhout, Netherlands (1981)
Also RAE Technical Report 82038 (1982)

8 P.R. Edwards. A controller for random and constant amplitude loading on resonant and electrohydraulic fatigue machines. RAE Technical Report 72226 (1973)

9 Vera J. Pike, W.T. Kirkby. Prediction of crack growth in damage-tolerant design - a basic parametric study. R & M 3822 (1978)

10 Vera J. Pike, W.T. Kirkby. Influence of assumed crack growth pattern on damage-tolerance life prediction for corner cracks at holes. RAE Technical Report 80017 (1980)

11 I.S. Raju, J.C. Newman Jr. Stress intensity factors for corner cracks at the edge of a hole. NASA TM 78728 (1978)

12 S. Pearson. Initiation of fatigue cracks in commercial aluminium alloys and the subsequent propagation of very short cracks. RAE Technical Report 71209 (1971)

13 L.P. Pook. Various aspects of the fatigue damage threshold in mild steel. Proc. SEE Conference "Fatigue Testing and Design", London (1976)

14 R.C.J. Howland. On the stresses in the neighbourhood of a circular hole in a strip under tension. Phil.Trans. Royal Society, Vol.A229, P.50 (1930)

15 Several Authors. Description of a Fighter Aircraft loading standard for fatigue evaluation. Joint Report of NLR, IABG, LBF, F+W (1976)

16 M. Matsuiski, T. Endo. Fatigue of metals subjected to varying stress. Paper presented at the Kyushu District meeting of the JSME (1968)

17 J.R. Heath-Smith, Judy E. Aplin. The effect of an application of heat on the fatigue performance under random loading of a notched specimen of DTD 5014 (RR 58) material. RAE Technical Report 71209 (1971)

18 P. Truyens. Crack growth under variable loads in ships. Thesis, University of Gent (1976)

19 J. Schijve. Differences between the growth of small and large fatigue cracks. The relation to threshold K-values.

20 W. Elber. Fatigue crack propagation under random loading: an analysis considering crack closure. Paper presented to the 11th Conf. of the ICAF, Stockholm (1969)

21 W. Elber. Einfluss der plastischen Zone auf die Rissausbreitung unter Schwingbelastung Materialprufung 12, 189-192 (1970)

ACKNOWLEDGEMENT

The Authors would like to thank Vera Pike for deriving the stress intensity factor solution used in this Report.

TABLE 1

NOMINAL MECHANICAL PROPERTIES AND CHEMICAL COMPOSITION OF MATERIAL

Specification BS 2L65

MECHANICAL PROPERTIES

0.1% Proof Stress	U.T.S.	Elongation
MN/m^2	MN/m^2	%
371	432	8

CHEMICAL COMPOSITION

Cu	Mg	Si	Fe	Mn	Zn	Ni	Ti
0.32	0.66	0.77	0.30	0.73	0.04	0.04	0.03

Balance Aluminium

TABLE 2

CONSTANT AMPLITUDE TEST LIVES TO FAILURE

Results from Ref.7 (R=-1)

Spec.No.	Peak Net Surface Stress (MNm^{-2})	Life (cycles)
35	147	5.56^{5}
27	184	1.36^{5}
25	184	2.28^{5}
34	129	8.94^{5}
29	165	1.64^{5}
30	147	1.92^{5}
28	184	1.24^{5}
26	221	7.52^{4}
31	129	3.53^{5}
24	184	6.90^{5}

Results of Strain Gauged Tests (R=-1)

Spec.No.	Peak Net Surface Stress (MNm^{-2})	Life (cycles)
WO817	147	3.67^{5}
WO815	147	4.16^{5}
WO901	184	1.18^{5}
WO814	147	3.73^{5}

Results of R=O Tests

Spec.No.	Peak Net Surface Stress (MNm^{-2})	Life (cycles)
WO803	184	6.91^{4}
WO205	184	1.29^{5}
WO103	184	1.05^{5}

Results of R=O (Half Rig)

Spec.No.	Peak Net Surface Stress (MNm^{-2})	Life (cycles)
WO907	156	1.90^{5}
WO818	156	1.81^{5}
WO710	193	1.31^{5}
WO908	193	1.12^{5}
WO915	193	1.33^{5}
WO905	136	3.21^{5}
WO910	156	1.85^{5}

Results of Tests with Stress Relief (R=-1)

Spec.No.	Peak Net Surface Stress (MNm^{-2})	Life (cycles)
P1	184	1.81^{5}
P2	147	2.24^{5}
P3	147	3.78^{5}

TABLE 3

VARIABLE AMPLITUDE TEST LIVES TO FAILURE (REF.7)

Gaussian Narrow Band Random Loading (R=-1)

Spec.No.	RMS Net Surface Stress (MNm^{-2})	Life (cycles)
39	65	7.22^{5}
16	78	1.26^{6}
17	78	8.70^{5}
42	85	2.52^{5}
38	91	2.12^{5}
22	91	1.94^{5}
20	91	2.46^{5}
19	91	2.27^{5}
41	104	1.18^{5}

FALSTAFF Loading

Spec.No.	Peak Net Surface Stress (MNm^{-2})	Life (cycles)
7	390	7.96^{6}
8	390	5.53^{6}

Spectrum Effects on the Growth of Short Cracks

by

B. I. Sandor, D. A. Haas, and T. Ozakat
University of Wisconsin
Madison, Wisconsin 53706

Summary

Several phenomena are discussed concerning creep-fatigue effects on crack initiation and propagation in notched 7075-T651 aluminum at room temperature. Background data show complete creep ruptures of smooth specimens in a time of 10^6 s at stresses about equal to the yield strength. Creep rate under a constant load decreases in the first half of the life and increases in the second half. In notched specimens ($K_t = 4$) tensile overloads with hold times result in additional extensions of the fatigue life beyond that of brief overloads. Additional extensions in life are 33%, 44% and 55%, for 100% initial overloads with hold times of 10^2 s, 10^3 s and 10^4 s, respectively. In specimens with part-through short cracks, the overload causes no crack extension, and it temporarily decreases the fatigue crack propagation rate. In specimens with through short cracks, the overload causes a distinct tunneling rupture during hold times of 100 s and 500 s, and a temporary retardation of the fatigue crack propagation rate.

Introduction

In this paper several phenomena are discussed concerning creep-fatigue effects on crack initiation and propagation in notched 7075-T651 aluminum at room temperature. Simple loading spectra involving overloads and hold times are used in the experiments. It is well known that overloads can alter the fatigue life of a notched member because of residual stresses generated in the plastic zone. Overloads with hold times have received little attention, in part because the possibility of creep in structural metals at room temperature is commonly ignored. However, such creep may occur altering the service life of a member.

Carroll (1) investigated the behavior of notched 7075-T651 aluminum plates, applying overloads, or overload-underload combinations, or sustained underload hold period immediately following the overload-underload combination. He found that the sustained underload hold periods shortened the fatigue life, and concluded that a hold period in any combination with an overload or underload would affect the residual stress (by creep and stress relaxation) in the plastic zone. McGee and Hsu (2) investigated crack growth in notched 2219-T851 aluminum plates, applying overloads, underloads, overload-underload combinations, and hold times at either overloads or underloads. They concluded that the underloads following overloads would decrease the retardation effect of the overloads, that underloads preceding overloads would have no effect, that hold periods in tension would increase the fatigue life, and that hold periods in compression would decrease the fatigue life.

The changes in fatigue life caused by hold times can be explained using the concept of localized creep strain. Freed and Sandor (3) determined that creep occurs in the plastic zones of notched steel and aluminum plates cyclically loaded with a mean stress at room temperature. The creep strain can be of the same order of magnitude as the cyclic plastic strains. In the case of an overload with hold time, there is a localized, time-dependent deformation which increases the residual stress upon unloading with respect to that of a brief overload.

Background information for the present investigation is obtained from monotonic tension tests of smooth specimens. The results are presented schematically in the first five figures which are based on extensive data provided by Freed and Duchon (4). In each specimen the longitudinal direction and loading axis coincide with the rolling direction of the plate. Figure 1 shows that the 7075-T651 alloy has a bilinear stress-strain curve with nearly flat-top yielding. On the average, yield and ultimate strengths are σ_y = 515 MPa and σ_u = 580 MPa, respectively. Quite unexpectedly, dilatation vs. true stress (Fig. 2) is also bilinear. This implies the existence of triaxial stresses in a uniaxially loaded notched member (caused by volume change differences), and it complicates future analytical work concerning notched members. Figure 3 shows two typical curves for creep at room temperature. Stress vs. time to fracture is sketched in Fig. 4. When the stress is slightly above the yield strength, the time to fracture is about 10^6 s (about 12 days). Fracture data at stresses below σ_y are not yet available, but several test results show that creep occurs at stresses as low as 207 MPa at 29°C (5). Creep rate vs. t and stress relaxation rate vs. t are shown in Fig. 5. It is remarkable that a long period of decreasing creep rate may lead to an increasing creep rate culminating in fracture.

Experiments with Notched Specimens

The plate specimens of 7075-T651 aluminum are 6.4 mm thick, 25 mm wide, and 64 mm long between grips. Each specimen has a circular notch on one side with a theoretical stress concentration factor of 4. All tests are performed at room temperature in an electro-hydraulic, servo-controlled testing system. Load control is used at a frequency of 20 Hz. Crack length measurements are made with an accuracy of ± 0.06 mm by microscopically observing the crack tip location against a reference grid on the specimen surface.

Several tests are performed to determine base-line crack propagation rates and fatigue life under constant amplitude loading, with limits of 2.2 kN and 18 kN, both in tension. The fatigue crack is first observed between 8000 and 15,000 cycles, and the average fatigue life is 22,000 cycles. A typical test is illustrated by curve A in Fig. 6.

13-2 A group of tests is performed with 100% tensile overloads (36 kN) applied initially as in Fig. 6. The hold time t_o ranges from 1 s (the time for loading and immediate unloading) to 10^4 s. The brief overloads (t_o = 1 s) extend the fatigue life by about six times (Figs. 6 and 7), which is an expectable result. Hold times ranging from 10^2 s to 10^4 s cause additional extensions of fatigue life as seen in Figs. 6 and 7. In Fig. 7 the overloads with brief hold time (t_o = 1 s) are used for reference data. There is considerable scatter in the results, but the averages are nearly on a straight line. The additional extensions in life are 33%, 44%, and 55%, for 100% overloads with hold times of 10^2 s, 10^3 s, and 10^4 s, respectively. This phenomenon is most likely caused by localized creep at the notch root during the held overload, resulting in an increased compressive residual stress upon unloading.

The effects of brief overloads applied in various sequences are shown in Fig. 8. Here Curve A from Fig. 6 is reproduced for comparison. Curve B indicates that an overload applied at about $N_{fA/2}$ is almost as beneficial as an initial overload if no cracks are present at the time of the overload. Curve C represents three different loading patterns as summarized in Table 1. C_1 is an average test with a single initial overload of t_o = 1 s (Fig. 7). C_2 is the same as C_1, with a second overload applied at $N'_{f/2}$ = 65,000 cycles, where N'_f is the approximate expected fatigue life with a brief initial tensile overload. The second overload seems to be ineffective even though the specimen is not cracked at $N'_{f/2}$. Ten identical overloads applied initially (curve C_3) are also ineffective in comparison with one initial overload. This is in contrast to the results of Hudson and Raju (6) who found a much greater delay in crack growth in the same metal for ten initial cycles than for a single one. The reason for the difference is not known; probably the size of the plastic zone is a significant parameter.

Compressive overloads are detrimental as expected. In Fig. 9 Curve A is again reproduced from Fig. 6 for comparison. Curve D shows that an initial compressive overload reduces the fatigue life but not drastically. Curves E and F show that tensile overloads applied at about $N''_{f/2}$ eliminate the harmful effect of the initial compressive overload. N''_f is the approximate expected fatigue life with a brief initial compressive overload. Note that part-through small cracks present in specimens E and F when the tensile overloads are applied (Table 1) cause no crack extension (Fig. 9).

Crack growth with tensile overloads applied to fatigue cracked specimens is illustrated in Fig. 10. Curves G and H are for specimens that have part-through short cracks when the overloads are applied. These cause no immediate crack extension, but a retardation in crack propagation rate (note that H shows rapid fatigue crack growth before the delayed propagation). There are through cracks present in specimens I and J when the overloads are applied. These cause a time dependent crack extension in the middle of each specimen but none on the surfaces. This tunneling is observed after final fracture (a sharply defined, dark gray area between the light gray fatigue fracture surfaces). The maximum central crack advance during the overload is about 0.3 mm for t_o = 100 s, and about 1.3 mm for t_o = 500 s. A similar tunneling rupture has been previously reported only for Gatorized IN-100, a nickel based superalloy (7). Remarkably, resumption of fatigue loading in specimens I and J causes rapid crack growth at first, followed by a retardation in crack propagation rate. The number of delay cycles is the same, about 14,000, for the four specimens in Fig. 10. Thus, noting the similarities in final crack propagation rates, the differences in fatigue lives are due to different crack initiation lives, not to crack shapes, crack lengths (within about 2 mm), and hold times. These results are similar to those for specimens E and F in Fig. 9 (10,000 delay cycles for combinations of compressive and tensile overloads). The extent of scatter in the experiments involving cracked specimens is not yet known.

In conclusion, a given tensile overload with hold time is not necessarily equally beneficial in all cases. Three situations are distinguished in this work: a) No crack; a 100% overload, with hold times up to 10^4 s investigated, is beneficial for a member with a round notch; b) Part-through short crack; the overload causes no crack extension, and it temporarily decreases the fatigue crack propagation rate; c) Through short crack; the overload causes a distinct tunneling rupture during hold times of 100 s and 500 s, and a temporary retardation of the fatigue crack propagation rate. Work continues to investigate these phenomena.

References

1. Carroll, J. R., Jr., "Time Dependent Changes in Notch Stress/Notch Strain and Their Effects on Crack Initiation," Effect of Load Spectrum Variables on Fatigue Crack Initiation and Propagation, ASTM STP 714, 1980, pp. 24-40.

2. McGee, W. M. and Hsu, T. M., USAF Flight Dynamics Lab., "Effects of Underloads on Fatigue Crack Growth; Technical Summary," March 1977, Report No. AFFDL-TR-77-2, Vol. 1.

3. Freed, A. D. and Sandor, B. I., "Localised Time-Dependent and Cycle-Dependent Creep in Notched Plates," Gittus, J., ed., Cavities and Cracks in Creep and Fatigue, London: Applied Science Publishers, 1981, pp. 89-107.

4. Freed, A. D. and Duchon, D., University of Wisconsin-Madison, unpublished data.

5. Neulieb, R. L., USAF Flight Dynamics Lab., unpublished data (1975), communicated by Carroll, J. R., Jr., Lockheed-Georgia Company, 1981.

6. Hudson, C. M. and Raju, K. N., NASA Langley Research Center, "Investigation of Fatigue Crack Growth Under Simple Variable Amplitude Loading," March 1970, Report No. NASA TN D-5702.

7. Macha, D. E., Grandt, A. F., Jr. and Wicks, B. J., "Effects of Gas Turbine Engine Load Spectrum Variables on Crack Propagation," Effect of Load Spectrum Variables on Fatigue Crack Initiation and Propagation, ASTM STP 714, 1980, pp. 108-127.

Table 1

Curve	Loading	a Crack length before overload (mm)	N_f Fatigue life (cycles)
A	constant amplitude	-	22,000
B	T overload @ N = 11,000	0	102,400
C	C_1: T OL initially	0	128,100
(represents	C_2: T OL initially	0	
three	T OL @ N = 65,000	0	129,400
tests)	C_3: 10 cycles of T OL initially	0	129,700
D	C OL initially	0	14,100
E	C OL initially,	0	
	T OL @ N = 7000	0.38 (part-through crack)	20,500
F	C OL initially,	0	
	T OL (t_o = 100 s) @ N = 8500	crack at notch center	23,400
G	T OL @ N = 25,000	0.32 (part-through crack)	52,100
H	T OL @ N = 14,500 t_o = 1000 s	0.25 (part-through crack)	40,700
I	T OL @ N = 9000 t_o = 100 s	1.4 (through crack)	33,000
J	T OL @ N = 9500 t_o = 500 s	0.25 (through crack)	33,400

Notes: For any test, a = 2.2 kN, b = 18 kN, c = 36 kN,
T = tension, C = compression, N = cycles,
OL = overload, t_o = 1 s unless otherwise noted

Acknowledgment
This investigation was partially supported by Lockheed-Georgia Company.

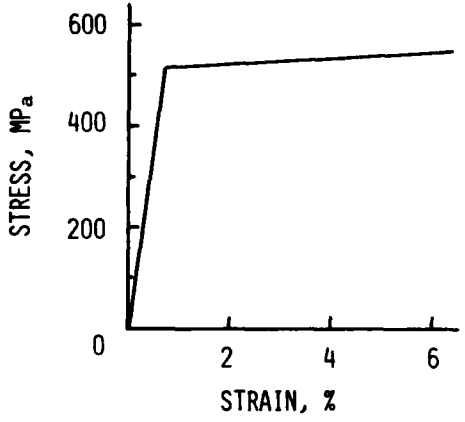

FIG. 1 STRESS-STRAIN CURVE OF 7075-T651 ALUMINUM

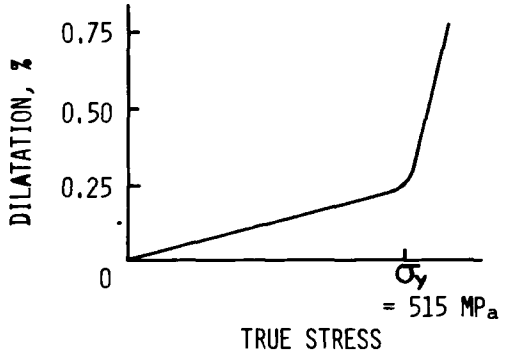

FIG. 2 DILATATION VS. TRUE STRESS

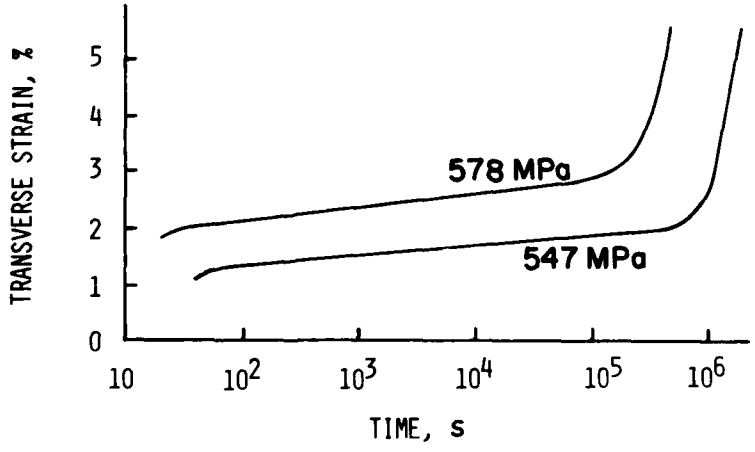

FIG. 3 CREEP CURVES

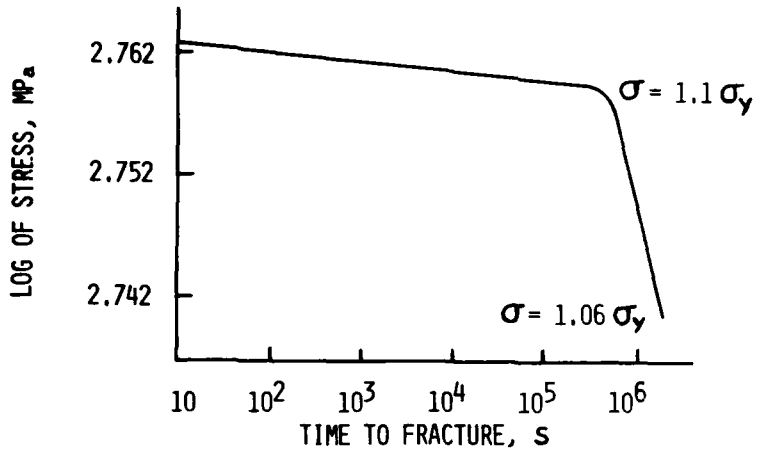

FIG. 4 CREEP RUPTURE TIMES

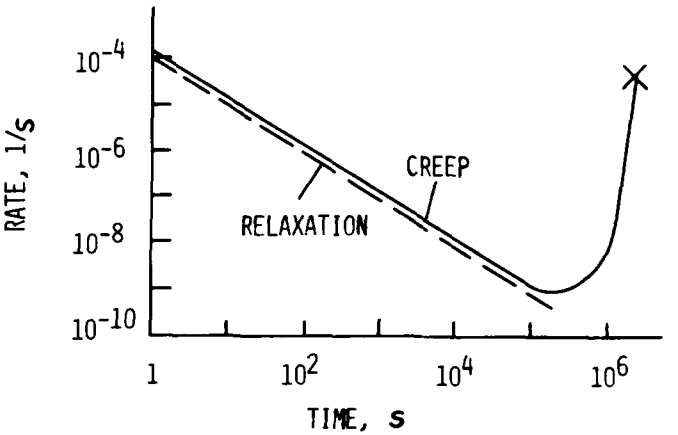

FIG. 5 CREEP AND STRESS RELAXATION RATES

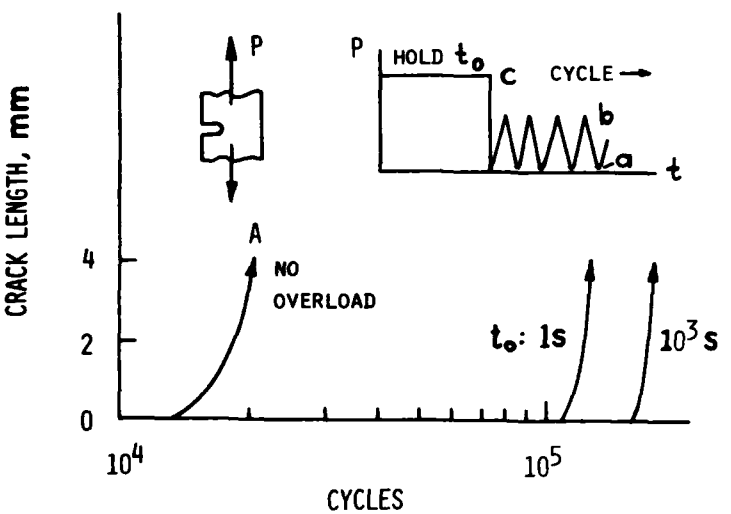

FIG. 6 CRACK PROPAGATION

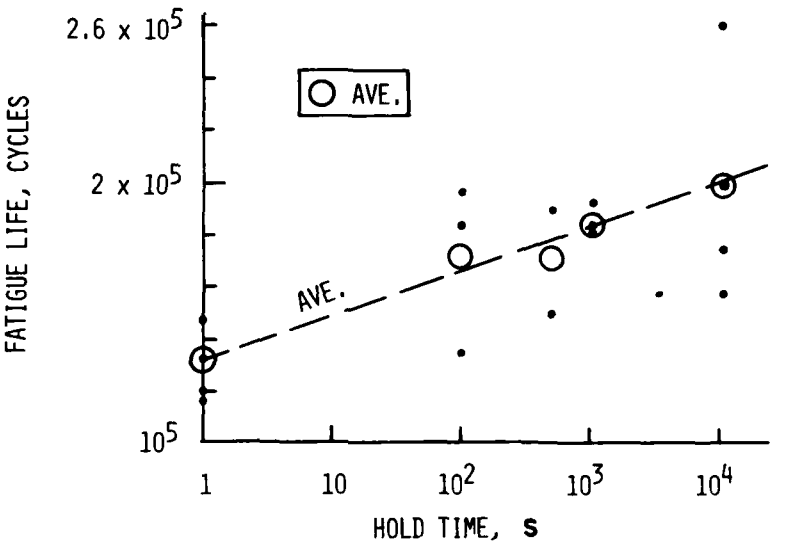

FIG. 7 FATIGUE LIVES WITH HOLD TIMES

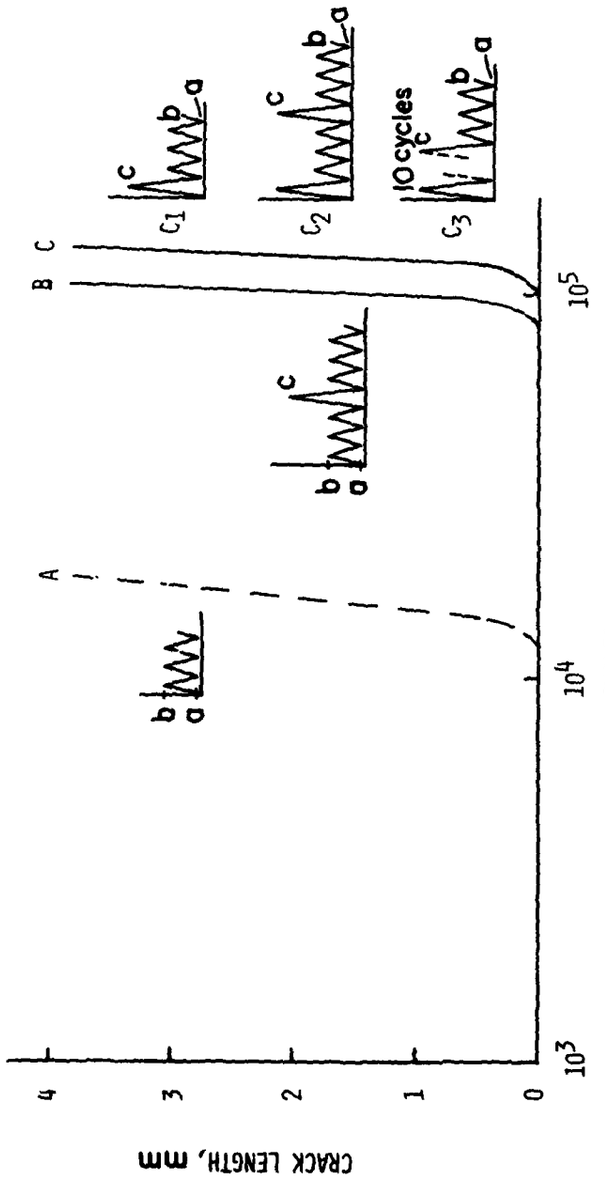

FIG. 8 CRACK GROWTH WITH MULTIPLE TENSILE OVERLOADS

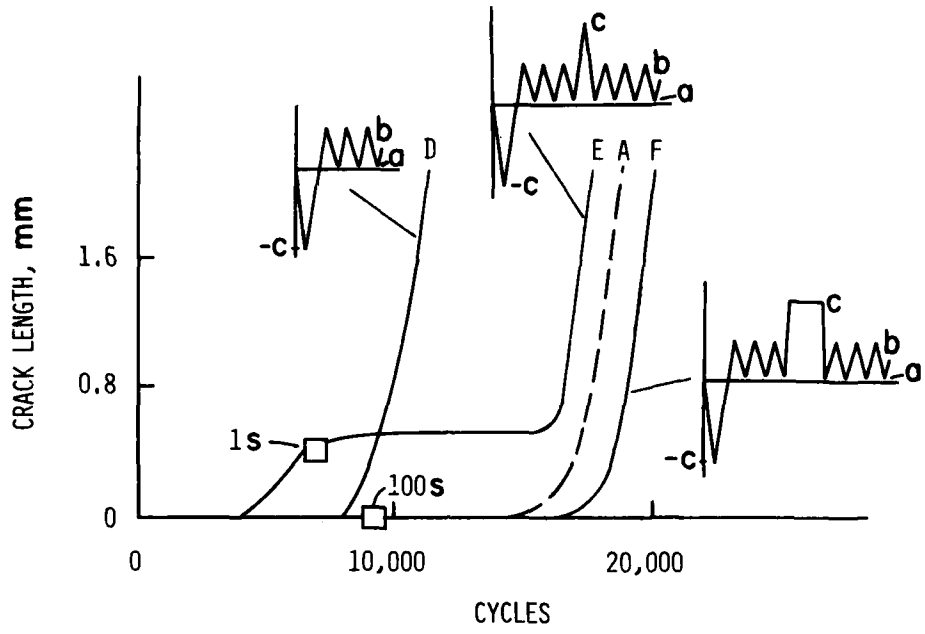

FIG. 9 CRACK GROWTH WITH INITIAL COMPRESSIVE OVERLOADS

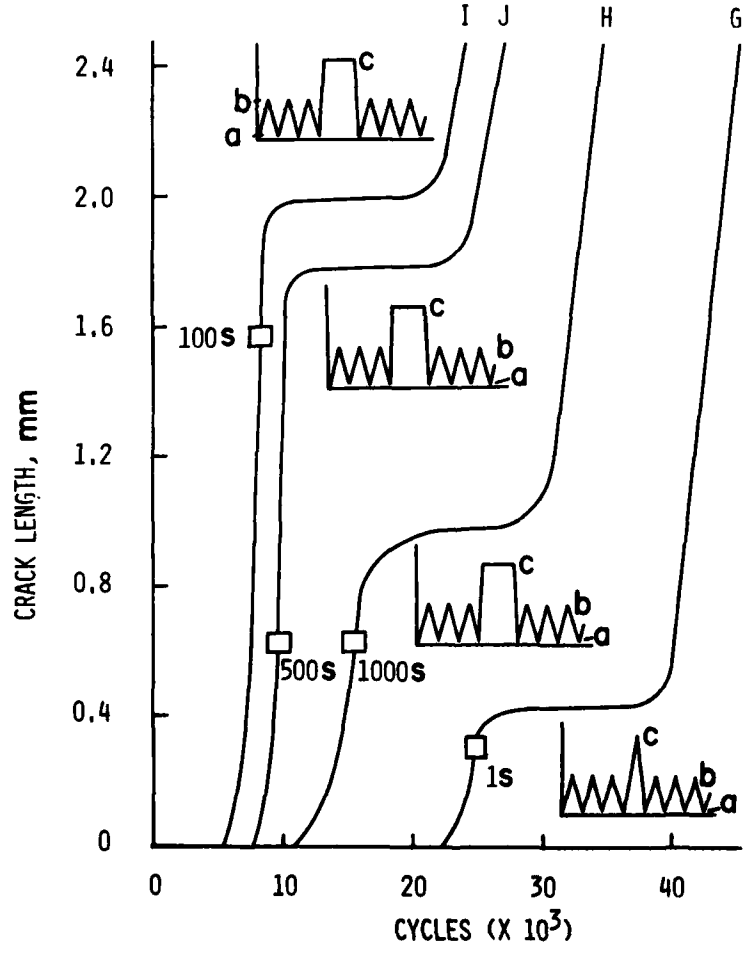

FIG. 10 CRACK GROWTH WITH TENSILE OVERLOADS

A STUDY OF SMALL CRACK GROWTH UNDER TRANSPORT SPECTRUM LOADING

14-1

by

D. Y. Wang

Douglas Aircraft Company
McDonnell Douglas Corporation
3855 Lakewood Blvd.
Long Beach, California 90846

SUMMARY

This paper describes a study of microcrack growth and statistical fatigue in terms of the initial quality of fastener holes in aluminum alloy. A special test procedure was used to obtain a statistically large sample of data under spectrum loading by testing a specimen containing 24 holes with maximum of 48 fatigue data sets. A total of seven specimens was tested. Small crack measurements were taken by fractography and surface observation. Marker cycles, which were designed to be part of the spectrum, served the intended purpose of identifying crack origin and microcrack growth rates using a scanning electron microscope. The phenomena of small crack growth have been analyzed from the extensive data. The essential physical defects in 2024-T3 and 7075-T6 aluminum alloys as origins of microfatigue cracking are the inclusions and tool marks.

INTRODUCTION

Analysis of fatigue crack propagation is utilized in the durability assessment of aircraft structure. A current specification, MIL-A-83444, requires that an equivalent initial flaw be assumed to exist in every fastener hole as a result of manufacturing and processing operations on material and structure. Damage tolerance requirements specify that small cracks of particular shape and length should not propagate to a critical size within the projected lifetime of a part. In practical cases, some failed airframe parts do show extensive crack growth during their service lives. Fairly rapid crack growth can be detected in the latter part of fatigue life. The small microcrack growth and the process of crack initiation occur during most of the fatigue life. Our understanding of small microcrack growth behavior is limited mainly because of the scale factor. The chance of finding a crack in a part increases with its size.

The range of a practical equivalent initial flaw size (EIFS) to be used for engineering analysis has been of great interest in the last several years. Several investigations have been conducted to define the statistical quantity of EIFS distribution in order to assess damage tolerance of military aircraft under the present military requirements (References 1 through 4). The general procedure for developing EIFS data consists of backward extrapolation of the crack growth curve to the zero cycle of loading. The experimental curves have been developed through regressive analysis of fractographic test data. However, it is not an easy task to obtain experimental crack growth curves to zero cycle from a non-precracked specimen. Instead, the experimental curves were correlated to the analytical curves, and the analytical curves were extrapolated to define the EIFS values.

It has been shown in the quality assessment in Reference 1 that EIFS values may be obtained through regressive analysis of experimental data only. In theory, EIFS should represent fastener hole surfaces of manufacturing quality independent of secondary variables, such as the types of load spectrum, stress level, material, and fastening system. These are the parameters that require further research.

The objective of this research is to investigate microcrack growth behavior and to assess EIFS distribution for production-quality fastener holes under a relatively long-life transport load spectrum. The statistical distribution has been established by using large quantities of test data developed in this investigation.

EXPERIMENTS

PROCEDURE

The test was conducted at Douglas Aircraft Company in a 100,000-pound (45,200 kg) MTS machine under uniaxial cyclic loadings. The loading was controlled by a computer preprogrammed for spectrum loads. Figure 1 shows the overall view of the test setup with specimen. A set of 0.5-in. (12.7 mm) steel plate buckling guides was clamped on both sides of the specimen to prevent buckling during the compressive ground load in spectrum.

The spectrum load tests were chosen for their representation of actual service loading conditions. The sequential loading characteristic also serves as a crack growth marker. The basic spectrum for the open hole specimens is a typical, simplified transport spectrum for a lower wing. A detailed description of the loads spectrum is presented in Reference 5 as the BS6.MISCG Spectrum. Figure 2 presents the loading profile of a flight, and Figure 3 shows the sequence of high peak loads in a repeat of the spectrum, which consisted of 3,843 flights. These high peak loads are arranged in such a way that the markers corresponding to the peaks are always identifiable in the fracture surface to the accumulated flight number.

The test specimens reported in this paper consist of the different configurations of 2024-T3 and 7075-T6 aluminum alloy sheet. The descriptions are listed in Table 1. The fastener holes were fabricated in the Manufacturing department.

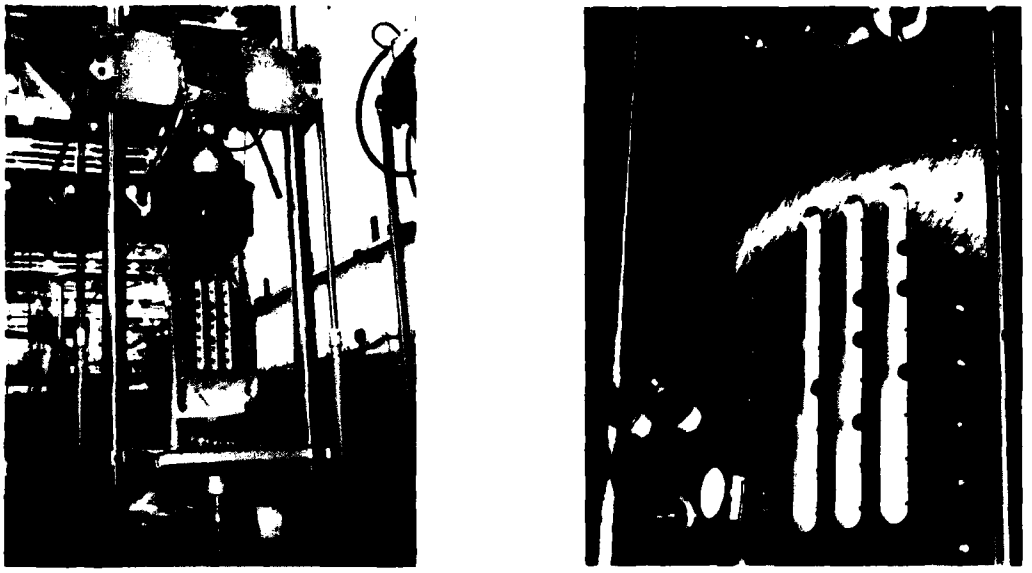

(a) (b)

FIGURE 1. SPECTRUM LOAD FATIGUE TEST SETUP FOR 24 MULTIPLE-DETAIL SPECIMENS

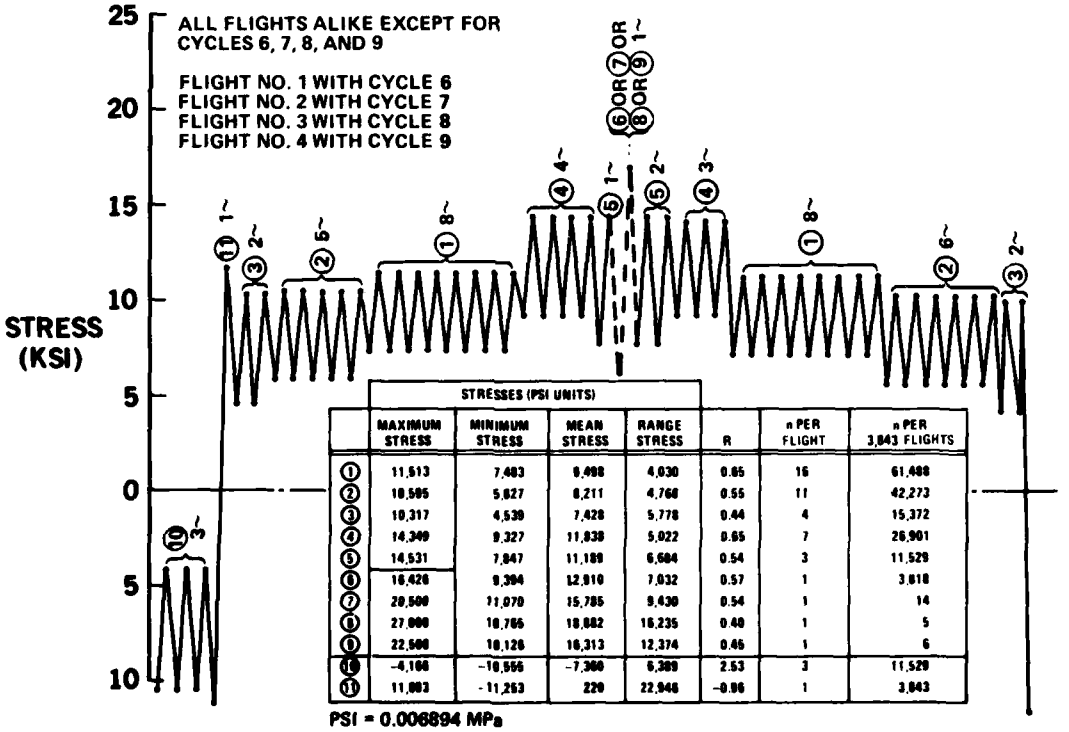

	STRESSES (PSI UNITS)						
	MAXIMUM STRESS	MINIMUM STRESS	MEAN STRESS	RANGE STRESS	R	n PER FLIGHT	n PER 3,843 FLIGHTS
①	11,513	7,483	9,498	4,030	0.65	16	61,488
②	10,595	5,627	8,211	4,768	0.55	11	42,273
③	10,317	4,539	7,428	5,778	0.44	4	15,372
④	14,349	9,327	11,838	5,022	0.65	7	26,901
⑤	14,531	7,847	11,189	6,684	0.54	3	11,529
⑥	16,428	9,394	12,910	7,032	0.57	1	3,818
⑦	20,500	11,070	15,785	9,430	0.54	1	14
⑧	27,000	18,765	18,882	18,235	0.40	1	5
⑨	22,500	10,126	16,313	12,374	0.45	1	6
⑩	-4,166	-10,556	-7,360	6,389	2.53	3	11,529
⑪	11,083	-11,263	220	22,946	-0.96	1	3,843

PSI = 0.006894 MPa

FIGURE 2. FLIGHT-BY-FLIGHT TEST SPECTRUM

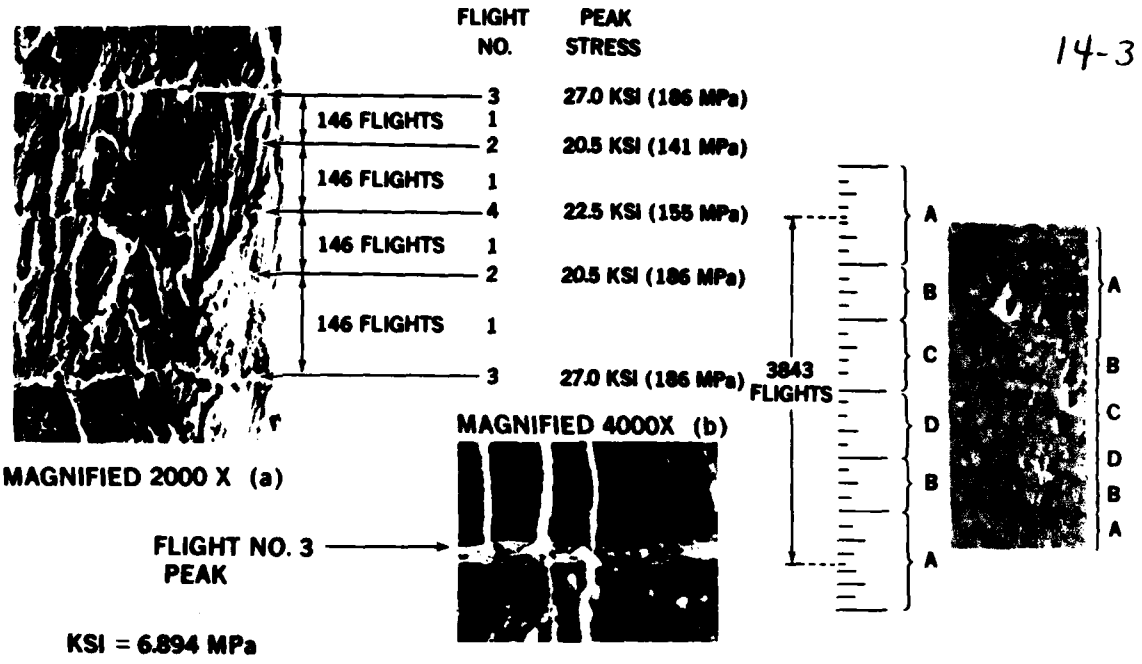

FIGURE 3. SEQUENCE OF APPLIED MARKER CYCLES AND EXAMPLE OF CORRESPONDING MARKERS ON A FRACTURE SURFACE

TABLE 1
STATISTICAL FATIGUE LIFE DISTRIBUTION IN OPEN HOLES AND HOLES WITH CLEARANCE FIT SCREWS IN 2024-T3 AND 7075-T6

SPECIMEN DESCRIPTION	NO. OF CRACKS	TOTAL FLIGHTS TO 0.10-IN. CRACK		LIFE IN MACROCRACK GROWTH FROM 0.010 TO 0.10 IN.		PERCENT OF LIFE IN MICROCRACK (a < 0.010 IN.) GROWTH INCLUDING CRACK INITIATION ± 1σ
		MEAN	ST DEV	(FLIGHTS)	(PERCENT OF TOTAL)	
0.071 IN. 2024-T3 COUNTERSINK OPEN HOLES	48	42,979	5,401	25,000	52 TO 67	33 TO 48
0.250 IN. 2024-T3 COUNTERSINK OPEN HOLES	96	48,000	7,998	20,000	32 TO 55	45 TO 68
0.250 IN. 2024-T3 COUNTERSINK HOLES WITH CLEARANCE FIT SCREWS	42	207,286	54,379	45,000	17 TO 29	69 TO 83
0.250 IN. 2024-T3 STRAIGHT OPEN HOLES	91	77,000	23,760	20,000	18 TO 41	59 TO 82
0.250 IN. 7075-T6 COUNTERSINK OPEN HOLES	42	48,619	19,638	5,000	7 TO 17	83 TO 93

0.010 IN. = 0.254 mm 0.250 IN. = 6.35 mm
0.100 IN. = 2.54 mm 0.071 IN. = 1.80 mm

A 24-detail, multiple-hole, 9- by 48-in. (23 by 122 cm) bow-tie specimen was selected for the test evaluation. Figure 4 shows an open-hole specimen and the tooling rig for drilling the multiple holes. Essentially, the identical 3/16-inch (4.76-mm) open holes are equally spaced in a three-column by eight-row configuration. This specimen design permits an identical stress level in each detail for a given applied load. This approach is aimed at achieving economy in a time-consuming transport spectrum load test; however, it requires a special test procedure.

Each detail was inspected periodically, the frequency depending on the length of the surface crack. Before any surface crack reached 0.050 in. (1.27 mm), the test was stopped at the end of each complete spectrum (3,843 flights) for inspection. After surface crack lengths of any hole exceeded 0.050 in. (1.27 mm), the inspection was performed at one-half or one-third of the spectrum. The inspection consisted of surveying the holes for surface cracks and recording the crack lengths using a pair of 30X stereo binoculars with a

14-4

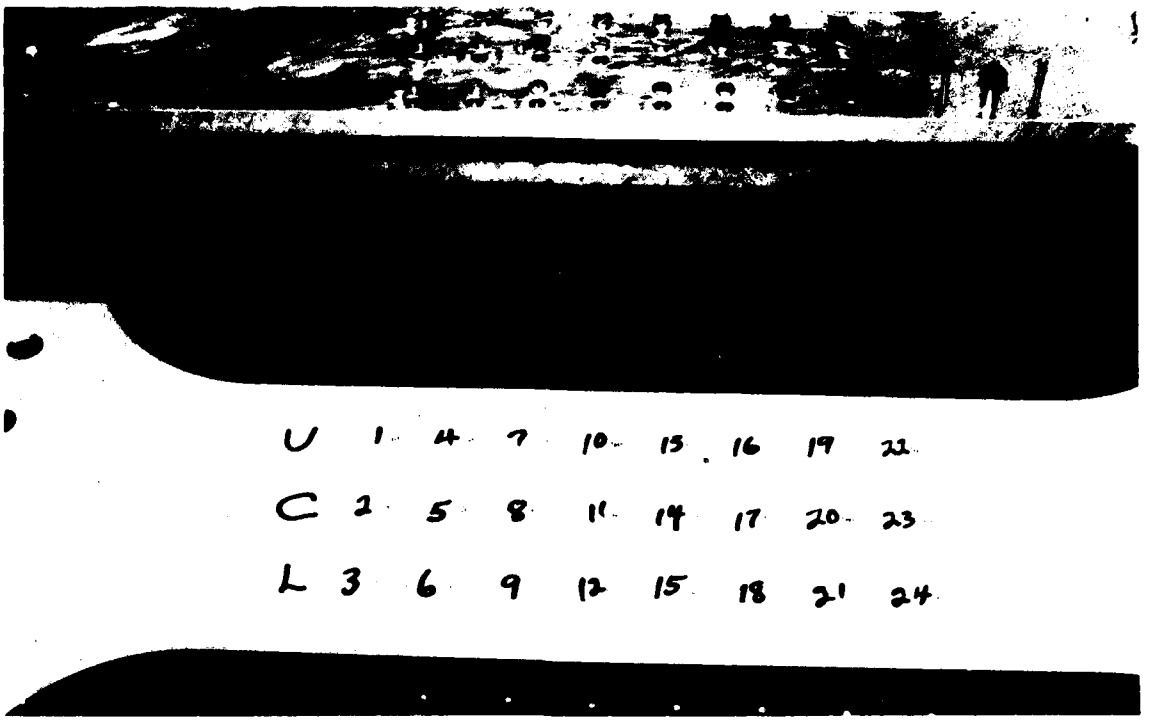

FIGURE 4. VIEW OF MULTIPLE-HOLE SPECIMEN AND THE TOOLING RIG FOR DRILLING THE HOLES

built-in scale such as shown in Figure 1(b). During the inspection, the specimen was under a positive static mean load to keep cracks open. Cracking usually occurred at the edge of the hole normal to the loading direction. A complete inspection of the 24 details required 96 discrete surveys, which included four per hole and two spots on each face.

A special procedure was developed to remove the cracked details when surface lengths exceeded 0.125 in. (3.18 mm). The procedure requires the use of a modified hole saw that makes a 0.75-in. (19 mm) cookie-shaped cut symmetrically about the center of the hole. Figure 5 illustrates a cookie-cut operation; Figure 6 shows a typical example of a cracked detail cut from the specimen. The 0.75-in. (19 mm) cookie-shaped hole in the specimen was then reamed to remove the rough surface and fitted with an interference fit plug to prevent cracking during further testing.

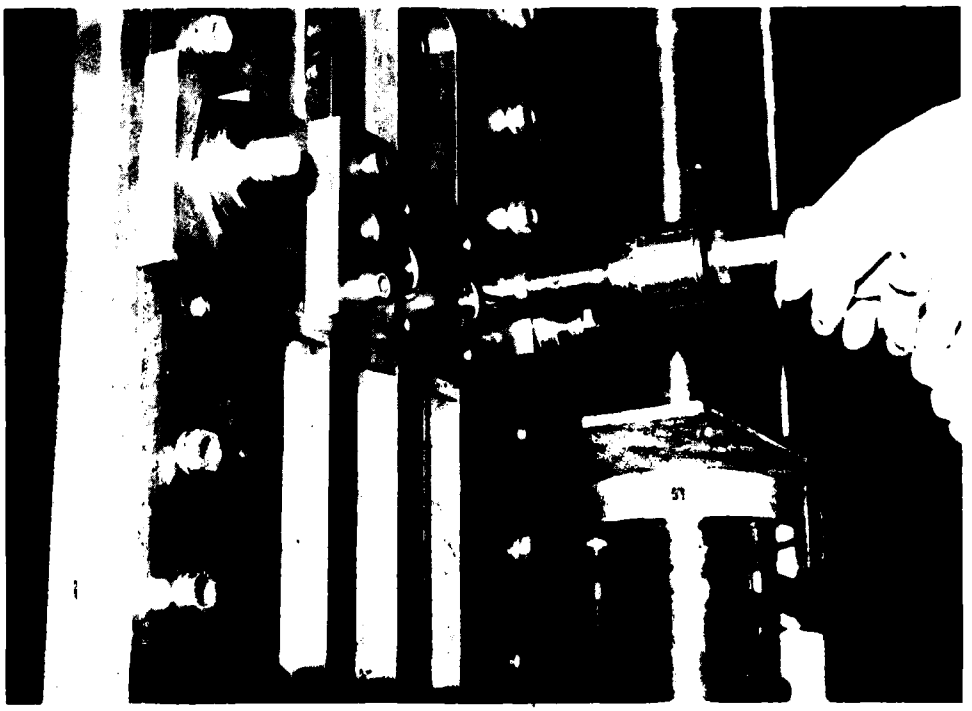

FIGURE 5. HOLE SAW OPERATION TO REMOVE A CRACKED DETAIL

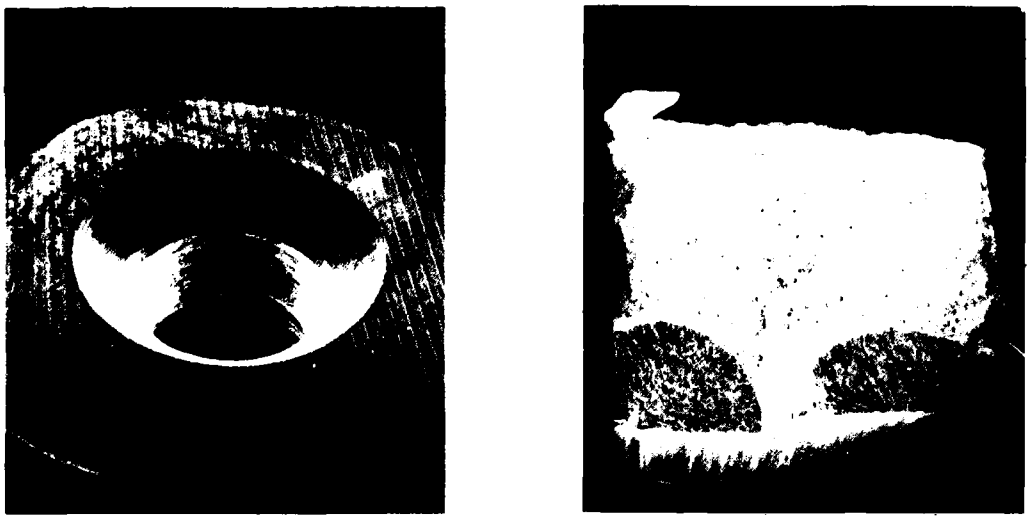

CRACKED HOLE CUT FROM SPECIMEN

FRACTURE SURFACE – SPLIT FROM CRACKED DETAIL

FIGURE 6. TYPICAL EXAMPLE OF CRACKED HOLE CUT FROM 2024-T3 SPECIMEN

RESULTS

FRACTOGRAPHIC DATA

In designing the spectrum load program, the marker cycles are built-in so that fatigue crack growth from the smallest scale may be identified in the fracture surfaces. The marker cycles that register identifiable markings on the fracture surface consist of repeatable infrequent high loads. Figure 3 shows a typical sequence of high peak stress and the corresponding markers on a fracture surface. The width of the striations resolvable under a scanning electron microscope is inversely proportional to the magnification up to a certain limit; i.e., a smaller width can be resolved only at a higher magnification.

In regions of very slow crack progression, only striations corresponding to the highest peak loads are resolvable. The markers provide a road map of the rate of crack growth in terms of the change in crack growth at a given interval of flights.

Fractographic observations provide two types of data, the rate of crack growth at various crack depths, and the pattern of crack progression from the origin of fatigue crack initiation. The physical origins of crack growth are particularly important from the standpoint of initial quality of the material and manufacturing process.

The identification of various types of common surface defects that result from the manufacture of the hole or from the combination of defects in the material with surface finish imperfections is an important part of defining fatigue quality. Some defects are more sensitive to fatigue cracking than others. Our approach is to examine the defects that are associated with cracking. This can be a byproduct of identifying the origin of the microcracks. The defects are observed along the bore of the hole at the edge of the fracture surface and the edge of the fracture plane where microcracks start and slowly grow (Figure 7).

The mechanical defects consist of various forms of tool marks. The material defects in 2024-T3 and 7075-T6 aluminum alloy are the insoluble constituent particles (inclusions). Some typical defects are described in Figures 7 through 10.

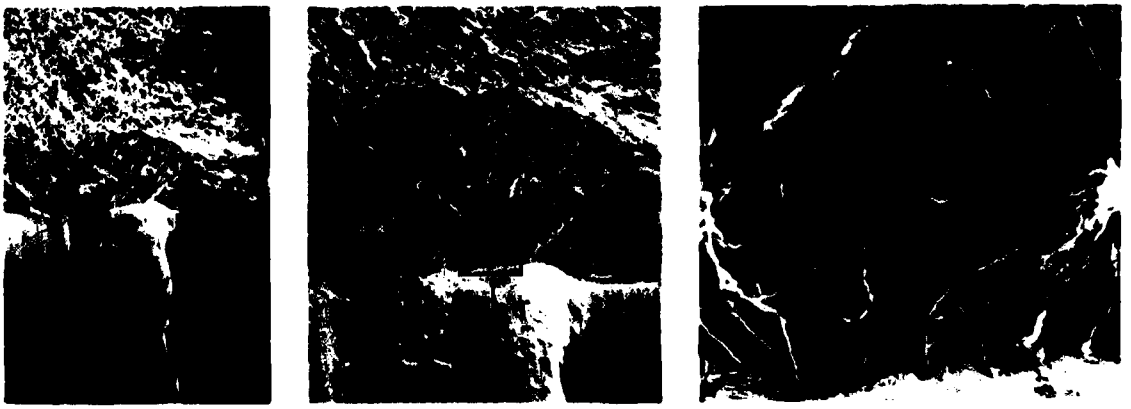

(a) 60 X (b) 150 X (c) 1500 X

FIGURE 7. PHOTOS SHOWING AN INTERCEPTING FATIGUE CRACK GROWTH PLANE AND SURFACE OF A HOLE CONTAINING A 0.010-INCH WIDE TOOL MARK

(a) 140 X (b) 200 X

FIGURE 8. CRACK ORIGINS AT TOOL MARKS

(a) 517-1-8E 120 X (b) 240 X

INTERFACE OF THE FOLDING TORN METAL AT THE CORNER OF DRILL EXIT CRACK GROWTH IN THE DIRECTION OF FRATURE TRACES

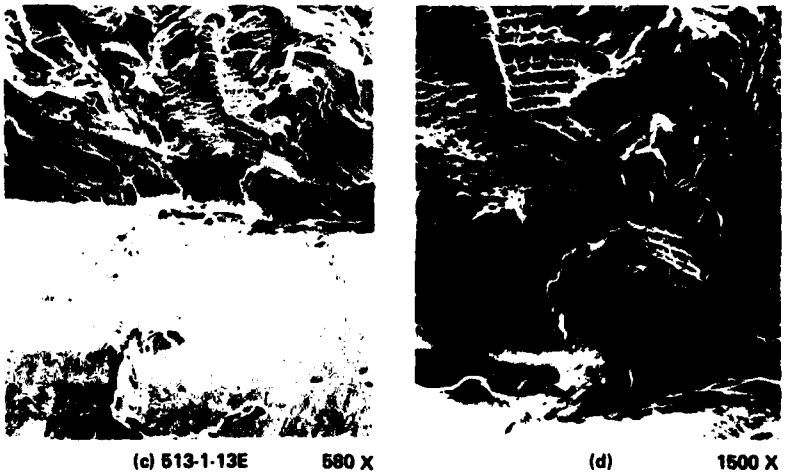

(c) 513-1-13E 580 X (d) 1500 X

VIEW OF INTERCEPTING HOLE SURFACE AND CRACK GROWTH PLANE AT AN INTERFACE OF TEAR/LAP FOLDING

FIGURE 9. VIEWS OF SOME FATIGUE CRACK ORIGINS

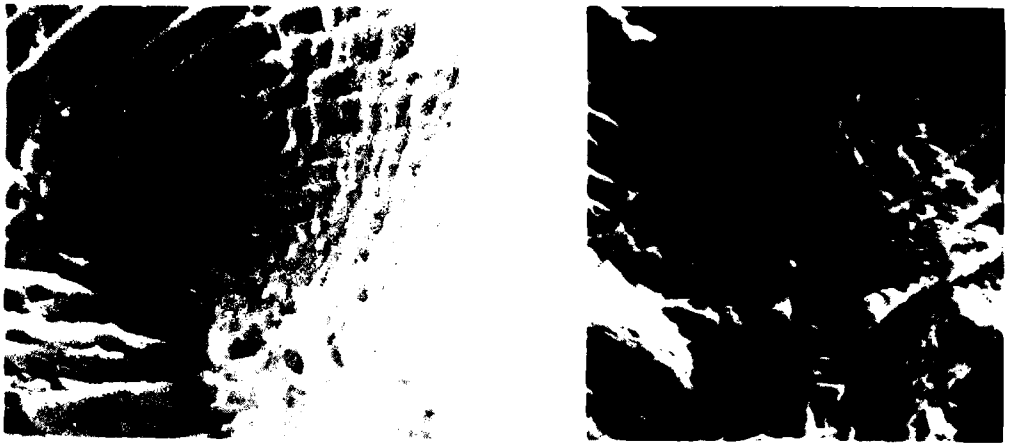

(a) 517-1-8W 2600 X (b) 513-1-13E 6000 X

FIGURE 10. FRACTURED INCLUSIONS AND MARKERS RINGED AROUND THEM CORRESPONDING TO VERY SLOW CRACK GROWTH

Figures 7 (a) and (b) illustrate a typical surface of a microfatigue crack of about 0.01-in. depth in a semicircular fan shape. The radiating lines, corresponding to folding lines of a fan, are "fracture traces." They are ridges on the fracture surface reflecting a change in elevations of local planes. These lines converge toward the origin of an expanding crack front. The marker cycles and striations observable under higher magnification are roughly normal to the fracture traces. Figure 7(c) shows the origin of microcrack growth from an intercepting hole surface and Figures 8 through 10 show some typical microcrack origins. An easily identifiable origin is an inclusion surrounded by rings of markers. In many cases, the inclusions cracked in a very brittle mode, as shown in the flat cleavage plane. However, many of the specimens surveyed do not contain well-defined markers at crack origins. The absence of the markers may have been a result of opposite surfaces rubbing against each other in subsequent cycling.

The rates of growth in microfatigue cracks, or cracks less than 0.01 in. (0.254 mm) long, were measured by counting the spacing of the marker cycles. These markers unequivocally represent crack growth under the highest peak load cycles. The distance between the markers was generated from crack growth of repetitive flights of the lower peak loads. The proof can be shown by matching the sequence of alternating marker spacing and the pattern of the high-load sequence in the spectrum (Figure 3). In the region of very slow crack growth at the origin, only the highest peak loads are resolvable under a high magnification. Nevertheless, the sequence of alternating spacings was similar, although on a smaller scale.

The microcrack growth curve may be derived from experimental data. Figure 11(b) shows a plot of microcrack growth versus the number of flights for a crack less than 0.0015 in. (0.038 mm) in length. Figure 11(a) shows the corresponding fractograph from which the marker cycle data were taken. In this case, it was quite easy to construct the growth curve by assuming that the surface of the bore, as the reference for the crack length, equaled zero, and that the interior edge of the inclusion at the first marker was the initial data point. As the crack grows away from its origin, the rate appears to increase exponentially. The markers are spaced further apart and become more difficult to locate then when they are situated closely together.

CRACK MEASUREMENTS

The crack growth rate measurements were taken by two methods, fractography and optical recording of the surface crack length during the test. The fractographic measurements were made only in the selected samples among various configurations of the specimens tested because of the time-consuming nature of the operation. Some of the results have already been presented in the preceding section. The surface crack length measurements of every crack were recorded during the tests.

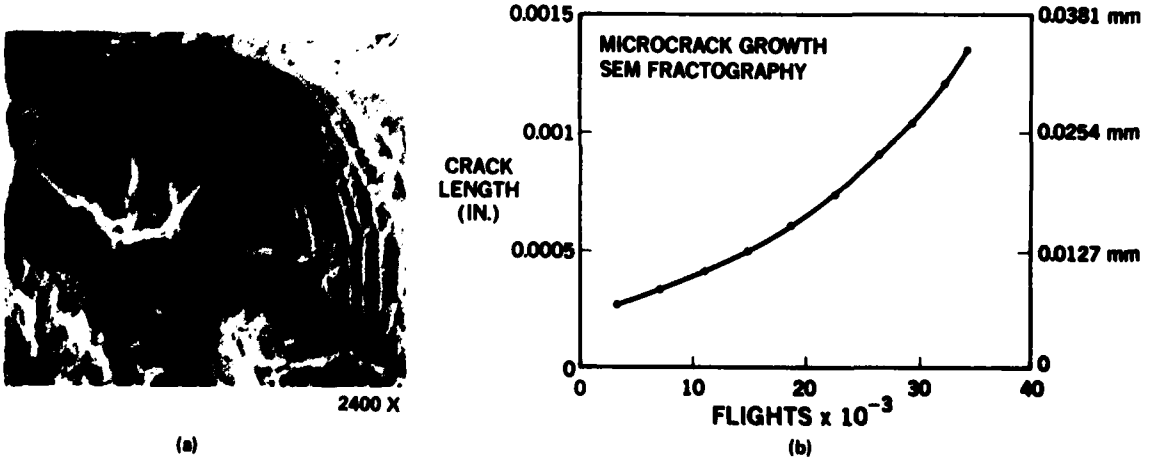

FIGURE 11. MICROCRACK GROWTH CURVE DERIVED FROM MEASURING MARKER SPACINGS IN A SEM FRACTOGRAPH

14-8

The full range of crack growth curves can and have been derived by fractographic means in a selected case, although this is time-consuming. Figure 12 shows the experimentally derived crack growth curves for a 7075-T6 open hole and a 2024-T3 filled hole starting at about 0.001 in. (0.0254 mm). These two curves have been constructed by integrating the representative growth rate shown on the fracture surface along the path of crack growth. Part of the fractographic records used to measure growth rates at some crack length is shown in Figures 13 and 14, respectively, for the above two curves. Several views of the fatigue fracture surface are shown at various

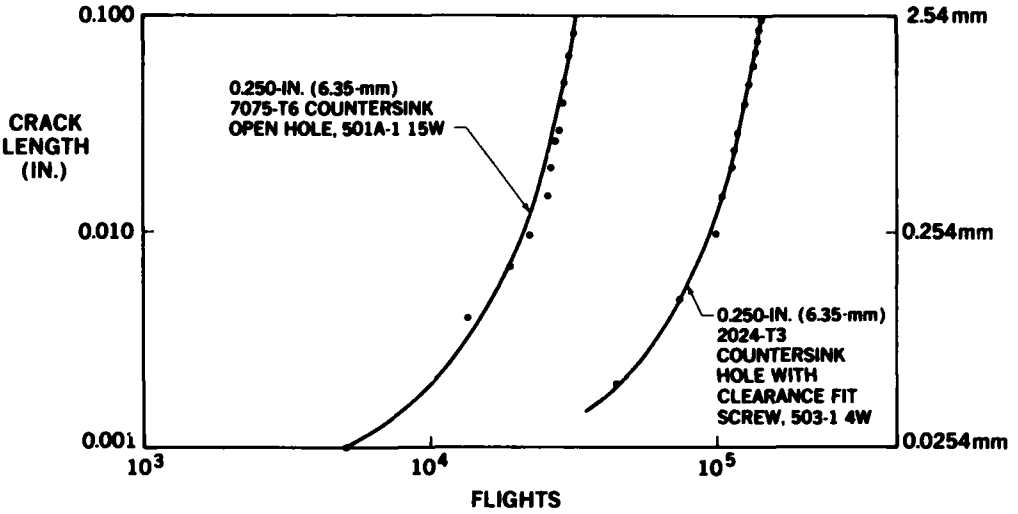

FIGURE 12. PLOTS OF CRACK GROWTH CURVES

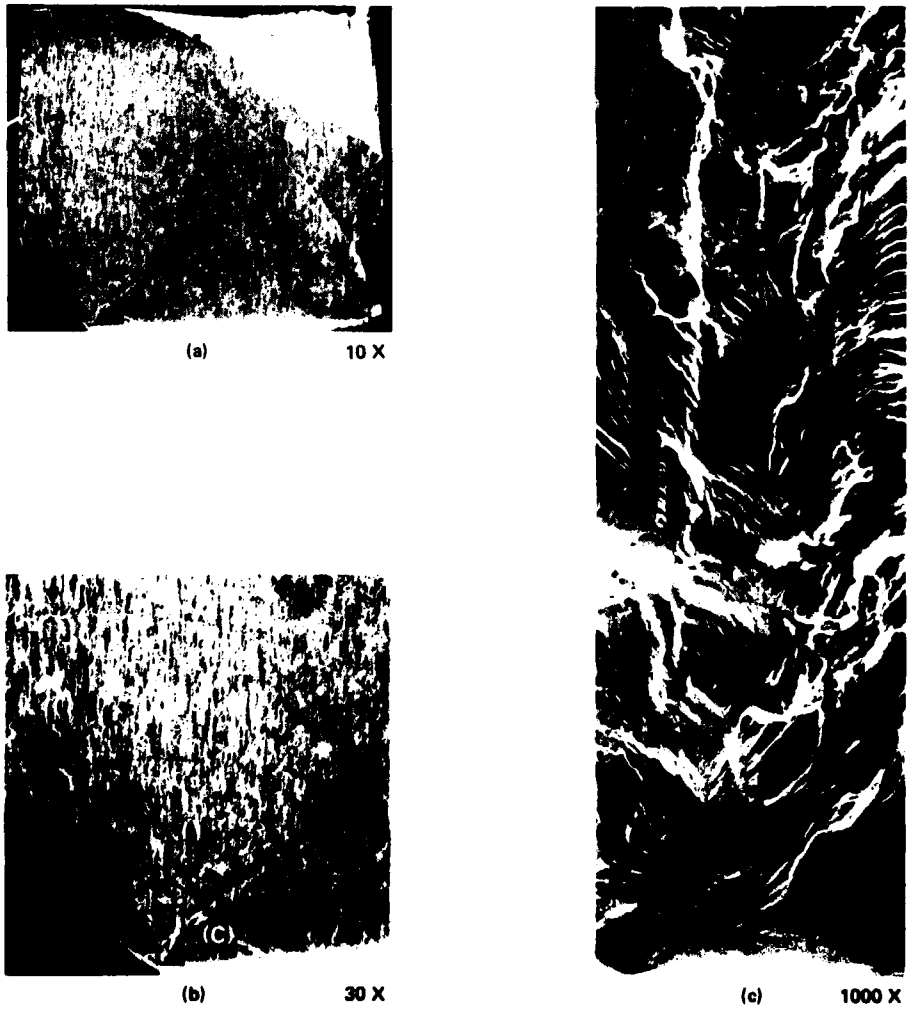

FIGURE 13. THREE-VIEW OF FATIGUE CRACK PLANE AND MARKERS FROM A CORNER ORIGIN IN A 0.250-IN. (6.35-mm) 7075-T6 COUNTERSINK OPEN HOLE

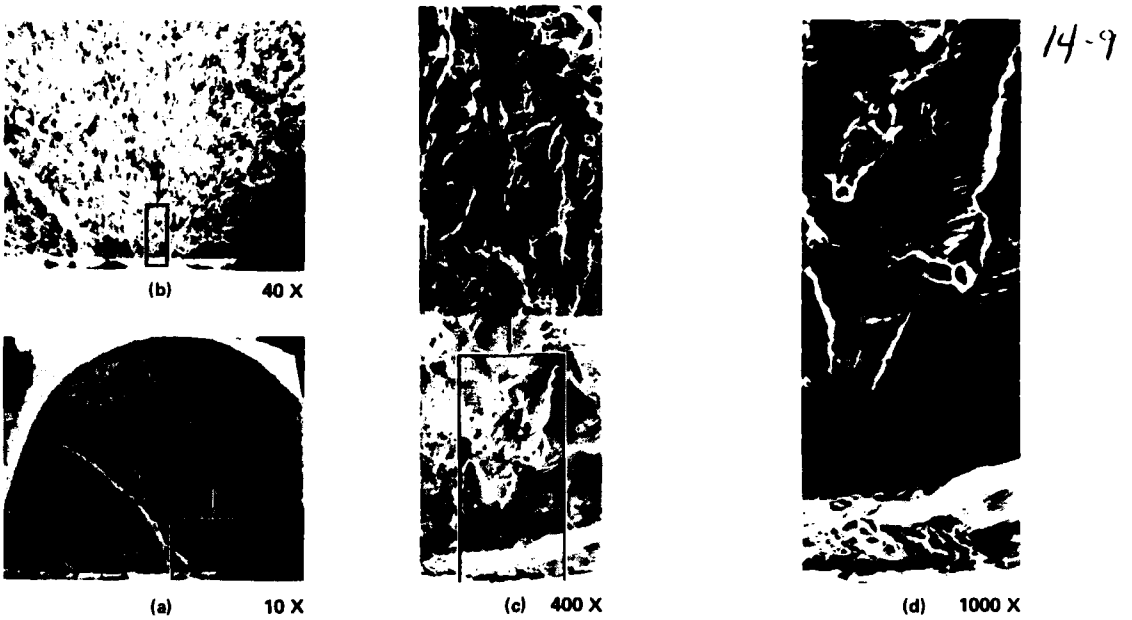

FIGURE 14. FOUR-VIEW OF A FATIGUE CRACK GROWTH PLANE AND MARKERS FROM AN ORIGIN IN A 0.250-IN. (6.35-mm) 2024-T3 COUNTERSINK HOLE WITH CLEARANCE FIT SCREW

magnifications in these figures to display the physical size of the crack. The low-magnification views show the overall crack shape and size, and the high-magnification views show the microcrack at the origin. Figure 15 shows the plots of crack growth per flight, $\Delta a/\Delta f$, along the maximum crack depth. These rates have been reduced from continuous series of fractographs of various magnifications where the distance between the interval of marker cycles for a given spectrum of flights was measured at various crack depths. The data show the rate of growth increasing with crack length on a log-log scale. Figure 16 shows the experimental crack growth curve for a 2024-T3 open hole crack obtained directly by counting the marker spacings along the path of the maximum crack length.

Quantitative surface crack growth data were recorded from surface measurements of each detail in every specimen, as discussed in the section on procedure. For convenience, any surface crack length readily measurable with a 30X binocular is defined as a macrocrack, roughly 0.010 in. (0.254 mm) and up. The separation of micro- from macrocrack growth is an arbitrary decision. The surface crack length rarely coincides with the maximum crack length in the interior except for the corner crack. The relationship depends on the shape of the crack front, which, in turn, depends on the locations of microcracks and the number of microcracks which develop into a dominant macrocrack front. Figure 17 shows a typical macrocrack progression pattern that was constructed by using the surface crack length data and a regressive count of the markers on the fracture surfaces along the path of the maximum crack length. The profile of

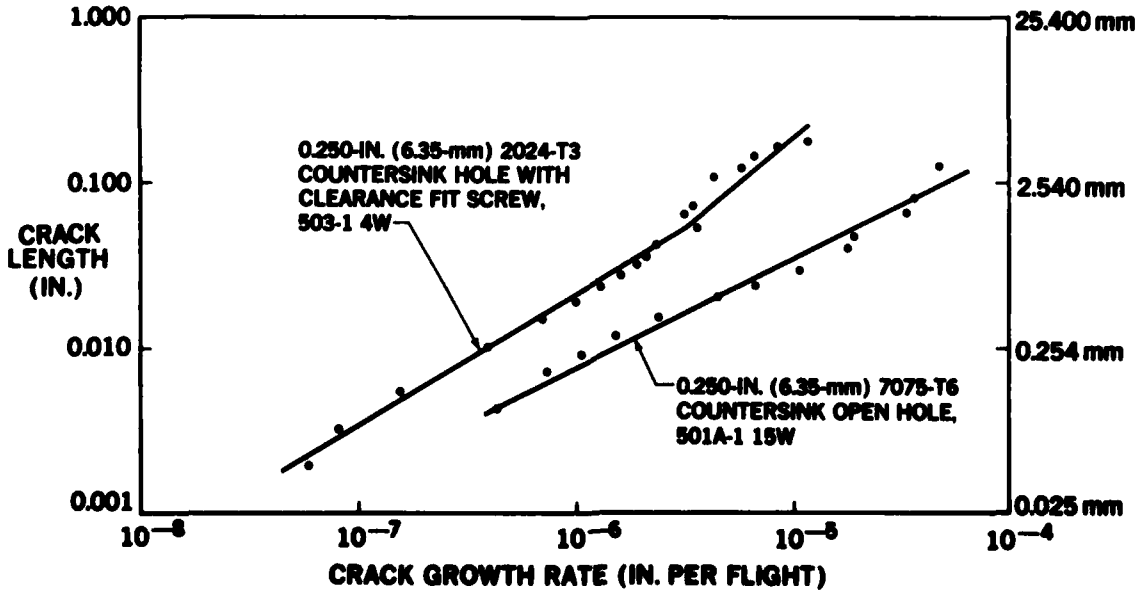

FIGURE 15. PLOTS OF CRACK GROWTH RATE VERSUS CRACK LENGTH

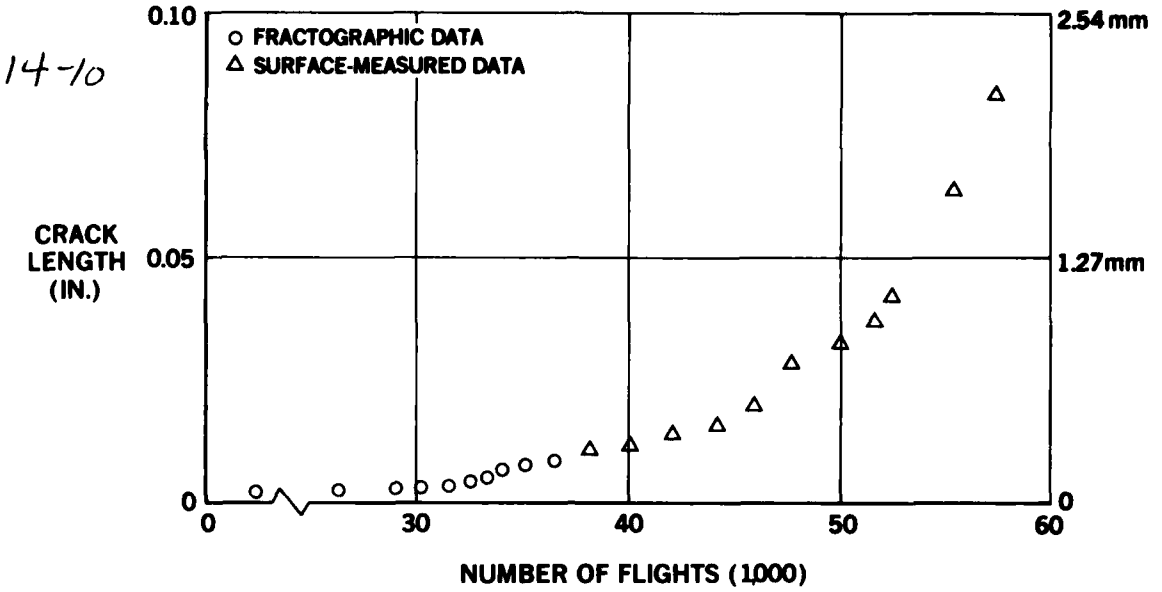

FIGURE 16. RESULTS OF COMBINED MICRO AND MACROCORNER CRACK GROWTH DATA FOR A COUNTERSINK HOLE SPECIMEN

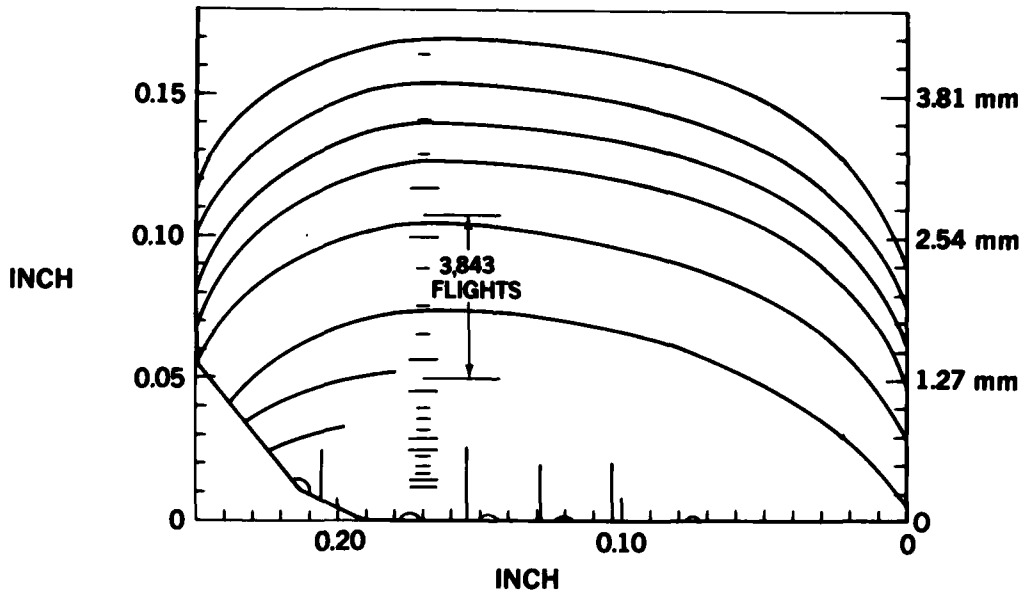

FIGURE 17. PLOT OF A TYPICAL INTERIOR MACROCRACK PROGRESSION PATTERN

the progressive crack front was constructed by connecting the front and back surfaces (both faces) of the crack lengths through appropriate marker locations at the particular flight number. The spacing of the profile lines does not represent the crack growth rate because it was not taken at a fixed interval of flight. However, the marker spacings shown do reflect crack growth under repeated sequences of spectrum loads (Figure 3). Figure 13 shows the fractographic view of a typical corner crack starting from the edge of a countersink open hole. The pattern of macrocrack progression markers is clearly defined. The surface crack length is almost equal to the maximum crack length.

STATISTICAL DATA

The statistical data of surface crack length at 0.1 in. (2.54 mm) were derived from raw data and were adjusted to normalize the results. Since the removal of the cracked hole is dictated by the first of the two possible cracks in a hole reaching 0.125 in. (3.18 mm) and the crack on the other side is small, the 0.10-in. (2.54 mm) crack life of the short crack is a projected value. The procedure involves adding the interval of macrocrack life from 0.010 to 0.10 in. (0.254 to 2.54 mm) to the short crack i.e., the interval is 20,000 flights for a corner crack in a 2024-T3 open hole. This interval of surface crack life is dependent on the crack shape. Therefore, each crack shape has to be identified. A detailed discussion on surface crack growth is presented in a later section on crack shape. Figure 18 shows a typical 0.010-in. (2.54 mm) crack life distribution in the form of a histogram.

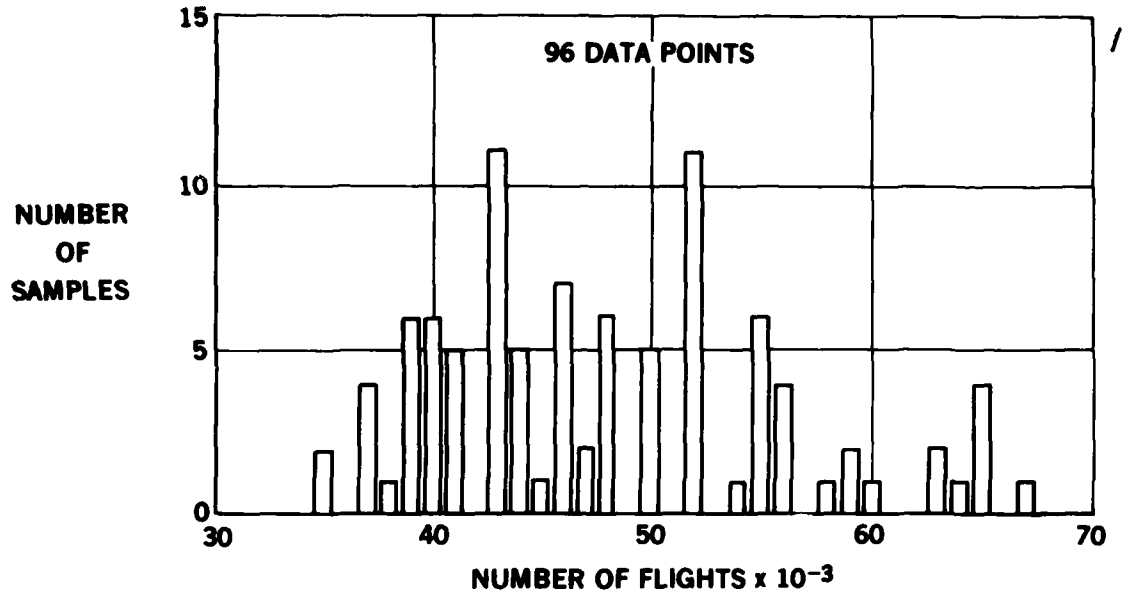

FIGURE 18. FATIGUE-LIFE DISTRIBUTION AT A 0.10-INCH (2.54-mm) SURFACE CRACK FOR OPEN-REAMED 3/16-INCH COUNTERSUNK HOLES IN 0.250-INCH (6.35-mm) 2024-T3

DISCUSSION

CRACK GROWTH

The crack initiation appears to take only a small fraction of the total life of the open hole or clearance-fit fastener-filled hole specimens. The full range of crack growth curves shown in Figure 12 correlates almost exactly with the total flights in the tests. These curves start at a very small crack length of about 0.001 in. (0.0254 mm). These results generally may apply to the other cracks in these types of fastener hole specimens. The markers are not easily identifiable in the early part of microcrack growth in many open hole specimens, probably as a result of repeated surface rubbing during compression cycles. The markers are better defined in the microcrack growth phase for fastener-filled holes than for the open holes because the fastener tends to prevent pressing on the cracked surface during compressive loading.

Under this type of spectrum loading, the microcrack growth rate increases continuously with crack length (or depth) from the small size, starting either in an inclusion or surface defects. The plots of increasing crack growth rate versus crack length are shown in Figure 15. This behavior is contrary to the finding of reducing rate under constant-amplitude loading in Reference 6. The only exception to this is in the data for a crack starting from a heavy burr at the drill exit side of the hole because of the residual stress field.

The local geometry around a microcrack appears to influence its growth rate. In Figure 19, the plots show the comparison of microcrack growth curves of different hole configurations in 2024-T3 material. The countersink increases the local stress concentration; therefore, the crack growth rate is faster in a countersink hole than in a straight hole. The knife edging effect of a countersink in 0.071-in.-(1.80 mm) thick specimen is amplified greatly in the crack growth rate. Along the bore of a hole in a 1/4-in.-(6.35 mm) thick material, the growth of microcracks starting at various locations such as those shown in Figure 17 does not seem to be different.

Crack Shape

Among all the fracture surfaces of the specimen surveyed, the cracking patterns (shapes) from fastener holes were of two general types, the corner crack and the interior crack. The corner crack emanates from one corner at either the drill entry or exit sides of the hole, such as shown in Figure 13. The interior crack originates in the microcrack locations (usually multiple origins), as shown in Figure 17. There are other types of crack shapes which are somewhat inbetween these two. For surface cracks, the maximum length of an interior crack is greater than the length of a corner crack. The measured crack growth rate is significantly faster for an interior crack than for a corner crack because of the difference in maximum crack length. Figure 20 shows the schematic of surface and maximum crack growth curves for corner and interior cracks. The figure indicates considerable scatter in the rate of crack growth in the surface-measured data. To use the surface crack growth data for analysis, it is necessary to identify the type of crack shape for that particular crack. Figure 21 shows a comparison of typical experimental surface crack growth curves for interior and corner crack types. In fact, surface crack growth life is quite consistent among the same type of cracks.

Effects of Hole Filling

The effect of hole filling is to reduce the crack growth rate drastically, especially in the microcrack range. The increased fatigue life is a result of a slower crack growth rate rather than slower crack initiation since full-range crack growth starting from a very small crack has been observed in the filled hole. In the presence of a clearance-fit screw in the 0.250-in.-(6.35 mm) thick 2024-T3 countersink hole, the mean total crack life increased by a factor of 4. The microcrack life increased by a factor of 5.46. The macrocrack life increased by a factor of more than 2. Table 1 shows the differences.

14-12

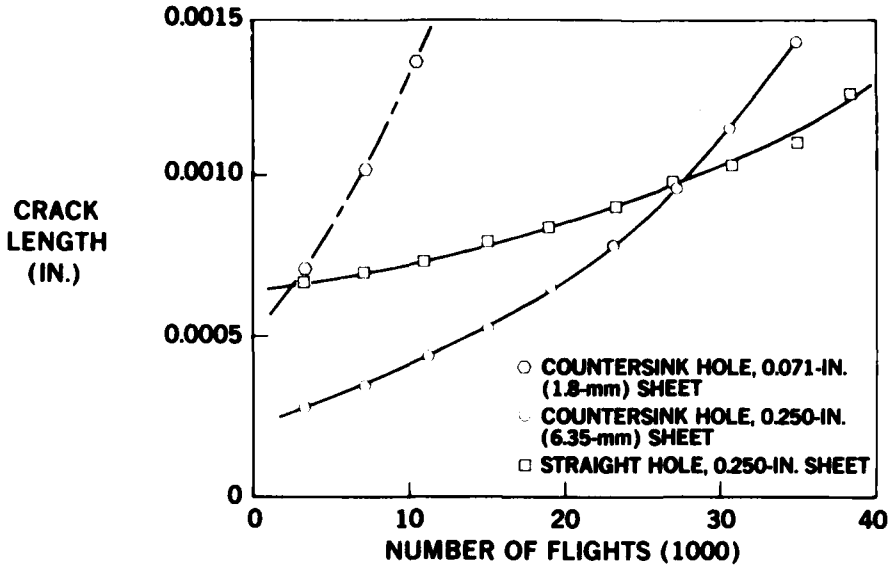

FIGURE 19. MICROCRACK GROWTH CURVES IN DIFFERENT HOLE CONFIGURATIONS AND MATERIAL THICKNESSES FOR 2024-T3

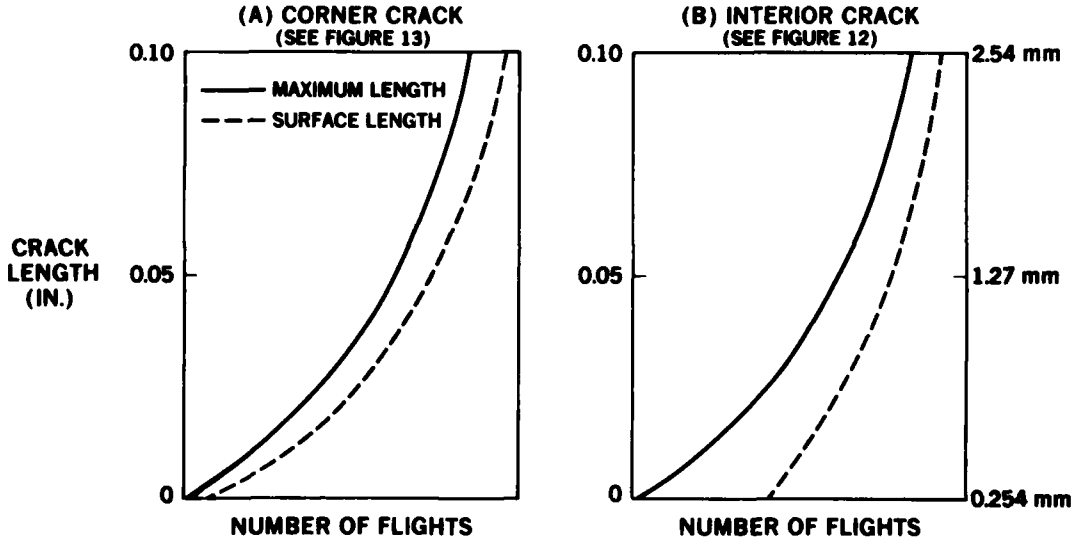

FIGURE 20. SCHEMATIC OF SURFACE AND MAXIMUM CRACK GROWTH CURVES FOR CORNER AND INTERIOR CRACKS

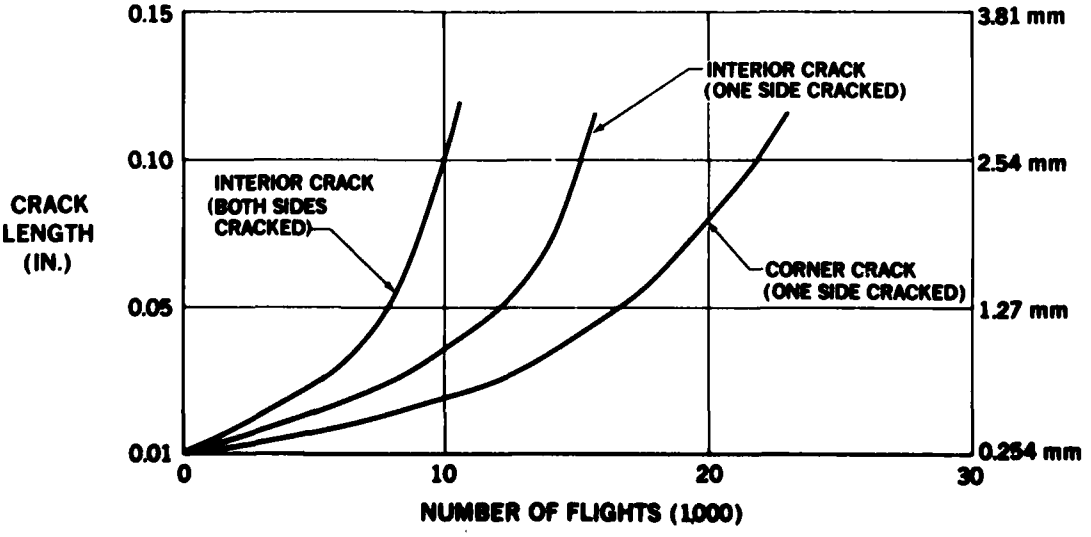

FIGURE 21. COMPARISON OF SURFACE-MEASURED CRACK GROWTH CURVES OF VARIOUS CRACK PROFILES FOR 0.250-INCH (6.35-mm) 2024-T3

One of the benefits of the fastener filling the hole is to prevent the crack from being subjected to spectrum compressive stresses. The range of the stress cycle is therefore smaller in the filled hole than in an open hole. This is substantiated indirectly from the experimental observations. The striation markers in the fracture surface of a filled hole, such as shown in Figure 14, are generally much better defined than those in an open hole because the fastener prevents the cracked surface from crushing. The fastener also restraints contraction of the hole due to Poisson's effect.

A number of specimens with rivet-filled holes and with interference-fit fasteners have been tested under the same spectrum as well as under a modified spectrum (30 percent higher stress than the basic one shown in Figure 2). None of these specimens developed any cracks after 100,000 flights except for the 0.071-in. (1.80 mm) specimens with rivets which developed a few cracks starting outside of the hole.

FATIGUE LIFE PREDICTION

The fatigue process of an open or clearance-fit fastener hole consists of; (1) the initiation of one or more microcracks; (2) growth of extremely small microcracks into macrocracks, and (3) growth of the dominant macrocrack to failure. If the initiation period is indeed negligible, as suggested by some experimental crack growth curves starting from an extremely small microcrack, then the fatigue life prediction may be handled by the crack growth analysis. The crack growth analysis is one form of durability analysis which predicts fatigue from crack growth only, starting from an equivalent initial flaw size.

Statistical Distribution

Fatigue life distribution may be analyzed by statistics in terms of the micro- and macrocrack growth period. The macrocrack growth life from 0.010 to 0.10 in. (0.254 to 2.54 mm) may be considered as a constant. The life of microcrack growth (where the crack length is less than 0.01 in.) is the principal variable in the scatter. The scatter is proportional to the percentage of life consisting of microcrack growth. Table 1 lists the statistical distribution of crack life for several configurations of open holes and one with clearance-fit screws. In one extreme, in the 0.071-in. (1.8 mm) 2024-T3 countersink open holes, the microcracks grow rather rapidly because of the knife edging effect of countersink in a thin sheet. The scatter is quite low, and the microcrack growth period is usually less than half of the total life. On the other extreme of high scatter, the 7075-T6 has a short macrocrack growth period, as low as 10 percent, because the macrocrack growth rate is much higher than in 2024-T3. The crack life of 0.250-in (6.35 mm) 2024-T3 countersink holes with clearance-fit screws has a longer microcrack growth period than the open holes in 2024-T3 because hole filling affects the microcrack growth rate more than in the macro range.

For a given material and hole configuration, the microcrack growth period depends on the initial size of the crack or physical defect and the rate of microcrack growth. A large starting crack will have a shorter microcrack growth period than a small starting crack. Therefore, the distribution of the defect size is partly responsible for the scatter in the total life. The other factor is the rate of microcrack growth in inverse proportion.

The microcrack growth curves do not correlate well with the analytical curves using existing linear-elastic fracture mechanics crack growth analysis models which correlate well in the macrocrack range i.e., where the crack length is greater than 0.05 in. (1.27 mm). The reasons for the discrepancy are beyond the scope of this paper. Instead, a typical crack growth has been experimentally derived for different hole configurations to evaluate fatigue life in terms of equivalent initial flaw size.

The master curve defines a complete crack growth relationship between crack lengths and the number of flights. This curve provides the reference between the data for crack length versus fatigue life to an equivalent initial flaw size. Figure 22 exhibits a composite master curve derived from the experimental results for the straight and countersink open holes in 0.250-in. (6.35 mm) 2024-T3. The curve consists of two parts, a microcrack ranging from the smallest practical length to 0.01 in. (0.254 mm), and a macrosurface corner crack starting from 0.01 in. to more than 0.10 in. The scale is expressed in reverse order, starting at zero flights for 0.10-in. crack length.

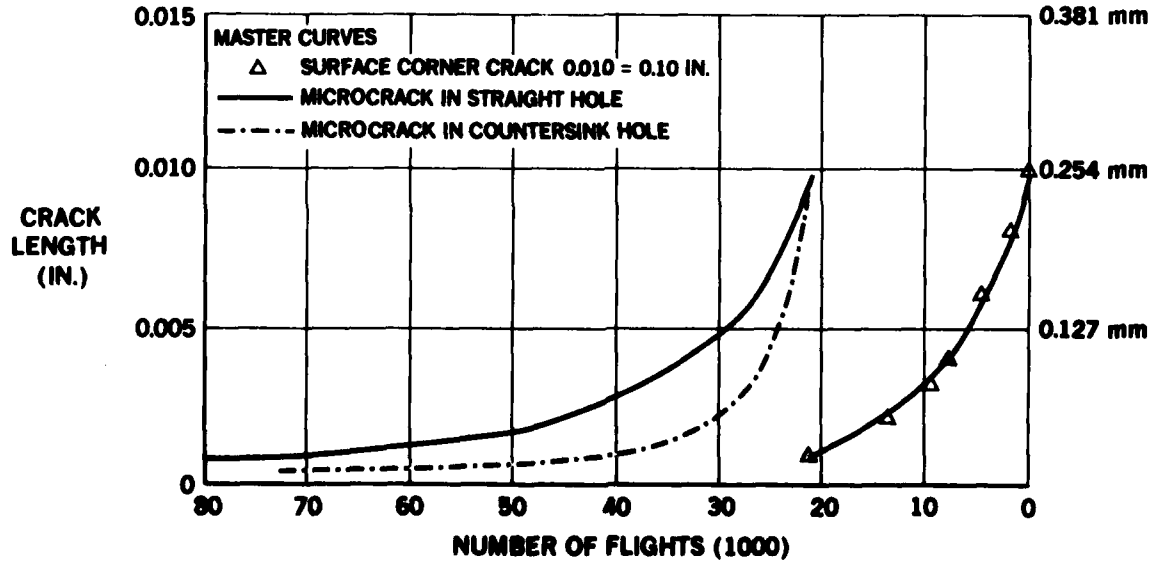

FIGURE 22. RELATION BETWEEN NUMBER OF FLIGHTS TO REACH A 0.10-INCH (2.54-mm) SURFACE CORNER CRACK IN STRAIGHT AND COUNTERSINK HOLES OF 0.250-INCH (6.35-mm) 2024-T3

The crack growth rate depends on the crack length, the crack shape, and the load spectrum. For a given crack shape under a particular load spectrum, the crack growth curve should be identical at any of the 24 details in a specimen. By isolating some secondary effects, the results of crack growth in both the micro- and macrorange were quite consistent. Figure 22 represents typical crack growth curves with no secondary effects. In Reference 3, the fastest growth curve was chosen as the master curve. In the microrange, the crack growth curve is influenced by the geometrical factors of a hole. The countersink increases the local stress concentration; therefore, the crack growth rate is faster in a countersink hole than in a straight hole. Figure 19 shows the typical microcrack growth curve for three hole configurations. In the macrocrack growth, the difference in rates among hole configurations is not the same as in microcrack growth. In 0.250-in.-(6.35 mm) thick specimens, the rate is essentially the same for a straight or countersink hole. Because of these characteristic differences, it is necessary to establish a master crack growth curve for a given material thickness and hole configuration combination.

Equivalent Initial Flaw Size

The concept of equivalent initial flaw size, or the equivalent crack length at zero life, may be used to define the fatigue property of a fastener hole. For a given spectrum loading, the fatigue life is inversely proportional to EIFS and consists of the growth of micro- and macrocracks. The master crack growth curve provides the relationship for transforming the normalized fatigue data to an expression in terms of EIFS. This procedure involves two assumptions: (1) the period for crack initiation is treated as equivalent to additional time to propagate a smaller original microcrack than one that does not involve crack initiation, and (2) EIFS is in the form of a singular microcrack that develops into one corner macrocrack since that was the basis of the master curve derived from experimental results.

In reality, many samples involve multiple microcrack and interior macrocrack shapes that result in a faster crack growth than the corner crack. In these cases, the assigned EIFS is a larger value than the physical size of the defect, as a compensation for slower crack growth of the singular corner crack.

Figure 23 shows the statistical distribution of EIFS for the countersink hole specimens in the form of a histogram. Figure 24 shows the comparison of the statistical cumulative probability plots of EIFS for straight and countersink holes, respectively. It would be noted that the mean EIFS value, $\bar{x}$, of the two groups is quite close, but the standard deviation is twice as great for the straight holes than for the countersink holes. This probably reflects a greater exposure area in the straight hole than in the countersink hole subjected to microcrack initiation.

CONCLUSIONS

1. The special test procedure using a 24-hole specimen to obtain a statistically large sample of data is workable.

2. Microcracks initiated in the open holes or the holes with clearance-fit screws have been shown to grow quite early in the spectrum fatigue test.

3. Cracks have been observed to grow at an increasing rate with crack length in the entire range of crack lengths.

4. The essential physical defects in the aluminum alloys as the origins of microfatigue cracking are tool marks, burrs, and inclusions.

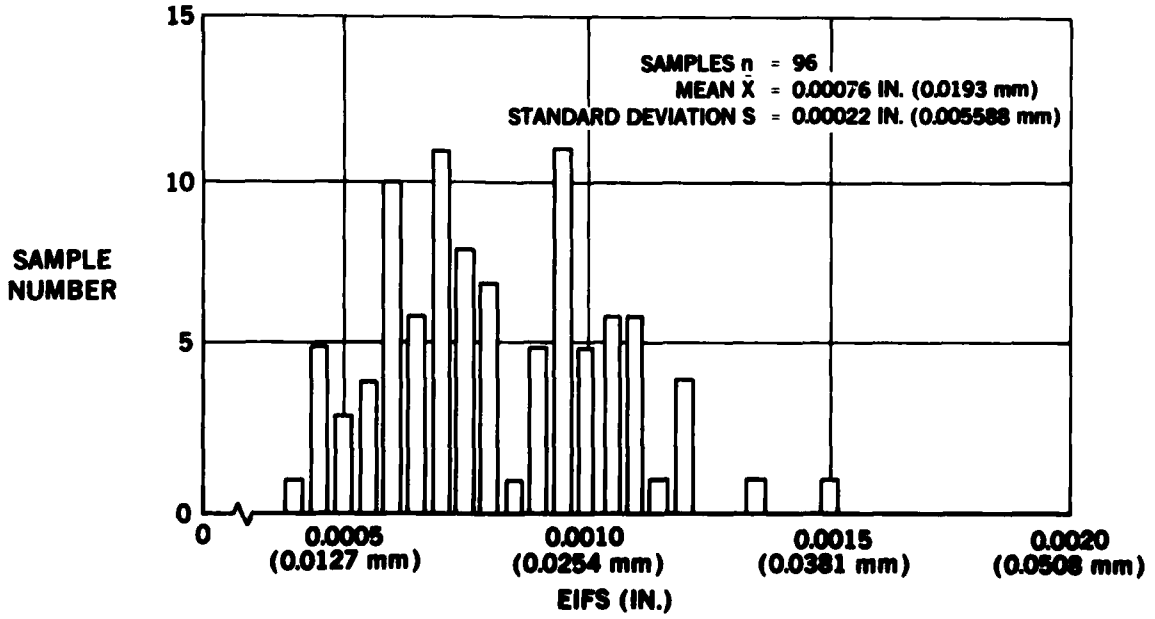

FIGURE 23. STATISTICAL DISTRIBUTION OF EQUIVALENT INITIAL FLAW SIZE FOR 0.250-INCH (6.35-mm) 2024-T3 WITH 3/16-INCH (4.76-mm) OPEN COUNTERSINK REAMED HOLES

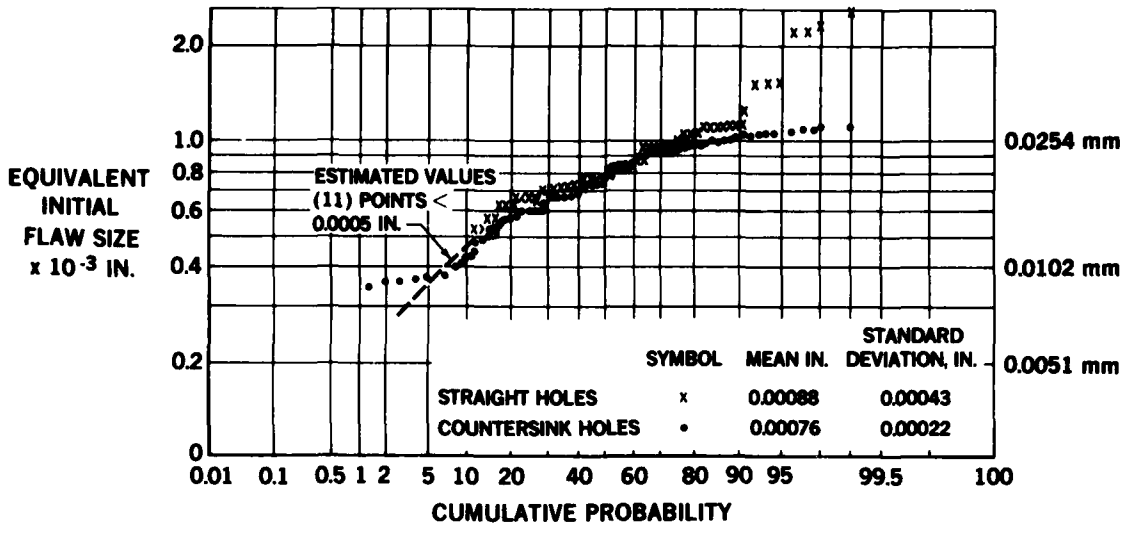

FIGURE 24. CUMULATIVE PROBABILITY PLOT OF EIFS FOR REAMED 3/16-INCH COUNTERSINK AND STRAIGHT OPEN HOLES IN 0.250-INCH (6.35-mm) 2024-T3

5. Statistical distribution of the equivalent initial flaw size based on quantitative data for the fastener holes was obtained using the method and the experimental procedure developed in this investigation.

6. Scatter in the statistical fatigue life distribution can be described in terms of equivalent initial flaw size, microcrack growth life, and macrocrack growth life. Scatter is a function of microcrack growth life, which is, in turn, a function of equivalent initial flaw size and microcrack growth rates.

7. The effect of clearance-fit screws in 3/16-in. (4.76 mm) countersink 2024-T3 fastener holes is to reduce the microcrack growth rate to one-fourth of that in an open hole.

REFERENCES

1. J. L. Rudd and T. D. Gray, Quantification of Fastener Hole Quality, presented at the AIAA/ASME 18th Structures, Structural Dynamics, and Materials Conference, San Diego, California, 24-25 March 1977, AIAA-P-77-382.

2. R. E. Pinckert, Damage Tolerance assessment of F-4 Aircraft, presented at the AIAA Aircraft System and Technology Meeting in Dallas, Texas, 27-29 September 1976, AIAA-P-76-904.

3. P. J. Noronha et al., Fastener Hole Quality, December 1978. Report AFFDL-TR-78-206, Vol 1.

4. S. D. Manning et al., Durability Methods Development, Vol 1, Phase I – Summary, June 1979, AFFDL-TR-79-3118.

5. P. R. Abelkis, Effect of Transport/Bomber Loads Spectrum on Crack Growth, November 1978, Report AFFDL-TR-78-134.

6. B. N. Leis and T. P. Forte, Fatigue Growth of Initially Physically Short Cracks in Notched Aluminum and Steel Plate, 1981, ASTM STP743.

ACKNOWLEDGMENTS

The author wishes to express his appreciation to Paul Abelkis, Don Smillie, and D. S. Warren for their technical advice; to E. Hayman, C. Thunell, and S. Watanabe for their contributions to the test program, and to Dennis Brown for fractography.

The information reported in this paper was developed under a McDonnell Douglas independent research and development program on fatigue and fracture mechanics.

SMALL CRACKS IN LARGE FORGINGS

by

Dr.-Ing. Walter Schütz

Industrieanlagen-Betriebsgesellschaft mbH
Einsteinstraße 20, 8012 Ottobrunn, Germany

1. Introduction

At the state of the art, it is not possible to produce large steel forgings for steam turbine rotors entirely without flaws. Although there have been considerable improvements in the quality of these forgings over the last 25 years and the type of flaws has changed from actual cracks to porosities or inclusions, see Figure 1 [1] their required size has also gone up dramatically, especially for the low pressure rotors, due to the enormously increased output of modern power stations (up to 1300 MW on one shaft).

According to statistics of a German steam turbine manufacturer and of several steel companies [2], about 8 per cent of the large forgings for turbine rotors have to be scrapped, see Figure 2, due to unacceptably large flaws as detected by the mandatory ultrasonic inspection.

In a further 20 per cent of the forgings smaller flaws are detected that require residual static strength and crack propagation calculations, in order to be able to decide if the forging in question can be accepted or has to be scrapped. Furthermore, the possible growth of at first acceptable flaws during service due to start-stop operations of the turbine requires repeated stringent NDI-inspections over the life of the turbine with the attendant prolonged shut-down periods, as well as further crack propagation calculations.

The engineering decisions leading to scrapping are based on two assumptions

- the ultrasonic indications are correct as to size and location of the flaw and
- the flaw behaves like a crack of identical size in the most unfavourable direction (at right angle to the tensile stress); that is, crack propagation starts with the first stress cycle of sufficient amplitude.

While the first assumption could be conservative or unconservative, the second one might be very conservative, since a potentially long crack initiation period is given away. Thus a number of expensive forgings might have been scrapped unnecessarily.

2. The Research Programme

The present programme was intended to answer the following questions:

- How do natural flaws behave under typical service stresses?
- Which typical geometries of such flaws are present in large forgings?
- Under which conditions (size of the flaw, magnitude of stress) do such flaws propagate?
- How do small flaws bunched close together propagate?
- How accurately is the actual size of flaws in the interior of large forgings indicated by ultrasonics?

In order to answer these questions the following research was decided upon by a working group consisting of five steam turbine manufacturers, five steel companies and the IABG.

First suitable forgings containing flaws of different types had to be selected. In all, four shafts and four discs weighing between four tons and one hundred tons each were found, see Figure 3. The forgings had 0,2 per cent offset yield strengths of 700 - 960 N/mm² (with the exception of forging A at $\sigma_{0,2} \approx 350 \div 440$ N/mm²) and tensile strengths of 740 to 1100 N/mm² (forging A 550 - 600 N/mm², see Figure 3.

The programme steps were as follows:

- The forgings were ultrasonically inspected by the highly qualified NDI personnel of the steam turbine manufacturers and/or the steel companies. One detailed inspection sheet per forging was prepared containing all the relevant particulars of the ultrasonic inspection, especially on the size, type and location of the flaws found (this was also done for all the following ultrasonic inspections).
- The forgings were next cut up into 2 - 6 segments and the ultrasonic inspections were repeated, in order to locate the flaws more precisely. Magnetic penetrant inspections were also carried out, because the cutting up of the forging might have

15-2

exposed flaws on the surface.

- Several (up to 17) rectangular bars of a size of 65 x 65 x 300 mm were then machined out of each segment in such a way that the flaws as indicated in the previous steps were in the interior if possible, see Figure 4. Many other specimens for Pellini-Charpy V- fracture toughness- tensile- and crack propagation-tests were also machined out of the forgings, see Figure 5.

- The rectangular bars were then again inspected ultrasonically and by the magnetic penetrant method.

All the above tasks were performed by the manufacturers and/or the steel companies, the following tasks by IABG.

The obvious purpose of the repeated ultrasonic inspections was to investigate the reliability of this NDI method with regard to size and location of flaws and different inspectors in successively smaller test pieces.

- In the next step 45 specimens in all were machined out of the bars with a test section diameter of 30 mm, see Figure 6, the largest diameter possible for the available 60 ton servohydraulic fatigue test machine. These cylindrical specimens were again ultrasonically inspected, this time by IABG personnel.

- Repeated loads of constant amplitude were then applied at a stress ratio of R = + 0,1. the corresponding stress amplitudes were calculated individually for each forging, so that the interior flaws would just show some growth in a maximum of 25 000 cycles, but complete fracture of the specimen would not occur. The corresponding maximum stresses typically were 60 to 80 per cent of the individual yield strengths. If flaw growth was detected by the potential drop method, the test was stopped. If no flaw growth was observed, the stress amplitudes were increased after 25 000 cycles and the test repeated.

  The number of 25 000 cycles was arrived at as follows: A large steam turbine is started up and shut down a maximum of 5 000 times over its lifetime. The necessary safety factor was assumed to be five, large because of the catastrophic nature of a turbine rotor burst in service. In the event, we were remarkably successful in producing small flaw growth usually at the first try.

- After the fatigue test, the specimens were again inspected by ultrasonics and magnetic penetrant.

- Next the specimens were broken at liquid nitrogen temperature in order to obtain brittle fracture through the largest flaw present.

- Examination of the fracture surface in the scanning electron microscope followed, in order to establish the actual original flaw size and type as well as the flaw growth due to the 25 000 cycles.

- The last step consists of supplementary tests to determine basic material data, such as da/dN, ΔK_{th}, tensile strength Pellini tests , SN-tests in the low cycle fatigue range etc. for the unflawed material of every forging utilised.

3. Preliminary Results

As the evaluation of the large number of results has not yet been fully completed only some preliminary results can be given.

3.1 Reliability of Ultrasonic Inspection

Figure 7 shows the results of the ultrasonic inspection of the flaws in some of the forgings compared to the actual size of the flaws as determined by scanning electron microscopy after breaking open the fracture surface. It is seen that there are conservative (below the 1 : 1 line) and unconservative (above the 1 : 1 line) predictions.

3.2 Typical Geometries of Flaws in Forgings and their Behaviour under Fatigue Loading

Some forgings, like shaft A, see Figure 8, contained a considerable number of spike-shaped flaws. They consist of aluminium oxydes. The fatigue cracks growing from these spikes tend to become more elliptical in shape, as predicted by fracture mechanics calculations, see flaws 1 and 2 in Figure 8.

In forging D, circular interior flaws were typical, see Figure 9. They tended to remain circular during fatigue crack growth. On closer inspection, see Figure 10, and in the SEM, Figure 10, lower half, each "flaw" actually consists of a very large number of small inclusions in the basic material.

In forging G the flaws are finely dispersed and cannot be recognised macroscopically on the fracture surface. Along the cylindrical part of the specimen many outside cracks however can be seen after the fatigue test, Figure 11. The original flaws, photomicrograph in lower right part of Figure 11 again are sharp-edged inclusions which grow to half-elliptical shape near the exterior of the specimen and to elliptical shape in the interior.

3.3 Behaviour of Flaws under Fatigue Loading

Some of the flaws did behave like fatigue cracks of the same size and shape, while others did not. One example of the latter case is shown in Figure 12, which will be explained in the following: The average propagation rate during the 25 000 applied stress cycles was calculated from the SEM photographs. In the case of flaw No 3 it was $4{,}2 \cdot 10^{-5}$ mm/cycle. The curve of dl/dN for unflawed material of forging D had been determined before with CT-specimens. The point of intersection between this dl/dN curve and line 3 gives an effective ΔK of 700 N/mm$^{3/2}$. At the stress amplitude applied this is equivalent to a flaw of 0,6 mm diameter. However, flaw No 3 actually had an 1,6 mm diameter; this results in an applied ΔK of 860 N/mm$^{3/2}$, and the intersection of line 3' with the dl/dN curve gives a crack propagation rate of 10^{-4} mm/cycle. So the flaw acted like a crack of 0,6 mm diameter, while it actually was 1,6 mm in diameter. Flaws 1 and 2 behaved similarly.

Obviously the reason for this may be that a crack initiation phase was present. We will look into this matter in more detail using the potential drop records we have obtained. One example is shown in Figure 13, left side, where there apparently was a long crack initiation phase of approximately 60 per cent of the complete life (9 700 out of 17 570 cycles). In shaft A, which contained sharp-edged inclusions, the flaws behaved practically like cracks, see Figure 14.

In addition, ΔK_{th} was determined for all materials, using CT specimens machined from unflawed regions of the forgings. The values obtained are compared here with the results of tests on the cylindrical specimens containing flaws in Figure 15. For several specimens out of forgings A and B, each of which contained several flaws of different sizes and therefore different stress intensity factors:

- Disc A, which contained sharp-edged inclusions: There was crack growth if the applied stress intensity factor range of the individual flaw was greater the ΔK_{th}. There was not, if it was below ΔK_{th}.
- Disc B, which contained half-elliptical flaws: There was no crack growth from one flaw in specimen B 12, even though the applied ΔK was nearly twice as large as ΔK_{th}. Four more flaws in specimens 7 and 8 did not propagate although ΔK was more than 50 % higher than ΔK_{th}.

Elsender in a paper at the Fracture Conference in Waterloo five years ago [3] showed some very similar results, see Figure 16.

4. Outlook

By the end of 1982 the report containing all the details as well as the conclusions to be drawn will be completed. A paper with the more important results will also be published in early 1983. A continuation comprising tests at typical rotor temperatures (+ 536° C) and at R = 1 is planned.

5. References

[1] Mayer, K. H., J. J. Meyer und W. Riess: Betriebsbeanspruchungen der Wellen moderner Dampfturbinen bestimmen die Anforderungen an die Schmiedestücke. VGB Kraftwerkstechnik, 58. Jhg., H. 7, Juli 1978, S. 529 - 541

[2] Mayer, K. H.: Critical Issue on the Necessity for Axial Boreholes in Rotor Forgings for Turbines and Generators. Presented at the EPRI workshop "Rotor Forgings and Generators", Palo Alto Ca, Sept. 14 - 17, 1980

[3] Elsender, A., R. Gallimore and P. A. Poynton: The Fatigue Behaviour of Macroscopic Slag Inclusions in Steam Turbo-Generator Rotor Steels. Fracture Conference 1977, Vol. 2, ICF4, Waterloo, Canada, June 19 - 24, 1977

15-4

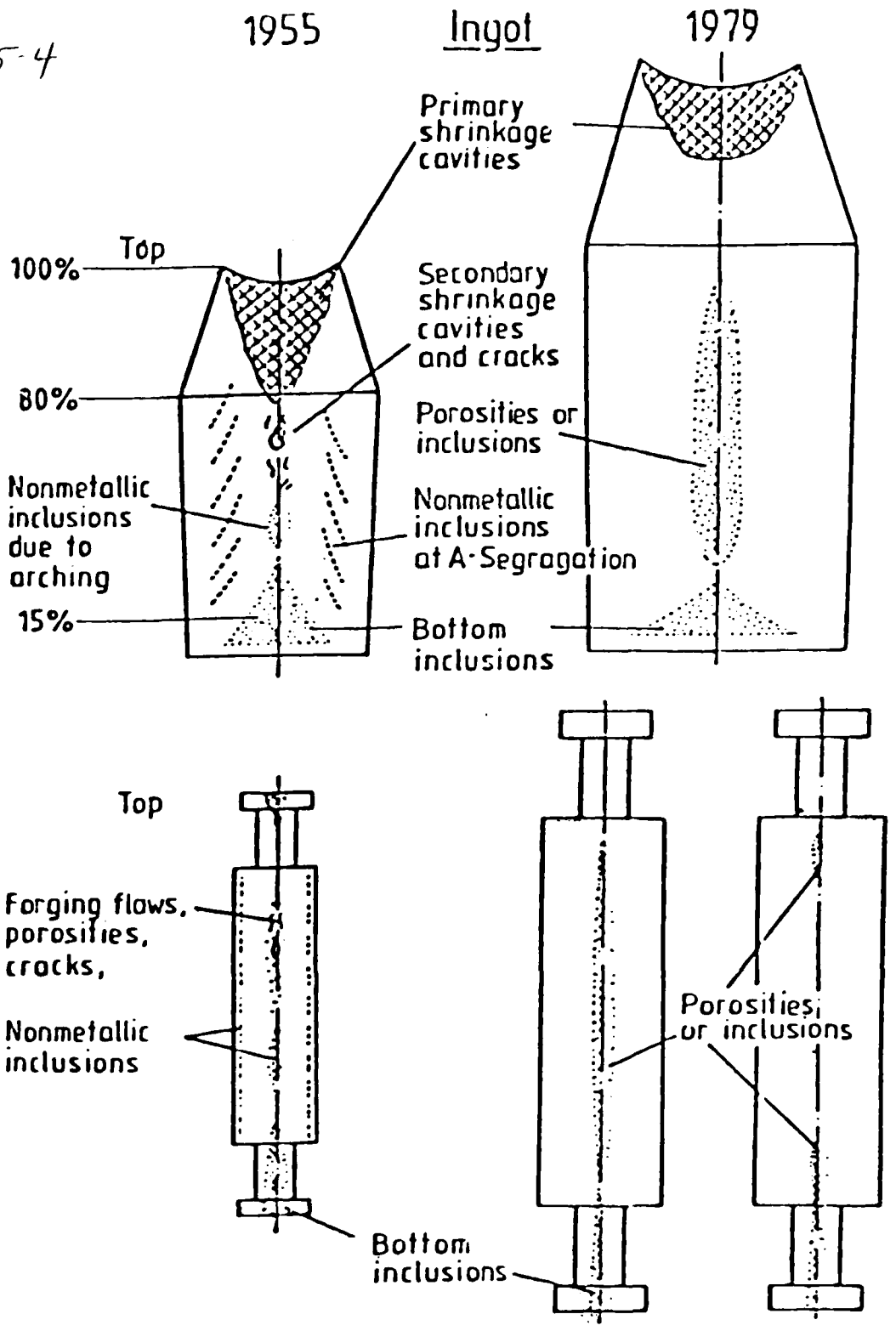

Fig.1 Possible flaws in ingots and rotors (improvements 1955 versus 1979)

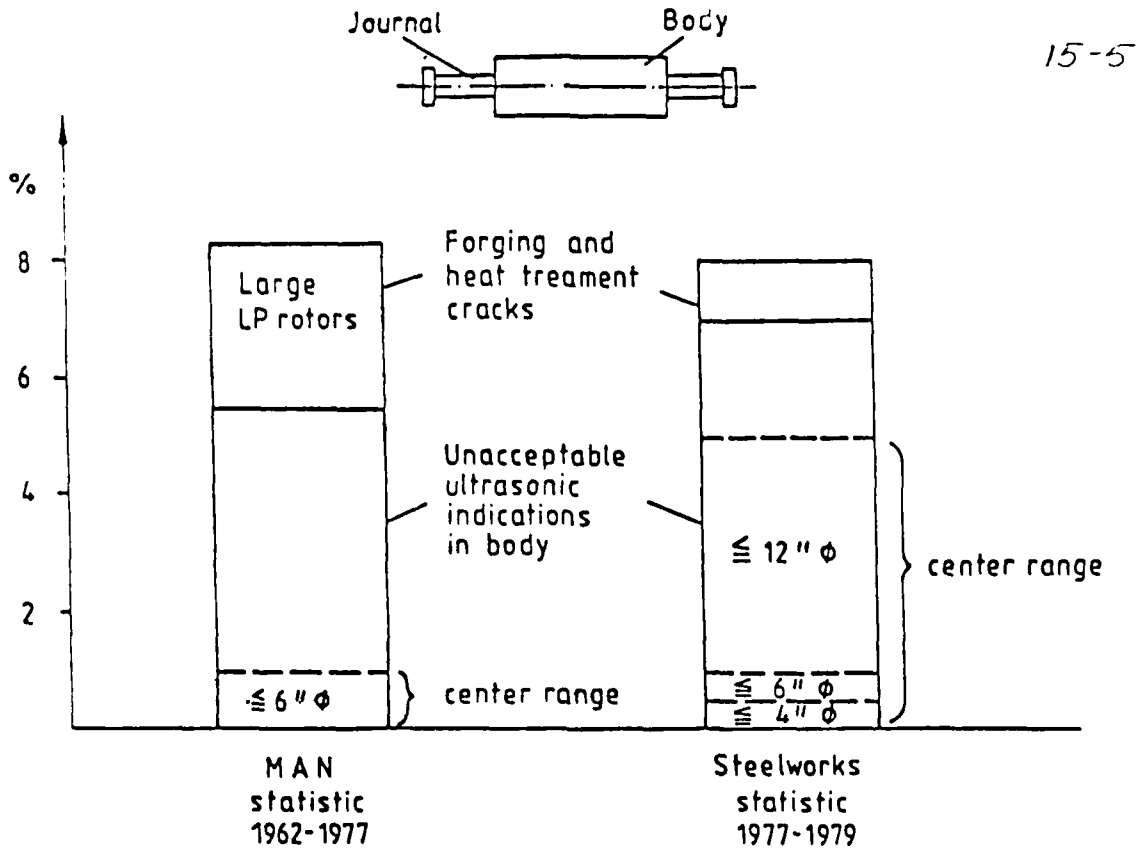

Fig.2 Percentage and type of flaws appearing in rotors during manufacture

Forging	Turbine Manufacturer, Steel company	Material	Tensile strength N/mm^2	0.2per cent Yield strength N/mm^2	Weight (tons) of the forging	Approximate size(mm) of the part tested
Shaft A	I , 1	26CrNiMo 4	550 - 600	350 - 440	38	965ϕ×8340
Shaft B	I , 2	27NiCrMo 85	800 - 880	700 - 750	30	750ϕ×3000
Disc D	II , 3	28NiCrMoV145	1000 - 1100	880 - 960	100	1500ϕ × 325
Disc E	II , 3	26NiCrMoV 85	800 - 880	700 - 790	19	1500ϕ × 208
Disc F	II , 4	26NiCrMoV115	920	780 - 820	100	3000ϕ × 441
Disc G	III , 5	23NiCrMo 747	800 - 830	640 - 700	12,5	1720ϕ × 260
Shaft H	IV , 4	21CrMoV 511	750	625 - 650	4,7	350ϕ × 10 10
Shaft J	V , 2	28CrMoNiV 49	740 - 800	600 - 660	not known	690 ×490×120

Fig.3 Description of the eight forgings utilised

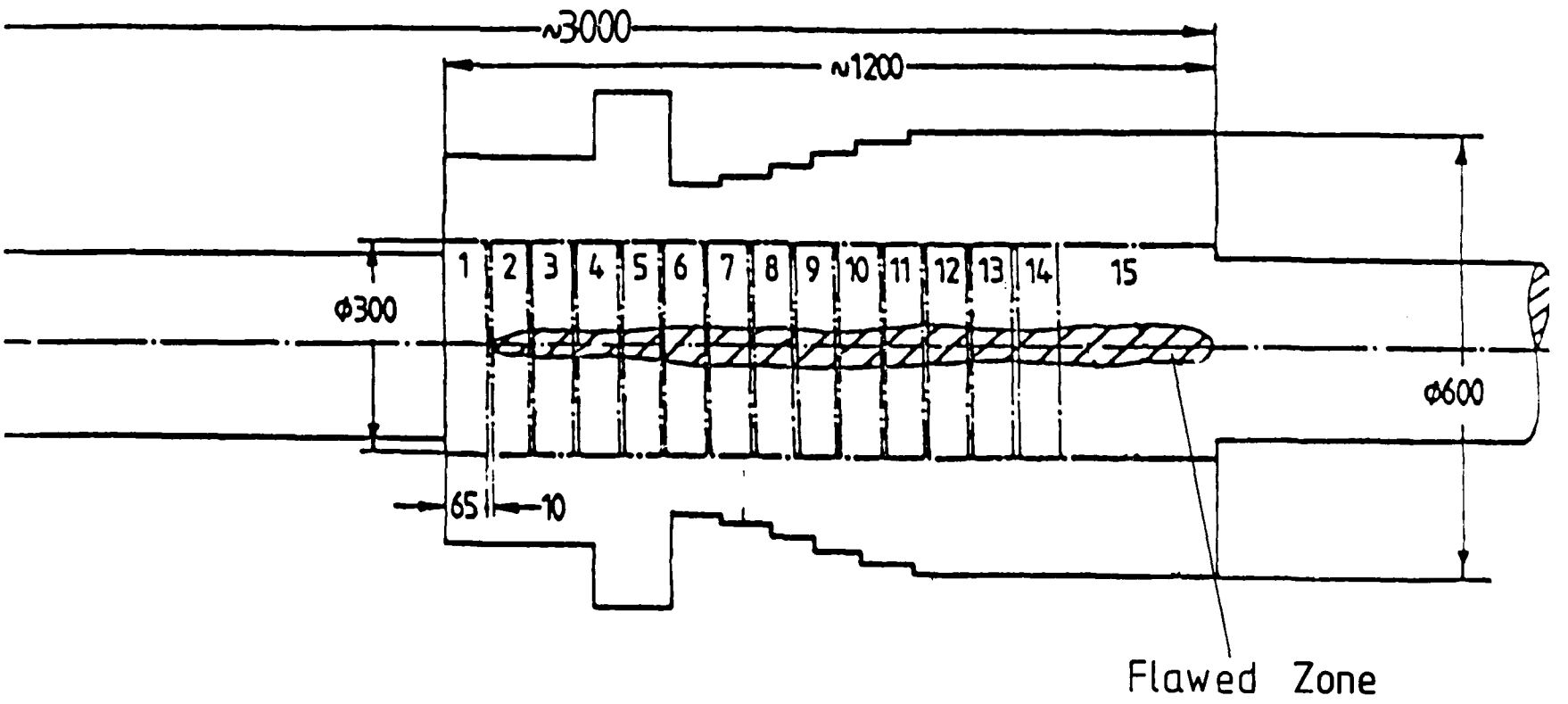

Fig.4 Sectioning of shaft B

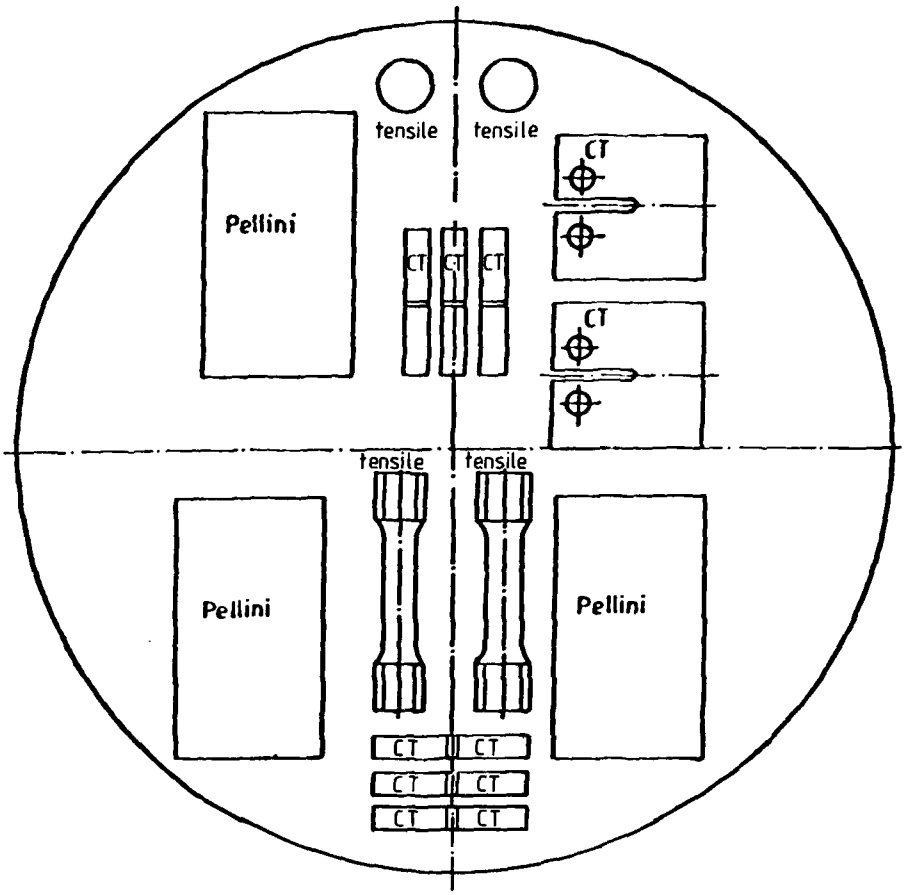

Fig.5 Specimens for Pellini - tensile - fracture toughness - and crack propagation tests

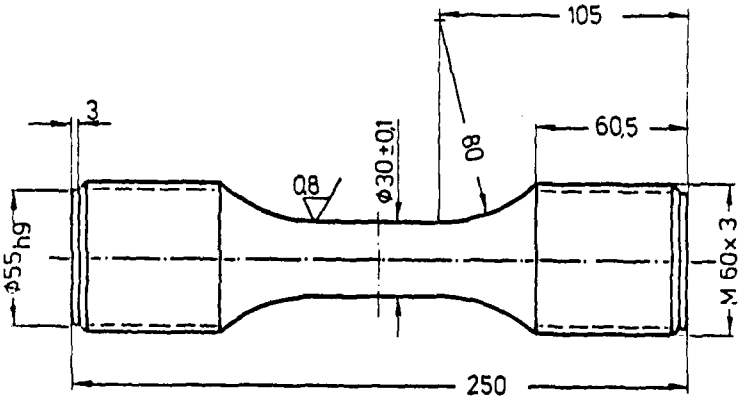

Scale 1:2

0,8 polished longitudinally

Fig.6 Specimen

15-8

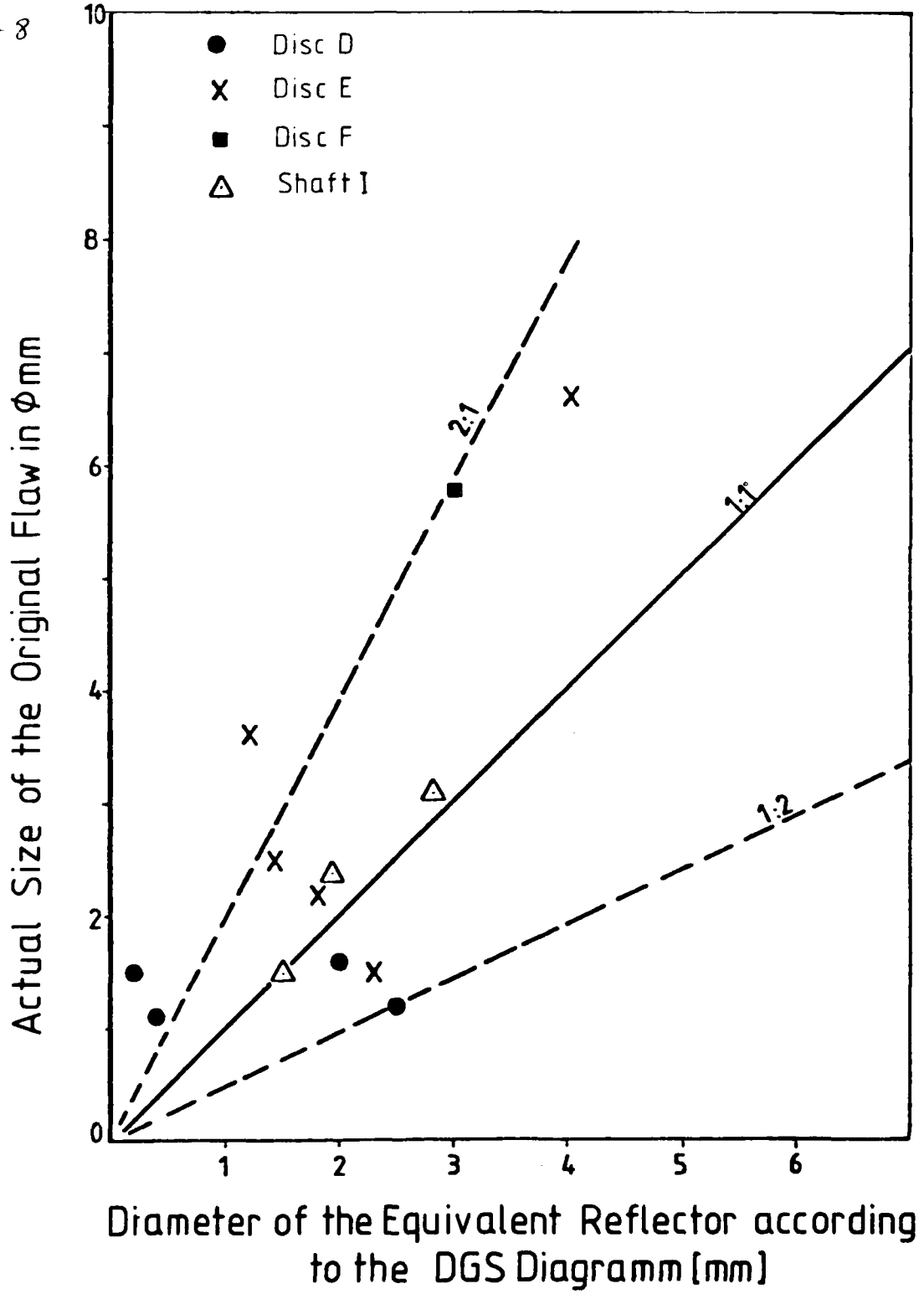

Fig.7 Reliability of ultrasonic inspection of forgings

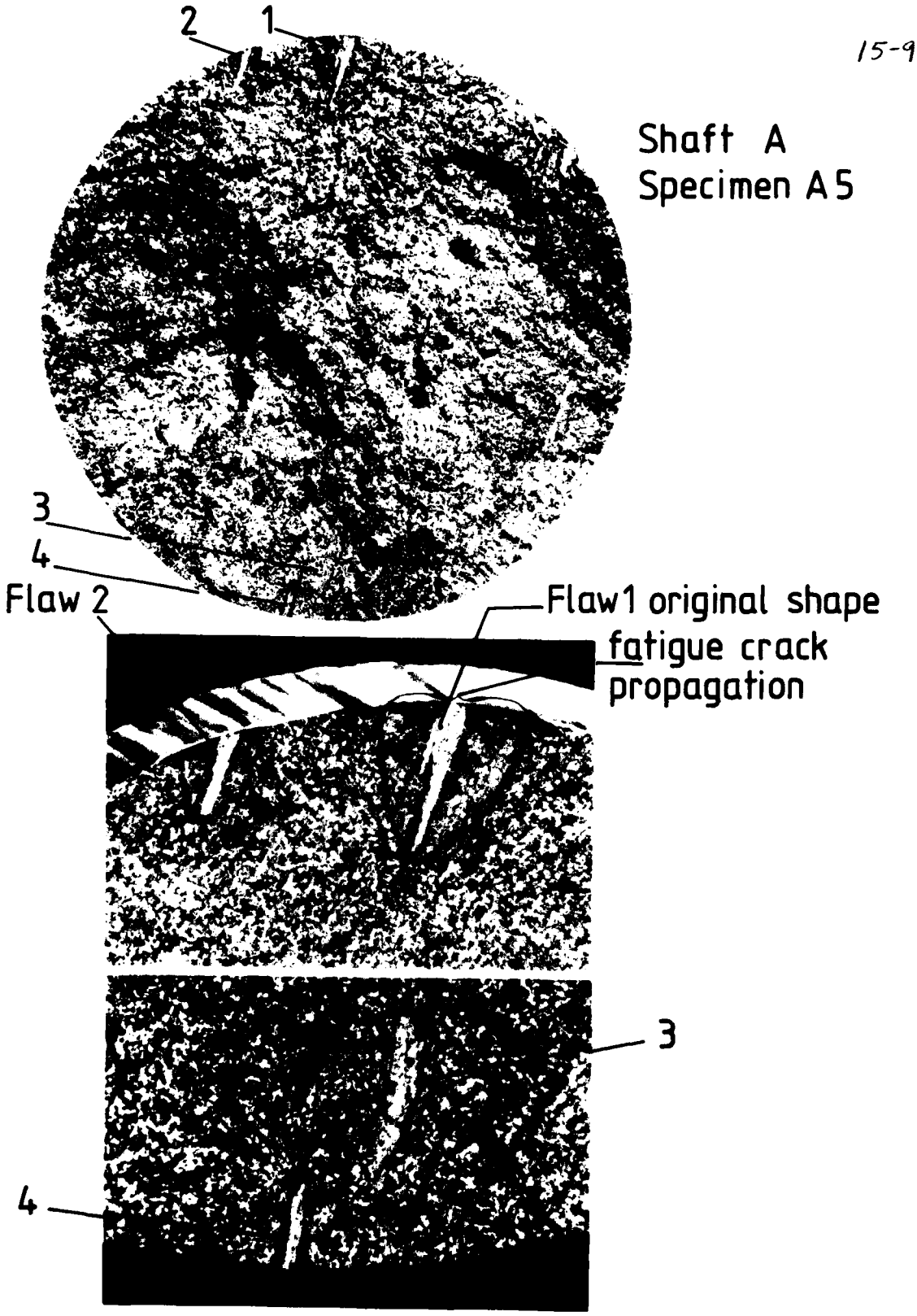

Fig.8 Flaws in shaft A

15-10

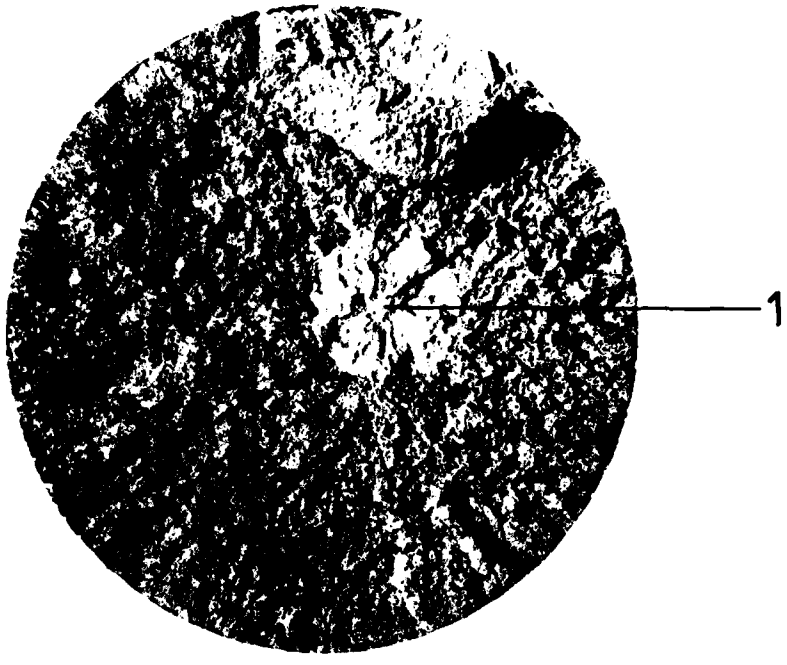

Specimen 2D 4

Fig.9 Flaws in disc D

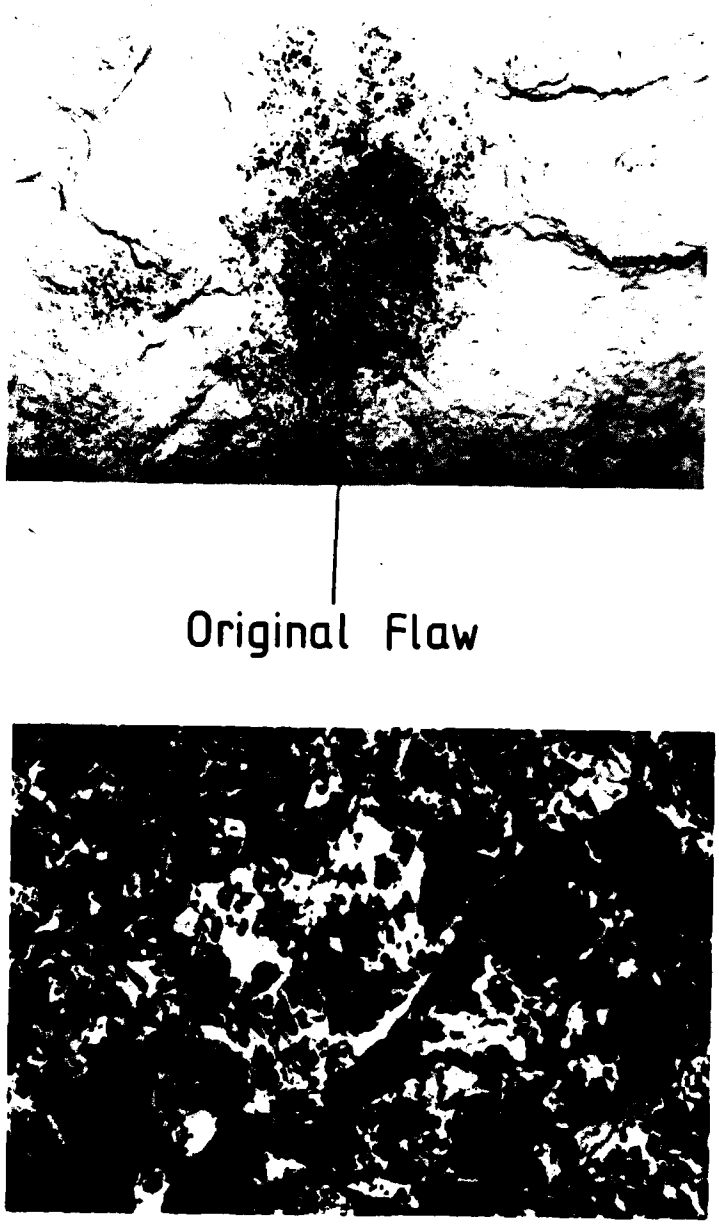

Fig.10 Flaws in disc D

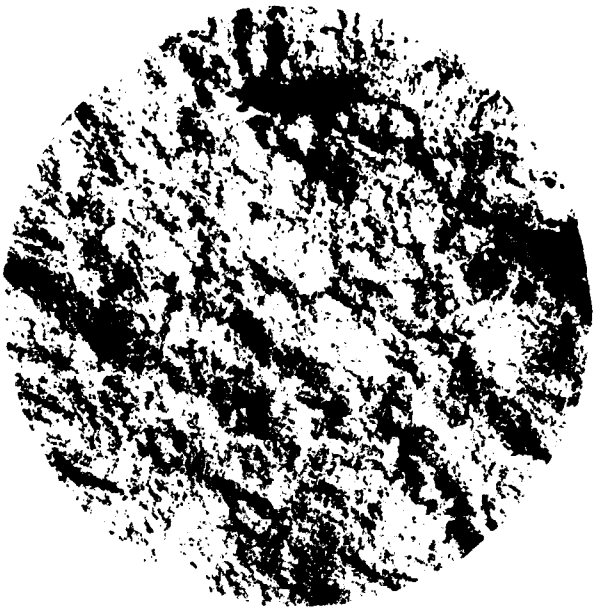

Disc G
SpecimenG14

Cracks in
Cylindrical Part of
Specimen

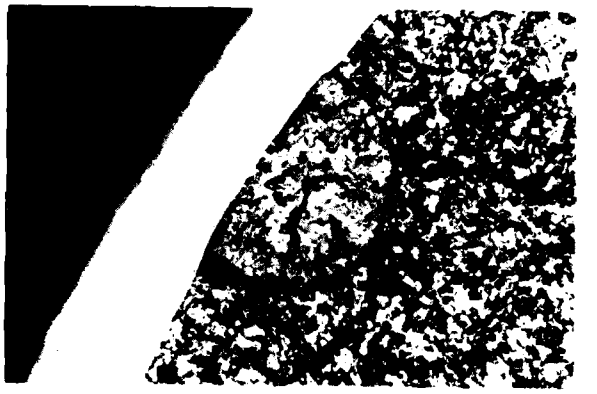

Flaws

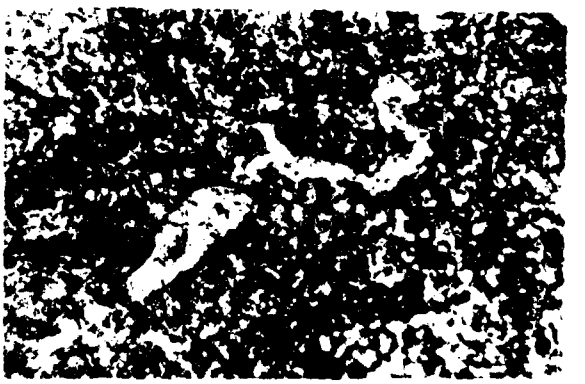

Fig.11 Flaws in disc G

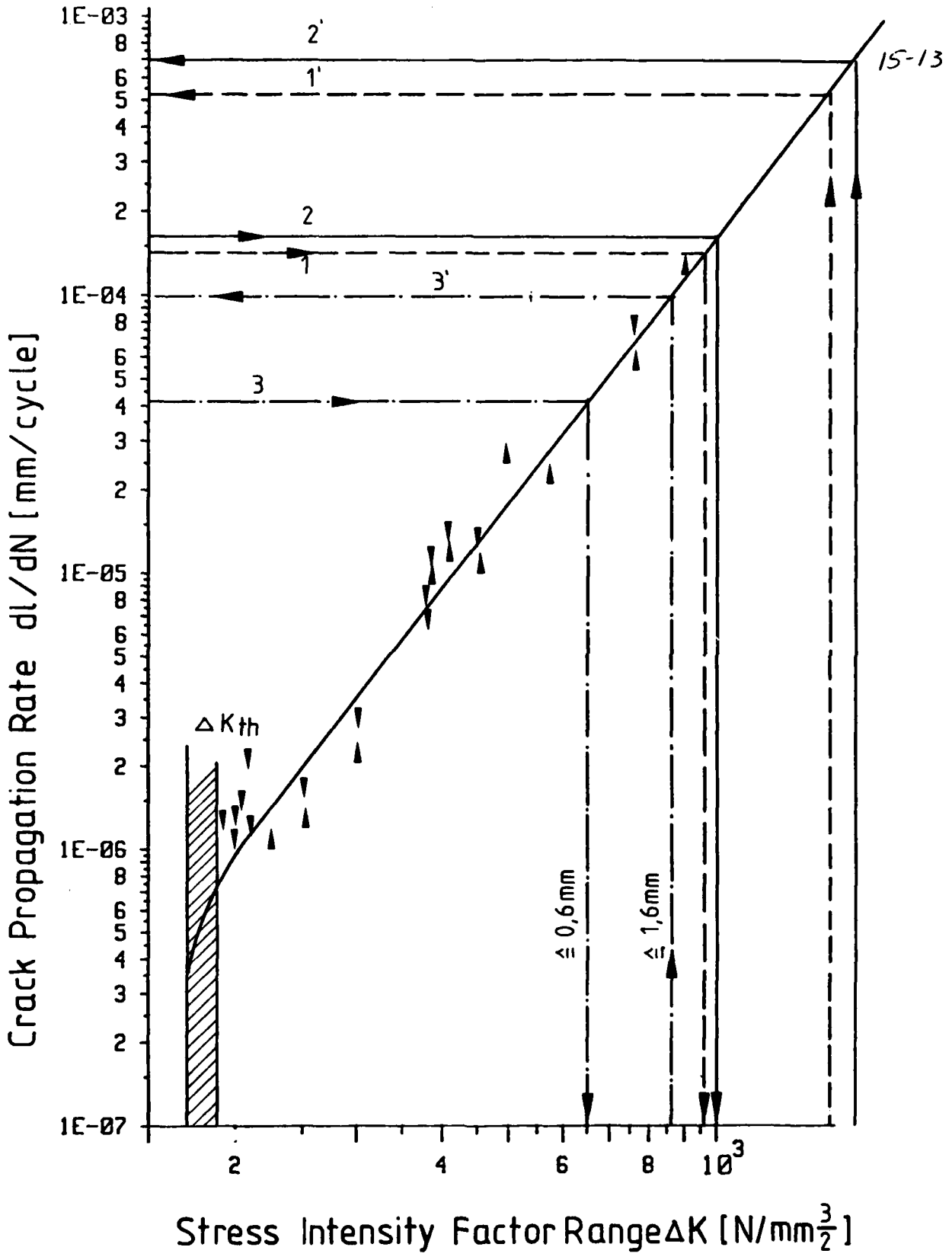

Fig.12 Crack propagation of flaws in disc D

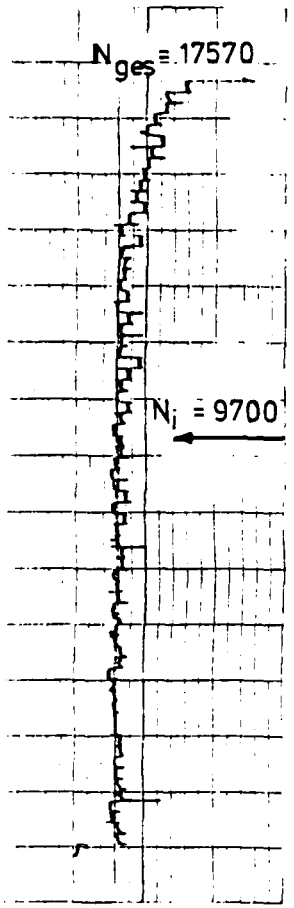

Potential Drop Record
R_0 = 1,487 mΩ – 1,539 mΩ

Disc E

Specimen E 5
σ_{max} = 600 N/mm²
17570 cycles

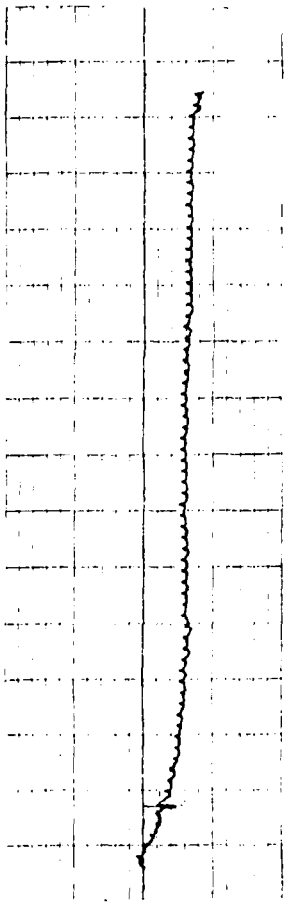

Temperature Record
T_0 = 30°C – 32,3°C

Fig.13 Potential drop measurements

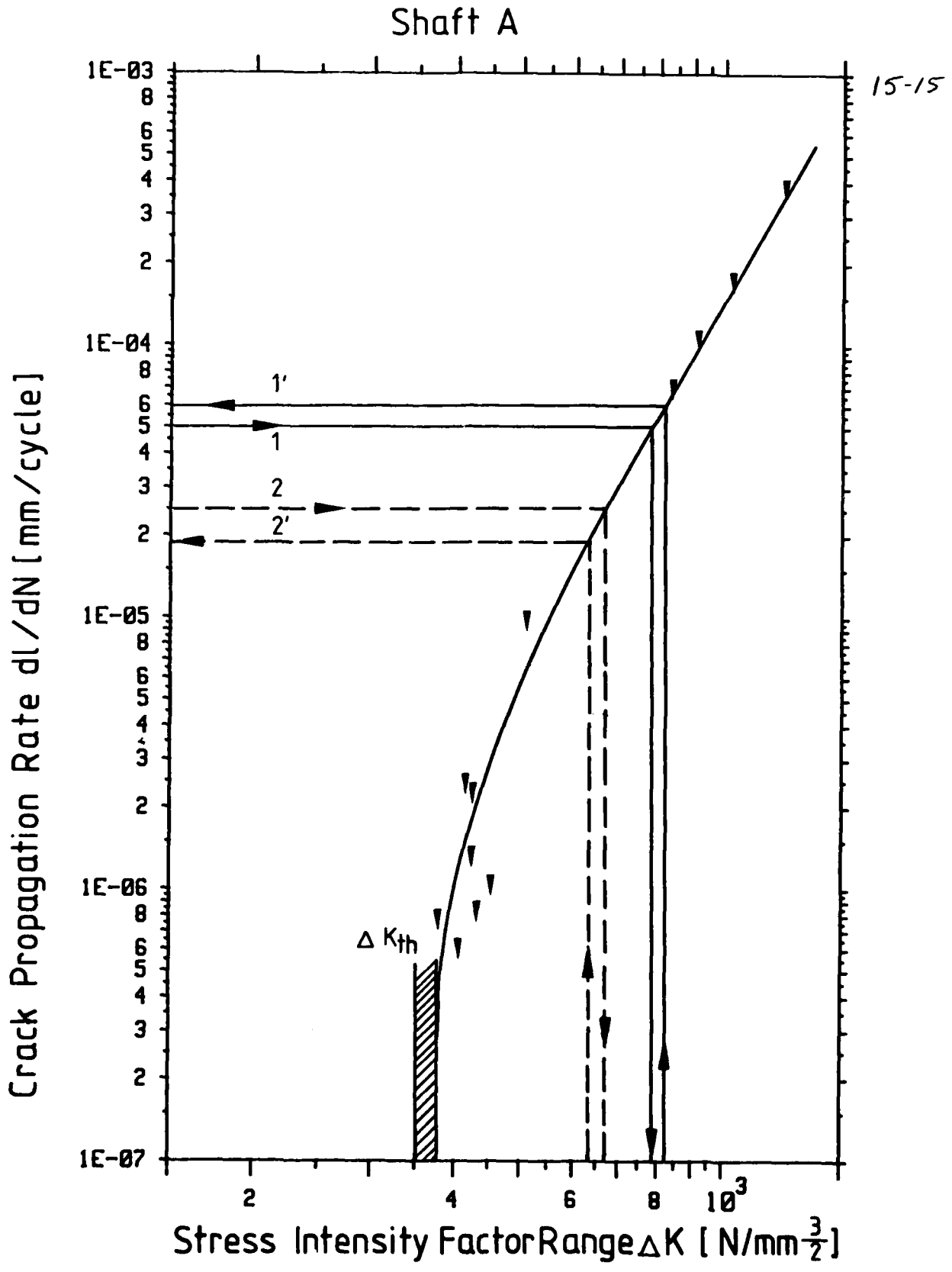

Fig.14 Crack propagation of flaws in shaft A

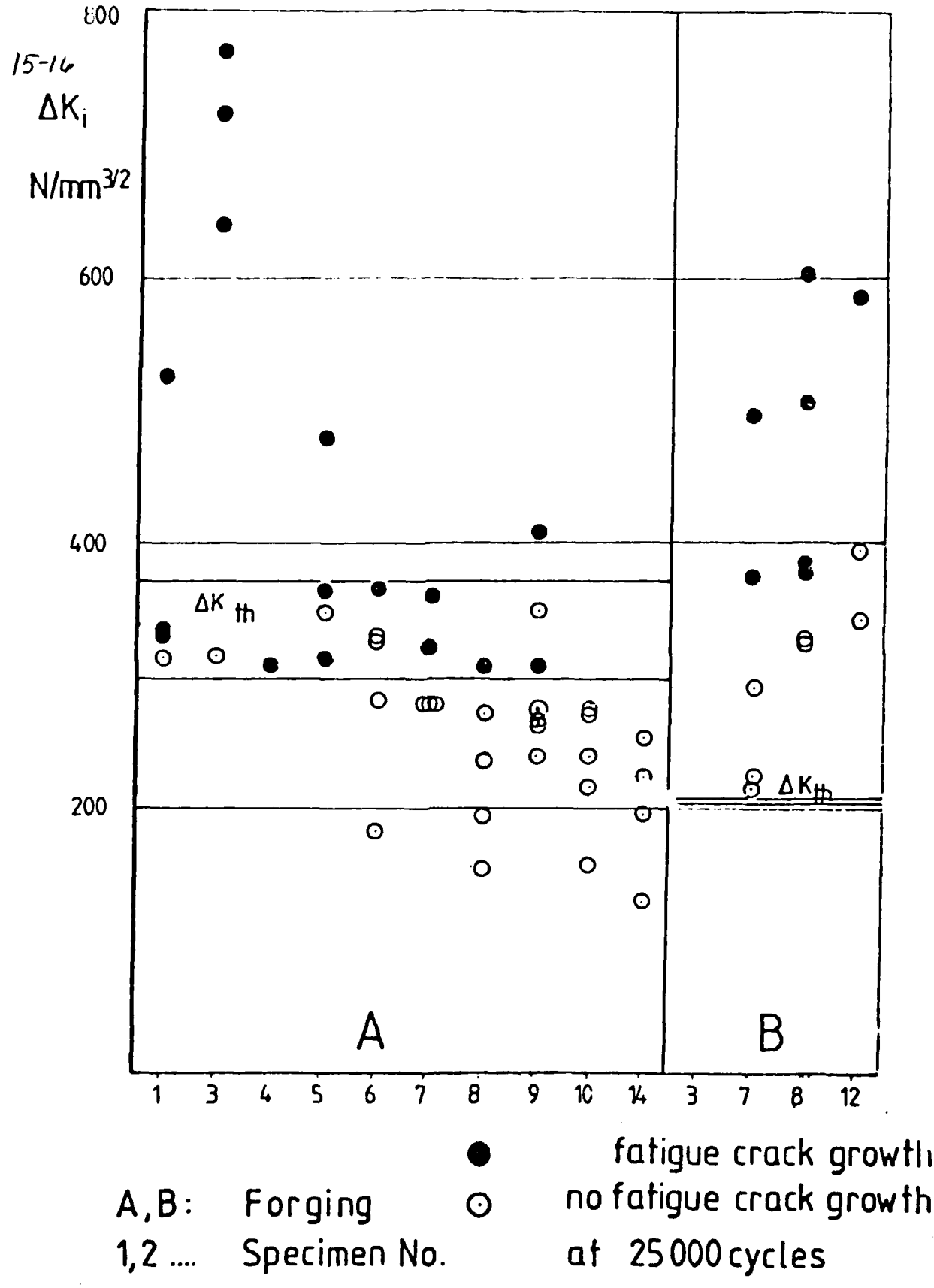

Fig.15 Crack propagation near ΔK_{TH} from flaws in shafts A and B

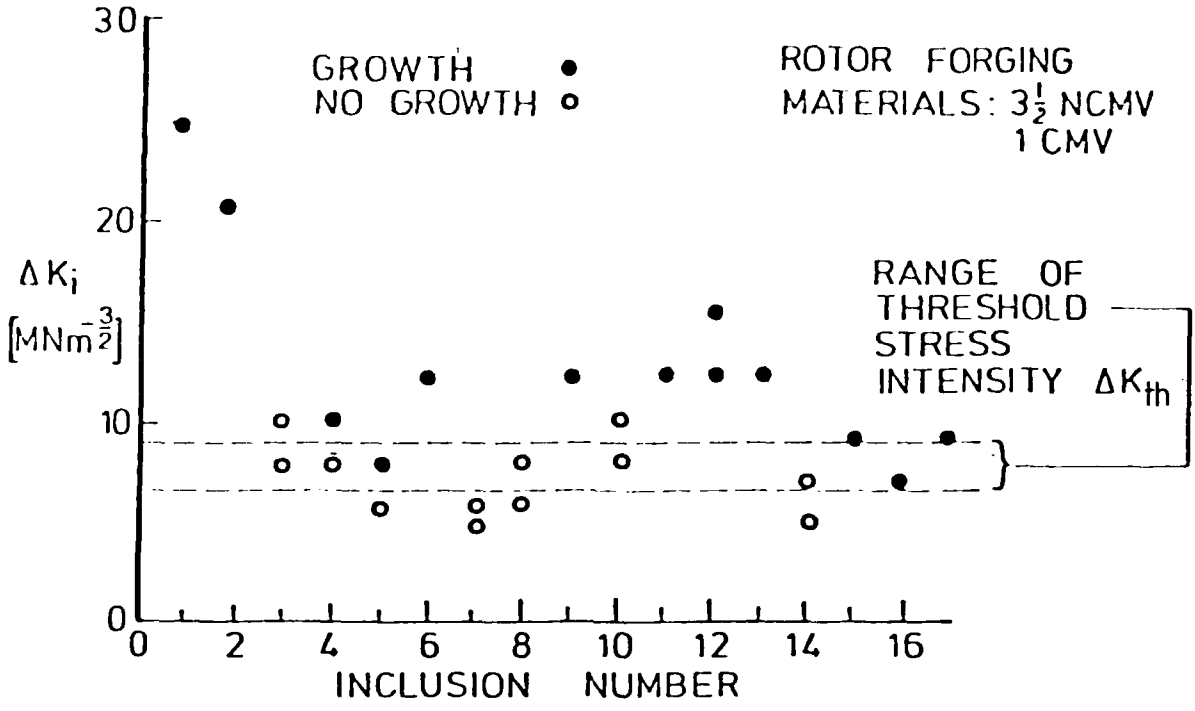

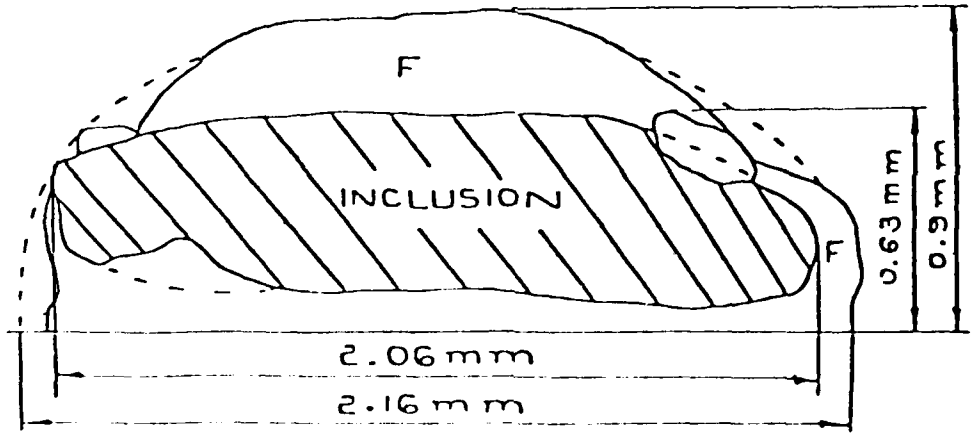

F = FATIGUE GROWTH

Fig.16 Crack propagation near ΔK_{TH} from flaws in a rotor forging after Elsender /3/

Round Table Discussion

"SHORT CRACK" FATIGUE DESIGN CONSIDERATIONS: MODELLING, CHARACTERIZATION, INTERPRETATION, DETECTION; PREDICTION OF BEHAVIOR

by

D.W.Hoeppner, Ph.D., P.Eng.
Department of Mechanical Engineering
University of Toronto
5 King's College Road
Toronto, Ontario M5S 1A4
Canada

This conference has attempted to focus on "short cracks" (or small cracks) rather than "long cracks". My remarks will be brief and of a summary context in relation to the papers presented at the conference and to stimulate thoughts for additional research.

Professor Ritchie in the first paper summarized various perspectives on the short crack problem. In a similar fashion, a recent report I wrote for the Metals Properties Council[1] emphasized the relativistic aspect of crack side and the necessity to be sure you have the proper set of boundary conditions (similitude) to apply Mode I linear elastic fracture mechanics to the fatigue crack propagation problem. This aspect can, in a sense, be discerned when the definition of a short crack is formulated using a dictionary. This definition would be:

Short crack

1A) Having little length, not extending far from end to end,
4B) Limited in distance,
5A) Not coming up to standard, measure, or requirement.

Since no standard exists to precisely define a short crack it is difficult to discuss it as we have seen from this conference. Each presenter presents a certain perspective on the problem and, at times, generalizes so much that the rest of us get very confused because of the many perspectives in which the short crack problem can be viewed. To an extent this was brought out by Professor Ritchie.

Subsequent to this brief conference one concludes that the short crack problem is a matter of perspective. That is that short must be compared to something. Thus, as engineers and scientists we are concerned with all of the following aspects of the short crack problem:

(1) Definition of a Crack,
(2) Definition of a Short (Small Crack),
(3) Size of crack with respect to microstructure (grain size, packet size, unit cell size etc.),
(4) Size of crack with respect to plastic zone size,
(5) Size of crack with respect to thickness (3, 4, 5 are all related),
(6) Size of the crack with respect to applicability of Mode I LEFM,
(7) Size of the crack with respect to crack detection capability [in an engineering sense we are concerned about our inspection capability (as discussed by Professor Packman) with respect to the crack size] in relation to crack size, location, and morphology,
(8) Crack size with respect to the tolerable crack size as determined by the Mode I fracture toughness (K_{Ic}) or other fracture instability material parameter,
(9) Crack size with respect to the overall fatigue design philosophy,
(10) Statistical aspects of the growth of short cracks, and
(11) The growth of short cracks in highly anisotropic materials (such as fiber composites or certain titanium alloys, aluminum forgings etc.) and potentially heterogeneous materials (such as powder alloys).

All of these aspects have been dealt with to an extent in this conference. Clearly, in dealing with the short crack problem we must precisely define the physical/chemical event to be dealt with, formulate the proper physical/mathematical

model, explicitly define the boundary conditions that relate to the specific crack size being dealt with, test the concepts and models, and establish behavioral relationships. This is a problem of physics and mathematics that requires the proper similitude. Many of these aspects must be researched further as pointed out in the conference and discussed in Reference 1. I would hope that future activities on the short crack concentrate on all of these areas so that we become more effective at dealing with the "short crack problem" since some people believe we have the "long crack" problem under control.

REFERENCES

1. Hoeppner, D.W. *Estimation of Component Life by Application of Fatigue Crack Growth Threshold Knowledge*, Fatigue, Creep, and Pressure Vessels for Elevated Temperature Services, pp.1-83, MPC-17, AME, NY, NY, 1981.

Discussion (Continued)

Subsequent to the regular program and the introductory discussion an extensive discussion resulted with many varied inputs. The committee reviewed the discussion and invided Dr Brian Leis to provide an extended written discussion to the conference. His input follows:

DISCUSSION OF THE SHORT CRACK EFFECT IN AIRFRAME MATERIALS AND COMPONENTS

Background

Author: Brian Leis
Battelle Memorial Institute
505 King Ave
Columbus, Ohio 43201
USA

This meeting has brought together a number of diverse interests, each with a different perspective on what a short crack is. The literature relevant to the short crack effect suggests that a short crack is any crack whose growth can't be correlated with handbook growth rate data using fracture mechanics technology, specifically linear elastic fracture mechanics (LEFM). The short crack effect is of interest to alloy designers because it may be a key to improving materials in the future. It is of interest to the scientist because it does not follow the commonly used analysis framework of LEFM. But most importantly for AGARD, it is of concern to the engineer in that the short crack literature indicates LEFM predictions of growth rate (when integrated crack size), inspection interval, and possibly critical crack size are often nonconservative in the presence of this effect.

The engineer may not be overly concerned with the causes of the short crack effect so long as he knows when to expect it and whether it be of consequence in his design. The desire is thus to establish crack sizes, materials, loadings, etc. for which the engineer must be aware of the short crack effect and its relative significance. Unfortunately, the occurrence and significance of the short crack effect depends on the structure and the loading, primarily through their influence on the critical crack size. For this reason, rules cannot be established to avoid design problems at the present time. Furthermore from an engineering viewpoint the effect is only of consequence if it radically alters the threshold for cracking and the total useful life of the structure or the inspection interval. In small highly stressed components the effect is therefore intuitively more significant than large panel structures. Rational design, however, is not based on intuition.

Causes of the Apparent Short Crack Effect

The engineer can avoid the problems associated with the short crack effect by careful consideration of the key assumption he makes in applying LEFM. The key assumption is that equal changes in the value of the stress intensity factor mean equal amounts of crack advance (equal crack driving force). That is, the concept of similitude is invoked. On the surface, the concept of similitude is straightforward however, its implementation in practical situations related to LEFM is not[1]. As detailed in a recent report[2], a breakdown in the similitude concept is central to the apparent short crack effect. The following summarizes the central issues related to similitude.

Mechanical Similitude

Provided the plastic zone is small compared to all length dimensions, and small with respect to the distance over which the first term of the elastic stress field solution is dominant, both the size of the plastic zone and the surrounding stress field are adequately described by the stress intensity factor, K. Under these restrictions, two cracks with equal K have the same plastic zone and stress field regardless of geometry: there is similitude.

Unfortunately, the similitude is still conditional. Most important there has to be equal constraint. Otherwise, σ_z and the plastic zone are different. Thus under circumstances of equal constraint and equal K, the response of two cracks should be the same. Therefore two cracks should show equal growth habits. Since both K_{max} and ΔK are of relevance, it follows immediately that

$$da/dN = f_1(K_{max}, \Delta K) = f_2(\Delta K, R). \quad (1)$$

Equation (1) is physically sound within the limitations invoked above. However, the functional forms of f_1 and f_2 cannot be derived from first principles and, therefore, they are obtained by interrogating the material through tests.

It should be pointed out that one similitude requirement has still been overlooked. This condition is that the plastic zone in the wake of the crack must also be equal in as much as they affect the local stress field through closure forces. More rigorously, similitude requires that the closure displacement and stress fields be the same as indicated schematically

AD-A131 150 BEHAVIOUR OF SHORT CRACKS IN AIRFRAME COMPONENTS CONFERENCE PROCEEDINGS O..(U) ADVISORY GROUP FOR AEROSPACE RESEARCH AND DEVELOPMENT NEUILLY.. APR 83 AGARD-CP-328 F/G 1/3 NL

3/3

UNCLASSIFIED

END
DATE FILMED
5 86

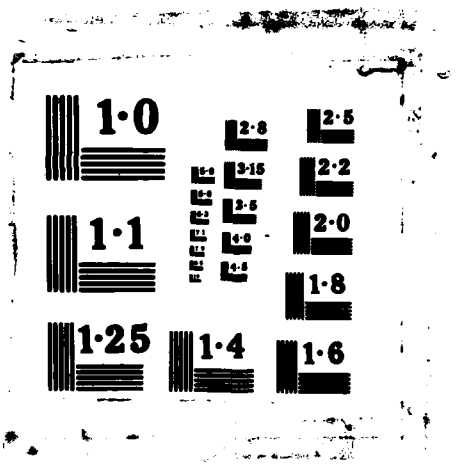
1·0
1·1
1·25
1·4
2·8
3·15
2·5
2·5
2·2
2·0
1·8
1·6

in Figure 1. Experience from tests has shown that the latter condition is reasonably fulfilled for long cracks growing under constant amplitude, since growth rates for long cracks tend to correlate on the basis of Equation (1) regardless of geometry. This implies that for small cracks, Equation (1) is a function of the K history as well as the current K_{max} and ΔK.

16-4

Metallurgical Similitude

In the derivation of Equation (1) it was tacitly assumed that metallurgical similitude existed. Although this may seem trivial, violation of metallurgical similitude can easily be overlooked when correlating the behavior of small and long cracks. Therefore, it is worthwhile to consider the conditions leading to metallurgical similitude.

Clearly, the material should be the same with regard to phase, orientation, dislocation density, particle density, etc. for it to respond in a unique manner to mechanically similar conditions. In the case of cracks with long fronts this condition is satisfied on the average even in multi-phase materials with high crystallographic anisotropy. However, if the crack front is short (e.g. of the order of several grains) this condition will generally be violated. Apparently, the condition translates into the geometrical requirement that the crack front be long with regard to metallurgical features.

Closely related is the similitude in crack growth mechanism, which is often quoted as an important condition. However, similitude in crack growth mechanism is not a condition. It is, rather, a consequence of the material's response to the mechanical and metallurgical similitude.

Differences in crack growth mechanisms, which may be considered a consequence of a breakdown in similitude, can affect the growth rate da/dN. The growth rate (crack advance over some cycle interval) is really a composite rate that reflects all operative modes and mechanisms of crack advance as suggested in Figure 2 and elaborated in the following. Most often long crack growth occurs by a sliding off mechanism at the crack tip in ductile engineering materials. For long cracks then, crack advance is associated with Mode I loading and the dominant Mode I mechanism is reversed slip which gives rise to striations. In contrast, short crack advance may be associated with both Mode I loading and localized Mode II loading. Moreover, the Mode I mechanisms may be related to reversed slip, ductile fracture, and brittle fracture and the local Mode II mechanisms could be related to local crystallographic fracture and local shear. Thus, the character of the growth rate process can be a factor in causing the short crack behavior.

In so far as the environment (temperature and chemistry) affect the mechanism and rate, it is clear that the local environments should be the same for complete similitude.

Similitude Conditions and Breakdown of Similitude

In summary, the similitude conditions are as follows:

- small plastic zone with respect to all length dimensions (including crack front length).
- small plastic zone with respect to the distance over which the first term of the stress field solution is dominant.
- equal K_{max} and ΔK.
- equal closure fields.
- long crack front with respect to metallurgical features.
- same environment.

When all of these conditions are satisfied the response of the crack will be the same. When any one condition is not satisfied, the bounds of validity of Equation (1) have been exceeded and thus dependencies of the type implied by Equation (1) become questionable.

If J is used instead of K as the mechanical similitude parameter the first requirement will be somewhat relaxed, but all others remain in force. Thus the extension of the validity of Equation (1), with K replaced by J, can bring only little solace to the small crack problem, and the comments that follow hold almost regardless of whether J or K is used as a similitude parameter. Moreover, if significant unloading is involved, the use of J becomes even more uncertain.

Similitude and Short Cracks at Smooth Surfaces

Provided that all similitude conditions are fulfilled, equal ΔK (and R) give rise to equal growth rate. For a given ΔK a smaller crack will require a higher stress. As long as the plastic zone is uniquely related to K, equal K means equal plastic zones. As a consequence the plastic zone to crack size ratio is larger for the small crack, so that the first similitude requirement tends to be jeopardized. For very small cracks the same ΔK requires stresses at or close to yield and the plastic zone becomes undefined. Then the first requirement is violated and for this reason alone correlation on the basis of Equation (1) becomes impossible.

It has been attempted to mend this problem by applying a plastic zone correction, most notably in the case of the threshold K_{th}. If K_{th} has a fixed value for a certain material, it follows that

$$\Delta\sigma_{th} = \frac{1}{\beta}\left(\frac{\Delta K_{th}}{\sqrt{\pi a}}\right) . \quad (2)$$

16-5

Naturally Equation (2) predicts $\Delta\sigma_{th} \to \infty$ for a ∞ 0, while for a = 0 one should and does find $\Delta\sigma_{th} = \Delta\sigma_e$ (the endurance limit), as shown in Figure 3. This is no surprise because for a = 0 all similitude requirements are violated. The difficulty can be avoided by using a plastic zone correction as follows.

$$\Delta\sigma_{th} = \frac{1}{\beta}\left(\frac{\Delta K_{th}}{\sqrt{\pi(a + r_p)}}\right) . \quad (3)$$

For fixed K_{th} the Irwin plastic zone is constant. In that case K_{th} is finite for a = 0. However, for a = 0 the plastic zone is certainly not r_p and therefore Equation (3) becomes untenable for small a. As a matter of fact Equation (3) has no merits beyond the 1975 equation of Ohuchida et al.[3] or the 1979 equation of El Haddad et al.[4] in which r_p is replaced by an empirical constant.

If a Dugdale solution is used for r_p instead, r_p will depend upon crack size, but since $r_p = 0$ for a = 0 (trivial) the solution still has little merit. From a technical point of view, Equation (3) would be fully acceptable if it would consolidate the data. It may do so for a certain case, but since both β and r_p depend upon geometry, it can hardly be expected that the (erroneous) equation will have generality. In addition, violation of several other similitude requirements dampens the expectations.

For short cracks the effect of local crack front irregularities and consequent local K and constraint variations are not averaged out. The shorter crack front length will further bring out the effects of micro-structural variations, which may even lead to different growth mechanisms. Finally, the closure stress field will be different for the short crack if it is only for the different history.

Similitude and Short Cracks at Notches

For short cracks at notches the problem is further compounded by the notch field. In general, yielding will occur due to the notch so that a residual stress field is introduced. The tip of a long crack would be outside this field, but the tip of a short crack is engulfed by the field. Thus the local fields at the crack tip are different. Another consequence can be that the short-crack tip is in a displacement controlled field and the long-crack tip in a load controlled field[4], as indicated in Figure 4. If the effect of this field is ignored, correlation of crack behavior on the basis of Equation (1) cannot be expected.

However, breakdown of the correlation is not, in the first place, due to a breakdown of similitude. Rather it is due to the fact that the condition of equal K is erroneously assumed. In principle it would be possible to account for the local field in the calculation of K and R. Provided this could be done properly, the problem of the short crack at the notch would be equivalent to that of the small crack at a smooth surface, and all comments on the breakdown of similitude given previously would apply.

The Literature on Short Cracks

There have been numerous reports in the literature that crack growth rate data taken for short cracks show two anomalous behaviors; considerable scatter about the long crack growth rate trend data, and an apparent higher than expected growth rate. These have been termed the short crack effect. Generally, data are said to show a short crack effect if they do not correlate when growth rate is plotted against stress intensity factor range, the common LEFM parameter. But in many of these cases, the failure to correlate may have been due to the way LEFM was implemented rather than to some inherent deficiency in the theory. For example, K has been used for short cracks where closure is a factor, even though it is well accepted that K alone is inadequate for long cracks (e.g., see Equation (1)). This kind of example illustrates why it cannot be conclusively stated that failure to consolidate short crack data is due solely to shortcomings in LEFM. On the other hand, there are also examples in the literature of data for which the underlying assumptions of LEFM have been violated and for which LEFM cannot apply.

There are factors other than the applicability of LEFM which are of consequence to the short crack effect. Data from the literature show that a host of both micro and macro mechanisms of the flow and cracking processes influence crack growth rate. Differences in the cracking process, particularly near threshold, are especially numerous. They include multiple growth modes and combinations of modes and three-dimensional nature of the fracture process[5-8], the length and configuration of the crack front involving dimensions of both the specimen and the microstructure[9-10], anisotropy[11], free surface effects on slip character including effects of surface treatment and crystollographic growth[7,8,12], multiple cracking processes including possible environmental effects[13-15], ragged crack fronts[16], and finally transient effects due to inclusions, grain boundaries, and grain to grain mis-orientation[17-19].

The factors just listed might be called materials related factors and they have their proponents who consider them to be the most important factors. There is another school which believes that the most important factors are mechanics-related. They credit the short crack effects to the effect of the plastic zone to crack length ratio on LEFM, anisotropic effects, surface residual stress and local closure effects due to plane stress surface flow confined by a plane strain

surrounding, crack bifurcation and ill-defined crack fronts, stress redistribution due to notch root yielding and to material transient deformation behavior, and macroscopic closure due to residual stresses and deformations. It may be that a preference for the mechanics factors or the materials factors as being the most important in long and short crack behavior is only a function of training and background. The truth is that all of these factors interrelate and must be considered together. Thus, for example, grain size should not be considered alone and as unrelated to yield strength, and conversely.

The process of going from a situation in which there is no crack on a scale on the order of the microstructure, to a situation in which a crack exists, is transient. The crack is tending toward a steady state condition, the limit of which is the long crack condition. During this transition the crack length can be small compared to the size of the crack tip plastic zone that is required to sustain a growing crack[20]. In this regime, short cracks violate the confined plasticity requirements of LEFM and LEFM is invalid. While this kind of argument about LEFM is true at the microstructural scale it is vacuous in an application to a single crystal. Yet a crack in a single crystal must still go through the transient phase. This is not to argue that LEFM is applicable to single crystals. To the contrary, it is to emphasize the transient nature of the process and note that it cannot be modeled by steady state theories regardless of how they correlate growth rate.

The mechanism of initiation will control the length the crack must attain before a steady state develops at its tip. Brittle initiations at inclusions localize the process and allow a sharp crack with a well defined tip and a continuous front to form. In contrast, ductile initiation involves a good deal of flow before slip band decohesion, for example, initiates a crack, often crystallographically and with a poorly defined tip and discontinuous front. Certainly, the second situation described will have to grow some to sharpen etc., and thus will not achieve a steady state as quickly as its brittle counterpart.

Brittle initiation tends to form a crack which grows stably from the beginning, with limited flow at the crack tip. In contrast, ductile initiation would initially tend to violate the plastic zone to crack length limitation of LEFM. Results in the literature indicate that active plastic zones in the ductile case are as large as 0.3 mm while those for the brittle case approach 10^{-3} mm (Ref.3). In this respect, brittle steady state exists soon after inclusions crack, at crack lengths as small as can be consistently resolved using even highly sophisticated measurement systems. Ductile steady state by contrast develops only after extensive cracking. Significantly, LEFM criteria are satisfied for the lower extreme of brittle intiation at a crack length of about 10^{-3} mm about the lower limit of detection. In contrast, LEFM criteria are violated at the upper limit of ductile initiation for cracks nearly 3 mm long.

For short cracks for which the plasticity requirements of LEFM are met (nominally brittle initiation), the literature suggests that metallurgical features are a controlling factor for cracks smaller than a few grains. Micromechanics is also a factor in this case in that local closure occurs due to plane stress flow on the surface that is contained within an unyielding plane strain field.* The growth of these cracks is strongly influenced by the transients associated with the mode and mechanism of initiation. Whether or not multiple initiation and/or branching occurs is also a factor. For this reason it is expected that naturally initiated cracks will show a short crack effect whereas artificially induced cracks will demonstrate it to a much lesser degree, or not at all.

Smooth specimen data show the short crack effect inconsistently, and then only to a limited extent at finite growth rates. In view of the preceding discussion, the limiting case of brittle initiation would not be expected to show any transient behavior, and only limited closure because of limited flow. This is in fact observed[21]. As more inelastic action occurs, these effects should and do become more pronounced[22]. Thus, the observed inconsistent nature of the short crack behavior is really not surprising, nor is it necessarily indicative of measurements scatter. Near the threshold, the short crack effect is more wide spread and consistent, an observation that can be rationalized easily in terms of both microstructural effects and mechanics (local closure). However, it has been demonstrated that the threshold may be wiped out under variable amplitude (service like) loadings[33]. In this respect the fact that the effect develops consistently near the threshold may be of little practical concern.

To be unquestionably accurate, damage tolerant and RFC analyses should make use of small crack thresholds. They may be substantially smaller than long crack thresholds. But once the crack is growing, inclusion of any short crack behavior will have a negligible effect. This is particularly true in the case of brittle initiation. It is difficult to give a quantitative estimate of the short crack influence on life for smooth specimens. However, the case of confined flow at a notch has analogous ingredients. By integrating the growth rate behavior shown in Figure 5 (Ref.24), a decrease in life of about 10 percent is obtained for the most extreme of these results. The magnitude of this decrease depends on the difference in growth rate, the crack length over which the short crack rates act, and the duration of the ensuing long crack propagation. Of course, the shorter the critical crack size, the shorter the LEFM growth and the more significant the short crack effect on life.

In the case of ductile initiation both small and larger cracks may initially violate the LEFM confined plasticity requirement because of large crack tip plastic zones. That plastic zone may be due only to the initiation process. It may also be due to yielding at a notch. In the first case the crack cannot behave as a long crack until it has grown beyond the initiation zone, and has developed its own steady state field. Again both micromechanics and metallurgical features are important considerations in regard to the transient growth process. Equally important are multiple initiation and

* "Local closure" cannot be of consequence in ductile materials at stress levels that lead to bulk plasticity. The significance of local closure is inferred from the fact that data which show a "brittle" intergranular initiation do not show the short crack effect whereas a "ductile" transgranular mechanism does[9].

branching. Again, because artificial flaws would tend to concentrate deformation and tend to cause a more brittle initiation, natural cracks are expected to show the short crack effect much more so than artificial preflawed samples. 16-7 When the plastic zone is due to notch inelastic action, not only may the contained plasticity requirement be violated, but the K solution is inappropriate. Cracks growing under this condition tend to be controlled primarily by the mechanics of the displacement controlled primarily by the mechanics of the displacement controlled inelastic zone.

Unlike the case of confined crack tip plasticity, integration of short crack growth rates for cracks growing at inelastically strained notch roots suggests large errors could develop. Analysis indicates of such data[25] indicated that non-conservative errors of more than an order of magnitude may develop when LEFM data and analyses are used in place of observed trends. Clearly, damage tolerant and RFC analyses need to use the appropriate short crack threshold and growth rates in this case.

The subject of short cracks to this point has been discussed without reference to environmental effects. However, airframe and engine components exist in an aggressive environment and some comment on environmental interactions with short cracks is appropriate.

Consideration of the nature of environmentally assisted cracking (EAC) suggests that environmental short crack effects may arise from several sources. First, many environmental processes generate reaction products which can serve to block small, tight surface cracks. This will prevent entry of the aggressive species to the crack tip and retard the process. Alternatively, if these reaction products are mechanically stiff and are resistant to compression fracture, they may serve to wedge open cracks[26]. This will locally reduce the range of the applied stress intensity factor, and thereby reduce at least the mechanical component of the growth rate. A second issue of consequence is the ready accessibility of short crack tips to the environment. In processes where transport of the aggressive species is of consequence, this would tend to enhance the growth rate for shorter crack (e.g., Reference 27). A number of parameters are significant in such situations, including CTOD and the nature of the environment. The final issue of consequence involves cracks whose length lies within the steady state environmental process zone that develops for long cracks. Clearly any crack smaller than the dimension of this zone will not be environmentally similar to its longer steady state counterpart.

Depending on environmental and mechanical factors, one would anticipate that environmentally affected small cracks may grow either slower or faster than their longer counterparts. Data in the literature show that wedging action develops for a variety of reaction products[26,28]. Of particular significance in engine applications are the hard oxides that develop on a range of engine materials. Such oxides possess mechanical properties which could effectively block and wedge cracks. Wedging would have its greatest effect when its thickness is on the order of the CTOD. Small cracks and threshold conditions thus are first to be susceptible to its effects. In view of results for wedging effects in long cracks in aqueous media[28], wedging may significantly reduce the growth rate under these susceptible conditions. Data in the literature also show that there is an evironmental short crack effect that significantly increases growth rates[27]. The first evidence of this effect, presented in Figure 6, appears in print before much of the current concern for short cracks[27]. More recent studies verify such trends at threshold[29] and finite growth rates[30]. Unfortunately, studies done to date do not permit determination of whether transport or nonsteady state environmental processes account for this increased rate.

Critical Discriminating Experiments

It is clear from a critical review of the literature[2] that there is a need for experiments which do two things:

- isolate conditions under which physically small cracks exhibit anomalous growth when properly analyzed via LEFM, and
- define those factors which control such growth in both smooth and notched specimens.

Since the effect appears to depend on the transient nature of the natural initiation process, naturally initiating cracks should be used. Furthermore, the effect appears to be fundamentally different at inelastically strained notch roots as compared to smooth specimens. Thus, both smooth and notched specimens should be used. Finally, differences in microcrack closure and fractographic features tend to most easily explain differences in short and long crack behavior in smooth specimens. Notched specimen behavior is likewise most easily explained by these factors, along with the fact that the local control condition is displacement control.

Discriminating tests that probe the influence of microcrack closure and fractographic transients would focus on smooth edge-cracked plate specimens precracked at their edges, to initiate well defined plane fronted cracks, i.e., a steady state crack. Use a simple edge-cracked geometry coupled with selective testing at a range of R values would facilitate direct LEFM analysis of the data, thereby removing uncertainty in K calculation from the study. Depth of cracking should be controlled to develop long crack (steady state) fractography. To ensure repeatability, the depth and minimum section size should be controlled via some closed loop measurement system such as a crack gage. Various crack depths can then be achieved using the classic Frost approach of machining off the sample edges.

Tests could be restarted on one set of samples at the same set of loads, with enough samples tested over a range of loads to develop a range of plastic zone sizes at crack tips. To circumvent the influence of prior plastic zones, all samples could be stress relieved with care taken to avoid grain refinement or growth. Growth rate should be monitored and

fractographic features studied after the test to ensure a steady state mode. These tests provide a closure free, transient free reference for all subsequent smooth specimens. They define the influence of plastic zone size to crack length ratio, in that a range of stress and crack lengths will be employed.

16-8

The influence of transients in growth due to differing growth mechanisms can be identified by running a corresponding set of experiments with naturally initiating cracks and comparing their growth against the steady state data. The effect of microcrack closure can be identified by selective testing to a similar matrix and thereafter removing material in the wake of the crack. Finally, the influence of grain size on fractographic features and microcrack closure can be studied by selectively performing certain of the above experiments on materials heat treated to refine or enlarge the grains, and therefore cold worked to yield the same strength level for all microstructures.

A similar series of selective discriminating tests should be run on notched samples. Here the center notched panel is appropriate. Different thicknesses can be studied to facilitate an examination of the influence of crack front length and geometry. Microcrack closure can be examined again by cutting away material in the wake of the crack.* Selective testing at a range of stresses and crack lengths facilitate direct study of the influence of notch plasticity. Since the influence zone of notch plasticity should scale with the linear scaling of the specimen planform, several geometrically similar samples of different relative size should be considered. Again, with the exception of the tests designed to study the corner crack configuration, the geometry chosen permits simple LEFM calculations.

SUMMARY

Considering the almost complete breakdown of similitude for short cracks, it is not surprising that short crack effects reported in the literature show no consistency. To some extent this may be because K had to be estimated or because the wrong K and R were used by ignoring the local (notch or closure) field. However, even if these artifacts could have been mended, correlations on the basis of Equation (1) (whether in terms of J or K) may still break down when other similitude conditions, as for example environment, are violated.

For equal K the nominal stress will be higher for a short crack than for a long crack. Eventually the stresses will exceed yield so that the plastic zone becomes undefined. Before that K becomes less and less a measure of similitude. This means that the "short crack effect" will depend upon the yield properties of the material.

Since also the metallurgical similitude breaks down for small cracks (which means that the growth rate is no longer an average taken over many grains) the local circumstances will be more reflected in the material's response. If the material is elastically or plastically anisotropic (differences in modulus and yield stress in different crystallographic directions) the local grain orientation will determine the rate of growth. A similar effect will occur in multi-phase materials. Crack front irregularities and small second phase particles or inclusions affect the local stresses and therefore the material's response. In the case of long cracks (which have long fronts) all of these effects are integrated and averaged over many grains, but for short cracks with short fronts only the local circumstances count.

It then follows that the magnitude of the small crack effect will depend upon:

- the yield properties of the material
- crack front irregularity (affecting stresses and mechanism)
- crystollographic anisotropy (stresses and mechanism)
- phases
- particles
- environment.

Several of these items are interrelated, so that the above separation is somewhat arbitrary, but it serves the purpose of showing the factors involved. Indeed the literature confirms this expectation. As such many publications are of interest, but they hardly provide insight beyond those gained through physical arguments.

A certain number of publications simply ignore all physical reality and carry Equation (1) beyond all its explicity limits, sometimes attempting to patch discrepancies through artificialities such as Equation (3). It is hardly surprising that they meet with only limited success.

Another set of publications seeks the answer entirely in the mechanical factors. Clearly, mechanical similitude has to be invoked, but it has to be invoked rigorously. Therefore, any attempts in which local fields and closure forces are ignored, have no chance to succeed, and any incidental correlations are fortuitous.

Departure from stress field parameters in favor of a geometrical parameter such as CTOD certainly has merits. However, the most expedient way to obtain CTOD solutions, through a Dugdale model, is still limited to contained yielding. Yet the big advantage of Dugdale solutions is that closure and other local fields can be accounted for, be it

* The advantage here is that K before and after cutting is the same so that growth rate trends provide a clear cut assessment of this factor. (Samples do not have to be heat treated to remove the prior plastic zone.)

with difficulty. In this respect the work by Newman in this publication and Seeger and Fuhring[31-35] is very valuable as a starting point.

Naturally, mechanical similitude alone will not completely solve the problem. To the extent that crack growth is a geometrical consequence of slip, CTOD is certainly a measure of crack extension. But it is not a unique measure, because the local crack tip profile depends upon crystallographic orientation, phase, etc. Automatic averaging at long crack fronts alleviates the problem, but for small cracks with short fronts da/dN cannot be uniquely correlated with CTOD. The extent to which this presents a problem cannot be judged a priori. It can only be ascertained that it will be strongly material dependent. Once a satisfactory model for mechanical similitude is developed, the significance of metallurgical similitude will become obvious.

It is concluded that the short crack effect arises primarily because of crack tip plasticity, transients from the initiation process, and incorrect or incomplete implentation of LEFM. The phenomenological data tend not to discriminate between which of these is significant, when, and why. Thus, discriminating tests are required. CTOD appears to be a viable basis to track the growth of small (short) cracks[2]. Its use as a measure of the crack driving force warrants continued study.

Regarding papers of this conference in light of AGARD's interest in airframe structural fatigue, several conclusions can be drawn. Potter et al., and Wang[36] present data which indicate growth rate data for cracks from fastener filled holes correlate with long crack data. These trends, which are contrary to open hole results, may be explained by the fact that compression loads do not develop differing closure conditions as the crack extends. Closure does not develop because (1) the cyclic loading considered was predominantly tensile and (2) load transfer occurs across the fastener in compressive cycles in filled holes and (3) interference fit fasteners (if used) prop holes open. Thus, one would not expect a major short crack effect in growth rate behavior. However, this does not mean that the threshold behavior would not differ from that developed for long cracks, particularly in situations where large compression loads develop. Data developed by Topper et al.[37] confirm the earlier Japanese work which shows threshold tends to be reduced in the presence of block cycling[38]. Significantly, data of both Potter et al. and Wang[36] do show crack propagation occurs at levels below the usual long crack threshold. Aside from the reduction in threshold, the paper by Anstee[39] thus reasonably summarizes the problem of short cracks for panel like elements of airframe structures.

However, many questions remain for the AGARD committee to answer to the significance of short crack growth in other geometries for which closure effects are not circumvented by load transfer through fasteners. Particularly significant in this context are metallurgical factors such as anisotropy, the effects of end grain in forgings, etc. Of equal concern are components subjected to aggressive environments. Given that in these situations, relatively high strength materials are used for which brittle initiation occurs, the integrated effect of the short crack behavior will occur only over a fairly short crack length (a few grains). Provided that critical crack lengths are very large compared to the grain size, the integrated effect of the short crack behavior will cause a limited reduction in life as compared to the usual LEFM prediction. But, if the critical crack size is small, there may be a major reduction in life.

In materials which exhibit ductile initiation under conditions where the plastic zone is large compared to the crack length over a significant portion of the life, life predictions based on LEFM may be very nonconservative due to the short crack effect. Fortunately, these situations tend not to be widespread in airframe materials and structures. However, such situations are not uncommon in highly stressed hot path components in engines. Particular care, therefore, should be taken in applying LEFM in engine design and RFC analyses. Attention should be focused on this and other similar situation by the AGARD committee.

16-10

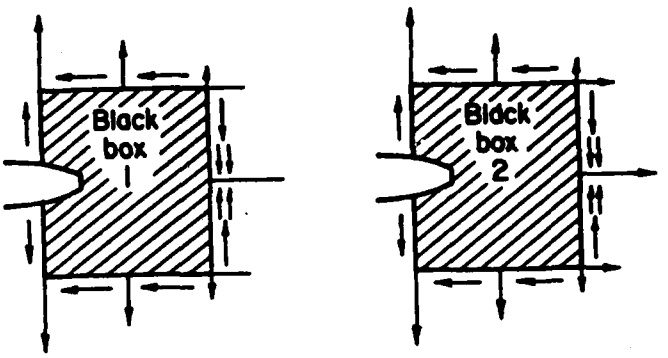

a. Similitude: Black boxes are equal so that ΔK is equal and thus da/dN is the same.

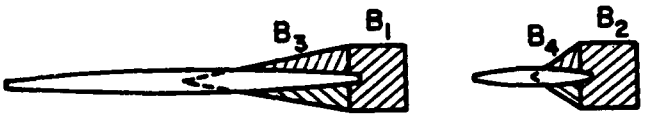

b. Questionable similitude: $B_1 = B_2$ so that ΔK is equal: $B_3 = B_4$ so that closure differs and thus da/dN will not be equal.

Fig.1 The concept of similitude

CONTRIBUTIONS TO CRACK ADVANCE PER CYCLING OF LOADING

	SHORT CRACK	LONG CRACK
MODE I	Δa Ductile (Dimples, Tearing) Δa Brittle (Cleavage) Δa Striations	Δa Striations
MODE II	Δa_{Shear} / Δa_{Total} (Short)	Δa_{Total} (Long)

Clearly $\Delta a^{Short}_{Total} > \Delta a^{Long}_{Total}$

Thus $\frac{\Delta a^{Short}}{\Delta N} > \frac{\Delta a^{Long}}{\Delta N}$

For the *same* ΔK and Local Closure

Fig.2 Modes and mechanisms of growth for short and long cracks

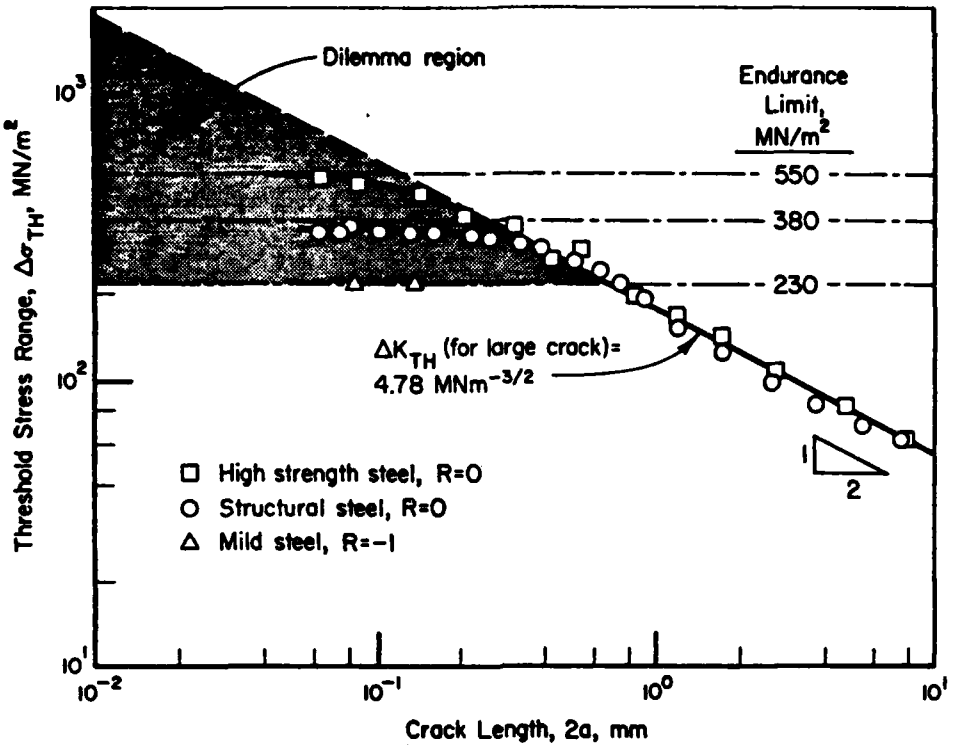

Fig.3 Breakdown of LEFM as crack size decreases (from Reference 2)

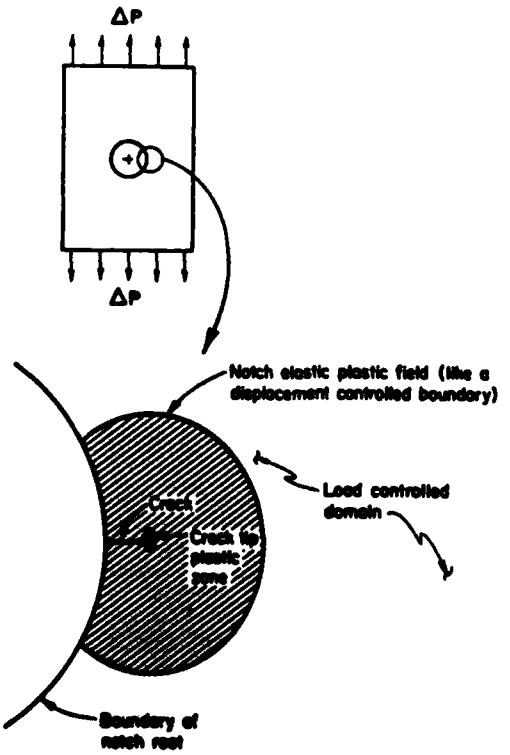

Fig.4 Short cracks grown in displacement control of inelastic notch field (after Leis[5])

16-12

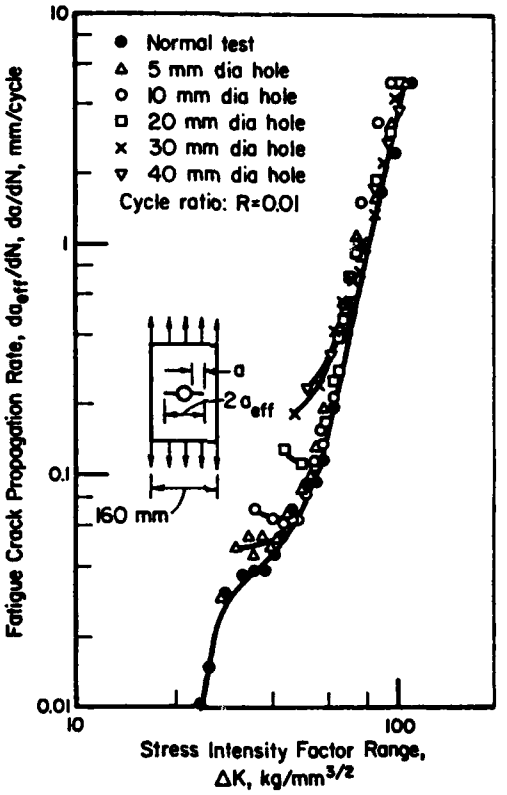

Fig.5 Crack growth rate data for a structural aluminum alloy (after Broek[24])

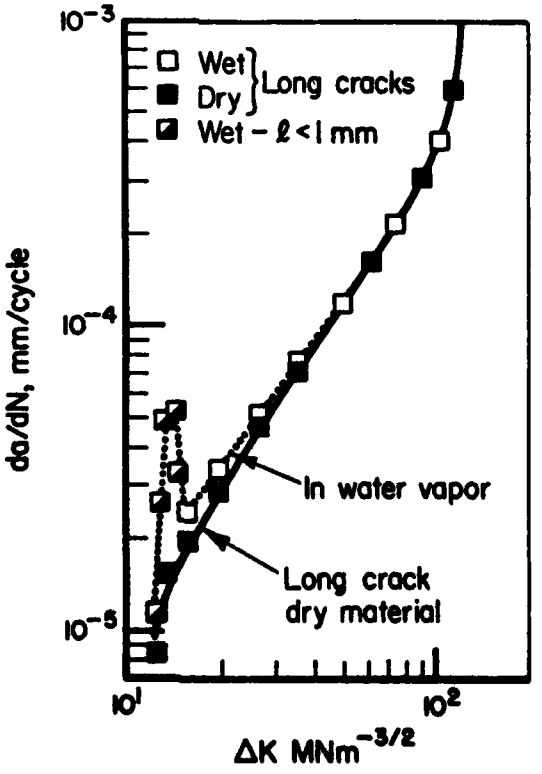

Fig.6 Effect of environment on short crack versus longer crack (after Holder[27])

REFERENCES

1673

1. Broek, D.
   Leis, B.N.
   Similitude and Anomalies in Crack Growth Rates, Materials Experimentation and Design in Fatigue, Proceedings of Fatigue '81, March, 1981.

2. Leis, B.N.
   et al.
   A Critical Review of the Short Crack Problem in Fatigue, AFML-TR, to appear.

3. Ohuchida, H.
   Usami, S.
   Nishioke, A.
   Fatigue Limit of Steel with Cracks, Bulletin of the JSME, Vol.18 No.125, November 1975

4. El Haddad, M.H.
   Smith, K.M.
   Topper, T.H.
   Fatigue Crack Propagation of Short Cracks, ASME Vol.101, No.1, 1979.

5. Leis, B.M.
   Displacement Controlled Fatigue Crack Growth in Elasticplastic Notch Fields and the Short Crack Effects, Engineering Fracture Mechanics, to appear.

6. Yokobori, T.
   Kamei, A.
   Yokobori, A.
   Fatigue Crack Propagation Under Mode II Loading, Int. Journal of Fracture, 1976.

7. Minakawa, K.
   McEvily, A.J.
   On Crack Closure in the Near-Threshold Region, Metallurgica, Vol.15, pp.633-636, 1981.

8. Vincent, J.N.
   Remy, L.
   On the Mechanisms of Threshold Behavior, Advances in Fracture Research, Vol.3, 1981.

9. Cook, T.S.
   Lankford, J.
   Sheldon, G.P.
   Research on Growth of Microcracks in Nickel-Base Superalloys, Final Technical Report No. AFML-TR-78-133 to Wright Patterson Air Force Base, September 1978.

10. Mahajan, Y.
    Margolin, H.
    Low Cycle Fatigue Behavior of Ti-6Al-2Sn-4Zr-6Mo: Part 1. The Role of Microstructure in Low Cycle Crack Nucleation and Early Crack Growth, Metallurgical Transactions, Vol.13A, February 1982.

11. Ohji, K.
    et al.
    Fatigue Behavior of Anisotropic Rolled Steel Plates Under Cyclic Torsion, Bulletin of the JSME, Vol.19, November, 1976.

12. Helle, H.P.E.
    An Investigation of Ship Propeller Fatigue, Ph.D. Thesis, Technische Hogeschool Te Delft, November, 1981.

13. Musuva, J.K,
    Radon, J.C.
    Threshold of Fatigue Crack Growth in a Low Alloy Steel, Advances in Fracture Research, Vol.3, 1981.

14. Sukuki, H.
    McEvily, A.J.
    Microstructural Effects on Fatigue Crack Growth in a Low Carbon Steel, Metallurgical Transactions, Vol.10S, April, 1979.

15. Tanaka, K.
    Masuda, C.
    Nishijima, S.
    Analysis of Fatigue Crack Growth Data for Various Steels with Special Reference to Fracture Mechanisms and Metallurgical Structures, Materials, Experimentation and Design in Fatigue, Proceedings of Fatigue '81, March 1981.

16. Leis, B.N.
    Galliher, R.D.
    Growth of Physically Short Center Cracks at Circular Notches, Low Cycle Fatigue and Life Prediction, ASTM STP 770, pp.399-421, 1982.

17. Morris, W.L.
    James, M.R.
    Buck, O.
    Growth Rate Models for Short Surface Cracks in Al 2219-T851, Metallurgical Transactions, Vol.12A, January, 1981.

18. Morris, W.L.
    . Trans. A, Vol.10A, pp.5-11, 1979.

19. Hatanaka, K.
    Yamada, T.
    Effect of Grain Size on Low Cycle Fatigue in Low Carbon Steel, Bulletin of the JSME, Vol.24, October 1981.

16-14

20. Seika, M. Kitaoka, S. Ko, H. — *Change of Material Properties at the Tips of Fatigue Cracks Subjected to Macroscopic Tensile and Shear Stresses for Propagation (in Rotary Bending Cyclic Torsion)*, Bulletin of the JSME, Vol.19, October, 1976.

21. Friedl, K.H. Scarlin, R.B. Zelizko, V. — *The Propagation of Short Fatigue Cracks in 12% Chromium Steels*, Advances in Fracture Research, Vol.2, 1981.

22. Tanaka, K. Nakai, Y. Yamashita, M. — *Fatigue Growth Threshold of Small Cracks*, International Journal of Fracture, October, 1981.

23. Kikukawa, M. et al. — *Fatigue Crack Propagation and Crack Closure Behaviour Under Varying Loading Conditions*, Fracture 1977, Vol.2, June, 1977.

24. Broek, D. — *The Propagation of Fatigue Cracks Emanating from Holes*, Report No. TR 72134 C to the National Aerospace Laboratory, 1972.

25. Leis, B.N. — *Fatigue Crack Propagation Through Inelastic Gradient Fields*, Int. J. Pres. Ves. & Piping, 10, pp.141-158, 1982.

26. — Private Communication L.F.Coffin of General Electric Co. to B.N.Leis of Battelle, June, 1982.

27. Holder, R. — *Environmental Effects on Fatigue Crack Initiation and Propagation in Cast Low Alloy Steels*, In: Mechanisms of Environment Sensitive Cracking of Materials, Proceedings of an International Conference organized by the Metals Society and held at the University of Surrey, Guildford, April, 1977.

28. Velden, D. Schultze, W.A. Ewalds, R.V. — *Anomalous Fatigue Crack Growth Retardation in Steels for Offshore Applications*, In Corrosion-Fatigue: Mechanics, Metallurgy, Electro-chemistry and Engineering, ASTM STP, to appear, October, 1981.

29. Usami, S. Shida, S. — *Elastic-Plastic Analysis of the Fatigue Limit for a Material with Small Flaws*, Fatigue of Engineering Materials and Structures, Vol.1, pp.471-481, 1979.

30. Gangloff, R.P. — Res. Mechanics Letters, Vol.1, pp.299-306, 1981.

31. Seeger, T. — *Ein Betrag für Berechnung von statisch und myblisch belasteten Rebocheichen nach dem Dugdale-Barenblatt Modell*, Institüt für Statick und Stahlban, Darmstadt (1973). (A Contribution to the Calculation of Statically and Cyclically loaded Cracks with the Dugdale-Barenblatt Model.)

32. Fuhring, H. — *Berechnung von elastisch-plastischen Beanspruchenoablaufen in Dugdale-Ribscheiben mit Ribüferkontakt auf der Grundlage nichtlinearer Schwingbruch mechanich*, Institüt für Statick und Stahlban, Darmstadt (1977). (Calculation of elastic-plastic loading in Dugdale Cracks with Crack Closure on the Basis of Non-linear Fatigue Fracture Mechanics.)

33. Fuhring, H. Seeger, T. — *Remarks on Load-Interaction Effects Based on Fatigue Fracture Mechanics Calculations*, ICAF Proceedings, 1977.

34. Fuhring, H. Seeger, T. — *A Suggestion for Systematic Load Interaction Studies on Fatigue Crack Growth*, Int. J. of Fracture, 12, pp.307-310, 1976.

35. Fuhring, H. Seeger, T. — *Structural Memory of Cracked Component Under Irregular Loading*. ASTM STP 677, pp.144-167, 1979.

36. Wang, D.Y. — *A Study of Small Crack Growth Under Transport Spectrum Loading*, this publication.

37. Au, P. Topper T.H. El Haddad, M.L. — *The Effects of Compressive Overloads on the Threshold Stress Intensity for Short Cracks*, this publication.

38. Kikukawa, M. et al. — *Fatigue Crack Propagation and Crack Closure Behavior Under Varying Loading Conditions*, Int. Journal of Fracture, 13, 1977.

39. Anstee, R.W.F. — *An Assessment of the Importance of Small Crack Growth to Aircraft Design*, this publication.

16-12

AGARD

NATO ⊕ OTAN

7 RUE ANCELLE · 92200 NEUILLY-SUR-SEINE

FRANCE

Telephone 745.08.10 · Telex 610176

DISTRIBUTION OF UNCLASSIFIED AGARD PUBLICATIONS

AGARD does NOT hold stocks of AGARD publications at the above address for general distribution. Initial distribution of AGARD publications is made to AGARD Member Nations through the following National Distribution Centres. Further copies are sometimes available from these Centres, but if not may be purchased in Microfiche or Photocopy form from the Purchase Agencies listed below.

NATIONAL DISTRIBUTION CENTRES

BELGIUM
Coordonnateur AGARD – VSL
Etat-Major de la Force Aérienne
Quartier Reine Elisabeth
Rue d'Evere, 1140 Bruxelles

CANADA
Defence Science Information Services
Department of National Defence
Ottawa, Ontario K1A 0K2

DENMARK
Danish Defence Research Board
Osterbrogades Kaserne
Copenhagen Ø

FRANCE
O.N.E.R.A. (Direction)
29 Avenue de la Division Leclerc
92320 Châtillon sous Bagneux

GERMANY
Fachinformationszentrum Energie,
Physik, Mathematik GmbH
Kernforschungszentrum
D-7514 Eggenstein-Leopoldshafen 2

GREECE
Hellenic Air Force General Staff
Research and Development Directorate
Holargos, Athens

ICELAND
Director of Aviation
c/o Flugrad
Reykjavik

ITALY
Aeronautica Militare
Ufficio del Delegato Nazionale all'AGARD
3, Piazzale Adenauer
Roma/EUR

LUXEMBOURG
See Belgium

NETHERLANDS
Netherlands Delegation to AGARD
National Aerospace Laboratory, NLR
P.O. Box 126
2600 A.C. Delft

NORWAY
Norwegian Defence Research Establishment
Main Library
P.O. Box 25
N-2007 Kjeller

PORTUGAL
Direcção do Serviço de Material
da Força Aérea
Rua da Escola Politécnica 42
Lisboa
Attn: AGARD National Delegate

TURKEY
Department of Research and Development (ARGE)
Ministry of National Defence, Ankara

UNITED KINGDOM
Defence Research Information Centre
Station Square House
St. Mary Cray
Orpington, Kent BR5 3RE

UNITED STATES
National Aeronautics and Space Administration (NASA)
Langley Field, Virginia 23365
Attn: Report Distribution and Storage Unit

THE UNITED STATES NATIONAL DISTRIBUTION CENTRE (NASA) DOES NOT HOLD STOCKS OF AGARD PUBLICATIONS, AND APPLICATIONS FOR COPIES SHOULD BE MADE DIRECT TO THE NATIONAL TECHNICAL INFORMATION SERVICE (NTIS) AT THE ADDRESS BELOW.

PURCHASE AGENCIES

Microfiche or Photocopy
National Technical
Information Service (NTIS)
5285 Port Royal Road
Springfield
Virginia 22161, USA

Microfiche
Space Documentation Service
European Space Agency
10, rue Mario Nikis
75015 Paris, France

Microfiche or Photocopy
British Library Lending
Division
Boston Spa, Wetherby
West Yorkshire LS23 7BQ
England

Requests for microfiche or photocopies of AGARD documents should include the AGARD serial number, title, author or editor, and publication date. Requests to NTIS should include the NASA accession report number. Full bibliographical references and abstracts of AGARD publications are given in the following journals:

Scientific and Technical Aerospace Reports (STAR)
published by NASA Scientific and Technical
Information Facility
Post Office Box 8757
Baltimore/Washington International Airport
Maryland 21240, USA

Government Reports Announcements (GRA)
published by the National Technical
Information Services, Springfield
Virginia 22161, USA

Printed by Specialised Printing Services Limited
40 Chigwell Lane, Loughton, Essex IG10 3TZ

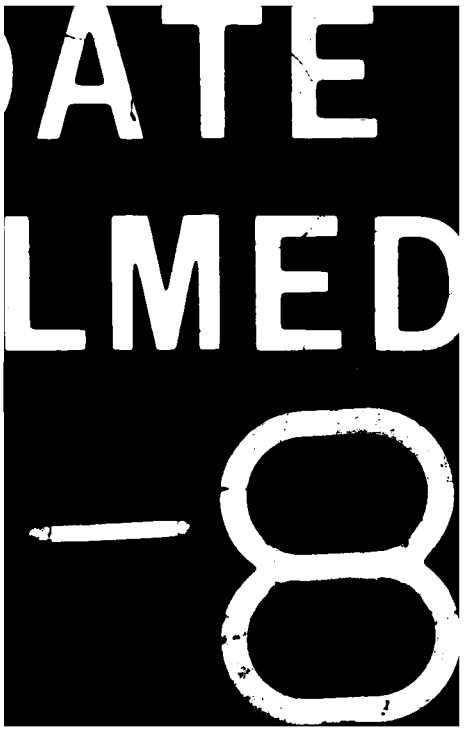
ATE
LMED
-8